DEVELOPMENT OF NEXT GENERATION MIXED MATRIX HOLLOW FIBER MEMBRANES FOR BUTANE ISOMER SEPARATION

A Dissertation
Presented to
The Academic Faculty

by

Junqiang Liu

In Partial Fulfillment
of the Requirements for the Degree
Doctor of Philosophy in the
School of Chemical & Biomolecular Engineering

Georgia Institute of Technology
December 2010

DEVELOPMENT OF NEXT GENERATION MIXED MATRIX HOLLOW FIBER MEMBRANES FOR BUTANE ISOMER SEPARATION

Approved by:

Dr. William J. Koros, Advisor
School of Chemical & Biomolecular Engineering
Georgia Institute of Technology

Dr. Victor Breedveld
School of Chemical & Biomolecular Engineering
Georgia Institute of Technology

Dr. Christopher W. Jones
School of Chemical & Biomolecular Engineering
Georgia Institute of Technology

Dr. Carson Meredith
School of Chemical & Biomolecular Engineering
Georgia Institute of Technology

Dr. Sankar Nair
School of Chemical & Biomolecular Engineering
Georgia Institute of Technology

Dr. Ronald R. Chance
Distinguished Scientific Advisor
ExxonMobil

Date Approved: October 8, 2010

A Dedication to
My Wife Hongxia

ACKNOWLEDGEMENTS

I want to thank my parents for their unconditional love and support throughout my life. They devoted all their limited resources and unlimited love to support my journey to be a scholar. Without their love and encouragement, I cannot arrive here. I am blessed to have Dr. Koros as my advisor. If someone asks me which intellectual influenced me mostly, I have to say it is Bill. His passion at work, trust on people, positive thinking set a superb role for me to follow in my future career and life. Under his guidance and encouragement, research becomes a fascinating adventure I totally immersed in. I feel grateful to my committee members, Dr. Christopher Jones, Dr. Sankar Nair, Dr. Victor Breedveld, Dr. Carson Meredith and Dr. Ronald Chance. I was fortunate to have so many world-class intellectuals almost as my co-advisors through the unique Georgia Tech-ExxonMobil research project. Their advices throughout my four year Ph. D study by the monthly GT-EM monthly discussions are greatly appreciated.

I must also thank those friends and colleagues in the GT-EM projects. Tae-Hyun Bae provided all the crucial zeolite samples, which make this research possible. Kayode Olanrewaju gave many advices on the phase separation and rheology of polymer solutions. Jung-Hyun Lee did the AFM for me and provided many insightful discussions on the polymer-zeolite adhesion. Omoyemen Esekhile gave me tremendous help on experiment work and theory development.

I also received numerous help from past and present Koros group members. Dr. Wulin Qiu synthesized all the 6FDA polymers used in my research. With his help, I was able to receive synthesized polymers within two weeks whenever I have a need. I want to thank Dr. Shu Shu, my college classmate at ECUST, for recommending me to Koros group. Special thanks to Dr. Shabbir Husain for tutoring me through my first year research. I appreciate the helpful advice from Dr. Ryan Adams, Dr. Jason Ward, Dr. Mita Das on the mixed matrix membrane works. Liren Xu and Chien-Chiang Chen, Naoki Bessho, Dhaval Bhandari, Ryan Lively helped me a lot on fiber spinning. JR Johnson and Oguz Karvan were always happy to help me find the solutions to numerous technical problems. I appreciate the help from Chen Zhang for proofreading my dissertation.

I want to thank my friends, Canghai Ma & Hongjuan Cui, Xue Ning, Kuang Zhang & Xuan Shi, Yanhui Yuan & Yi Ding, for their continuous help and encouragement during my stay at Atlanta. I also want to thank Jasmine and Jason Chen, Carol and Neale Hightower for their helps to me and my wife during our stay at Atlanta.

At last, I want to thank my wife, Hongxia, for her accompany these years. Her trust and encouragement are the fuel drives me to this stage. This dissertation cannot be completed without her care these years and intellectual contribution from a chemistry point of view.

To all the people impacted and helped me, thank you very much!

TABLE OF CONTENTS

LIST OF TABLES

LIST OF FIGURES

SUMMARY

Mixed matrix hollow fiber membranes maintain the ease of processing polymers while enhancing the separation performance of the pure polymer due to inclusion of molecular sieve filler particles. This work shows the development process of high loading mixed matrix hollow fiber membranes for butane isomer separation, from material selection and engineering of polymer-sieve interfacial adhesion to mixed matrix hollow fiber spinning.

The matching of gas transport properties in polymer and zeolite is critical for forming successful mixed matrix membranes. The nC4 permeability in glassy commercial polymers such as Ultem® and Matrimid® is too low (< 0.1 Barrer) for commercial application. A group of fluorinated (6FDA) polyimides, with high nC4 permeability and nC4/iC4 selectivity, are selected as the polymer matrix. No glassy polymers can possibly match the high permeable MFI to make mixed matrix membranes with selectivity enhancement for C4s separation. Zeolite 5A, which has a nC4 permeability (~3 Barrer) and nC4/iC4 selectivity (essentially ∞), matches well with the 6FDA polymers. A 24% nC4/iC4 selectivity enhancement was achieved in mixed matrix membranes containing 6FDA-DAM and 25 wt% treated 5A particles. A more promising mixed matrix membrane contains 6FDA-DAM-DABA matrix and 5A, because of a better match of gas transport properties in polymer and zeolite.

Dual layer hollow fibers, with cellulose acetate core layer and sheath layers of 6FDA polyimides, were successfully fabricated. Successive engineering of the 6FDA sheath layer and the dense skin is needed for the challenging C4s separation, which is

extremely sensitive to the integrity of the dense skin layer. The delamination-free, macrovoid-free dual layer hollow fiber membranes provide a solution for the use of expensive 6FDA polyimides selective layer spinning. Mixed matrix hollow fiber membranes are spun based on the platform of 6FDA/Cellulose acetate dual layer hollow fibers. Preliminary results suggest that high loading mixed matrix hollow fiber membranes for C4s are feasible. Additional research is needed on the fiber spinning with well treated zeolite 5A nanoparticles.

The key aspect of this research is elucidating the three-step (sol-gel-precipitation) mechanism of sol-gel-Grignard treatment, based on which further controlling of $Mg(OH)_2$ whisker morphologies is possible. A $Mg(OH)_2$ nucleation process promoted by acid species is proposed to explain the heterogeneous $Mg(OH)_2$ growing process. Different acid species were tried: 1) HCl solution, 2) AlClx species generated by dealumination process and 3) $AlCl_3$ supported on zeolite surfaces. Acids introduced through the HCl solution and dealumination are effective on commercial 5A particles to generate $Mg(OH)_2$ whiskers in the sol-gel-Grignard treatment. Supported $AlCl_3$ is effective on both commercial and synthesized 5A particles (150 nm-1 μm) during the sol-gel-Grignard treatment, in terms of promoting heterogeneous $Mg(OH)_2$ whiskers formation. The $Al(OH)_3$ layer appears to separate the $Mg(OH)_2$ whiskers from zeolite surface, and leads to undesirable morphologies for polymer-zeolite interfacial adhesion. The elucidation of sol-gel-Grignard mechanism and importance of zeolite surface acidity on $Mg(OH)_2$ formation, builds a solid foundation for future development towards ‘‘universal’’ method of growing $Mg(OH)_2$ whiskers on zeolite surfaces.

CHAPTER 1

INTRODUCTION

1. 1 MEMBRANES FOR GAS SEPARATIONS

While commercial aqueous membrane separations, including micro and ultra-filtration, reverse osmosis, dialysis and electro-dialysis are well established, membrane based gas separation is a more recently emerging field with annual growth rate more than 10% [1]. Because of the low cost associated with equipment installation, and large potential energy saving advantages, membrane based gas separation also provide a competitive alternative to traditional cryogenic distillation and adsorption swing methods. During the past 20 years, sales of membrane gas separation equipment have grown to become a $150 million/year business [2]. A diverse array of gas processing applications using membranes has been identified. Much of the membrane application involves the separation of non-condensable gases: nitrogen from air; carbon dioxide from methane. However, as shown in Table 1.1, a large potential market for membrane gas separation lies in separating mixtures containing condensable gases such as the C^{3+} hydrocarbons from methane or hydrogen, propylene from propane, and n-butane from i-butane. These applications require the development of new membranes and processes [2].

1.1.1 Polymeric Membranes for Gas Separations

Polymeric membranes are relatively inexpensive, and can be processed into hollow fibers with good mechanical properties, which is the currently preferred industrial form of membrane for gas separation; however they have limits in separation efficiency

as well as chemical and thermal stability. The performance of polymeric membranes has been shown to suffer from a trade-off curve between gas permeability and selectivity as illustrated by Robeson's upper bound [3].

Table 1.1 The future membrane market, adapted from [2]

	Membrane market ($ million, 2000 dollars)		
Separation	2000	2010	2020
nitrogen from air	75	100	125
oxygen from air	<1	10	30 (?)
hydrogen	25	60	100
natural gas	30	90	220
vapor/nitrogen	10	30	60
vapor/vapor	0	30	125 (?)
other	10	30 (?)	100 (?)
total	150	350	760

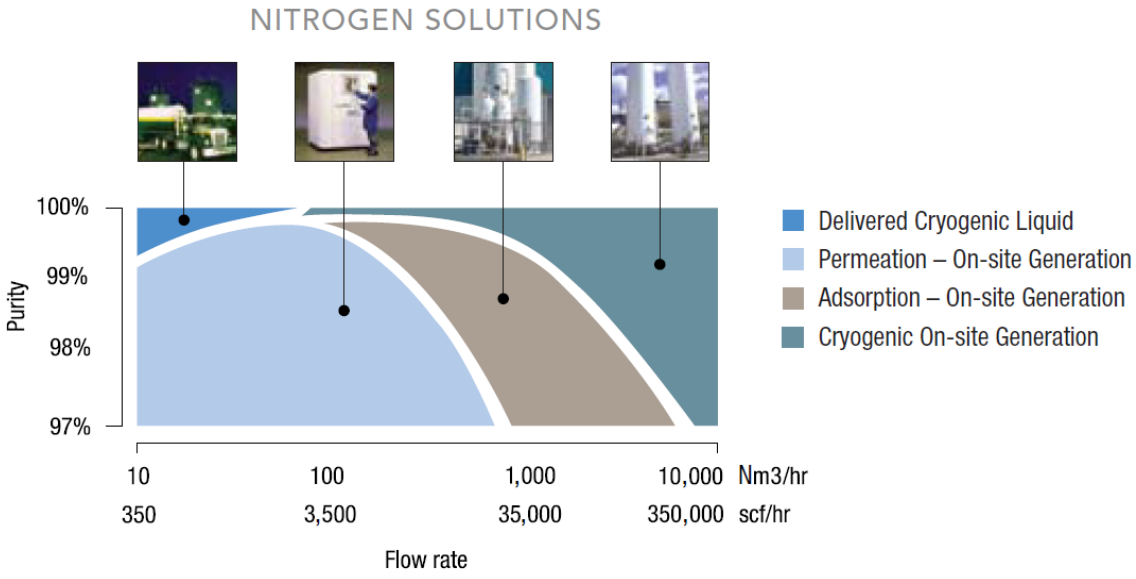

Figure 1.1 Most economical separation methods for Nitrogen enrichment from air at various technical requirements, adopted from PRISM® brochure, Air Products

In general, polymeric membranes are economical when low flow rates are required or when low impurities can be tolerated, because polymeric membranes have

generally limited selectivity over different gas molecules. Fig. 1.1 shows the most economic way of nitrogen enrichment at various quantity and purity requirements. In order to get high purity nitrogen, the faster permeating oxygen has to diffuse through the membrane to the permeate side and to be removed to maintain an oxygen driving force at downstream, where the retentate side of oxygen concentration is very low. A significant amount of high pressure nitrogen also diffuses through the membrane to the permeate side and makes removal more costly. The selectivity of polymer membranes has to be raised in order to have wider economic membrane application for diverse gas separations, even beyond the simple O_2/N_2 case.

1.1.2 Mixed Matrix Membrane for Gas Separations

Advances in either permeability or selectivity improve the economies of membrane based gas separation. The throughput of the membrane can be improved by a thinner membrane thickness, more membrane area, and optimized module geometry. The hollow fiber form of membrane has more than an order of magnitude higher membrane surface to module volume ratio compared to forms like flat sheet and spirally wound flat sheet. Together with the inexpensive fabrication costs, the efficiency of such hollow fiber modules makes fibers the ideal form for economical gas separations. Economical improvement of selectivity is the most critical factor for practically separating most large scale gas streams, especially those requiring higher purity gas products.

Zeolites membranes offer significantly higher selectivity than polymeric membranes because of ‘‘molecular-sieving’’ properties; however their properties make them prohibitively expensive to process into membranes. Organic-inorganic, or “mixed matrix”, materials may provide the basis for the next generation of economical, high

performance membranes [4]. Although the viability of the mixed matrix concept for gas separation has been demonstrated, many technical challenges as well as fundamental science questions remain to be addressed properly [5-7]. This research aims to enhance the performance of mixed matrix membranes by understanding the fundamentals and by engineering the interface adhesion, to extend work done by former researchers. The final goal will be to demonstrate the ability to spin high loading mixed matrix hollow fibers with advanced separation performances.

1.2 PREVIOUS RESEARCH ON MIXED MATRIX MEMBRANE

Numerous research efforts have sought to incorporate high separating-performance zeolites into polymeric membrane to make mixed matrix membranes [8-13]. Successful mixed matrix membranes were reported either using rubbery polymers [8, 9], or at temperatures close to the glass transition temperature (T_g) of the glassy polymer [10, 11]. In other words, at a state where the polymer chain is flexible enough to accommodate stresses due to the inserted sieves. The incorporation of sieves into glassy polymer membranes, which would have better separation performance, has proven much more difficult because of defective interfaces between polymer and zeolite. Intensive effort has sought to make mixed matrix membranes, and the so-called ‘‘Maxwell model’’ provides a simple, quantitative framework to predict the transport properties of mixed matrix materials when the transport properties of the constituent phases are known. This expression is most effective at relatively low dispersed phase volume fractions, where sieve-sieve interactions are minimized. However it also has been useful as a first approximation at higher loadings. Eq. 1.1 relates the permeability in mixed matrix

material, where, P_c and P_d refer to the permeability in the continuous and dispersed phases, respectively. The volume fraction of the dispersed phase is φ_S.

$$P_{MMM} = P_P[\frac{P_S + 2P_P - 2\varphi_S(P_P - P_S)}{P_S + 2P_P + \varphi_S(P_P - P_S)}] \qquad (1.1)$$

Zimmerman *et al* published criteria for selecting molecular sieves and compatible polymers for a given separation to yield a substantial mixed matrix effect [6]. Previous researchers Mahajan and Moore in Koros group have identified four undesirable morphologies at the polymer-sieve interface, which need to be overcome in order to create a successful mixed matrix platform [7]. These includes: (i) *Matrix Rigidification, (ii) Sieve in a cage*, (iii) *Leaky interface and (iv) Plugged sieves.* Subsequently, many efforts have sought to modify either the zeolite surface chemistry or the polymeric matrices in order to improve adhesion at the interface. One direction of zeolite surface modification was to covalently bond via silane treatment [14-17]. The silane reagents were carefully selected to modify the zeolite surface, but not plug its pores. Some successful mixed matrix dense films were reported to show separation performance enhancement. No defect free mixed matrix hollow fibers have been spun via silane treatment, even though a few cases showed enhancement after annealing the fiber [18].

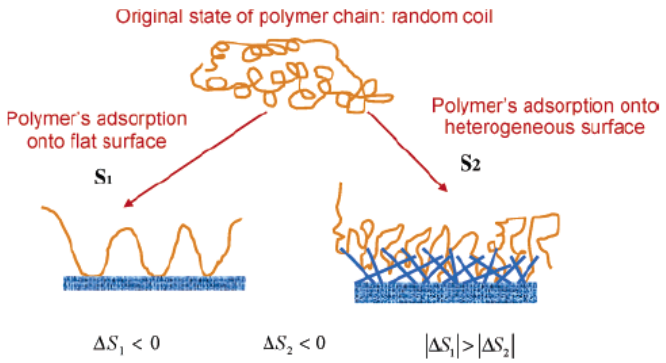

Figure 1.2 Schematic of enhanced bonding with whiskered structure on zeolite surface

Only recently, a reliable method of mixed matrix formation has been established and shown to be extendable to practical asymmetric fiber membrane has been established. Shu and Husain applied a Grignard treatment method to modify the zeolite surface [19-21]. This treatment significantly improved the interfacial adhesion between zeolite and polymer, which is the biggest problem facing mixed matrix application [6, 7]. The selectivity enhancement in mixed matrix dense film indicates improved interfacial adhesion by minimizing the entropy penalty for accommodating random coils of the matrix, as shown in Fig. 1.2. The Grignard treatment involves growing $Mg(OH)_2$ whiskers, consisting of two steps: (i) the crystal seeding step and (ii) the direct crystal growing step. The Grignard process starts from zeolite with alumina in the framework like zeolite 4A. The dealumination step provides nanocrystal seeds on the surface. Nano-scale $Mg(OH)_2$ whiskers form, possibly because of the large amount of the crystal seeds formed. The Grignard treatment was later applied to those zeolites, or silica, which lack alumina in the framework, by transferring seeds from other sources. Even more recent work in Jones/Nair group has explored the creation of similar whiskers via a similar "solvothermal method" [22].

As noted above, since the preferred conformation state for most polymers is as random coils, when a polymer chain adsorbs onto bare surface of zeolite, it must obviously be in much more ordered configurations than the initial random situation. In this unmodified case, there is a large entropy penalty, however, for the roughened particle surface, a polymer coil need not change much and the entropy penalty, is reduced. From an enthalpy view point, the base property of $Mg(OH)_2$ may also promote bonding with polymer.

Using the Grignard treatment approach, S. Husain successfully spun mixed matrix hollow fibers using SSZ-13, and 4A nanoparticles [23, 24]. Fig. 2 shows the outer skin layer of mixed matrix hollow fiber. Good sieves dispersion and bonding between SSZ-13 and Ultem® can be observed.

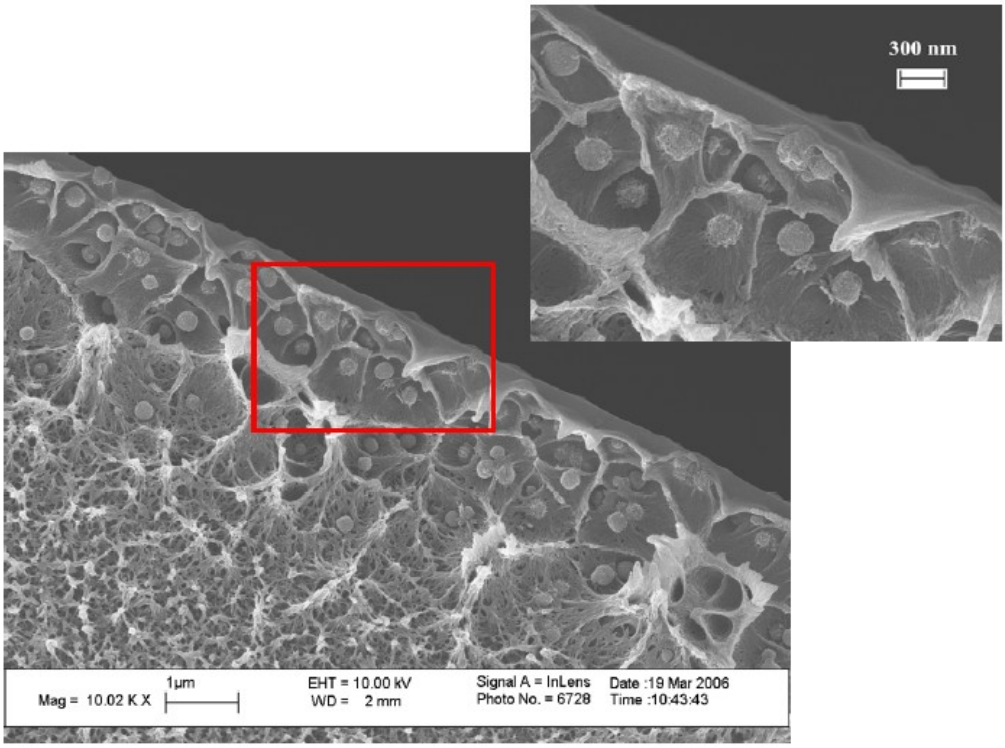

Figure 1.3 Skin layer of Ultem® mixed matrix hollow fiber with 4A nanoparticles [24]

S. Husain suggested an explanation regarding the mechanism for $Mg(OH)_2$ enhanced dispersion and adhesion in spinning environment. Agglomeration, driven by van der Waals attraction between nanoparticles, is detrimental to membrane separation performance. Husain suggested that the $Mg(OH)_2$ surface formed during Grignard treatment enhanced the electrostatic repulsion between charged particles, effectively countering the van der Waals attraction, and therefore, stabilized the dispersion of zeolite nanoparticles [24].

The $Mg(OH)_2$ whiskers formed in Grignard treatment were hypothesized to be a reaction product of Grignard reagent and moisture carried in by isopropanol. The detailed mechanism of whisker formation was not explained by former researchers. This work will need further in depth investigation to understand and optimize the Grignard treatment process. The original Grignard treatment showed success to grow $Mg(OH)_2$ whiskers on Al-containing zeolites like 4A and SSZ-13. In this work, Grignard treatment had to be adjusted to treat pure silicalite MFI. The effectiveness of Grignard treatment on zeolite nanoparticles also needed to be investigated for mixed matrix hollow fiber spinning.

1.3 MEMBRANES FOR BUTANE ISOMER SEPARATION

Since the petrochemical refining industry is seeking alternatives to methyl tertiary butyl ether (MTBE), alkylation processes and related technologies have been developed where i-butane (iC4, kinetic diameter (dk) 0.50 nm, boiling point (bp) 261K) formed by isomerization of n-butane (nC4, dk 0.43 nm, bp 272.3K) is an essential ingredient in production of alkylates [25]. The alkylation process catalytically combines C3-C5 olefins with iC4 to produce motor fuel alkylates, which is ideal for producing reformulated gasoline. However, the current process producing iC4 uses a large, energy intensive distillation column to recycle unconverted nC4 back to a reactor [26]. Table 1.2 and 1.3 show the specifications of one industrial scale C4s fractionators, which is bulky in size and energy intensive to operate. The boiler itself consumes about 5% the energy content of C4s, which it intends to separate.

The efficiency and cost-effectiveness of isomerization process can be improved by using a membrane separation unit that would significantly reduce capital and

operating costs associated with C4s separation. The main obstacle is reproducible preparation of a suitable membrane [25].

Table 1.2 Industrial column specifications for the n/iC4 fractionator, adapted from [26]

Column Specifications		
Number of Trays		74
Feed Flow Rate	kg/h	26234
Bottoms Flow Rate	kg/h	28229
Distillate Flow Rate	kg/h	8115
Reflux Flow Rate	kg/h	92838
Reflux Temperature	C	18.5
Column Top Pressure	kPa	658.6
Feed Pressure	kPa	892.67
Boiler Duty	MW	10.24

Table 1.3 Industrial column performance data of n/iC4 fractionator, adapted from [26]

Species	Compositions, Mass Fractions		
	Feed	Top	Bottom
Propane	0.015	0.053	0.003
i-Butane	0.294	0.935	0.003
n-Butane	0.677	0.002	0.981

1.3.1 Molecular Sieve Membranes for Butane Isomer Separation

Considering the effective ‘‘kinetic’’ diameters of the two gas molecules (nC4, 4.3 Å, iC4, 5.0 Å) [27], two molecular sieving zeolite candidates were considered based on previous research: aluminosilicate Zeolite 5A and pure silicate MFI.

Zeolite 5A is the Ca^{2+} form of first commercial and most widely used zeolite A. The 5A name comes from the approximately 5Å pore diameter. Zeolite 5A has been reported to selectively adsorb nC4 over iC4 [28]. The iC4 is essentially totally excluded from the zeolite pores because of the larger size. The selectivity of nC4/iC4 is practically ∞ in zeolite 5A. However, the diffusivity of nC4 in zeolite 5A is on the order of

magnitude of 10^{-9} cm^2/s [29], which is several orders of magnitude slower than the nC4 diffusivity in MFI (~10^{-6} cm^2/s) [30], therefore, the permeability of nC4 in MFI is 3 order of magnitude higher than that in 5A (assuming the solubility to be the same).

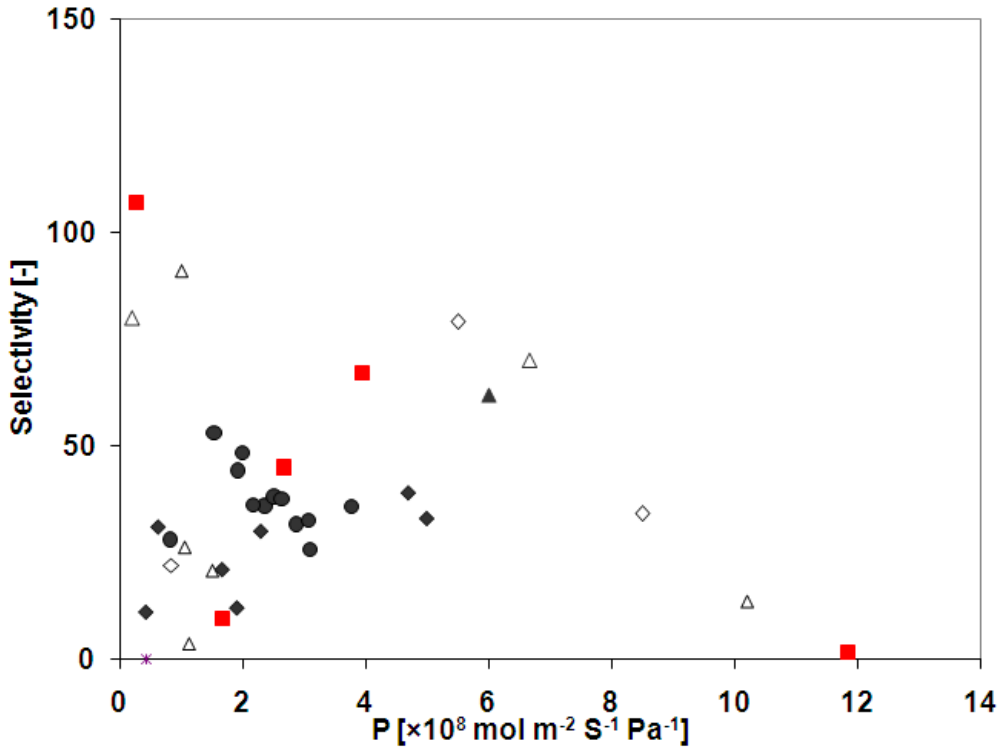

Figure 1.4 Butane isomer separation performance of different MFI membranes, open points are results from pure gas permeation tests, filled points are results from mixture gas permeation tests, filled square points are membranes with post caulking treatment. Data are adopted from [32-36]

MFI with a zigzag crosslinking circular (5.4 ± 0.2 Å) and elliptical (5.7-5.8 × 5.1-5.2Å) channels was reported to have high selectivity and permeability for C4s separation. The permeability of nC4 was very high, because of the large pore size of MFI. Additionally, silicalite MFI is hydrophobic and organophilic, and selectively adsorbs organic molecules over water [31]. These properties are attractive because moisture blocks aluminosilicate zeolite pores easily. Water exists everywhere to be avoided, from the water quenching bath during spinning, to atmospheric moisture during storage, and

many times the feed gas contains some amount of water. Therefore, MFI also seems like an attractive sieve candidate for C4s separation. High silica MFI membranes, either in flat sheet form [32-35], or tubular form [36, 37], have been extensively studied for C4s separation. Fig. 1.4 shows a summary of C4s separation performances of high silica MFI membranes synthesized by the above authors. The selectivity of nC4/iC4 is reported to range from about 1.5 to 90, which depends on the quality of membranes synthesized. The difficulty of pure MFI membrane fabrication has prevented the application of MFI membranes for large scale C4s separation application.

1.3.2. Polymeric and Mixed Matrix Membrane for C4s separation

There have been few studies on polymeric membranes for C4s separation for several reasons. First, butane is highly condensable near room temperature, and plasticizes polymers to a degree that low separating performance typically results. Accordingly, high temperature (low activity) is required for butane isomer separation using polymeric membranes. Clearly, dealing with flammable gases at high temperature is a potential safety issue. Moreover, the molecular sizes of butane isomers are so large that butane diffusion is hundreds of times slower than smaller gases like N_2 or O_2, according to Okamoto's estimation [38]. Until now, only limited membranes were reported for C4s separation using few most permeable polymers. Zendel Copolymer-I (Union Carbide) were reported to has nC4 permeability of 1890 Barrer and an ideal selectivity of 7.27 at 50 °C [39]. PDMS has nC4 permeability of 14,400 Barrer and an ideal selectivity of 2.38 [40]. The so called most permeable glassy polymer PTMSP were reported at 50 °C to have nC4 permeability of 36900 Barrer, and an ideal selectivity of 2.72 [41]

Mixed matrix membranes, with highly selective molecular sieve particles dispersed in an appropriate flexible polymer matrix, can have both high separation performance assisted by high performing molecular sieves, and economical fabrication due to reliance on a similar processing approach to that used for simple pure polymeric membranes. Woo loaded MFI micron particles to polymer PTMSP and found increased nC4 permeability and maximum 56% higher n/i C4s selectivity at 50 wt% loading compared to pure polymer [41]. However, the unstable PTMSP cannot be expected to be useful for real applications. Fig. 1.5 summarizes the performance of published C4s separation performances using polymeric and mixed matrix membranes. Membranes of glassy polymers, which possess higher selectivity and are easier to form into hollow fiber membranes, have not been investigated thoroughly for C4s separation.

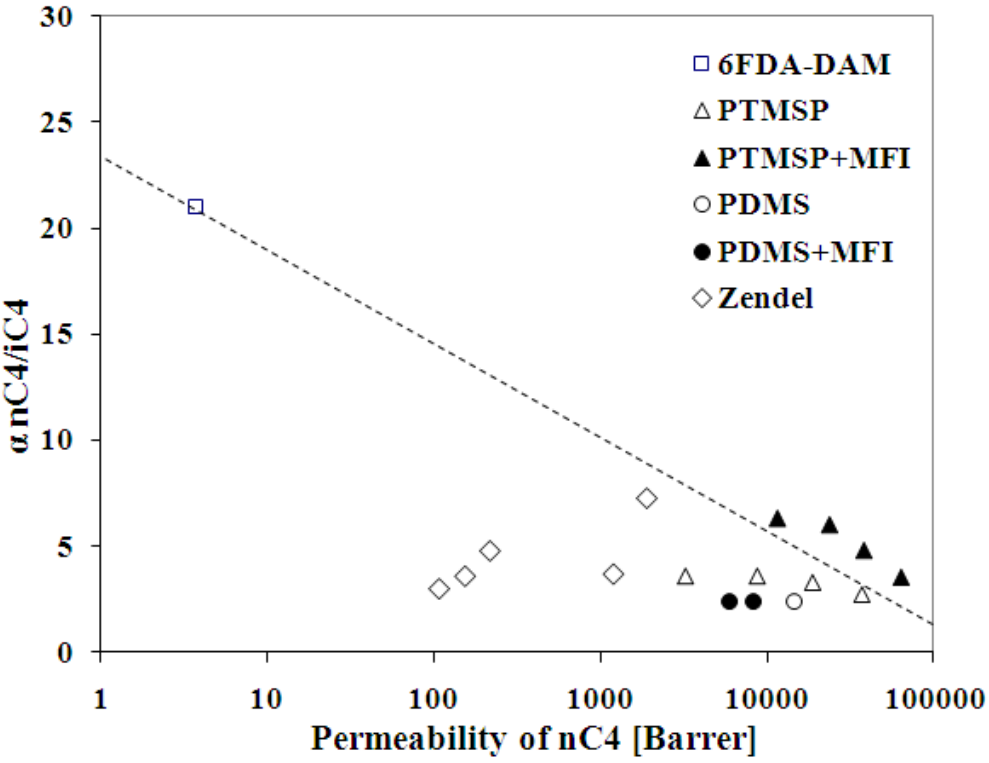

Figure 1.5 Summary of butane isomer separation performances on polymeric and mixed matrix membranes, pure gas permeation test

1. 4 RESEARCH OBJECTIVES

The overall goal is to create mixed matrix hollow fiber membranes for butane isomer separation. In order to achieve that, several objectives have to be fulfilled.

Objective 1: Identify proper sieve and polymer for butane isomer separation

Research recently identified a series of large Free Volume Fraction (FFV) fluorinated polyimides that have both high selectivity and permeability, and are on the boundary of the trade off curve for many gas separations. This high free volume in the glassy polymers provides more space to accommodate the penetrating gas and to enable diffusion, so a higher permeability is possible. Nevertheless, since the polymer chains in these polymers are very rigid due to the large fluorinated groups, these polymers are also quite selective at the same time. Polymer will be chosen among these polymers to make mixed matrix membranes, and as discussed previously, two zeolite candidates, 5A and MFI, will be tested for C4s separation.

To finally decide upon the best sieve and polymer choice, mixed matrix dense films with surface treated sieve particles will be tested on C4s permeation. The Maxwell model will be used to help select the best pair of sieve and polymer for C4s separation.

Objective 2: Surface modify the sub-micron sieves for good adhesion and dispersion

The $Mg(OH)_2$ whiskers formed on the sieve surfaces proved to be effective to improve the adhesion between polymer and sieve, in both mixed matrix dense films and hollow fibers. Unfortunately, insufficient knowledge exists regarding the $Mg(OH)_2$ formation, especially for treatment of nanoparticles, during which agglomeration is a problem. Grignard treatment method will be explored to find the mechanism of $Mg(OH)_2$

formation and treat appropriate zeolite particles, which will be used for mixed matrix hollow fiber membranes fabrication.

Objective 3: Spin dual layer hollow fibers using 6FDA polymers.

6FDA polymers are prohibitively expensive for spinning single layer fibers. A dual layer fiber design is used to reduce the cost. An inexpensive, commercial polymer is preferred to act as a support layer, which has porous structure. 6FDA polymers are only used in the sheath with a dense skin for separation purposes. This design can effectively cut the cost by 80-90% according to our calculation.

A support polymer is needed for 6FDA dual layer fiber spinning. The polymer should have the following properties: 1) be commercially available, 2) form porous structure after phase separation, so that negligible substructure resistance is added and 3) exhibit good adhesion with 6FDA polymers. Finding a proper polymer that adheres well with 6FDA polymers under spinning conditions is a challenging task. In order to have good bonding between support and sheath layer, the support layer probably needs to be miscible with 6FDA polymers. At the same time, spinning conditions need to be optimized to provide enough time for polymer chains to diffuse between interfaces prior to phase separation. Given the early state of the art in composite spinning, considerable trial and error will be required to optimize the conditions.

Objective 4: Spin dual layer mixed matrix hollow fibers.

Until now there has no report regarding high loading mixed matrix fiber spinning. There are multiple areas that need investigation: 1), how to improve the stabilization and interfacial bonding at high loading under spinning conditions; 2), how the zeolite changes rheology, phase separation and solvent diffusion rate during mixed matrix hollow fiber

spinning. This dissertation makes a preliminary step toward forming a practical dual layer mixed matrix membranes for the C4s separation.

1.5 DISSERTATION OUTLINE

Chapter two includes the theory and background for this research. All the materials and experimental procedures in this work are summarized in chapter three. Chapter four explains the mechanism of the Sol-Gel-Grignard treatment. The effectiveness of the Sol-Gel-Grignard treatment on different zeolite (surface acidity control) is also discussed in chapter five. Discussion of mixed matrix membranes for C4s separation containing appropriate polymers and treated zeolites is in Chapter six. The matching pair of zeolite 5A and 6FDA polymers is selected as the materials for next step hollow fiber membrane formation. To save cost on expensive 6FDA polymers for fiber spinning, a dual layer design is used in this research. Chapter seven details the research on dual layer 6FDA hollow fiber spinning, using a cellulose acetate as the support layer. The preliminary work on mixed matrix hollow fiber spinning is shown in chapter eight. Chapter nine is the final conclusion and recommendation.

1.6 REFERENCES

[1] H. Strathmann, *AICHE*, **2001**, 47(5), 1077-1087

[2] R. W. Baker, *Ind. & Eng. Chem. Res*., **2002**, 41(6), 1393-1411.

[3] L. M. Robeson, *J. Membr. Sci.,,* **1991**, 62, 165–185

[4] W.J. Koros, *J. Membr. Sci.,*, **2000**, 175(2), 181-196

[5] R. Mahajan, *J. Appl*. *Polym*. *Sci*, **2002**, 86(4), 881-890

[6] C.M. Zimmerman, *J. Membr. Sci.,,* **1997**, 137(1-2), 145-154

[7] T. Moore*, J. of Mole Struct*., **2005**, 739(1-3), 87-98

[8] M. Jia, *J. Membr. Sci*., **1991**, 57, 289-296

[9] J. M. Duval, *J. Membr. Sci*., **1993**, 80, 189-198

[10] J. M. Duval, *J. Membr. Sci*., **1994**, 54, 409-418

[11] T. M. Gur, *J. Membr. Sci*., **1994**, 93, 283-289

[12] M. G. Suer*, J. Membr. Sci*., **1994**, 91, 77-86

[13] I. F. J. Vankelecom, *J. Phys. Chem*., **1995**, 99, 13187-13192

[14] T. W. Pechar, *J. Membr. Sci*., **2006**, 277, 210

[15] R. Mahajan, *Ind. & Eng. Chem. Res*., **2000**, 39, 2692

[16] M. D. Guiver, *J. Polym. Sci.: Polym. Sci*. **2003**, 40, 4193

[17] Y. Li*, J. Membr. Sci*., 275(1-2), **2006**, 17-28

[18] L. Jiang, *J. Membr. Sci.,* **2005**, 252, 89-100

[19] S. Shu, *Chem. Mater*. **2007**, 19, 4000-4006

[20] S. Shu*, J. Phys. Chem. C*, **2007**, 111, 652-657

[21] S. Shu*, Ph. D thesis*, Georgia Institute of Technology, **2007**

[22] T. Bae, *J. Am. Chem. Soc.*, **2009**, *131*, 14662–14663

[23] S. Husain, *J. Membr. Sci*., **2007**, 288, 195-207

[24] S. Husain, *Ph. D thesis*, Georgia Institute of Technology, **2006**

[25] P. Hrabánek, *Desalination*, **2008**, 224, 76–80

[26] K. T. Klemola*, Ind. Eng. Chem. Res*., **1996**, 35, 4579-4586

[27] A.J. Burggraaf, *J. Membr. Sci*., **1998**, 144, 77-86

[28] S.H. Cho, Adsorption separation and purification apparatus and process for high purity isobutane production, *US patent*, **2000**

[29] B. Millot, *Micropor. Mesopor. Mat*., **2000**, 38, 85-95

[30] H. Yucel*, J.C.S. Faraday I*, **1980**, 76, 71-83

[31] E. Flanigen, *Nature*, **1978**, 271, 512-516

[32] G. Xomeritakis, *Micropor. Mesopor. Mat*., **2000**, 38, 61-73

[33] M. Jiang, *Sep. Purif. Technol*., **2001**, 25, 287-295

[34] K. Tanaka, *J. Membr. Sci*., **1996**, 121, 197-207

[35] K. Kusakabe, *J. Membr. Sci*., **1996**, 116, 39-46

[36] M. P. Bernal*, Catal. Today*, **2001**, 67, 101–107

[37] K. Kusakabe, *J. Membrane Sci*., **1996**, 116, 39-46

[38] K. Okamato, *J. Membrane Sci.*, **1997**, 134, 171-179

[39] M.L. Santos, *J. Appl. Polym. Sci*. **1974**, 18, 727-734

[40] M. Jia*, J. Membr. Sci*., **1991**, 57, 289

[41] M. Woo, *Micropor. Mesopor. Mat*., **2008**, 110, 330-338

CHAPTER 2

THEORY

Gas transport in polymers and zeolites are by similar sorption and diffusion mechanisms. Despite the general similarities, there are also differences in the detailed sorption and diffusion procedures. In this chapter, theory of these different transport processes is discussed firstly. Several gases (N_2, CO_2, nC_4, iC_4) in various materials (rubbery polymer PDMS, glassy polymer ethyl cellulose, zeolite 5A) are shown as examples. Modeling of transport through the polymer-zeolite composite, and the matching of polymer and zeolite for mixed matrix membrane formation material is also discussed. The chemical and physical methods for zeolite-polymer interfacial adhesion enhancement are shown for defect free mixed membrane formation. The fabrication of hollow fiber form of composite membrane is discussed at the end of this chapter.

2.1 TRANSPORT IN POLYMERS

Fick's law applies to mass transport processes in both polymers and zeolites. Consider a process that molecule A diffuses through a thin membrane with thickness δ, the concentration of A at two sides of membrane are C_{A0} and $C_{A\delta}$, partial pressure of A in the two side gas phase are p_{A0} and $p_{A\delta}$, respectively. As shown in Eq. 2.1, the mass transfer flux (N_A) is proportional to the driving force, concentration gradient: $(C_{A0}-C_{A\delta})/\delta$. D_A is known as the diffusivity coefficient of molecule A. Suppose there is a linear relationship between pressure and concentration in the membrane, as shown in Eq. 2.2, Eq. 2.1 can be rewritten into Eq. 2.3. The driving force for mass transfer is now the pressure (actually partial pressure, p_A) difference ($p_{A0}-p_{A\delta}$) and P_A is known as the

permeability coefficient of molecule A. The permeability is the product of the solubility and diffusivity of compound A, as shown in Eq. 2.4. Permeability is defined as the amount of gas molecules diffuse in specific time through a membrane with specific thickness and area, under standard pressure difference. The unit for permeability is Barrer (1 Barrer = 10^{-10} cm^3 (STD)·cm·cm^{-2}·s^{-1}·$cmHg^{-1}$).

$$N_A = -D_A \frac{(C_{A0} - C_{A\delta})}{\delta} \tag{2.1}$$

$$C_A = S_A \times p_A \tag{2.2}$$

$$N_A = -D_A \times S_A \frac{(p_{A0} - p_{A\delta})}{\delta} = -P_A \frac{(p_{A0} - p_{A\delta})}{\delta} \tag{2.3}$$

$$P_A = D_A \times S_A \tag{2.4}$$

It is convenient to use the permeability coefficient to determine the ideal selectivity between different gas molecules. The selectivity between gas molecule A and B is the ratio of permeability of the two gases for the case with a negligible downstream pressure (p_{A0} &p_{B0}). As shown in Eq 2.5, it can be separated into two part, solubility selectivity (α_S) and diffusivity selectivity (α_D). The separation factor, as shown in Eq. 2.6, should be used to determine the gas separating performance in real situations. In Eq. 2.6, x is the mole fraction of molecule *A* and *B, P* and *F* indicate permeate and feed side.

$$\alpha_{AB} = \frac{P_A}{P_B} = (\frac{S_A}{S_B}) \times (\frac{D_A}{D_B}) = \alpha_S \times \alpha_D \tag{2.5}$$

$$separation\ factor = \frac{x_{A,P} / x_{B,P}}{x_{A,F} / x_{B,F}} \tag{2.6}$$

Robeson summarized the permeability (P_A) and ideal selectivity (α_{AB}) in different membranes for various gas pairs, and found an empirical trade-off relationship between

the P_A and α_{AB} [1]. Freeman further explored the trade-off relationship between permeability and selectivity theoretically [2] and theoretically established the relationship between gas permeability and selectivity, as shown Eq. 2.7. The exponential parameter, n, is related to the size difference of molecule A and B. The parameter k depends on the relative condensabilities of the two gases and the polymer properties.

$$P_A = k\alpha_{AB}^{\ n} \tag{2.7}$$

Ideal selectivity can be used as the initial parameter to determine the membrane separation performance on A and B gas mixture, only under the assumption that molecule A and B do not affect each other's transport process through the membrane. It should also be keep into mind that gas permeability is also not a real constant, as both diffusivity and solubility depend on concentration of molecule A and temperature in polymeric membranes.

2.1.1 Sorption in polymers

Sorption in rubbery polymers obeys Henry's law for low pressure, as shown in Eq. 2.2. The solubility coefficient for one gas in a specific rubbery polymer is determined by two parameters: the condensability of the gas and the interaction strength between the gas molecule and polymer chain. Fig.2.1 shows the solubilities of four kinds of gases, N_2, CO_2, iC_4, nC_4 in one rubbery polymer polydimethylsiloxane (PDMS). All gases obey Henry's law. The solubility coefficient follows the order of $S_{N2} < S_{CO2} < S_{iC4} < S_{nC4}$, the same order of condensability, which depends on the critical temperature (T_C). Table 2.1 shows the critical temperature of the four important industrial gases. Butane isomer show little difference in terms of solubility because of close boiling point, shown in former chapter. The high solubility of CO_2 comes more from both high T_C and strong

interaction with PDMS due to its polarizable property. N_2 has neither high condensability nor strong interaction with PDMS, therefore, the solubility is tens of times lower than those of C4s. The much higher solubility of hydrocarbons than the permanent gases in rubbery polymers are utilized to make reverse selective membranes. The bigger but more condensable molecules permeate faster than the smaller but less condensable molecules, which is contrary to the size selective mechanism.

Table 2.1 Kinetic diameters [6] and critical temperature of different gases [7]

	CO_2	N_2	nC_4	iC_4
kinetic diameter σ [nm]	0.33	0.36	0.43	0.50
critical temperature T_C [K]	304.1	126.2	425.2	408.2

Sorption in glassy polymers is more complicated due to non-equilibrium chain packing. There is a kind of unrelaxed chain packing, which forms packing defect or ‘‘holes’’, in glassy polymers. Gas molecules can also adsorb into these preexisted holes, which can be described by a Langmuir form, besides the sites in equilibrium packing chains which follows Henry’s law like rubbery polymers. Barrer [8] firstly found the phenomena and successfully described the dual mode sorption in glassy polymers, as shown in Eq. 2.8.

$$C_A = k_D p + \frac{C_H' bp}{1 + bp} \tag{2.8}$$

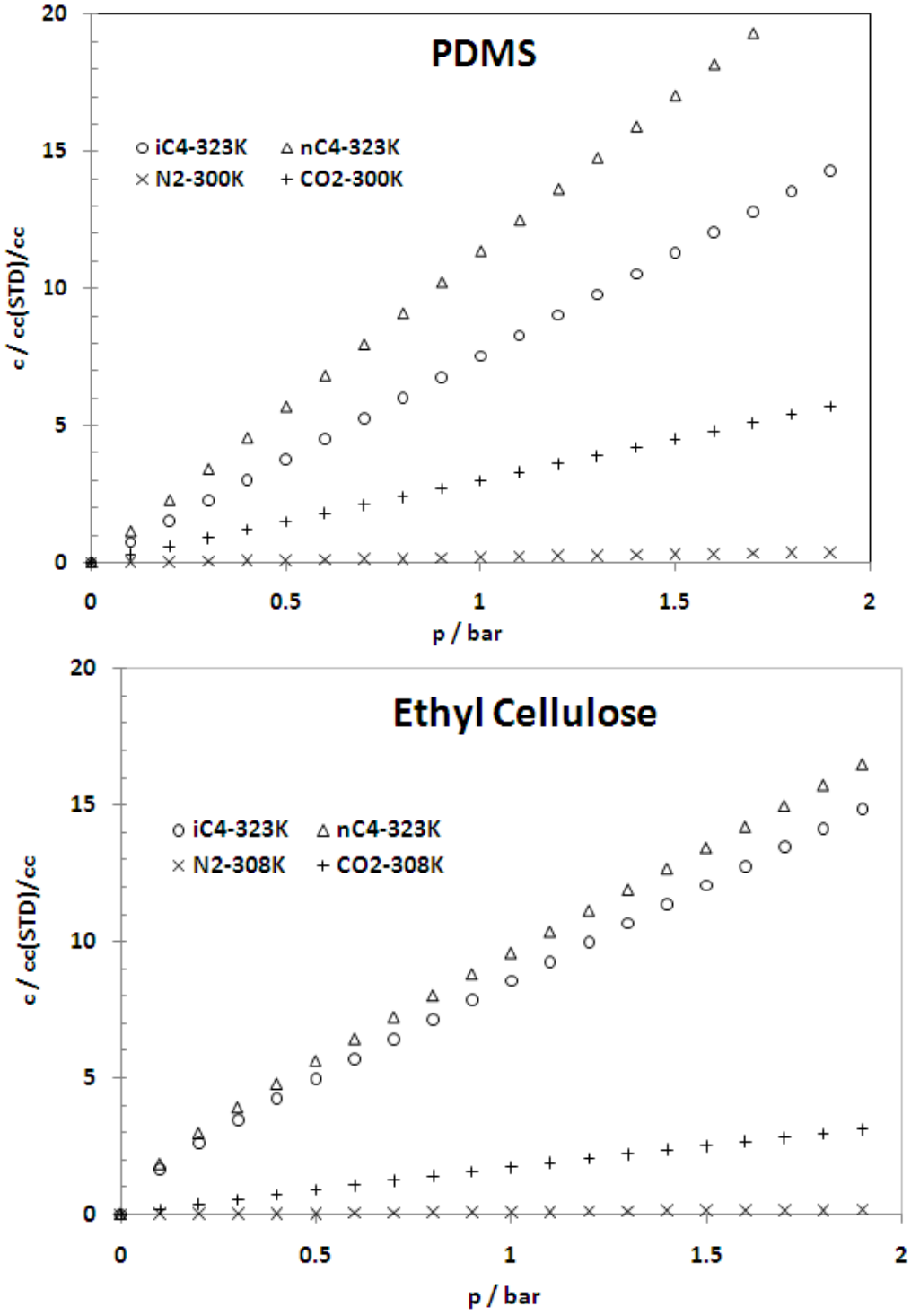

Figure 2.1 Gas sorption isotherms in PDMS and ethyl cellulose polymers. The data points are generated by the Eq. 2.8 using the parameters from, gases in PDMS [3], N_2, CO_2 in ethyl cellulose [4], and nC4, iC4 in ethyl cellulose [5]

The Henry's law constant k_D is the ordinary solubility coefficient in the equilibrium packing region, C_H' is the Langmuir constant in the gap packing region, while *b* describes the affinity of the gas for the Langmuir sites. As shown in Fig. 2.1, solubility of different gases in ethyl cellulose follows the same order as that in rubbery PDMS. The isotherm deviates not too much from Henry's law, because the Langmuir region (or free volume) sorption is low in ethyl cellulose. Unrelaxed volume related to deviation between the glassy volume and the extrapolated rubbery volume below the glass transition (Tg) is used to describe the holes concentration in glassy polymers. Traditionally Langmuir constant (C_H') in sorption measurement was used to derive the unrelaxed volume, as shown in Eq. 2.9 [5], where M is the molecular weight of the sorbent gas, ρ is the gas density as it is in the holes. Molecules of higher critical temperature, such as the C4s, C5s are used because of the simplicity of estimation of their in-hole packing densities. However, it is under debate whether all of the holes are accessible to such big molecules.

$$unrelaxed\ volume(\%) = \frac{C_H' M}{\rho \times 22400} \tag{2.9}$$

The unrelaxed volume of ethyl acetate is 1-2 %, which makes the polymer chain close to ideal packing. In this work a family of fluorinated polyimide is used. The unrelaxed volume can reach 15-20 % because of the large amount of non-ideal rigid chain packing [9].

2.1.2 Diffusion in polymers

Diffusion in polymers occurs through a transient opening between polymer chains due to thermal fluctuation. Gas molecules can jump through these transient openings, as Fig. 2.2 shows. A three dimensional diffusion coefficient can be derived from random

walk theory. As shown Eq. 2.10, ν is the jump frequency through the transient opening, which is big enough for the diffusing molecule, and l is the average jump length. The diffusivity coefficient describes the easiness for the molecule jump, which is determined by the polymer chain stiffness and molecular size.

$$D = \frac{1}{6} \nu \, l^2 \tag{2.10}$$

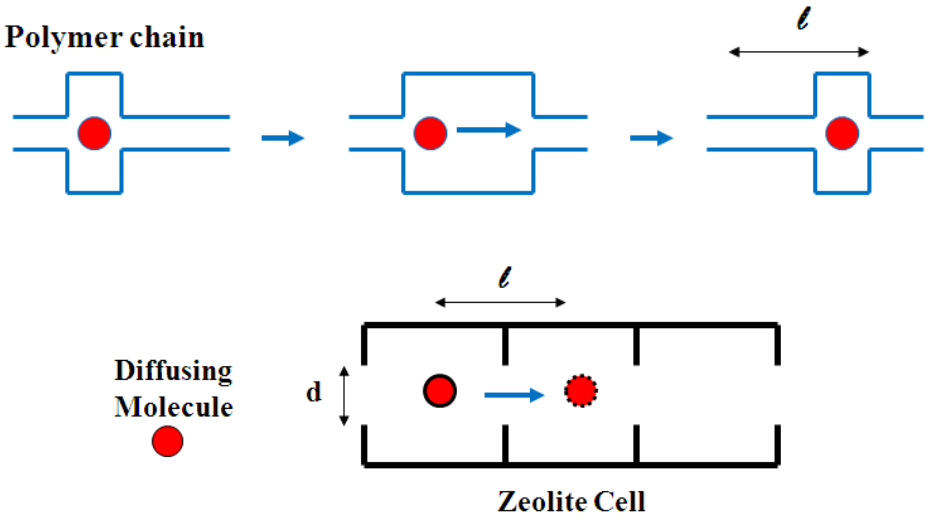

Figure 2.2 Diffusion mechanism of a penetrate molecule through polymer chains and zeolite channels

Similar to the sorption difference in rubbery and glassy polymers, the diffusion is also quite different in the two kinds of polymers. Rubbery polymer chains have more flexibility to generate large transient openings so molecules can make random jumps more frequently. The drawback of flexible chain is the indiscriminative ability to let molecules of different sizes to diffuse through, *i.e.*, the diffusivity selectivity is low in rubbery polymers. As shown in Fig 2.3, the diffusivity selectivity of N_2/iC_4 is only ~5.

Diffusion in glassy polymer is through two modes. Partial Immobilization Model suggested diffusion in Langmuir region has limited mobility [10]. The effective diffusivity in rigid glasses can be quite different, as shown in Fig 2.3. The diffusivity selectivity of N_2/iC_4 is ~ 40, which is far higher than that in rubbery polymer due to the different chain rigidity.

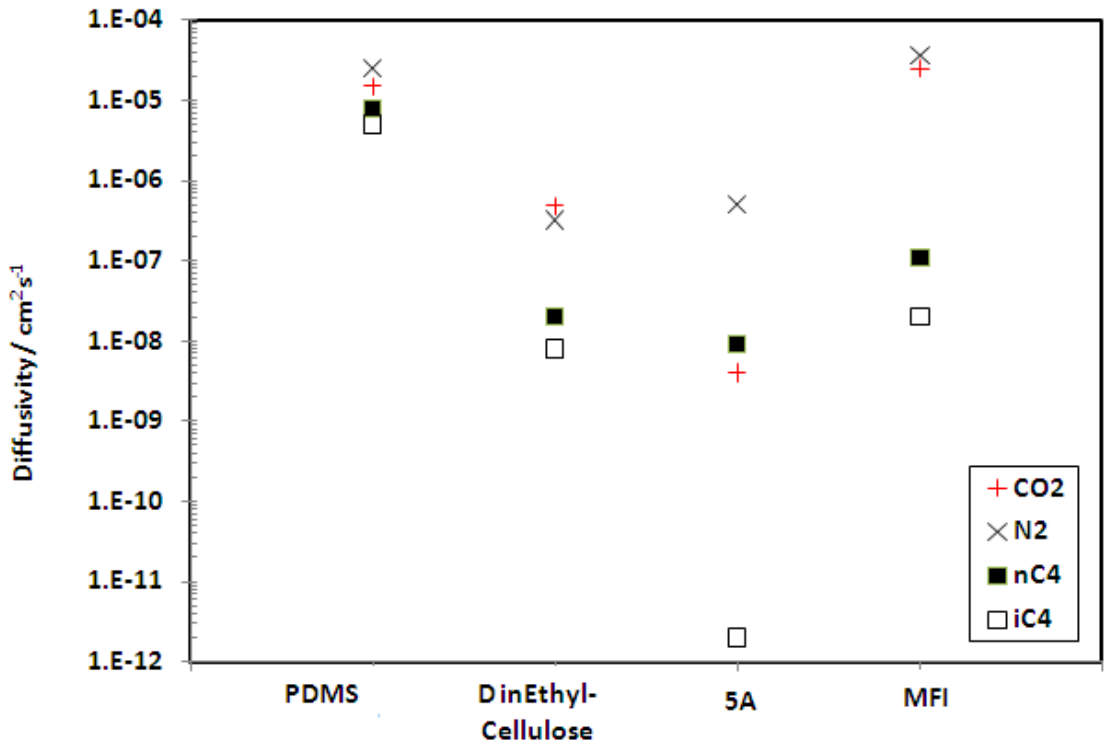

Figure 2.3 Gas diffusivity in different materials, PDMS data from [11], D_{eff} in ethyl cellulose at low pressure [4,5], corrected diffusivity D_0 in 5A [4, 12], D_0 in MFI [13]

2.2 TRANSPORT IN ZEOLITES

IUPAC terminology divides porous materials into three regions: macroporous (r_p > 50 nm), mesoporous (2 nm< r_p <50 nm), and microporous (r_p < 2 nm). This division is based on the difference in the types of forces which control adsorption behavior in the

difference size ranges. Zeolites with molecular sieving ability commonly have pore size of 3-5 Å, which fall well into microporous region. The solution-diffusion model can also be applied to transport in zeolites. Therefore, solubility and diffusivity are two most important parameters for the transport process.

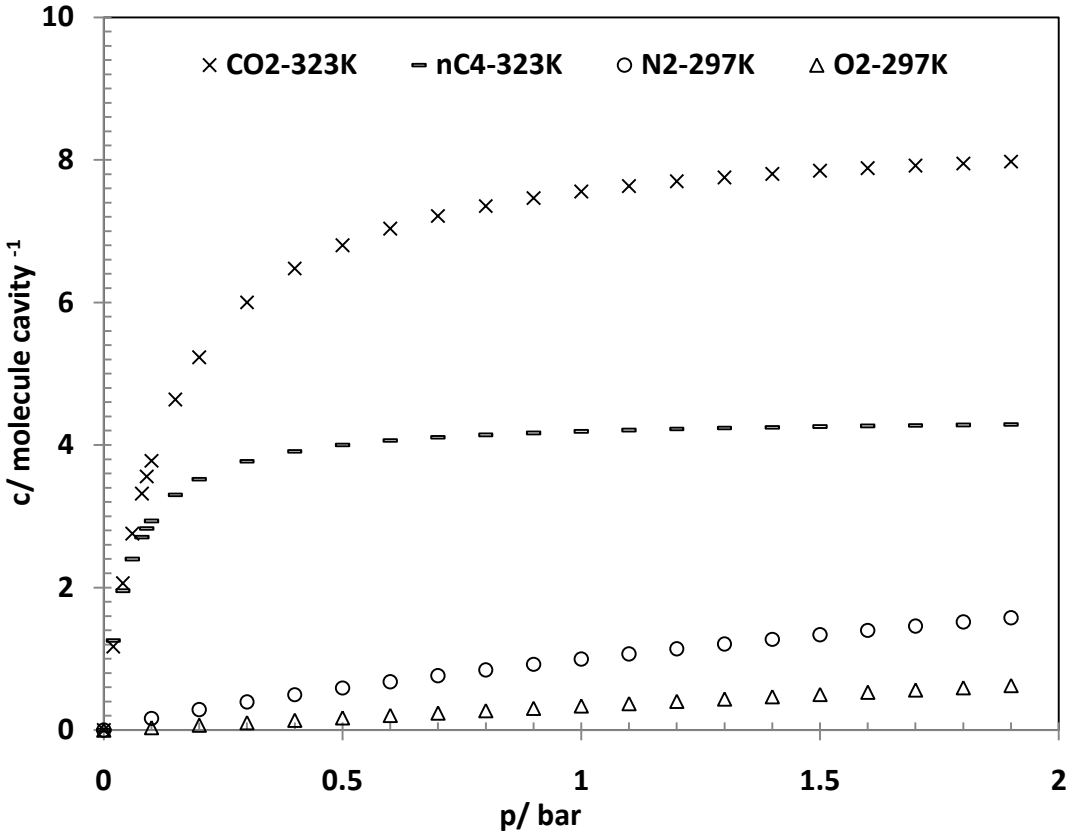

Figure 2.4 Solubility of gases in zeolite 5A, data is generated by Eq. 2.11 using parameters from literature O_2, N_2 [14], CO_2 [15], nC_4 [5]

2.2.1 Sorption in zeolites

A Langmuir model, as shown in Eq. 2.11, is usually used to describe gas sorption in zeolites, assuming the sorption sites in zeolite pores to be uniform. C_H' is the Langmuir constant, and *b* describes the affinity of the gas in the Langmuir sites.

$$C_A = \frac{C_H' bp}{1 + bp} \tag{2.11}$$

This simplified model provides very good agreement with experimental results in most of the zeolites. Fig 2.4 shows solubility in zeolite 5A of four different gases. More CO_2 molecules can pack into one zeolite cell than nC_4 because of its smaller molecular size. Sorption of O_2 and N_2 stays in Henry's region up to relatively high pressure. Sorption and diffusion of these less adsorbed gases can be modeled, assuming adsorbed gas molecules do not affect each other in an ideal state. CO_2 and nC_4 reaches equilibrium from very low pressure due to their strong affinity with zeolite structures. The Langmuir constant C_H' can be used to derive the porosity of zeolites similar as polymer free volume calculation using Eq. 2.9.

2.2.2 Diffusion in zeolites

For diffusion through zeolite pores, steric effects are important, and diffusion is an activated process. The activated state, or transient state occurs when diffusion molecules undergo specific configurational accommodation with the pore walls to travel through the narrow pores [16]. As shown in Fig. 2.5, zeolites consist of relatively large cages connected through smaller windows. For example, zeolite 5A has cages of ~1.12 nm, and windows as small as ~0.42 nm in diameter. Therefore, molecules in cage can be considered as the equilibrium state, and molecules passing through the window as the transient state. The self-diffusivity ($\mathscr{D}$) in micropores can be analyzed as in the following Eq. 2.12, where l, n_c stand for the jump length and cavity density (determined by zeolite micropore structure), f_g' and f^+ represent partition function for gas phase, and transition phase, $V_0' = (\mu^* - \mu_g)$ is the difference in potential energy between gas phase and transition state, *p and q* stand for pressure and adsorbed phase concentration. The probability for a

jump through the window depends on the energy difference between the two states. The molecular (mobility) sieving effect in zeolite is based on activated energy difference among diffusion molecules through the micropores.

From Eq. 2.12, we can know self diffusivity is concentration dependent because of the nonlinearity between pressure and sorbent concentration. Under ideal thermodynamic conditions, or Henry's law regime ($p \propto q$), and interactions between diffusion molecules are negligible, the self diffusivity becomes constant, denoted as $\mathscr{D}$.

$$\mathscr{D}(q) = \frac{l^2 n_c}{h} \frac{f^+}{f_g^{'}} \frac{p}{q} e^{-V_0^{'}/kT} \tag{2.12}$$

There are more complexities regarding the difference between ideal self-diffusivity and measured apparent transport diffusivity. Diffusivity according to Fick's first law stands for the resistance coefficient of mass transport under the driving force: concentration gradient (C_A). However, the true driving force of mass transfer is the gradient of chemical potential (μ_A). Because of the nonlinearity relationship between chemical potential and concentration, the Fickian diffusivity, also called transport diffusivity is normally concentration dependent. The relationship between Fickian diffusivity and ideal self-diffusivity was derived by Darken [17], as shown in Eq. 2.13. Because of the typical Langmuir type adsorption in zeolites, ($d \ln p / d \ln q$) > 1, Fickian diffusivity increases at higher concentration.

$$\frac{D}{\mathscr{D}} = \frac{d \ln p}{d \ln q} \tag{2.13}$$

Table 2.2 Corrected diffusivity of nC4 in 5A and MFI by different techniques [16]

Sorbent	Technique	T (K)	D_0 (m^2s^{-1})
Lab synth. 5A	NMR (PFG)	400	8×10^{-13}
	NMR relaxation	400	1×10^{-11}
Own 5A	Gravimetric	400	9×10^{-13}
Linde 5A	Gravimetric	400	5×10^{-15}
Own 5A	ZLC	400	6×10^{-13}
		400	5×10^{-15}
Linde 5A	Chromatography	400	9×10^{-15}
MFI (300 μm)	Membrane	334	1.1×10^{-11}
MFI (300 μm)	Membrane	334	3.7×10^{-12}
MFI (300 μm)	NMR (PFG)	334	1.5×10^{-10}

The concentration dependence of transport diffusivity comes from two factors: concentration effects on: *1)* the molecular mobility and *2)* the driving force. The molecular mobility dependence on concentration is relatively low, therefore it is considered constant, which has been experimentally verified in several systems. From equation, when $q \to 0$, $d \ln p / d \ln q \to 1.0$, $\mathscr{D} = D_0$, which is known as ‘‘corrected diffusivity’’. Transport diffusivity can be generated using corrected diffusivity (D_0) from Darken equation for practical purposes. The corrected diffusivity is also theoretically easy to understand because of its physical meaning as the molecular mobility. Different methods can be used to measure the diffusivity in zeolites. Tab. 2.2 shows the somewhat inconsistent nC4 corrected diffusivity in zeolites by various techniques. There is debate on the reliability of different techniques, which can be found in multiple literatures, but generally diffusivity results from different methods converge to a reasonable degree (factor of about 100).

2.3 MIXED MATRIX MEMBRANES

As discussed in the introduction, enhancement of selectivity can increase the feasibility of membrane separation method compared to other separation methods. Theoretically, the mixed matrix membrane method is promising to raise the membrane selectivity to cross the trade-off boundary. There are two prerequisites for a successful mixed matrix membrane: 1) good matching between gas transport properties of polymer and zeolite; good interfacial adhesion at the zeolite-polymer boundary.

2.3.1 Polymer-zeolite matching

As shown in the introduction, Maxwell model is commonly used to model the transport properties in the mixed matrix membranes. In the model Eq. 1.1, there are four interrelated parameters: permeability in mixed matrix membrane (P_{MM}), polymer (P_P) and sieve (P_S), the volume fraction of sieve (Φ_S). With any of the three known, the fourth one can be derived. There are several theoretical presumptions for the Maxwell model: 1), the addition of zeolite particles does not affect the properties of polymer; 2) the particles are spherical and gas transport in particles is three dimensional; 3) the concentration of particles is sufficiently low to neglect the interference between particles;

Real mixed matrix membranes can deviate from the aforementioned presumptions. First, there are studies showing that the addition of nanoparticles alters the free volume distribution and the intrinsic polymer transport properties [18, 19]. Polymer can rigidify the zone around nanoparticles, and voids can form at the polymer-zeolite interface (sieve-in-a-cage) because of the stress during the membrane fabrication step. Moore [20] used a three phase Maxwell model to account for the non-idealities of rigidified polymer and voids. Second, diffusion in zeolite can be anisotropic. For zeolites with one dimensional

pores, for example $ALPO_4$, only pores in the direction of gas flow contribute to the flux [21]. Gas molecules diffuse at different rate in the two kinds of channels for MFI [22]. Percolation can happen at higher zeolite loading, when molecules will selectively pass through least resisting zeolite materials, so the Maxwell model has clear limitations. Petropoulous has shown adequate application of Maxwell model upto high level of solids concentration for approximate purposes [23]. Zimmerman explains the importance of polymer-zeolite matching for the fabrication of mixed matrix membranes with good separation performance, using O_2/N_2 separation as an example [24]. Below, the matching between one imaginary polymer (Permeability of faster gas is 1 Barrer, selectivity is 10) and various imaginary zeolites is shown.

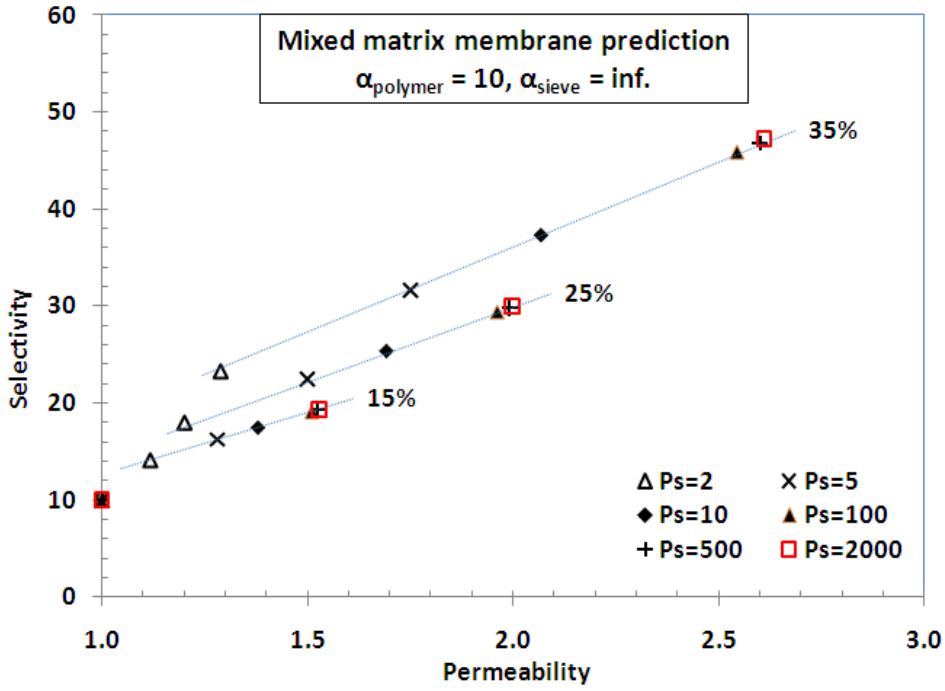

Figure 2.5 Maxwell modeled permeability and selectivity in mixed matrix membranes, using polymer $P_{polymer}$=1 Barrer for faster gas, $\alpha_{polymer}$=10, and sieves with ideal infinite selectivity and various faster gas permeability for 15 %, 25 % and 35 % sieve loadings

Fig. 2.5 shows the mixed matrix membrane performance according to Maxwell model, using zeolites of various permeabilities (Ps), and selectivity of infinity (*i.e.* total blocking of the slower gas). There are clearly few cases of infinite selectivity for the separation in zeolites, such as zeolite 5A for straight chain and branched chain hydrocarbon separation [25], separation of smaller molecules (H_2, He) from bigger molecules (C3+) using zeolite 4A. In these cases, zeolites with various permeabilities all act as the same ideal barrier material (total blocking) for the slower gas molecules, but enhance differently for the faster gas molecule. As shown in the figure, permeability and selectivity both are higher with more permeable zeolites at the same solid loading. However, mixed membranes show negligible difference of separation performance, using the zeolites with permeability of 500 Barrer and 2000 Barrer. This is because the permeability of faster gas in mixed matrix membranes containing the two zeolites are the same. In other words, there is a maximum permeability for mixed matrix membrane based on the polymer performance and zeolite loading. For example, at 35% zeolite loading, the maximum permeability of mixed matrix membrane is 2.62 times of that in polymer, and selectivity is 4.73 times of than in polymer, by adding an imaginary ideal zeolite with infinite permeability and infinite selectivity.

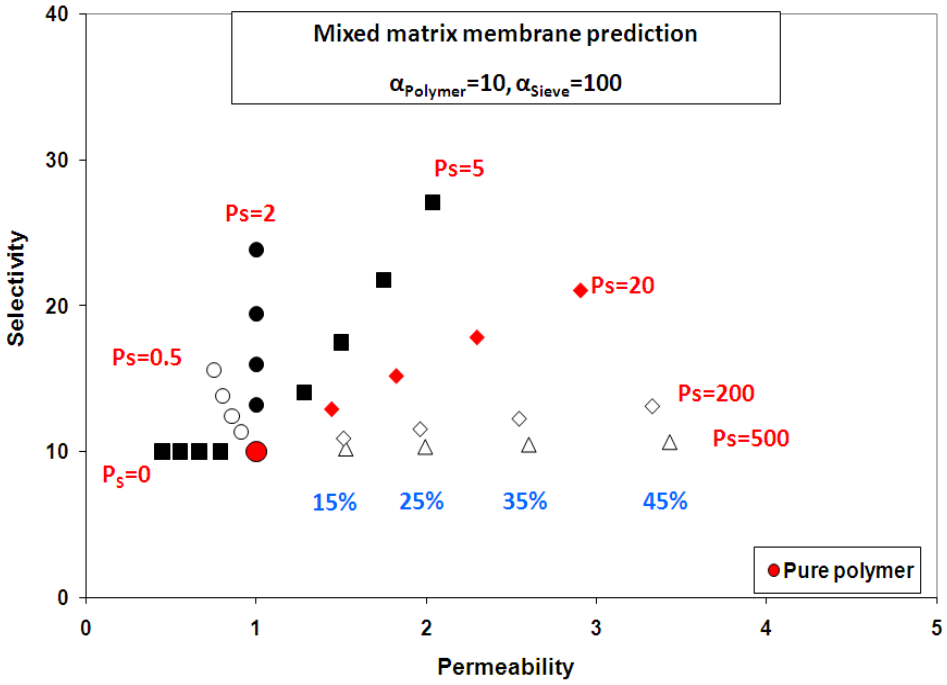

Figure 2.6 Maxwell modeled permeability and selectivity in mixed matrix membranes, using polymer Ppolymer=1 Barrer for faster gas, αpolymer=10, and sieves with selectivity of 100 and various faster gas permeability

For most cases, selectivity in zeolites is higher than polymers, but lower than infinity. In other words, the slower gas can also pass through the zeolites pores. For example, nC4 molecules permeate ~ 50 times faster than iC4 molecules in MFI pores [13], O_2 molecules permeate 37 times faster than N_2 molecules in zeolite 4A [24]. Fig. 2.6 shows the mixed matrix membrane performance using the matrix polymer (P=1, α=10) imaginary zeolites of different permeabilities and the same selectivity of 100. For extreme cases of Ps above 500, the slow gas also gets the same amount of permeability enhancement through the addition of zeolite, therefore, *no selectivity enhancement should be anticipated theoretically*. There is an optimal permeability of zeolite (selectivity of 100), 5.5 times of that in matrix polymer (selectivity of 10), in order to achieve the highest selectivity enhancement in mixed matrix membrane. The ratio of perfect

matching permeability in zeolite and polymer can change depending on the relative selectiveness of zeolite and polymer. It is worth noting that in real applications, more choices exist for polymer transport properties than that in zeolites. Different polymers with various transport properties should, therefore, be used to match some selective zeolites for specific gas separations. The Maxwell model will provide a useful guideline for the initial polymer and zeolite selection.

2.3.2 Polymer-zeolite interfacial adhesion

Glassy polymers are promising material for gas separating membranes because of their high selectivity and easiness to form high surface area hollow fiber membranes. Despite their attractive properties, the rigid chains of glassy polymer cause the stress induced sieve-in-a-cage morphology, which is detrimental to the mixed matrix membrane performance. There are generally two ways to increase the adhesion between polymer and zeolite surface: chemically tune the hydrophobicity of zeolite, and generate polymer chain length scale physical interlocking sites on zeolite surfaces.

Adhesion enhancement between hydrophilic zeolite and hydrophobic polymer were tried using a silane treatment. The silane treatment was intended to modify the abundant –OH groups on zeolite surface (> 1/nm^2 density), and turn them into more hydrophobic –Si-R groups [26, 27]. There are limited successes of enhanced adhesion using silane treatment, presumably because the molecular layer of –Si-R groups cannot provide sufficient adhesion force. The following researches were carried out by modifying the zeolite surface into more hydrophobic surfaces by forming –Si-CH_3, through a much stronger reaction with Grignard reagent. Success was reported on mixed matrix hollow fiber membranes using Grignard treated SSZ-13 and Ultem [28]. The

effectiveness of chemical modification is more zeolite and polymer specific. For example, SSZ-13 or MFI are considered to be more hydrophobic because of high silica content. Ultem has polymer chains which are less rigid than Matrimid. All these factors may have influence on the effectivess of the chemical modification methods.

The physical interlocking methods are considered more universal by locking the polymer chains to the zeolite surface using the nanoscale structures, such as mesopore and nanowhisker. As shown in Fig. 2.7, mesopores and nanowhiskers on zeolite surface can provide sites for polymer chains to penetrate in and anchor. Successful mixed matrix membranes with enhanced selectivities were reported using the Matrimid and mesopore containing MFI [29]. Shu created zeolite 4A with nanowhiskers using a Grignard method, which provide the locking sites for polymer chains [30]. The whiskered 4A and Ultem showed improved adhesion, confirmed by gas separation properties and mechanical strength. The two interlocking method by mesopore and whisker can be considered related mechanisms, which are more universal because the intrinsic hydrophobicity of zeolite and rigidities of polymer chain seem play less role on the zeolite-polymer adhesion. Research is needed to investigate the controlled formation of the mesopores or nanowhiskers on zeolite. The mesopores on MFI is reported to be a byproduct during the synthesis step [29]. The density and morphology of the mesopores, which should have a significant role on adhesion, was not controlled. There is also a lack of researches on the formation of mesopores on other attractive zeolites, such as zeolite A, SSZ-13, *etc*. The optimal nanowhisker density and length were not investigated for the Grignard treatment. The effectiveness of the Grignard treatment on other zeolites also needs to be investigated. In this research, Grignard treatment will be used for interfacial adhesion

enhancement between zeolite and polymer. The morphology of $Mg(OH)_2$ and its effects on adhesion will be investigated.

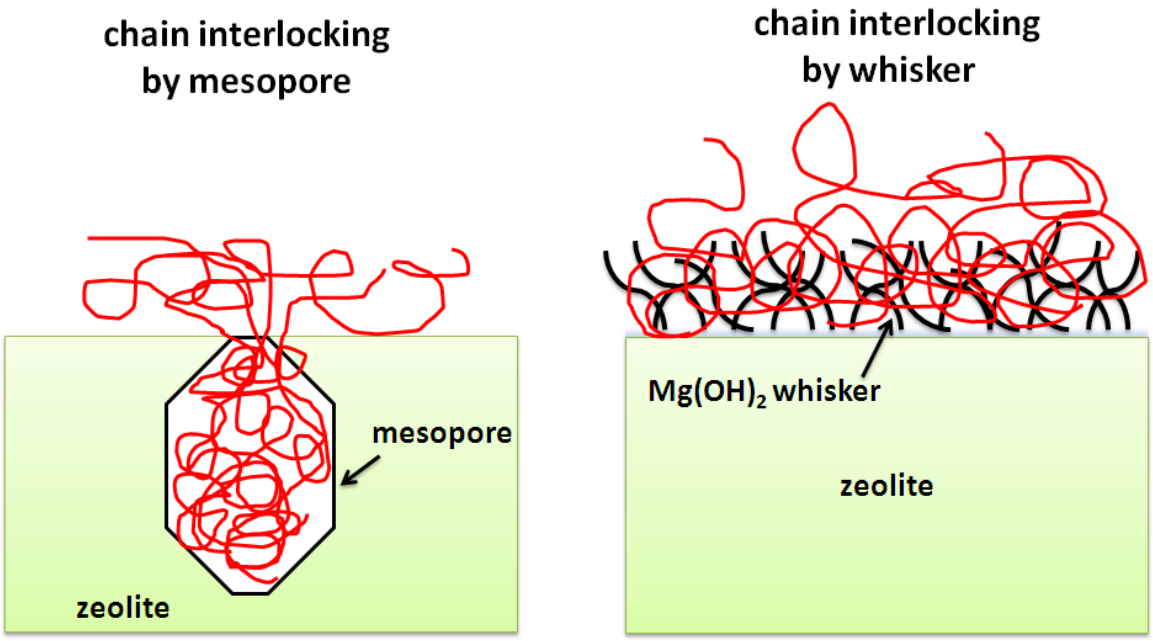

Figure 2.7 Two polymer chain locking mechanism by mesopore and whisker for adhesion enhancement between zeolite and polymer

2.4 MIXED MATRIX HOLLOW FIBER MEMBRANES

Hollow fiber membranes are fabricated using a dry jet/wet quench process. A sketch of the hollow fiber spinning apparatus is shown in Fig 2.8. Polymer solution, referred to as ‘‘dope’’, is fed by a high pressure pump into a spinneret. Simultaneously, a thermodynamically neutral solution comprising a mixture of water and an appropriate solvent, referred to as the bore fluid, is fed into the spinneret. The ‘‘solvent neutrality’’ of the bore fluid allows one to define the hollow core of the fiber without excessively vitrifying the lumen of the fiber. When the fiber enters the quench bath it will phase separate, becoming rigid. The fiber is “strung-up” onto the take-up drum. Dope extrusion rate combined with take-up rate and the size of the annular die determines the

size of the fibers produced. Within the air gap, the nascent selective skin layer is formed by evaporation of volatile component. The porous structure is formed by phase separation of spinning dope in the quench bath. This support layer under the skin adds negligible permeating resistance, and supports the separating skin layer in the presence of high pressure.

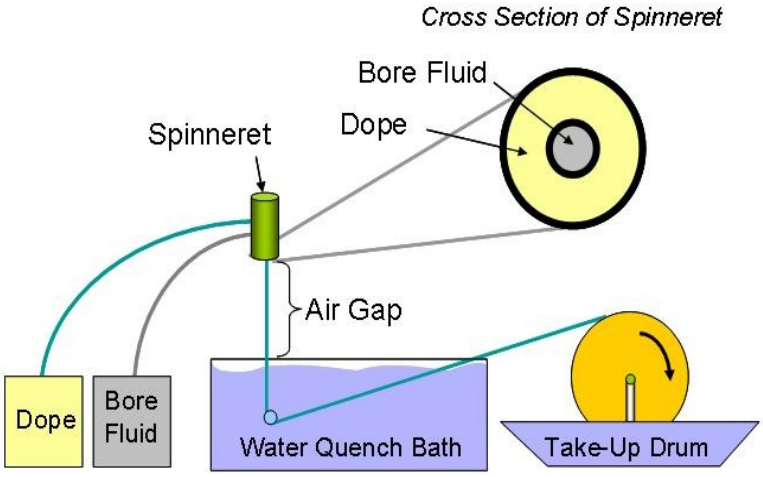

Figure 2.8 Asymmetric hollow fiber spinning apparatus

In our case, fluorinated polyimides have high separating performance, but are extremely expensive. Dual layer fibers, with an inexpensive support layer, are preferred to reduce cost. The dual-layer hollow fibers are prepared by the dry-jet wet spinning process using a triple orifice spinneret. Molecular sieves will be added only to the outer layer, and only part of that layer is vitrified to form the dense selective layer. By adjusting the dope viscosity and the porosity of the inner layer, the dual-layer hollow fibers can exhibit excellent mechanical strength compared to integrally skinned single-layer hollow fibers, with less cost.

The fiber spinning process can be affected by many factors. Until the introduction of the Grignard treatment, defect free mixed matrix fibers could not be created and the

full reason for this requires better understanding. The addition of zeolite into fiber spinning can be complicated from three factors.

Adding nanoparticles introduces rheological complexity. The polymer dope needs to have moderate strength to undergo stretching in the air gap. Macroscopically, the addition of zeolite can reduce the flexibility and strength of fiber, which makes fiber spinning difficult. Microscopically, the polymer chain packing can be affected by the zeolite nanoparticles, especially at high loading. This factor will change polymer chain response to stress, i.e. chain relaxation process. During spinning of highly rigid chain polymers, like fluorinated polyimide, I speculate that the chains orient to some degree during the spinning stretching step and become vitrified from solvent evaporation before the chain has enough time to relax. Such fiber membranes may show lower permeability and higher selectivity. It is anticipated that the nanoparticles will add restriction to the chain movement, hence a longer relaxation time to react to spinning stress. Kayode Olanrewaju in Dr. Breedveld's research group is working on this aspect. The chain relaxation time change after addition of nanoparticles is being measure using a capillary thinning method is their group. More fundamental rheological understanding can guide the mixed matrix fiber spinning. Close cooperation will be pursued to cast more light on this issue.

The second possible influence of zeolite is in the area of changes in phase separation factors. A defect free skin layer and a resistance-free support layer are two parameters required in a successful hollow fiber. A dense skin layer is promoted by solvent evaporation in the air gap. The spinning dope composition is selected to be close to the phase separating line in a phase diagram, in order to promote quick phase

separation. There are two reasons the addition of zeolite complicate the phase separation. First, the phase separation line was determined via the cloud point method by making different composition dopes. It is hard to judge when the mixture is cloudy as the dope with particles itself is cloudy. The second reason is the phenomenon recently found by Kayode Olanrewaju. A rheological difference from theoretical modeling was found after adding zeolite particles by them, and the difference was explained by the sorption of solvent in the porous sieves. The sieves sorb large amount of solvent or non-solvent depending on chemical properties. This can change the real composition of polymer dope, hence the phase separation rate. So, information of solvent sorption in sieves provided from Kayode can give a better guide for hollow fiber spinning.

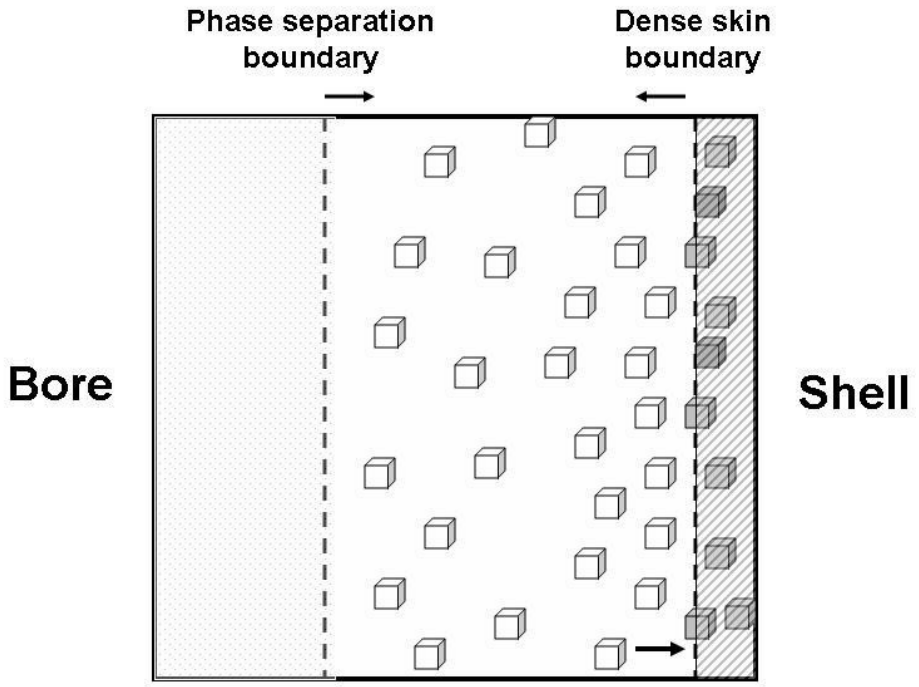

Figure 2.9 Formation of porous support and dense skin in mixed matrix fibers

Zeolite can also change the solvent and water diffusion rate in the dope and dense layer. A schematic diagram of hollow fiber membrane formation process is shown in Fig.

2.9. Highly permeable sieves in the skin layer can facilitate further evaporation of solvent and make a thicker dense skin layer. A hydrophilic sieve like zeolite A can enhance the water diffusion in the dope to make faster phase separation. Since different kinds of sieves will be added to spinning dopes, a careful examination of adsorption and other properties are needed. This zeolite effect can be investigated by spinning fibers with different kinds of sieves. ZSM-5 and 5A are two sieve candidate for the spinning, comparing the two can provide more fundamental understanding regarding sieves effect on spinning. Clearly, while these factors complicate engineering of the membrane structure, considerable expertise now exists to guide the engineering process [28].

2.5 REFERENCES

[1] L. M. Robeson, *J. Membr. Sci.*, **1991**, 62, 165-185

[2] B. D. Freeman, *Macromolecules*, **1999**, 32, 375-380

[3] T. C. Merkel, *J. Polym. Sci.: B: Polym. Phys*., **2000**, 38, 415–434

[4] A. Y. Houde, *J. Membr. Sci*., **1997**, 127, 171-183

[5] A. H. Chan*, J. Membr. Sci*., **1978**, 3, 117-130

[6] A. J. Burggraaf*, J. Membr. Sci.,* **1998**, 144, 77-86

[7] J. M. Prausnitz, *Molecular thermodynamics of fluid-phase equilibria*, 3rd edition, **1999**

[8] R.M. Barrer, *J. Polym. Sci*., **1958**, 27, 177.

[9] J. H. Kim*, Polymer*, **2006**, 47, 3094–3103

[10] W. J. Koros, *J. Polym. Sci.: Polym. Phys*., **1976**, 14, 687-702

[11] M. Jia, *J. Membr. Sci*., **1991**, 57, 289

[12] H. Yucel, *J.C.S. Faraday I*, **1980**, 76, 71-83

[13] B. Millot, *Micropor. Mesopor. Mat*., **2000**, 38, 85-95

[14] G. W. Miller, *AICHE*, **1987**, 33, 194-201

[15] H. Yucel*, J Colloid Interf. Sci*., **1980**, 74, 186-195

[16] J. Karger, *Diffusion in zeolites*, **1999**, John Wiley & Sons

[17] L. S. Darken, *Trans*. *AIME*, **1948**, 175, 184

[18] E. Marand, *Polym. Matl. Sci. and Engr*., **2001**, 85, 297-298

[19] T. C. Merkel, *Science*, **2002**, 296, 519-522

[20] T. Moore, *Ph.D*. *thesis*, UT Austin, **2004**

[21] D.S. Sholl, *J. Chem. Phys*. **1997**, 107, 4384-4389

[22] G. Xomeritakis, *Chem. Mater*., **1999**, 11, 875-878

[23] J. H. Petropoulous, *J. Polym. Sci.: Polym. Phys. Edi*., **1985**, 23, 1309

[24] CM Zimmerman*, J. Membr. Sci*., **1997**, 137(1-2), 145-154

[25] S.H. Cho, Adsorption separation and purification apparatus and process for high purity isobutane production, *US patent*, **2000**

[26] M. D. Guiver*, J. Polym. Sci.: Polym. Sci*. **2003**, 40, 4193

[27] Y. Li, *J. Membr. Sci.*, 275(1-2), **2006**, 17-28

[28] S. Husain*, J. Membr. Sci*., **2007**, 288, 195-207

[29] Y. Zhang, *J. Membr. Sci*.,**2008**, 325, 28-39

[30] S. Shu*, J. Phys. Chem. C*, **2007**, 111, 652-657

CHAPTER 3

MATERIALS AND METHODS

In this chapter, the materials and experimental methods used in this dissertation will be shown. The 6FDA polymers are synthesized by Dr. Wulin Qiu in Koros group. The zeolite MFI and LTA was synthesized by Dr. Chil Hung Cheng and Taehyun Bae in Jones& Nair group. The synthesis procedures for polymer and zeolites are shown in the first part. Zeolite surface roughening method, the sol-gel Grignard method is shown in the second part. The experimental conditions controlling the sol-gel reaction: pH, water amount, *etc,* are detailed. Three different ways of acidity control: addition of HCl, dealumination by $SOCl_2$, and deposition of $AlCl_3$ are shown. The methods to fabricate mixed matrix dense film and hollow fiber are shown subsequently. Sorption, permeation methods are shown in the last part, as the standard ways to evaluate the treatment effectiveness and mixed matrix membrane performance. Other testing methods, SEM, EDS, BET, XRD are also shown in this chapter.

3.1 MATERIALS

3.1.1 Polymers

6FDA polyimides are high performing polymers for gas separation membranes because of high free volume and rigid chain packing. Figure 3.1 shows the molecular structure of the three 6FDA polyimides used in this research. Table 3.1 shows the properties of these 6FDA polyimides. The free volume fraction (FFV) is higher than that of Matrimid®, which is one of the most permeable commercial glassy polymers. Due to

their high FFV, the gas permeabilities in 6FDA polyimides are very high, which suits well for the separation of big molecules, such as C4s.

The 6FDA polyimides were synthesized in the Koros group. The synthesis of polyimides is a two step process. The initial step involves a stoichiometric amount of dianhydrides reacting with a diamines to form a polyamic acid. The next step of condensation reaction is to close the ring structure of the polyamic acid in order to form a polyimide. The monomer concentration in the reaction solution is kept at ~ 20 w%, to keep appropriate viscosity for good mass transfer rate for high molecular weight polymers. The stoichiometry between the dianhydrides and diamines is essential for development of high molecular weight polyimides. All the monomers 6FDA (2, 2-bis (3,4-carboxyphenyl) hexafluoropropane dianhydride, 99% purity), 6FpDA ((4,4'-hexafluoroisopropylidene)diamine, 99% purity), DAM (diaminomesitylene, 98% purity) were purchased from Sigma and sublimed to further increase the purity, except for DABA (3,5-diaminobenzoic acid, 99% purity). All the monomers are dried in a vacuum oven overnight at 70 °C to remove the moisture before polymerization.

Table 3.1 Published properties of various polymers

Polymer	FFV [-]	Tg [°C]	ρ [g·cm^{-3}]
Matrimid® [1]	0.17	305	1.20
6FDA-6FpDA [2]	0.175	298	1.50
6FDA-DAM-DABA(3:2) [3]	0.180	-	1.41
6FDA-DAM [2]	0.190	372	1.33

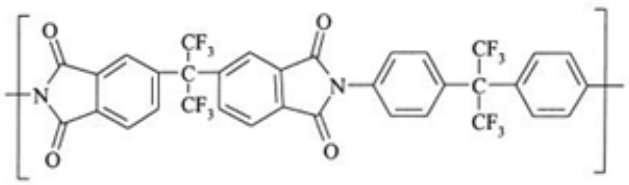

6FDA-6FpDA

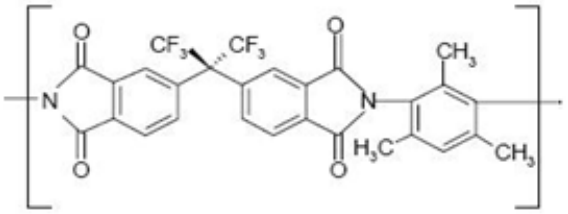

6FDA-DAM

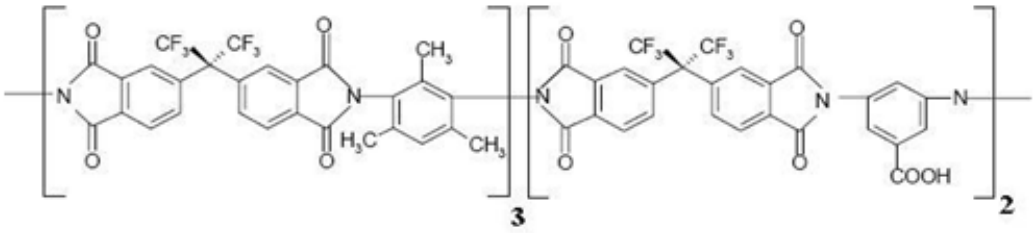

6FDA-DAM-DABA(3:2)

Figure 3.1 Molecular structures of different 6FDA polyimides

There are two methods used for the second step imidization: chemical and thermal imidization. In thermal imidization method, the ring closing reaction is carried out by raising solution temperature to above 190 °C. The formed water is removed by forming azeotropy with dichlorobenzene. In the chemical imidization method, the conversion of polyamic acid to polyimide is achieved through the use of triethylamine (TEA) and acetic anhydride (AcAn). The TEA acts a catalyst for the ring closing reaction and the acetic anhydride reacts with the water that is given off by the ring closure, forming acetic acid.

Cloudy polymer solutions were found using the thermally imidized 6FDA polyimides, possibly because of a trace of undesired crosslink reaction [4], which does not affect dense film membrane formation for gas separation, but the insoluble parts may

bring in unpredictable gas separation properties. Clear polymer solution were later made possible by using the chemically imidized 6FDA polyimides. In Table 3.2, the polymers used in this research and their synthesizing methods are shown.

Table 3.2 Synthesized 6FDA polyimides in this research

Polyimide	Batch #	Imidization	Mw
6FDA-DAM	WQ0807	Thermal	81500
6FDA-DAM	JQ0801	Chemical	119000
6FDA-DAM	WQ0912	Chemical	48300
6FDA-DAM-DABA (3:2)	WQ0903	Chemical	-
6FDA-6FpDA	WQ0804	Thermal	-

Ultem® 1000 polyetherimide (GE Plastics), Udel® Polyethersulfone (Solvay), Cellulose Acetate (Eastman) were selected as the support polymer candidates for 6FDA dual layer hollow fiber spinning. PDMS (GE) was used to make MFI-PDMS mixed matrix dense films.

3.1.2 Zeolites

Two kinds of zeolites were used in this research for C4s separation. Except for the 2 μm commercial 5A bought from Sigma, all MFI and LTA of different sizes were synthesized in Jones and Nair group. The zeolite properties are shown in Tab. 3.3.

Table 3.3 Selected properties of zeolites, (Permeability calculated as $D_0 \times S$ at 25 psi)

	nC4 permeability at 25 psi [Barrer]	nC4/iC4 selectivity	Pore size [Å]	Density [g cm-3]
5A	~ 10 [5]	∞ [7]	4.3 [9]	1.55 [9]
MFI	~ 24000 [6]	~ 50 [8]	5.2-5.4 [10]	1.75 [10]

Zeolite MFI

MFI is a pure silicalite zeolite. There are two kinds of interconnected channels composed of ten-oxygen-rings. As shown in Fig. 3.2, the straight channels have higher selectivity for nC4/iC4 separation, than the zig-zag channels. The molecule diffusion in MFI is anisotropic because of the size difference between channels in two directions. It is reported that the straight channels has higher selectivity for butane isomers, because the iC4 diameter (5.0 Å) is approaching the critical channel size (5.2 Å). As shown in Fig. 3.3, MFI 2 μm crystals are flat ‘‘coffins’’ and become more cubic at smaller sizes. MFI crystals are in favor of growth along a, and b axis, therefore, more straight channels are available for diffusing molecules in bigger MFI crystals. This will be discussed in later chapters.

High silica MFI particles with an average diameter of 150 nm, 300nm, 2 μm and 5 μm were synthesized using the procedures described in detail elsewhere [10]. The XRD pattern showed by previous work that all the MFI particles maintain the MFI-crystal structure. Nitrogen physisorption results showed the same amount of micropore volume as larger micron MFI crystal particles. The synthesis used 105 g of tetraethylorthosilicate (TEOS, 98%, Aldrich) that was added dropwise into tetrapropylammonium hydroxide (TPAOH, 40% w/w aqueous solution, Alfa Aesar) solution while stirring. After stirring at room temperature for 1 hour, water was added to this mixture and the resultant mixture was stirred vigorously at room temperature for another 24 hrs. The reaction mixture prepared was then transferred to a 700 ml autoclave reactor (HR-700, Berghof Inc.) to perform the hydrothermal reaction. The TEOS to TPAOH molar ratio and synthesis duration were parameters to control the particle sizes.

The resulting suspension was centrifuged and the supernatant was discarded. The solid was redispersed into deionized water by sonication and was centrifuged afterward. This centrifugation-sonication cycle was repeated 5 times until the pH of the supernatant was below 8. The organic template is larger than the pore and therefore must be removed by chemical or thermal decomposition to yield the microporous MFI [10]. In this study MFI particles with organic template inside the pores (termed uncalcined- MFI) was synthesized without calcination, while the porous MFI (termed calcined- MFI) was calcined at 550 °C for 8 h in air to remove the organic template.

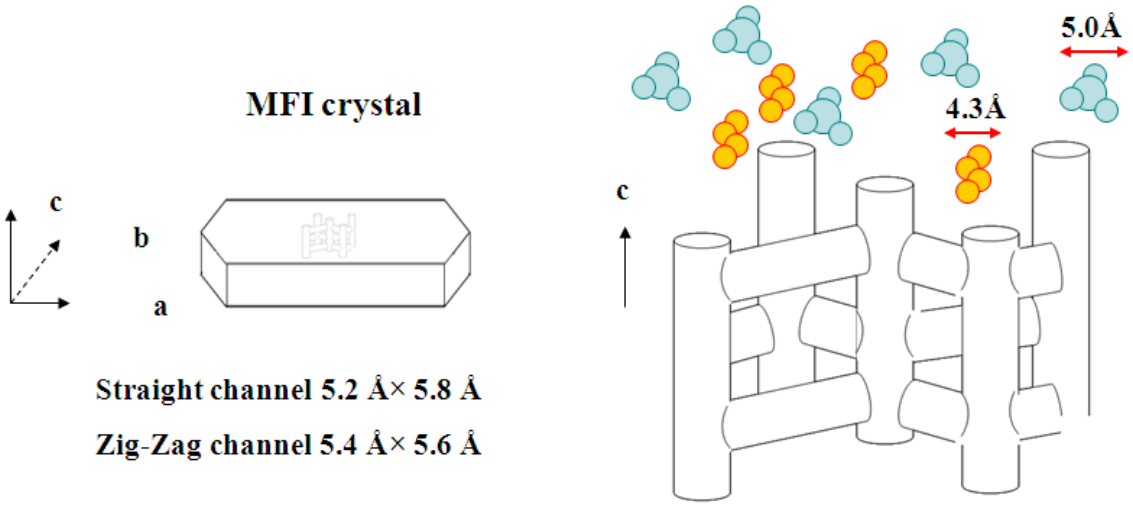

Figure 3.2 Crystal channel orientation and pore structures of MFI

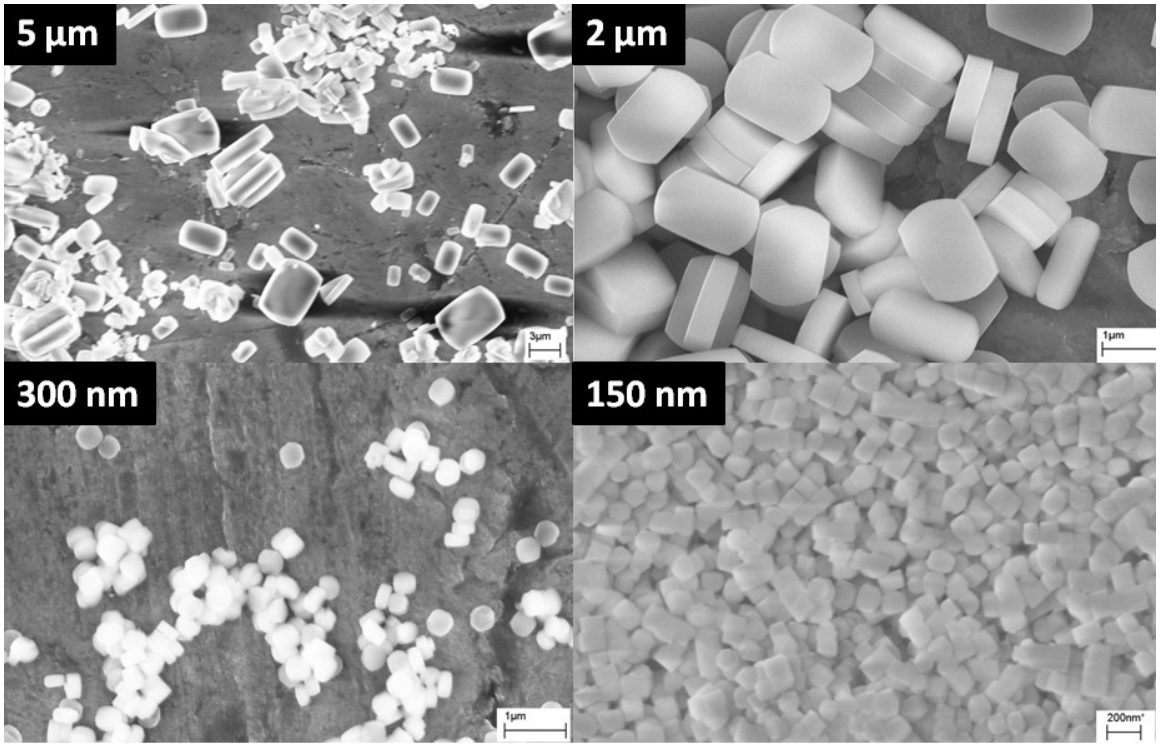

Figure 3.3 Synthesized MFI particles of different sizes

Zeolite LTA

Fig. 3.4 shows the structure of zeolite A, the vertices stands for either Al or Si atoms, the oxygen atoms is in the middle. Because of the relative sizes, the Al and Si atoms are so small that they are effectively buried in the spaces between larger oxygen ions. The lines can be considered as the diameter of oxygen ions. The α-cage, also called cell, connected by six eight-oxygen-ring apertures in three dimensions, is the main route for molecular diffusion. The pores of zeolite A are constructed by eight member oxygen rings with free aperture of 4.3 Å when not obstructed by a cation. In one cell, there are 12 monovalent (or 6 divalent) cations to make zeolite neutral overall. There are three types of cation sites, S_1, S_2, S_3 in the order of their energy [12].

S1. at the center of the six-oxygen-rings (8 equivalent sites per pseudo cell)

S2. within the eight-oxygen-ring windows (3 equivalent sites per pseudo cell)

S3. against a four-oxygen-ring

If there are less than 8 cations (e.g., 4 Na^+, 4 Ca^{2+}), all of them can be accommodated to low energy states S1, therefore the eight-ring aperture will be free of cations and totally open. If there are more than 11 cations (e.g., 10 Na^+, 1 Ca^{2+}), only 8 cations can be accommodated to S1 sites, the eight ring apertures are totally blocked by the remaining three cations at S2 sites. Table 3.4 shows the fraction of open windows at different ion exchange extent. It is called 5A when Ca^{2+} makes more than 67% of cations, and windows are totally open. It has been known when Ca^{2+} content near 67%, or transition from NaA to CaA, the gas diffusion properties can be dramatically dependent on the ion content. Yucel found that the corrected diffusivity (D_0) of nC4 at 100 °C in 65% CaA is about 3 times lower than that in 95% CaA [5]. It is therefore, desirable to reach Ca content well above 67% to make sure a complete open pore CaA is achieved.

Table 3.4 Fraction of open windows at different extent of cation exchange extent, adopted from [12]

Cations per Cell	Fraction of open windows
12 Na^+	0
10 Na^+, 1 Ca^{2+}	0
8 Na^+, 2 Ca^{2+}	1/3
6 Na^+, 3 Ca^{2+}	2/3
4 Na^+, 4 Ca^{2+}	1.0
2 Na^+, 5 Ca^{2+}	1.0
6 Ca^{2+}	1.0

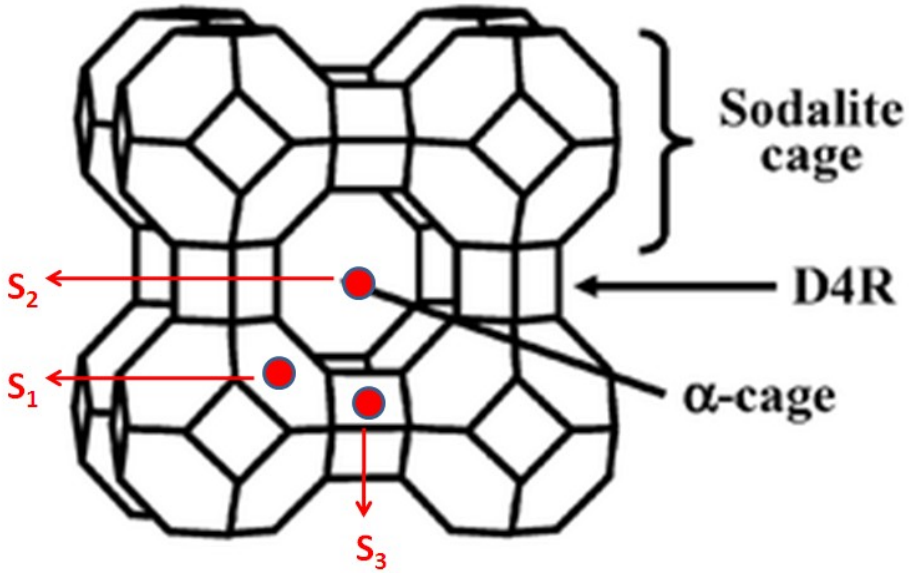

Figure 3.4 Pore structures of zeolite A and different sites of cations

Fig. 3.5 shows different sizes of LTA particles. The 2 μm 5A particles were bought from Sigma Aldrich. Zeolite LTA (Na form) particles were synthesized hydrothermally based on the procedure published by Larlus [13]. Colloidal silica (Ludox HS-30) and aluminum isopropoxide were used as silicon and aluminum sources respectively and the structure directing agent was TMAOH. For 150 nm and 300nm particle synthesis, a clear precursor solution with molar ratio of 0.2NaOH: $1SiO_2$: $1Al(OiPr)_3$: 4TMAOH:$170H_2O$ was prepared at room temperature and treated hydrothermally at 60 °C for 1day, and at 100 °C for 1 day, correspondingly. Large crystal LTA, approximately 1-2 μm, was also prepared from the solution with molar ratio of 0.2NaOH: $1SiO_2$: $1Al(OiPr)_3$: 3TMAOH:$170H_2O$. The hydrothermal reaction was conducted at 120 °C for 4 days. After the reaction, zeolite particles were washed with DI water by repetitions of centrifuge and dispersion at least 5 times and dried at 80 °C. Calcination was performed at 550 °C for 8hr in air.

The synthesized LTA (Na-A) were then ion exchanged into Ca-A form to make open pores in LTA. A sample of 6-8 g of Na-A was dispersed into a 150 ml 0.25 M $Ca(NO_3)_2$ solution for at least 3 hrs, at room temperature. As shown in Appendix, the hydrated Na^+ and Ca^{2+} are close to the size of LTA pores, therefore, enough time was given to make sure the equilibrium is reached. The LTA particles were centrifuged out at ~8000 rpm for 10 minutes, and the supernatant solution was removed. New $Ca(NO_3)_2$ solution was put in and another cycle of ion exchange was performed. Three times of exchange at room temperature and one time at 60 °C were performed to make sure enough Ca^{2+} ion exchange is reached. Five to six times of DI water washing steps were carried out following the ion exchange steps, to remove the extra-framework ions. The conductivity of supernatant water drops from few hundreds to about 10 $\mu s \cdot m^{-1}$. The thoroughly washed zeolite particles were dried under vacuum at 50 °C for few hours to remove the majority of water. The temperature is increased later to 180 °C to remove the remaining water in the micropores of zeolite LTA. Sorption kinetics and capacity of nC4 gas is used to probe the integrity of zeolite 5A after ion exchange steps.

Table 3.5 shows the elemental analysis results of different LTA crystals by EDS (Electron Dispersion Spectroscopy) measurement. The synthesized LTA has close to ideal atomic ratio of: 1Na:1Al:1Si. The 5A by ion exchange has Ca:Al ratio of 0.47, which is close to the ideal ratio of 0.5. The commercial 5A has some Na+ ions remaining in the LTA crystal, and the Ca:Al ratio is 0.38. As shown in table 3.4, LTA with more than 67% of Ca^{2+} cation, or Ca:Al > 0.33 has totally open pores, and are called 5A. Both the commercial 5A and synthesize-exchanged 5A should have the same gas diffusion properties, which will also be proved by sorption measurement in later chapters.

Table 3.5 Atomic percentage of commercial and synthesized LTA

	O	Na	Ca	Al	Si
synthesized 4A	**66.6**	**11.0**		**11.1**	**11.3**
synthesize-exchanged 5A	**61.9**	-	**7.1**	**15.0**	**16.0**
commercial 5A	**55.6**	**5.2**	**6.4**	**16.7**	**16.1**

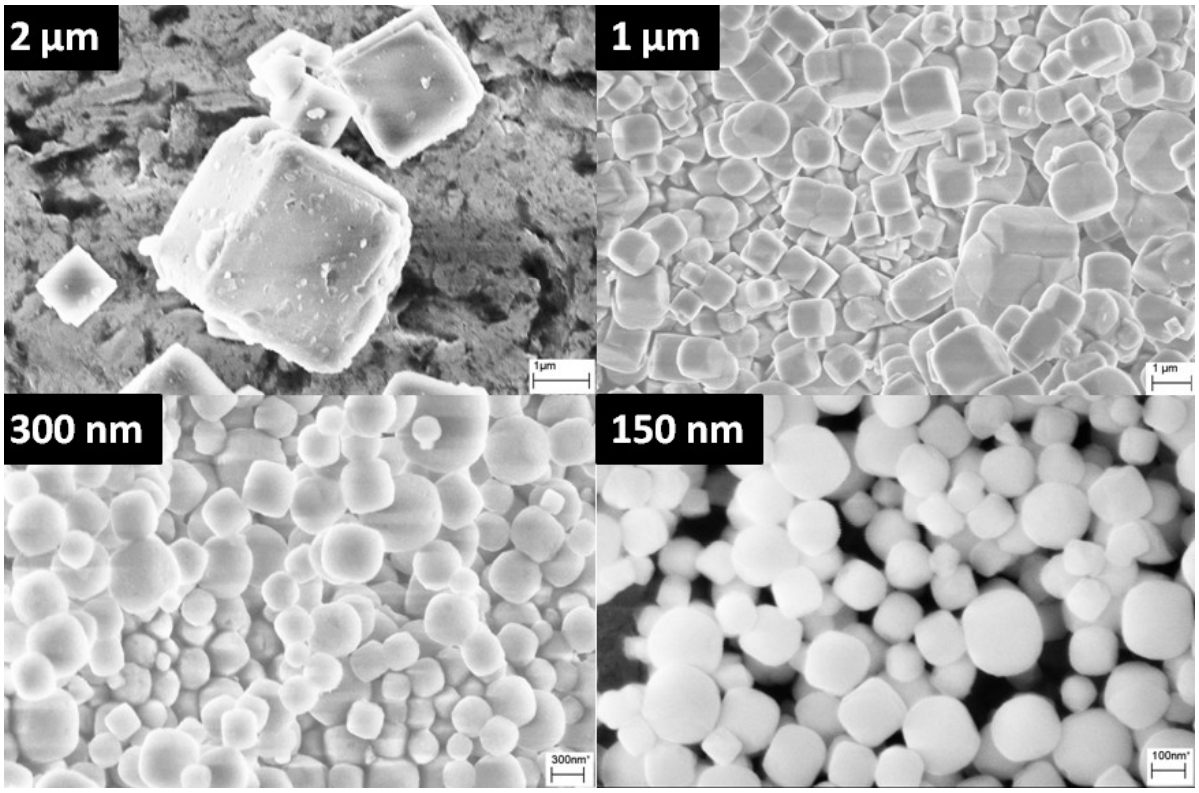

Figure 3.5 Commercial (2 µm) and synthesized zeolite LTA (1 µm, 300 nm, 150 nm) particles as received

3.1.3 Gases and chemicals

Compressed O_2, N_2, CO_2, CH_4 (all research grade, 99.99% purity) Butane isomers (99.99% purity) are bought from Air Gas. It is worth noting that the purity of iC4 needs to be extremely high, because small amount of impurities (usually He or air) can permeate far faster than the bulky iC4 molecules in polymer membranes. The iC4 permeability is inaccurate using even slightly impure iC4 gases. The evidence of impurity existence is the lack of time lag (or unclear time lag) in the permeation test.

Fig. 3.6 shows the activity coefficient of butane isomer vapors at different temperature and pressure. Because of their close-to-room temperature boiling point, the C4s vapors' activities are very high. It is well known that high activity hydrocarbon can plasticize (swell) the glassy polymers, hence reduce the separation performance of the polymer membrane. To avoid this adverse effect, permeation test on polymer membranes were performed only at 100 °C, 25 psi, when the activity of C4s is lower than 0.15. The sorption tests showed no non-Fickian diffusion in polymer membranes at this condition, thus proving that no significant plasticization happens.

Toluene (99.8% purity), Tetrahydrofuran (THF 99.8% putiry), N-methyl-pyrrolidinone (NMP 99% purity), 2-propanol (99.5% purity), were bought from Aldrich and used without further purification. Sol-gel Grignard treatment reagents, thionyl chloride (99.5% purity, Fe < 5 ppm), alumina chloride (99% purity, powder), and methymagnesium bromide (3.0M solution in diethyl ether) are all moisture sensitive and need to be transferred carefully through a syringe or weighed quickly to avoid exposure to moisture in air.

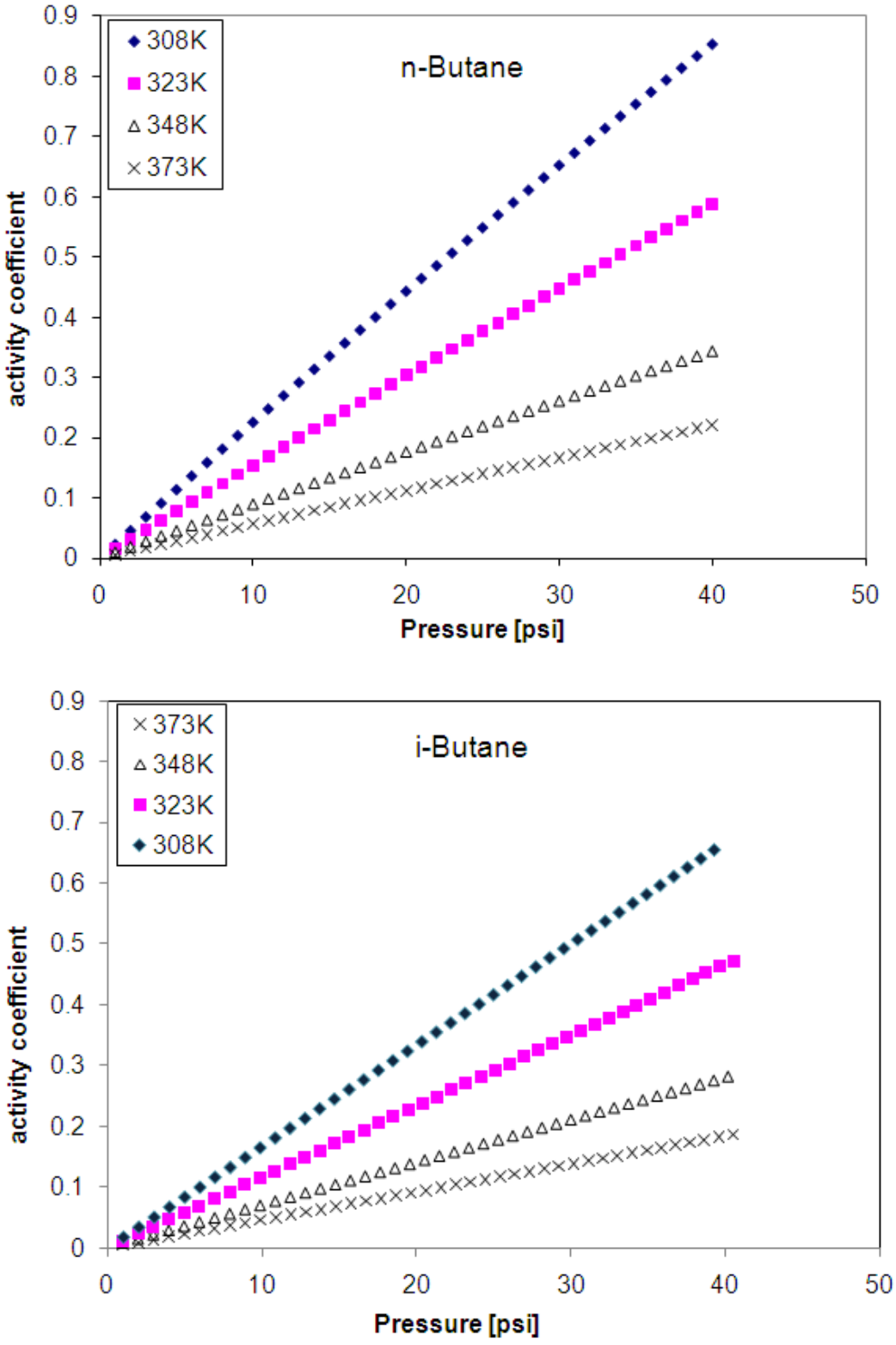

Figure 3.6 Activity coefficient of butane isomer vapor at various temperature, obtained from National Institute of Standard and Technology (NIST) database

3.2 ZEOLITE SURFACE MODIFICATION

Former researchers Shu and Husain established a two step treatment method to form $Mg(OH)_2$ whiskers on zeolite surfaces [14]. However, the $Mg(OH)_2$ formation mechanism was not fully known and the treatment is limited to only Al-containing zeolites, such as LTA. In this research, I found the plausible whisker formation mechanism: sol-gel reaction using the Grignard reagent. In order to have whiskers formed on zeolite surfaces, acidic sites on zeolite surface (heterogeneous acidic sites) are needed. Former researchers established a way to generate AlClx species by dealumination [15]; however, the treatment partially destroys the zeolite structure and cannot be applied to zeolites without Al content. In this work, heterogeneous acidic sites were formed by anchoring $AlCl_3$ to zeolite surface through its reaction with surface –OH groups. The experimental methods are shown as following.

3.2.1 Sol-gel-Grignard treatment

Zeolite in sol-gel precursor

Zeolite 5A, with an average crystal size of 2 μm was purchased from Aldrich. Samples of 8 g of 5A particles and a magnetic stir bar were placed in a 200 ml reaction flask. All the particles and glassware were dried overnight at 150 °C in a vacuum oven. Amounts of 80 ml of Toluene (99.8% Aldrich) and 20 ml of methylmagnesium bromide (3.0 M solution in diethyl ether, Aldrich) were added into the reaction flask. The dispersion was kept in a sonication bath overnight, before 80 ml of isopropanol (99.5%, Aldrich) was added slowly to react with the methylmagnesium bromide. The milky sol dispersion product was divided into six 50 ml centrifuge vials.

Zeolite in sol-gel

Water was added into the vial of dispersion dropwisely. Sonication was used to assist the H_2O dispersion after every four drop of water addition, by an inserted type sonication horn (VCX130, Sonics) with a 55 W power and 10 seconds duration. The pH of H_2O added was adjusted to 7.0, 1.0 and 0 by adding adequate amount of HCl to the DI water. The resultant dispersion was aged overnight without disruption.

Sol-gel precipitation

The particles and reaction product were separated from the dispersion by centrifuge. The supernatant was decanted and isopropanol was added to wash away the remaining toluene, 3 times of sonication with a 55 W power and 30 seconds duration were applied to assist the washing. Zeolite particles were centrifuged out of the isopropanol phase and water was then added, followed by 3 times of sonication with a 55 W power and 30 seconds duration. Sonication and centrifuge were repeated until the conductivity of supernatant dropped below 30 $\mu S \cdot m^{-1}$. The final collected particles were dried overnight in a vacuum oven at 180 °C.

3.2.2 Acidity modification of zeolite

Zeolite LTA dealumination

Thionylchloride is a chlorination reagent, which can turn the –OH groups on zeolite surface into –Cl groups by the following reaction [16].

$$-Si-OH + SOCl_2 \rightarrow -Si-Cl + SO_2 + HCl \qquad (3.1)$$

Previous researchers [15] found the dealumination of LTA using the $SOCl_2$ reagent, assisted by sonication. The AlClx species are assumed to also be generated on

the surface of LTA particles. In the sol-gel Grignard treatment, the –Si-Cl groups or AlClx species formed by dealumination reaction act as acidic sites for sol-gel reaction. In this research, the extent of dealumination was controlled by varying the amount of $SOCl_2$ and reaction time. The experiment was carried out in the following procedures.

A sample of 8 grams of 5A particles in a 250 ml flask was firstly dried thorough at 150 °C overnight in a vacuum oven. Specific amount of $SOCl_2$ (10-20 ml) and 80 ml of toluene was added. The dispersion was stir by a magnetic bar for 15 minutes, before putting into a sonication bath for a specific amount of time (10-25 hrs) sonication. The flask was then put in an oil bath to raise temperature to 90-110 °C, and a continuous flow of nitrogen was used to evaporate the liquid in a fume hood. A water trap was used to collect the unreacted $SOCl_2$ in the vapor. The collected particles was then dried at 80 °C for two hours in a vacuum oven before adding the Grignard reagent for the next step of treatment.

$AlCl_3$ deposited on zeolite

The acidic AlClx species can be generated by the dealumination reaction through $SOCl_2$. These AlClx can promote the one dimensional $Mg(OH)_2$ whisker formation in the sol-gel reaction. However, the dealumination reaction also changes the properties of LTA crystal, which is discussed in chapter 4. Another way of generating acidic AlClx sites on zeolites is by anchoring $AlCl_3$ to zeolite surfaces through the abundant –OH groups, as shown in Eq. 3.2. Research shows a close to 100% conversion rate was achieved at modest reaction conditions [17]. Different amount of $AlCl_3$ was used in this study to find the optimal acidity.

$$-Si-OH + AlCl_3 \rightarrow -Si-O-AlCl_2 + H_2O \qquad (3.2)$$

A sample of 8 grams of 5A particles in a 250 ml flask was first dried thoroughly at 150 °C overnight in a vacuum oven. Specific amount of $AlCl_3$ (0.04-0.32 g) and 80 ml of toluene was added. The flask was then put in an oil bath to raise temperature to 80 °C, and kept stirring for 4 hours to make sure the reaction was complete. A slow flow of nitrogen was used to keep the inert atmosphere and avoid the toluene pressure building up. The flask was then taken out of the oil bath and let cool down to room temperature. The dispersion was then ready to add Grignard reagent for the next step sol-gel treatment.

3.3 MIXED MATRIX DENSE FILM FORMATION

3.3.1 6FDA polymer and mixed matrix membrane

A 20 wt% polymer dope was prepared beforehand with dried 6FDA-DAM and tetrahydrofuran (THF). The dope was rolled on a mixer overnight to dissolve the polymer. The zeolite sieve particles were first dried in a vacuum oven at 180 °C overnight, in order to remove any moisture in the pores. A small amount of tetrahydrofuran was added to the dried sieve and a few bursts of sonication (55W, 30s) were applied to assist the sieve in dispersing in THF. The polymer dope was carefully added to the sieves to achieve the desired particle to polymer ratio. The polymer-sieve dope was rolled and sonicated to assist the dispersion of sieves. The dopes were poured onto a glass plate, which was placed in glove bag presaturated with THF vapor for at least 4 hours. The dope was cast into the desired thickness (typically 30 micron) using a draw knife with appropriate specific clearance. The film was left in the glove bag overnight to let the THF solvent evaporate slowly. The film was further dried in a vacuum oven at 180 °C overnight to remove any remaining solvent.

3.3.2 PDMS and mixed matrix membrane formation

The PDMS membrane was prepared with two parts commercial polymer A and crosslinker B (GE). The two parts with a ratio of 10:1 was added to isooctane to make a 10 wt% solution. For mixed matrix membranes, MFI particles were first dried overnight at 150 °C in a vacuum oven, then added into isooctane to make a 10 wt% dispersion. A sonication horn was used to assist the dispersion. The commercial PDMS and crosslinker were then added to the MFI-isooctane dispersion. The solutions containing polymer or with MFI particles were poured onto a Teflon dish, and dried overnight at 50 °C in a vacuum oven. The dried membranes were put in an oven and dried at 350 °C for 2 hours before permeation tests.

3.4 HOLLOW FIEBR SPINNING

The dual layer hollow fibers were spun, with Ultem, polyethersulfone (PES), and Cellulose acetate (CA) as the support layer for the 6FDA polymer sheath. The dope compositions are shown in table 3.6. In order to determine the dope composition, a three phase diagram was first constructed. The spinning dopes were made close to the phase separation lines. NMP and THF were used as solvents, and EtOH, H_2O and $LiNO_3$ were used as non-solvents for the spinning dopes. All the solvent and non-solvent were mixed first, then the dried polymers were poured into the liquid mixture. Shaking and rolling were used to assist the polymer dissolving process.

Table 3.6 Compositions of various dopes for dual layer hollow fiber spinning

Spin #	JQ10	JQ03	JQ11	JQ11	JQ33
	Ultem	PES	CA	DAM	DAM-DABA
Polymer	32	34	25	22	23
NMP	56	60	64	40	28
THF	9			13	11.5
EtOH				19.4	32
H_2O			11		
$LiNO_3$	3	6		5.6	5.5

The mixed matrix dopes were prepared slightly differently from pure polymer dopes. Table 3.7 shows the composition of mixed matrix sheath dopes. Grignard treated (GT) particles were firstly dispersed in the NMP and THF mixtures, sonication bath and horn were used to assist the nanoparticle dispersion depend on the agglomeration degree. Sonication was stopped when no visible agglomerates could be found. As discussed in chapter 1, it is found that Grignard treated particles are ready to disperse with slight sonication applied because of electrostatic stabilization. NMP solution containing about 10% of the total polymer was firstly added to the zeolite dispersion slowly. The remaining solvent and dried polymer solids were then added to make dopes the desired composition. The dopes were rolled overnight before put into pumps for spinning.

Table 3.7 Compositions for mixed matrix sheath dopes

Spin #	JQ08	JQ09	JQ12	SH56
	20%-MFI-Ultem	40%-MFI-Ultem	40%-4A-Ultem	35%-MFI-6FDA-DAM-
Polymer	28	21	21	14.7
NMP	49	49	49	-
THF	16	16	16	77.5
GT-Zeolite	7	14	14	7.8

The core and sheath dopes, together with bore fluid were coextruded through a dual layer spinneret (Recessed 1). The typical parameters for dual layer hollow fiber spinning were: bore/core/sheath flow rates (60/180/30 ml/hr), air gap distance (10 cm), water bath temperature (25 °C), take-up rate (15 m/min), spinneret temperature (50 °C). The fibers were kept in DI water for 3 days (change water everyday) before solvent exchange. Three times of methanol and three times of hexane solvent exchanges (20 minutes each time) were performed subsequently. Then the fibers were kept in the hoods to dry for 30 minutes, followed by a vacuum drying at 110 °C for one hour. The dried fibers are then ready to make modules and test for gas separations.

3.5 ZEOLITE AND MEMBRANE TESTING METHODS

3.5.1 Pressure decay sorption

Sorption measurements were done using a pressure decay method. Solubility of C4s in zeolites and polymers was calculated from the pressure change before and after sorption. A small experimental error of less than ±5 % is expected from the relatively accurate pressure measurement, and volume calibration. Diffusivity of C4s in 6FDA polymer films was obtained from the relation curve between M_t/M_∞ (M_t and M_∞ are the masses sorbed at time t and t=∞, respectively) and $(Dt/l^2)^{1/2}$ (D, t, l are diffusion coefficient, time and film thickness respectively), assuming a Fickian type one-dimensional diffusion takes place in the polymer thin films.

99.5% purity n-butane and i-butane were used as the sorption gases. Polymer thin films or porous cylinder filled with zeolites were loaded into cell (B) and degassed for overnight. A differential amount of sorption gas was first introduced into the reservoir

(A), then the connecting valve was quickly open for 3 second and closed. The pressure signal in both volume A and volume B were recorded continuously.

The sorption in both zeolites and polymers was calculated through molar balance: adsorbed amount equals to decreased amount in reservoir A minus increased amount of gas in cell B, as shown in Eq. 3.3.

$$C = \frac{\frac{V_A}{RT}\left(\frac{P_{A0}}{Z_{A0}} - \frac{P_{Af}}{Z_{Af}}\right) - \frac{V_B}{RT}\left(\frac{P_{Bf}}{Z_{Bf}} - \frac{P_{B0}}{Z_{B0}}\right)}{V_{polymer}} \tag{3.3}$$

The diffusivity coefficient in polymer films was calculated by fitting the sorption curves onto the ideal Fickian's sorption model curve. The model has three assumptions. *1) One-dimensional diffusion process in the thin films; 2) D is constant during an incremental sorption step; 3) Local equilibrium at boundary condition.*

The diffusion equation and its boundary conditions become Eq. 3.4:

$$\begin{aligned}
&\frac{\partial C}{\partial t} = D\frac{\partial^2 C}{\partial x^2} \\
&initial: \\
&C = C_0,\ 0 < x < l \\
&Boundary: \\
&x = l, C_B = C_B(t)\ (\text{from Crank solution}) \\
&x = 0, \frac{\partial C}{\partial x} = 0
\end{aligned} \tag{3.4}$$

Crank developed the solution for this equation, as shown in Eq. 3.5, 3.6:

$$\frac{M_t}{M_\infty} = 1 - \sum_{n=1}^{\infty} \frac{2\alpha(1+\alpha)}{1+\alpha+\alpha^2 q_n^2} \exp(-Dq_n^2 t / l^2) \tag{3.5}$$

$$\tan q_n = -\alpha q_n \tag{3.6}$$

The adsorbed percentage to the total amount of adsorbing molecule is shown as f. The adsorbed percentage was calculated through Eq. 3.7.

$$\alpha = \frac{(\frac{P_{start}}{Z_{start}} - \frac{P_{finish}}{Z_{finish}})}{(\frac{P_{start}}{Z_{start}})} \tag{3.7}$$

A further assumption was made that solubility coefficient C is proportional to pressure during one incremental sorption step, even though the sorption curve C to P was concave on a larger pressure range. Then the experimental Mt/Minf can be calculated from pressure change. It was defined in equation (8)

$$\left(\frac{M_t}{M_{\inf}}\right)_{\exp} = \frac{(\frac{P_{B0}}{Z_{B0}} - \frac{P_{A0}}{Z_{A0}})}{(\frac{P_{B0}}{Z_{B0}} - \frac{P_{A\infty}}{Z_{A\infty}})} \tag{3.8}$$

The experimental result M_t/M_{inf} was fitted into ideal curve by trying different diffusion coefficients. The best fitting D was determined to be the local diffusion coefficient from pressure P to P+ΔP. By differentially increase the adsorbent pressure, a pressure dependent solubility and diffusion coefficient were obtained.

Considering the diffusion coefficient of nC4 in zeolite 5A ($1\times10^{-8}cm^2/s$) and MFI ($5\times10^{-6}cm^2/s$), it is impossible to observe the sorption kinetics using zeolite crystals about 1 μm in size. The time scale of kinetic sorption is less than one second, which is impossible to detect using pressure decay method. However, diffusion in zeolites, especially LTA is reported to slow down dramatically after harsh treatments, such as steaming, dealumination, plugging by chemical reagents, *etc.* [12]. The commercial LTA particles have gas diffusivities several orders of magnitude lower than the ideal values

[5]. The sorption kinetics turns out to be a very convenient tool to check if the zeolite is still the same for gas diffusion after Grignard treatment. Many treatment conditions induced the slow sorption kinetics, and ways to avoid the slow kinetics are discussed in chapter 4. A sorption kinetic test of the treated zeolite is needed to ensure the particles' quality before mixed matrix membranes are made using these treatment particles.

3.5.2 Permeation

Permeation test of butane isomers were carried out at 100 °C to avoid the possible plasticization of polymer membranes. The system was heated by a 750 W silicon coated heating tape, and insulated by a 1.5 inch thick fiberglass wall. Both the upstream and downstream transducers were kept inside the box to maintain a constant temperature.

For dense film permeation test, high temperature epoxy (Duralco® 4525, Cotronics, Brooklyn, NY) was used to avoid the plasticization of tape adhesive by C4s gases, in addition to other standard procedures, shown in other places [19]. One gram of epoxy and crosslink reagent were mixed thoroughly with a ratio of 100:8, waited for 10 minutes to degas and cure initially, and then applied to the interface of adhesive tape and membrane, as shown in Fig. 3.7. The cell with membranes mounted was pulled to vacuum at downstream, at room temperature for overnight to cure the epoxy thoroughly. The temperature was then raised to the permeation test conditions. For mixed matrix film permeation test, moisture in the air can contaminate the zeolite in the mixed matrix film over time. Films need to be dried in vacuum oven at 180 °C overnight to remove the moisture in zeolites, mounted onto cell, and quickly connect to permeation system.

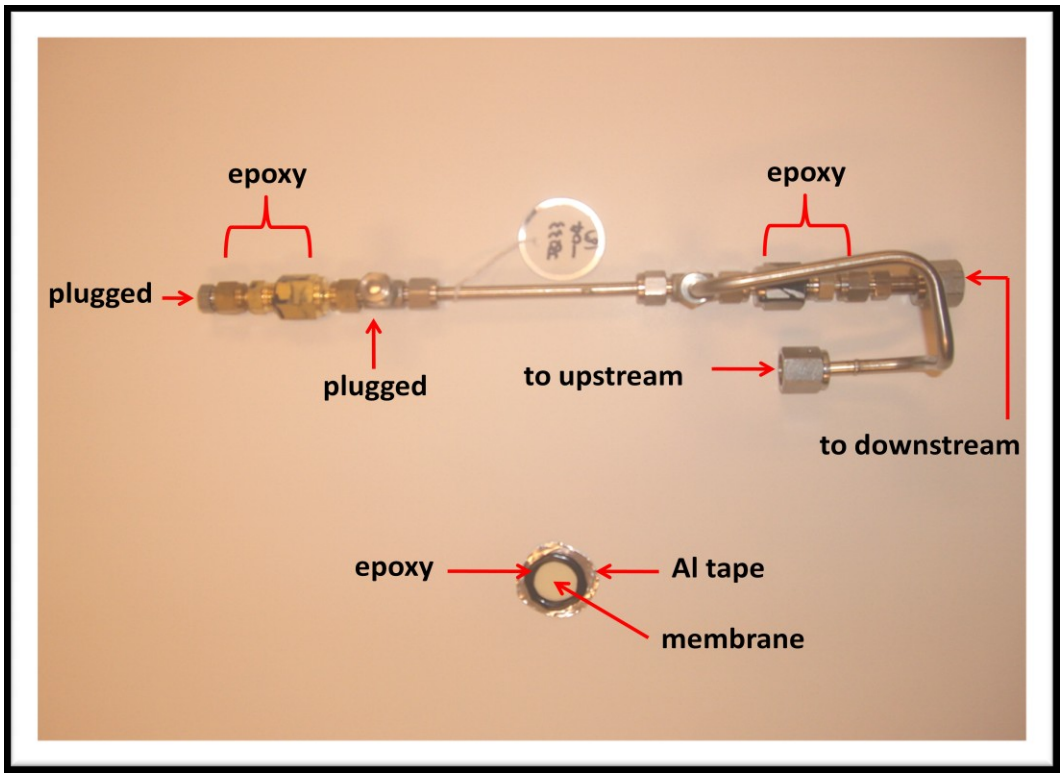

Figure 3.7 Dense film masking and hollow fiber module connection for permeation tests, using upstream dead flow/downstream pressure build up method

The permeation result at steady states was taken (after ten time lags). After n-butane (time lag 1-2 hours) permeation test, membranes were vacuumed for more than one day to degas before the slower i-butane (time lag 10-20 hours) permeation test.

The downstream vacuum permeation method was also used to test the hollow fiber membranes, considering the leak free safety requirement for C4s gases at high temperature. Modules with 5-10 fibers, 19 cm in length were made using the standard procedures shown in former works [20]. A high temperature epoxy (from Emerson & Cuming, Billerica, MA) was used to plug the two ends of fiber modules. Epoxy and crosslink reagent were mixed at ratio of 100:9, and degassed briefly in a vacuum oven, before pouring into the two ends of modules. One end of module with epoxy was first cured overnight, before applying epoxy to the other end. The fibers modules were

connected to the permeation system using some tube connection to fit into permeation systems, and vacuumed overnight before doing gas permeation test. The vacuum time and steady state permeation results were done in the same way as dense films. Considering the hollow fiber membranes has typically 20 times thinner skin and 10 times larger surface area, the gas permeation time lag was significantly lower, and permeation rate far faster than those in dense films.

3.6 OTHER EXPERIMENTAL METHODS

SEM images were obtained with SEM machines LEO 1530, LEO 1550, equipped with a thermally assisted field emission gun operating at 3.5 kV or 1.5 kV for zeolites and 10 kV for polymers films. In order to see the fine structures on zeolite surfaces, no metal sputtering was applied to zeolites to avoid the formation of nm scale metal particles. Lower voltage is preferred to dim the electron beam and observe the fine structures, such as $Mg(OH)_2$ whiskers. For polymer or mixed matrix membrane observation, a layer of gold was sputter-coated on top of sample to increase the electron conductivity, using current of 20 mA for 1 minute. Elemental content was analyzed by EDS measurement, which measures composition more than 2 μm deep from surfaces. Compared to XPS for surface measurement, EDS measures the overall elemental compositions for the submicron zeolite particles.

Micropore volume by t-plot method and BET surface area were calculated from nitrogen physisorption measurements performed on a Micromeritics ASAP 2020 or 2010.

Powder X-ray diffraction (XRD) patterns were obtained on a Philips X'pert diffractometer equipped with X'celerator using Cu Kα radiation.

3.7 REFERENCES

[1] *Matrimid Product Data Sheet*, **2000**, Vantico, Inc.: Brewster, NY.

[2] J. H. Kim, *Polymer*, **2006**, 47, 3094-3103

[3] W. Xu, *J. Membr. Sci*., **2003**, 219, 89-102

[4] M. Das, Ph. D. thesis, *Georgia Institute of Technology*, **2009**

[5] H. Yucel, *J.C.S. Faraday I*, **1980**, 76, 71-83

[6] B. Millot, *Micropor. Mesopor. Mat.*, **2000**, 38, 85-95

[7] S.H. Cho, *Adsorption separation and purification apparatus and process for high purity isobutane production*, US patent, **2000**

[8] G. Xomeritakis, *Chem. Mater*., **1999**, 11, 875-878

[9] T.B. Reed, *J. Am. Chem. Soc.*, **1956**, *78*, 5972–5977

[10] E. Flanigen, *Nature*, **1978**, 271, 512-516

[11] C.H. Cheng, *J. Phys. Chem. C*, **2008**, 112, 3543-3551

[12] J. Karger, Diffusion in zeolites, **1999**, *John Wiley & Sons*

[13] O. Larlus, *Microporous Mesoporous Mater*., **2006**, 96, 405

[14] S. Shu, J. Phys. Chem. C, **2007**, 111, 652-657

[15] S. Shu, *Ind. Eng. Chem. Res.,* **2007**, 46, 767-772

[16] T. Tao*, J. Am. Chem. Soc.,* **2000**, 122, 3118-3126

[17] X. Hu, *J. Catalysis*, **2000,** 195, 412-415

[18] J. Crank, Mathematics of Diffusion, **1980**, *Oxford university press*

[19] T. Moore, Ph.D. thesis, *University of Texas Austin*, 2004

[20] S.Husain, Ph.D. thesis, *Georgia Institute of Technology*, 2005

CHAPTER 4

SOL-GEL-GRIGNARD TREATMENT

4.1 OVERVIEW

A facile three step sol-gel-precipitation process is used to synthesize $Mg(OH)_2$ nanowhiskers on micron-sized zeolite 5A particle surfaces at room temperature. The putative amorphous gelation product, $Mg(OH)_n(OR)_{2-n}$, forms first by a controlled hydrolysis and condensation reaction of magnesium isopropoxide and water, followed by precipitation to form $Mg(OH)_2$ structures on the zeolite surface. The optimum conditions for one dimensional $Mg(OH)_2$ whisker formation were found to be: 6 times the stoichiometric amount of water with1M HCl as the catalyst for the sol-gel reaction. The one-dimensional $Mg(OH)_2$ whiskers have an average diameter of 5-10 nm and length of 50-100 nm. The zeolite micropores are not affected by the $Mg(OH)_2$ whiskers formed on the surface. The surface roughened zeolite 5A, with a $Mg(OH)_2$ content of about 9.2 wt%, showed improved adhesion between the zeolite and the polymer in a mixed-matrix composite membrane.

4.2 THE ORIGINAL GRIGNARD TREATMENT

The original Grignard treatment was originally designed to introduce methyl groups on the zeolite surface, making the solid hydrophobic, via reaction with methylmagnesium bromide. However, it was serendipitously found that a significant coating of $Mg(OH)_2$ was deposited on the zeolite particles as a result of the aqueous

work-up used in the reaction. This $Mg(OH)_2$ cotaing resulted in a zeolite that adhered well to commercial polyetherimide used in membrane fabrication.

Subsequent investigation of the Grignard treatment method suggested that the process involved growing $Mg(OH)_2$ whiskers on the zeolite surface in two steps. First dealumination products comprising NaCl and $AlCl_3$ were formed by $SOCl_2$ treatment of the aluminosilicate, with the latter proposed to act as nucleation sites for creation of $Mg(OH)_2$ whiskers on the surface [7]. Then methylmagnesium bromide was added to the mixture, followed by quenching in isopropanol, as shown in Eq. 4.1, to form isopropoxide magnesium bromide [8, 9]. In previous reports, the $Mg(OH)_2$ was assumed to be formed by reaction between methylmagnesium bromide and H_2O, as shown by Eq. 4.2. However, complete elucidation of the reaction pathway has not been achieved, and the original synthesis is somewhat difficult to control.

$$2CH_3MgBr + 2(CH_3)_2CHOH \rightarrow 2CH_4 + MgBr_2 + Mg(OCH(CH_3)_2)_2 \quad (4.1)$$

$$2CH_3MgBr + 2H_2O \rightarrow 2CH_4 + MgBr_2 + Mg(OH)_2 \quad (4.2)$$

In this work, we have reconsidered the reaction pathway in light of what is known about sol-gel chemistry of magnesium alkoxides, such as the species shown in Eq. 4. 1. In addition, a streamlined, highly reproducible process has been developed that facilitates efficient coating of the zeolite crystals with $Mg(OH)_2$ nanostructures without the need for surface pretreatment.

4.3 SOL-GEL-GRIGNARD TREATMENT ON COMMERCIAL 5A PARTICLES

An efficient way to have the majority of Grignard reagent form $Mg(OH)_2$ is via first conversion of the Grignard to a magnesium alkoxide, followed by controlled hydrolysis and condensation of the magnesium sol, viz.,

Magnesium alkoxides have been widely used to synthesize $Mg(OH)_2$ and MgO with high surface area porous structures through sol-gel reactions, consisting of hydrolysis reactions (Eqs.4.3, 4.4) and condensation reactions (Eqs. 4.5, 4.6) [10-14]. It is known that there are two critical factors affecting the sol-gel products: (i) the amount of water and (ii) the pH of the reactions. In the present work, a sol-gel-precipitation method is used to synthesize $Mg(OH)_2$ whiskers on zeolite LTA surfaces, and the whisker morphology is controlled by the sol-gel reaction conditions via manipulation of the amount of water and the pH.

$$Mg(OCH(CH_3)_2)_2 + H_2O \rightleftarrows HOMgOCH(CH_3)_2 + (CH_3)_2CHOH \quad (4.3)$$

$$HOMgOCH(CH_3)_2 + H_2O \rightleftarrows HOMgOH + (CH_3)_2CHOH \quad (4.4)$$

$$-MgOCH(CH_3)_2 + -MgOH \rightleftarrows -MgOMg- + (CH_3)_2CHOH \quad (4.5)$$

$$-MgOH + -MgOH \rightleftarrows -MgOMg- + H_2O \quad (4.6)$$

4.3.1 Effect of magnesium/water ratio and pH on sol-gel $Mg(OH)_2$ morphology

The most important parameter for the sol-gel reaction is the amount of water used, which determines the extent of the hydrolysis and condensation reactions involving the Grignard reagent. The stoichiometric amount of water needed to react with magnesium isopropoxide was calculated according to Eq. 4.7. The amount of magnesium isopropoxide generated by methylmagnesium bromide, as shown in Eq. 4.1, in each vial is 0.005 moles (total of 0.015 mol, separated into 3 vials). One stoichiometric (denoted as 1S) amount of water to react with the magnesium isopropoxide according to Eq. 4.7 is 0.18 grams.

$$Mg(OCH(CH_3)_2)_2 + 2H_2O \rightleftarrows Mg(OH)_2 + 2(CH_3)_2CHOH \quad (4.7)$$

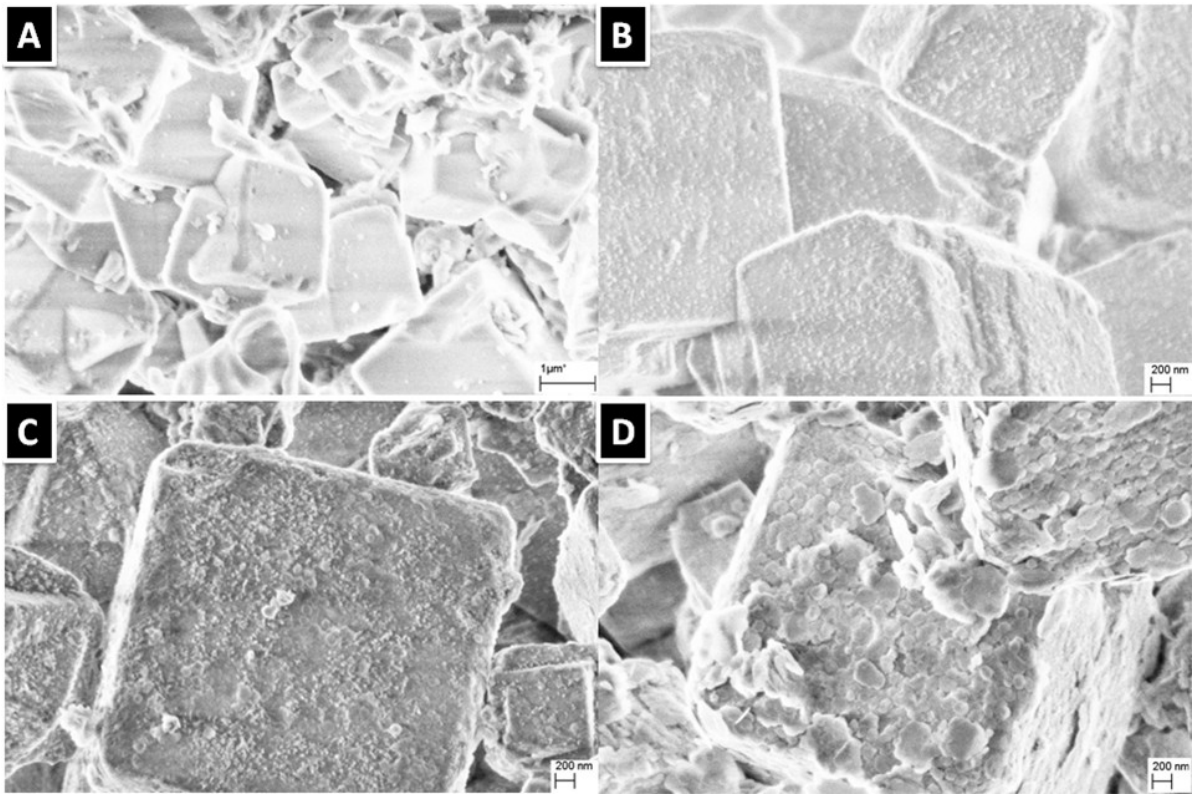

Figure 4.1 Different morphologies of $Mg(OH)_2$ formed by adding various amounts of water to the reaction (pH = 7.0): A, B, C, D have two, four, six and eight times stoichiometric amount of water

Research showed that hydrolysis reactions of magnesium alkoxides are equilibrium reactions, and the amount of $Mg(OH)_2$ generated depends on the reaction extent [10, 13]. Fig.4.1 shows the final $Mg(OH)_2$ morphology on a zeolite 5A surface after treatments with different amount of added water. Treatment with 2S amount of water showed bare zeolite 5A surfaces. This is likely because the hydrolysis reaction (Eq. 4.7) does not proceed to a large extent under these conditions, and the magnesium isopropoxide remains largely unreacted. The zeolite and sol-gel product mixture was later washed several times using de-ionized water to remove the water soluble reaction products. During the water washing steps, the water soluble magnesium isopropoxide is washed away and little solid forms on the zeolite surfaces. Therefore, during the water

washing step, the remaining magnesium isopropoxide does not hydrolyze and form $Mg(OH)_2$ to any appreciable extent. This supposition is consistent with visual observation of the reaction filtrate, which remained clear for an extended period of time and only became cloudy after a few weeks. It is reported that the presence of toluene significantly accelerates the hydrolysis reaction and gelation process of magnesium alkoxides [10], so the hydrolysis reactions start when water is added into the dispersion of magnesium isopropoxide /toluene /isopropanol. This hypothesis is further verified by the later discussion.

When the amount of water is 4S to 6S, $Mg(OH)_2$ solids in the form of short whiskers begin to form on the zeolite surfaces. This is likely because $Mg(OH)_n(OR)_{2-n}$ ($0<n<2$) species are formed as hydrolysis products, and these species are partially insoluble in water, precipitating onto the zeolite surfaces during the water washing step. As the water amount is increased, more water insoluble hydrolysis product is generated and these precipitate onto the zeolite surfaces. As shown in Fig. 4.1, more plate like $Mg(OH)_2$ is formed on the zeolite surfaces at 8S of water addition. With water addition in excess of 12S, the milky dispersion begins to phase separate into a clear top layer and white, cloudy, bottom layer. It can be concluded that at pH=7, only short whiskers or flakes can be generated after addition of varying amounts of water.

It is well known that reaction pH can affect the morphology of sol-gel products. Under acidic conditions, the hydrolysis reactions are promoted, condensation reactions are depressed, and one dimensional structures, such as nanoparticles, whiskers *etc.*, can be generated [16]. In the well studied sol-gel silicate case, acid-catalyzed hydrolysis with low H_2O:Si ratios produces weakly branched ‘‘polymeric’’ sols, whereas base-catalyzed

hydrolysis with large H_2O:Si ratios produces highly condensed ‘‘particulate’’ sols. To our knowledge, there has been no relevant research on the pH effects on $Mg(OH)_2$ morphologies using the sol-gel method.

In this work, the pH of the water was controlled by making 1 M (pH=0) and0.1 M (pH=1) HCl solutions. The acid solutions were added to the sol dispersion replacing the pure de-ionized water that was used in the base case. The other steps were performed exactly the same.

Fig. 4.2 shows the different morphologies of $Mg(OH)_2$ whiskers on the zeolite surfaces after treatments with water additions of different pH. Longer whiskers were formed in the more acidic environment. The whiskers from treatment at pH=1 appeared to be longer than those formed under neutral condition (pH=7). The $Mg(OH)_2$ content was about 3.0 wt% of the total solid, as shown in table 4.1. The whiskers from treatment at pH=0 were even longer and interlocked. The $Mg(OH)_2$ content was about 9.2 wt% of the total solid. These interconnected whisker structures may provide more stable chain polymer chain entanglement in composite films, as discussed below. The density of the whiskers on the zeolite surface was not evaluated exactly, but there seems to be no dramatic difference between the different treatments, judged by SEM images. The whisker density may be controlled by the density of nucleating sites on the zeolite surface, which is determined by the surface properties of the molecular sieve.

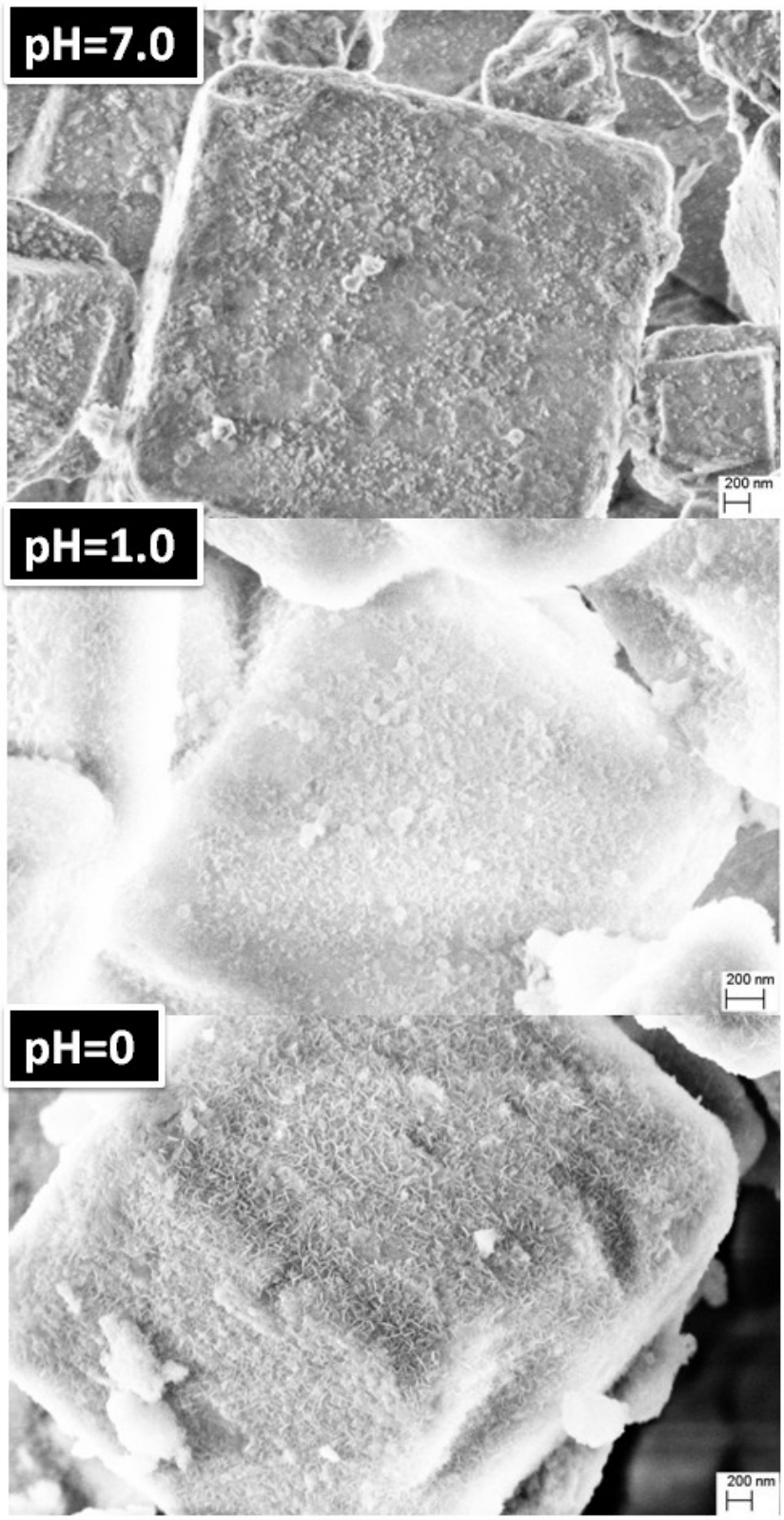

Figure 4.2 Different morphologies of $Mg(OH)_2$ formed on zeolite 5A surfaces by adding six times the stoichiometric amount of water at various pHs

Table 4.1 Elemental composition of different 5A particles by EDS measurement

	Atomic percentage %					
	O	Na	Mg	Al	Si	Ca
Bare 5A	54.3	4.9		16.0	16.8	8.1
GT-5A (6S H2O, pH=7.0)	63.7	3.2	0.4	13.6	13.8	5.4
GT-5A (6S H2O, pH=1.0)	65.9	2.8	1.1	12.3	12.2	5.4
GT-5A (6S H2O, pH= 0)	61.9	3.5	3.3	13.2	12.4	5.8

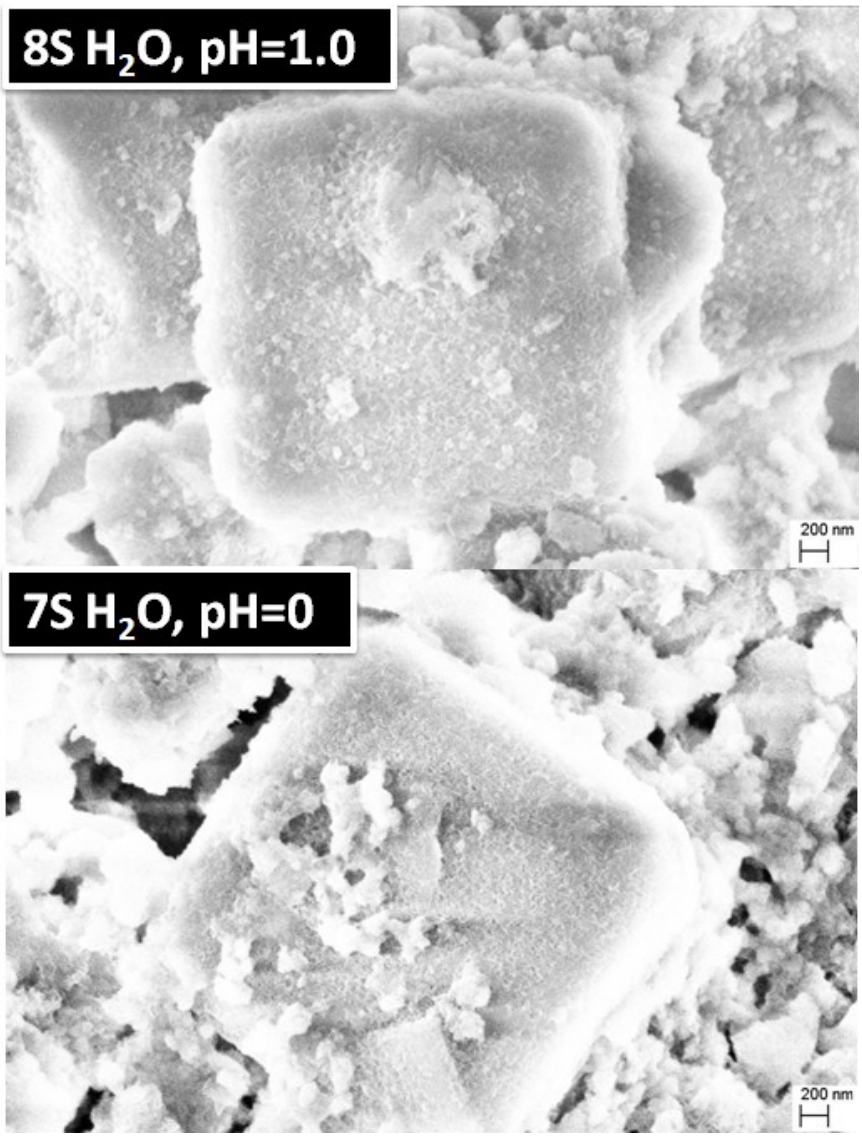

Figure 4.3 Independently formed $Mg(OH)_2$ after over amount of water addition

Fig. 4.3 shows the $Mg(OH)_2$ morphologies prepared via addition of water more than 6S equivalents. In these cases, free $Mg(OH)_2$ particles appear to have formed in solution and then deposited on the zeolite surfaces. This is likely due to homogeneous nucleation at higher hydrolysis levels.

4.3.2 Magnesium sol formation

Fig.4.4 shows the images of LTA zeolites at various stages of the $Mg(OH)_2$ functionalization process at different stages of the process under a fixed set of conditions (6S H_2O, pH=0). After quenching the methylmagnesium bromide with isopropanol, it is well known that magnesium bromide and magnesium isopropoxide are formed [8, 9]. Smooth zeolite surfaces were observed after this step. After water addition, an amorphous product on zeolite surface was observed, but no whisker morphology appeared present on the zeolite surface. After the first water wash, the zeolite surfaces were found to be covered by thick layer of sol-gel product. After three water washes, only $Mg(OH)_2$ whiskers were observed on the zeolite surfaces.

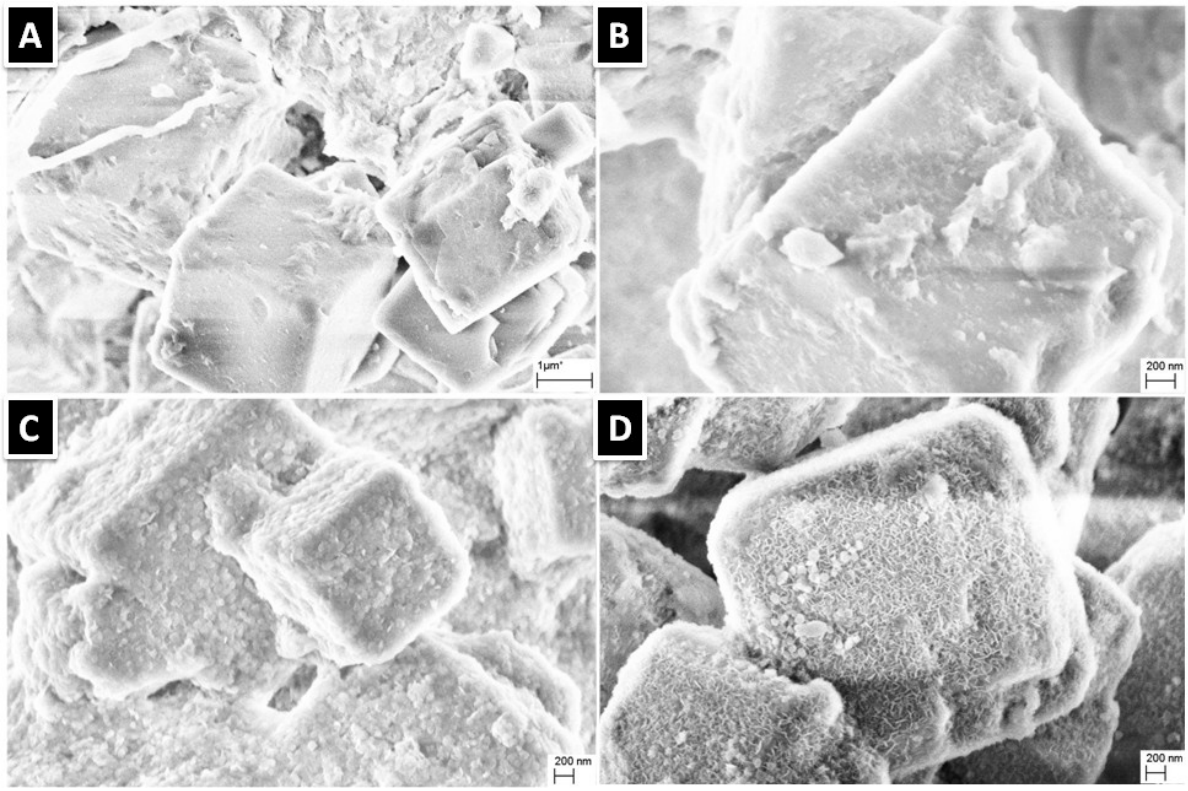

Figure 4.4 Morphology development at different stages of treatment (6S H2O, pH=0): A, zeolite in magnesium sol (after IPA quenching); B, zeolite in the magnesium sol-gel (after water addition); C, zeolite in with precipitated sol-gel (after one water wash); D, zeolite with precipitated sol-gel (after three water washes).

To better understand the process, the same treatment without addition of zeolite was performed, the products were collected by centrifuge analyzed by XRD (results shown in Fig. 4.5). The solid (precursor) separated from the magnesium sol in toluene/IPA, consisting of magnesium bromide and magnesium isopropoxide, showed a clear crystal pattern. After adding water to toluene/IPA dispersed sol, the sol-gel reactions started and the solid (sol-gel) was centrifuged out from the sol-gel dispersion. The crystalline pattern disappeared, consistent with the amorphous morphology suggested in Fig. 4.4. The hydrolysis and condensation reactions started after water was added, and the intermediate products can associate into polymer-like gels by –Mg-O-Mg-

bonding or hydrogen bonding between -Mg-OH groups [10], as shown in Fig. 4.6. Indeed, after addition of 5S of water, the gel formation was inferred by an increase of viscosity.

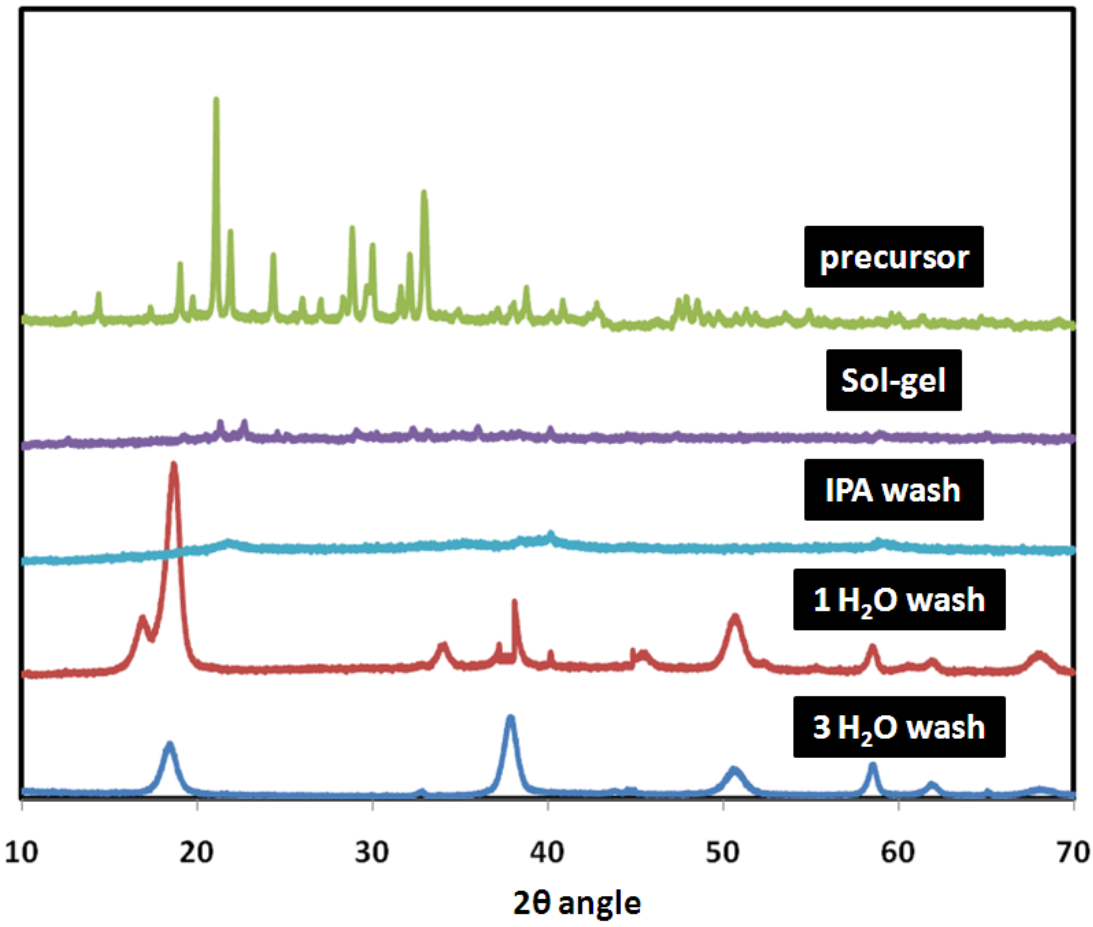

Figure 4.5 XRD patterns of sol-gel products at different steps of treatment

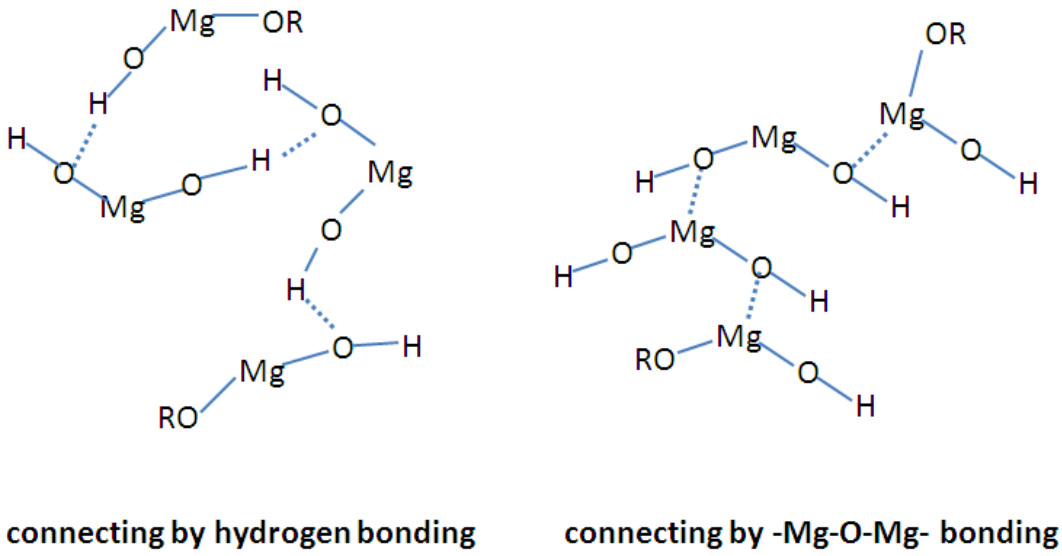

Figure 4.6 Examples of polymer like interconnected gel structures formed by hydrolysis and condensation reactions, -OR stands for the unhydrolyzed isopropoxyl group

Although there should be an equimolar amount of magnesium bromide and magnesium isopropoxide after the isopropanol quenching step, no strong $MgBr_2$ peaks were observed in the XRD pattern after the water addition step. This is probably because the $MgBr_2$ salt is strongly associated into the gel structure shown in Fig. 4.6, together with water. In the real situation, the polymer structures are probably surrounded not only by toluene and isopropanol solvent, but possibly by water and hydrated ions of Mg^{2+}, Br^-. It has been reported that the soluble salts are typically homogeneously dispersed in the sols to give well dispersed mixture products [16]. It is unknown whether the presence of $MgBr_2$ salts is this work affected the reactions of magnesium isopropoxide and the magnesium hydroxide precipitation process.The XRD pattern of the gel displayed little crystallinity. During the isopropanol wash that was used to remove the toluene from the sol-gel product, the amorphous nature of sol-gel product did not change. When the isopropanol phase was replaced by water, however, the collected sol-gel product showed

a clear crystalline pattern associated mainly with $Mg(OH)_2$, and small amount of other impurities, most probably $MgBr_2$. After three times of water washes assisted by sonication, only the strong $Mg(OH)_2$ pattern was observed. This agrees with images in Fig. 4.4 that suggest that most of the $MgBr_2$ and deposited particles were removed after three sonication and water washes. The conductivity of supernatant water for the first three water washes drops from few thousand to about 100 $\mu S \cdot m^{-1}$, which is probably due to the $MgBr_2$ being washed off. The originally embedded $MgBr_2$ diffusing out into the water solution may also affect the $Mg(OH)_2$ whisker morphology, but more research is needed to understand the process.

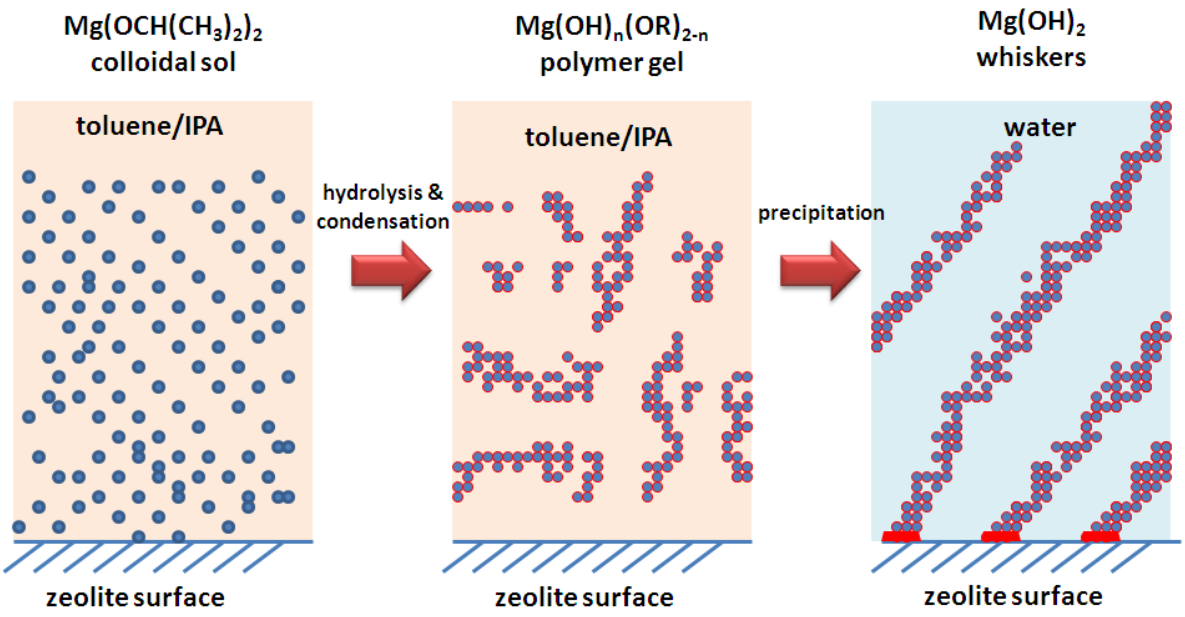

Figure 4.7 Morphology evolutions from magnesium alkoxide to magnesium hydroxide, during the sol-gel precipitation steps

It can be concluded that the $Mg(OH)_2$ whiskers were formed by a sol-gel-precipitation mechanism, as shown in Fig. 4.7. The magnesium isopropoxide sol first reacted with water and was transformed into a polymerlike amorphous gel. The amorphous gel, made of $Mg(OH)_n(OR)_{2-n}$ then precipitated onto the zeolite surfaces because of its limited solubility in water. The uncompleted hydrolysis reaction was completed and $Mg(OH)_2$ was generated with the abundant water washing.

4.3.3 $Mg(OH)_2$ precipitation

It appears the gel precipitated preferentially onto the zeolite surfaces, rather than forming homogeneous particles in solution. This suggests the zeolite surface provided heterogeneous nucleating sites. There is typically a high concentration of hydroxyl groups on zeolite surfaces [17]. Methylmagnesium bromide may react with the surface hydroxyl groups as shown in Eq. 4.8 [18]. Si-O-Mg- bonds can also be generated by condensation reactions, as shown by Eq. 4.9, between silanol groups and hydrolysis product of magnesium alkoxides [19]. Both of these routes leading to –Si-O-Mg- bonding could provide nucleating sites for $Mg(OH)_2$ precipitation and the potential for covalent bonding between the zeolite and $Mg(OH)_2$ structures. Additional research will be required to elucidate the true mechanism.

$$-Si-OH + CH_3MgBr \rightarrow -Si-O-MgBr + CH_4 \qquad (4.8)$$

$$-Si-OH + Mg(OR)(OH) \rightleftarrows -Si-O-Mg-OH + ROH \qquad (4.9)$$

4.4 SOL-GEL VS. GRIGNARD TREATMENT

From the discussion above, it can be suggested that two requirements are important in the formation of $Mg(OH)_2$ whiskers: (i) an appropriate amount of water, and (ii) an acidic catalyst in the sol-gel reactions. $Mg(OH)_2$ whiskers formed on zeolite LTA

were reported previously using the same chemical reagents. The two requirements were also met to some extent in the original synthesis [4].

In the original Grignard treatment, highly acidic AlClx species were generated by dealumination using the $SOCl_2$ reagent [7]. The AlClx can act as an acidic catalyst for the sol-gel reactions. It was also reported that without the $SOCl_2$ treatment [4], $Mg(OH)_2$ was also formed on the zeolite surfaces, but without a whisker morphology. This is similar to the treatment with pH=7 water addition in this work.

The amount of water needed for formation of an "ideal" morphology appears to be 6S, or 6.48 g on the scale used here. This large amount of water is hard to be carried in through the 80 ml of 99.5% purity isopropanol during the quenching reaction, as hypothesized in previous work. In the Grignard treatment setup [20], the reaction apparatus was connected to a water bubbler to monitor the CH_4 gas releasing reaction, as shown in Eq. 4.1. Because the quenching reaction is highly exothermic, the temperature of apparatus can reach high temperature after the reaction. When the reactor cooled down, the water in bubbler can be sucked back into the reaction flask in an uncontrolled manner. The water from backflow probably initiated the sol-gel reactions in a similar way as in this work.

It is highly possible the unknown $Mg(OH)_2$ formation mechanism in the Grignard treatment by former researchers [4] is through the same sol-gel-precipitation mechanism. Dealumination by $SOCl_2$ generated acidity species AlClx to catalyze the sol-gel reaction. Water comes in probably through backflow into the reactor unexpectedly.

4.5 POLYMER ZEOLITE ADHESION ENHANCEMENT

It has been reported that the $Mg(OH)_2$ nanowhiskers on zeolite surfaces may provide molecular scale interlocking interactions with polymer chains and enhance the adhesion between the zeolite and polymer [4]. The adhesion enhancement in this work was evaluated by butane isomer permeation tests using mixed matrix membranes containing treated 5A zeolite particles.

Zeolite 5A has pores that allow n-butane to pass through but totally block the passage of i-butane, *i.e.,* show effectively infinite selectivity for the normal butane isomer [20]. By adding zeolite 5A into polymeric membranes, the butane isomer performance should be enhanced if the zeolite and polymer are properly adhered. To check for the possibility for permeation of n-butane in zeolite 5A before and after the magnesium treatment, sorption measurements were performed and the results are shown in Fig. 4.8. The n-butane sorption capacity was not changed by treatment under the different conditions. The i-butane adsorbs to essentially no extent in all the samples. Therefore, the micropores of the zeolite were not affected by the acidic water added in the treatments. The ratio between HCl and magnesium isopropoxide was about 1:5, under the 6S water addition conditions, pH=0. The stability of the zeolite framework was good, as confirmed by the only small change of in the gas sorption capacity on the sorption measurement.

A defective interface (so called 'sieve-in-a-cage' morphology) was formed when bare zeolite 5A was added into the 6FDA-DAM polymer, as shown in Fig. 4.9. Gas molecules can bypass the zeolite through the defective interfaces. Pinholes can be generated if voids are interconnected in extreme cases. The treated zeolite with the most whisker-like $Mg(OH)_2$ morphology were those treated with 6S water addition, at pH=0

(Fig. 10). In the mixed matrix membrane containing the treated zeolite, the zeolite-polymer interfacial adhesion was improved significantly.

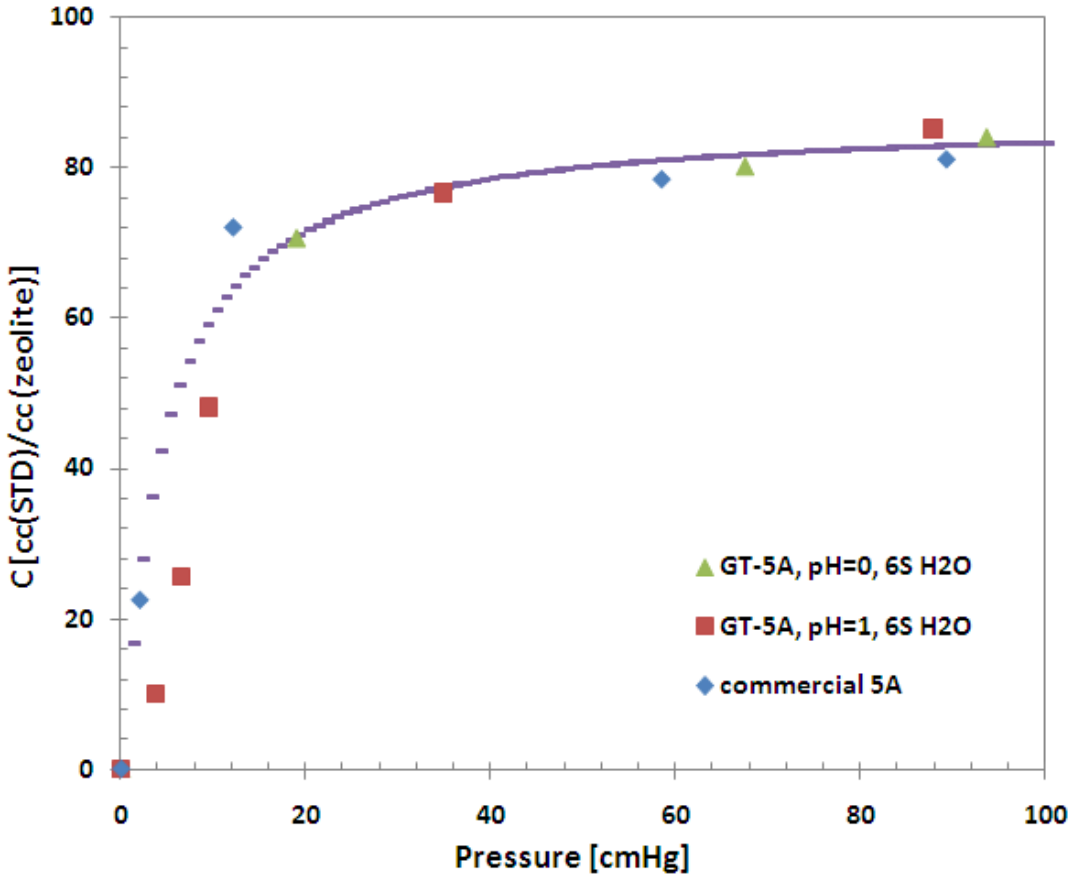

Figure 4.8 Sorption isotherm of n-butane in bare and treated 5A samples, at 50 °C. The points are from experimental results, the line is a Langmuir fitting

The permeation results for these membranes are shown in table 4.2. The mixed matrix membrane containing bare 5A had increased n-butane permeability, but the butane isomer selectivity was far lower than that in pure polymer. This is possibly due to pinholes generated by the defective interfaces. In the mixed matrix membrane containing treated zeolite 5A, the butane isomer selectivity increased about 24% due to the addition of i-butane blocking 5A particles. The n-butane permeability was not increased because

the rates of n-butane diffusion were about the same in the 6FDA-DAM polymer and zeolite 5A, which will be discussed in a separate paper. The selectivity enhancement in the mixed matrix membrane confirms the good adhesion suggested by the SEM images.

Table 4.2 Permeability and selectivity of C4s in polymeric and mixed matrix membranes, 100 °C, 25 psi at upstream, GT-5A is done with condition: pH=0, 6S water

	Permeability nC4 [Barrer]	Selectivity nC4/iC4 [-]
6FDA-DAM (WQ0912)	3.2 ± 0.2	21 ± 2
25wt%-bare 5A-6FDA-DAM	4.5 ± 0.3	2.5 ± 0.3
25wt%-GT-5A -6FDA-DAM	3.3 ± 0.2	25 ± 2

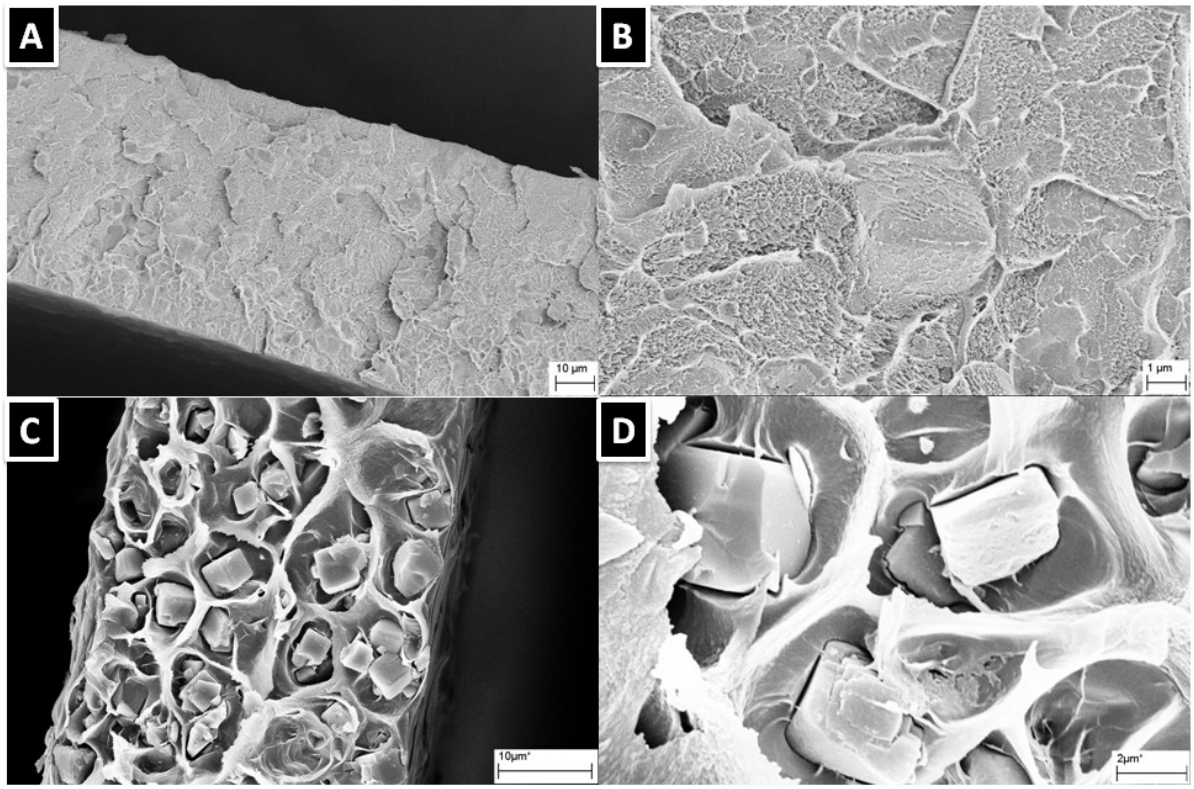

Figure 4.9 Cross section of mixed matrix films containing 6FDA-DAM polymer and 25wt% treated (6S water, pH=0) 5A (A, B) and bare 5A (C, D)

4.6 CONCLUSIONS

The three step sol-gel-precipitation treatment developed based on knowledge of the probable mechanism of $Mg(OH)_2$ formation on the zeolite surface successfully resulted in magnesium hydroxide nanowhisker functionalized zeolite 5A. Magnesium isopropoxide, the precursor for the sol-gel reaction, was formed by quenching the methylmagnesium bromide with isopropanol. After controlled water addition, the hydrolysis and condensation reactions started, and gelation occurred. The amorphous polymer-like $Mg(OH)_n(OR)_{2-n}$ then precipitates out of the water solution and onto the zeolite surfaces, because of its limited solubility. The amount of added water determined the extent of the hydrolysis reactions, and the composition of $Mg(OH)_n(OR)_{2-n}$ formed. When water was not added, $Mg(OH)_n(OR)_{2-n}$ was largely $Mg(OR)_2$, and nothing was formed on the zeolite surface, because the water soluble $Mg(OR)_2$ was washed away. When more water was added, $Mg(OH)_n(OR)_{2-n}$ trends closer to $Mg(OH)_2$ in composition and tended to precipitate out of the water solution. The amount of $Mg(OH)_2$ formed was controlled by the hydrolysis extent via the amount of water added. The addition HCl affected the hydrolysis and condensation reactions, and the structure of polymer gels formed. The high surface area whisker morphology was formed using acidic water for the sol-gel reactions. The formation of $Mg(OH)_2$ whiskers on the zeolite surfaces showed little effect on the microporosity of the zeolite 5A. The $Mg(OH)_2$ whiskers on the zeolite surfaces helped the interfacial adhesion between the zeolite and polymer, possibly by providing more surface area for entanglement of the polymer chains.

Figure 4.10 $Mg(OH)_2$ whiskers formed on 5A surfaces at treatment condition: 6 times of stoichiometric amount of water, pH = 0

4.7 REFERENCES

[1] W.J. Koros, *J. Membrane Sci.*, **2000**, 175 181-196

[2] R. Mahajan, *J. Appl. Polym. Sci.*, **2000**, 86 881-890

[3] T. Moore, *J. Mol. Struct.*, **2005**,739 87-98

[4] S. Shu, *Chem. Mater.*, **2007**, 19 4000-4006

[5] S. Shu, *J. Phys. Chem. C*, **2007**, 111 652-657

[6] S. Husain, *J. Membrane Sci.*, **2007**, 288, 195-207

[7] S. Shu, *Ind. Eng. Chem. Res.*, **2007**, 46 767–772

[8] L. F. Fieser, *Organic Chemistry*, Reinhold, New York, **1956**

[9] P. Y. Bruice, *Organic Chemistry*, Pearson Prentice Hall, New Jersey, **2007**

[10] Y. Diao, *Chem. Mater.,* **2002**, 14, 362-368

[11] S. Utamapanya, *Chem. Mater.,* **1991,** 3, 175-181

[12] V. Stengl, *Mater. Lett.*, **2003**, 57, 3998-4003

[13] T. Lopez, *J. Catal.*, **1991**, 127, 75-85

[14] L. F. Francis, *Mater. Manuf. Process*, **1997**, 12, 963-1015

[15] J. Liu, *J. Membrane Sci.*, **2009**, 343, 157-163

[16] C. J. Brinker, *Sol-Gel Science*, Academic Press, Inc. **1990**

[17] J.W. Ward, *J. Catal.*, **1967**, 9, 225-236

[18] M. Sato, *J. Catal.*, **1967**, 7, 342-351

[19] J. G. Yoon, *Appl. Phys. Lett.,* **1995**, 66, 2661-2663

[20] S. Shu, Ph.D. thesis, *Georgia Institute of Technology*, **2007**

CHAPTER 5

EFFECT OF ZEOLITE SURFACE ACIDITY ON SOL-GEL-GRIGNARD TREATMENT

5.1 OVERVIEW

The sol-gel-Grignard treatment was extended to lab-made 5A particles. $Mg(OH)_2$ flakes generated at pH higher than 1.0, changed to homogeneous $Mg(OH)_2$ whiskers at pH=0 during the treatment on lab made 5A particles. The homogeneously formed $Mg(OH)_2$ was probably due to the lack of nucleating sites on lab-made 5A surfaces. The three possible nucleating sites can be: 1) hydroxyl groups on zeolite surface (hydroxyl groups can be removed by dehydroxylation reaction during 550 °C calcination step for lab-made 5A); 2) nucleating sites produced from the commercial synthesis procedures, such as unreacted reagent not washed off after zeolite synthesis (water washing steps were repeated 5-10 times during the lab-made 5A synthesis), and defective sites (less defective sites using the template method during lab-made 5A synthesis). The similar treatment result on calcined and uncalcined lab-made 5A, which are dramatically different from that on commercial 5A, suggests less possibility of hydroxyl groups as the nucleating sites. It is highly possible the $Mg(OH)_2$ whiskers are generated on the second class of nucleating sites, which are insufficient on lab-made 5A particles. In light of the acid catalyzed sol-gel mechanism and dealumination promoted whisker formation discovered previously, a kind of acidic nucleating sites is introduced to lab-made 5A surfaces through two methods: 1) $AlCl_3$ generated on 5A surfaces through dealumination reactions; 2) $AlCl_3$ anchored to the zeolite surfaces. The dealumination treatment was less

effective on lab-made 5A to promote $Mg(OH)_2$ whisker formation, on the other hand, the gas transport properties of the lab-made 5A sieve were more adversely affected. The dramatic reduction of gas sorption capacity and molecular diffusion rate indicates the severe disruption of 5A crystals by the dealumination treatment. An external source of $AlCl_3$ was then used to anchor to the zeolite 5A surfaces. The amount of $AlCl_3$, therefore, can be easily controlled compared to the dealumination method. The 5A crystal structure is less affected by the outer layer of $AlCl_3$ (later hydrolyzed to $Al(OH)_3$) compared to the dealumination method. The amount and morphology of $Mg(OH)_2$ can be controlled by the amount of heterogeneous acidic sol-gel catalyst $AlCl_3$, which is anchored to the zeolite surface. Unfortunately, the treated 5A particles show an undesirable three layer structure: $Mg(OH)_2$ whiskers grow on $Al(OH)_3$ layer (from $AlCl_3$ hydrolysis), which is on top of the zeolite surface. When the tri-layer treated 5A particles are added to polymer matrix, good adhesion was apparent through the highly whiskered surface, which is observed by SEM. This fact notwithstanding, C4s permeation test on these mixed matrix membranes shows a typical ‘‘sieve-in-a-cage’’ phenomenon, *i.e.*, a huge increase of permeability and an unchanged or decreased selectivity. This is probably caused by the additional $Al(OH)_3$ layer generated by the $AlCl_3$ hydrolysis reaction. The gas molecules can bypass the zeolite through this presumably porous $Al(OH)_3$ layer. Less amount of $AlCl_3$ was tried in order to introduce a thinner $Al(OH)_3$ layer, but the decrease of acidity sites from $AlCl_3$ leads to insufficient $Mg(OH)_2$ whisker formation.

In summary, the sol-gel treatment on commercial 5A, with acidic catalyst of HCl and dealuminated AlClx species showed good results. The sol-gel-Grignard treatment is less effective on lab-made 5A, with acidic catalyst of HCl and dealuminated AlClx

species. Tri-layer structure ($Mg(OH)_2$ whisker-$Al(OH)_3$-Zeolite) is formed on both commercial and lab-made 5A by the Sol-gel-Grignard treatment, with acidic catalyst of anchored $AlCl_3$. The acidic catalysts have profound influence on the Sol-gel-Grignard treatment, and more thorough effort is needed on this aspect.

5.2 SOL-GEL-GRIGNARD TREATMENT USING HCL ACID AS CATALYST

Desired $Mg(OH)_2$ morphologies are formed on commercial 5A particles using a sol-gel-Grignard method, using HCl as the acidic catalyst, as shown in chapter 4. The same treatment was performed on the lab-made 5A particles, in the hope of treating nanometer lab-made 5A particles for mixed matrix hollow fiber spinning.

As shown in Fig. 5.1, $Mg(OH)_2$ flakes are formed on lab-made 5A surfaces at higher pH regions, which is similar to that on commercial 5A particles. The $Mg(OH)_2$ flakes turn to a whisker morphology at pH=0. The amount of water addition was adjusted to control the $Mg(OH)_2$ morphology. At lower amount of water addition (4S, 5S), the majority of 5A particle surfaces are not roughened probably due to the less amount of $Mg(OH)_2$ formed by the sol-gel method at lower hydrolysis extent. When the amount of water addition increases to 6S, majority of $Mg(OH)_2$ is formed independent of zeolite surfaces, which was probably due to a lack of nucleating sites on the lab-made 5A surfaces. The homogenous nucleation was preferred because the amount of heterogeneous nucleating site was insufficient. Compared to the successful $Mg(OH)_2$ formation on the commercial 5A particles, the sol-gel-Grignard treatment was less effective on the lab-made 5A particles using HCl acid as catalyst.

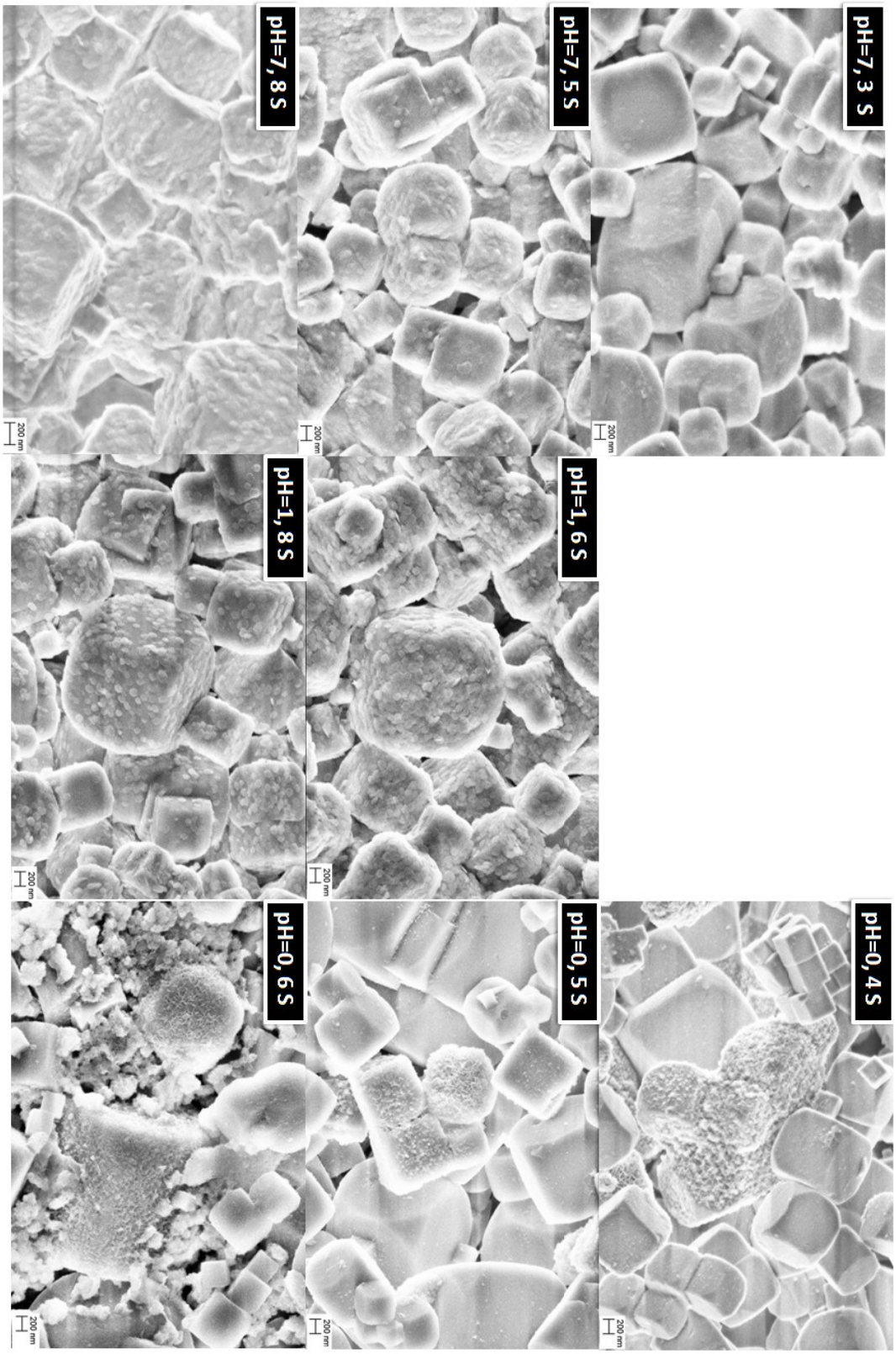

Figure 5.1 $Mg(OH)_2$ morphologies formed by the Sol-gel-Grignard treatment on lab-made 5A particles at various pH and amounts of water addition

The difference between the surface properties of commercial and lab-made 5A particles presumably causes the different morphologies of $Mg(OH)_2$ formed by the Sol-gel-Grignard treatment. The tendency of homogeneous formation of $Mg(OH)_2$ whiskers is presumably due to the lack of nucleating sites on the lab-made 5A surfaces. As noted earlier, the three possible nucleating sites can be: 1) hydroxyl groups on zeolite surface (hydroxyl groups can be removed by dehydroxylation reaction during 550 °C calcination step for lab-made 5A); 2) nucleating sites produced from the commercial synthesis procedures, such as unreacted reagent not washed off after zeolite synthesis (water washing steps were repeated 5-10 times during the lab-made 5A synthesis), and defect sites (less defect sites using the template method during lab-made 5A synthesis).

It is reported that abundant hydroxyl groups exist on zeolite surfaces [1]. As shown in chapter 4, the $Mg(OH)_2$ whiskers is probably chemically bonded to the zeolite surfaces through the surface hydroxyl groups. The -Si-O-Mg-OH chemical bonding can provide the sites for $Mg(OH)_2$ whiskers to continue to grow upon. The adjacent hydroxyl groups can be removed by thermal dehydroxylation reaction during calcinations steps to remove the organic template. A hydrophobic surface is generated and rehydroxylation is kinetically slow after calcination above 450 °C [2]. The commercial 5A particle is labeled as undried (synthesized using a template-free method, no need for calcination), no other calcinations information is available. The lab-made 5A particle is calcined at 550 °C for 10 hrs (in order to remove the template used for zeolite synthesis) after synthesis. There is an expected concentration difference of hydroxyl groups between the undried commercial particles and the calcined lab-made particles.

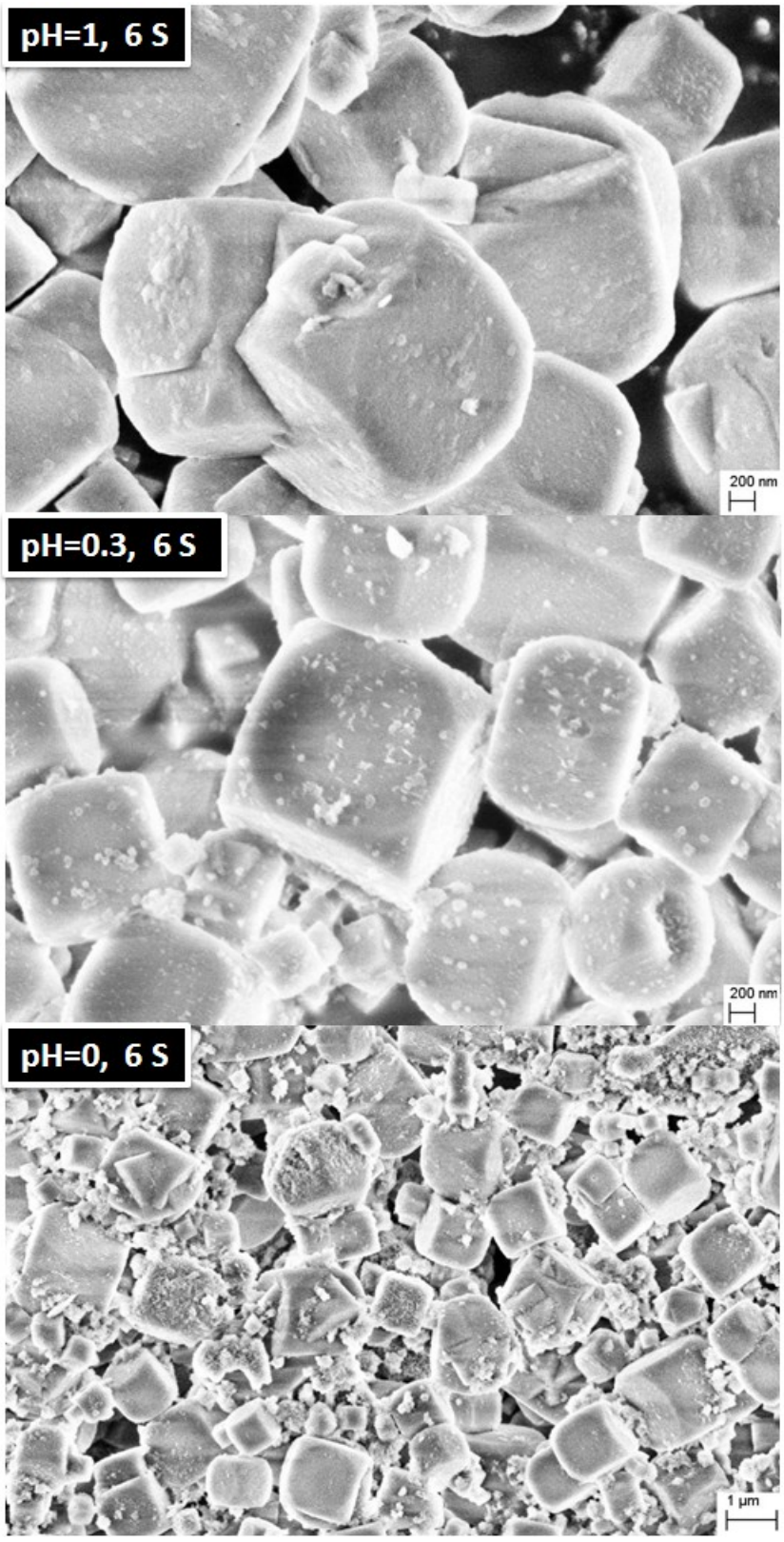

Figure 5.2 $Mg(OH)_2$ morphologies formed on the uncalcined lab-made 5A particles at various conditions

In order to verify the possibility of surface hydroxyl groups as the nucleating sites, uncalcined lab-made 5A particles were used, intended to have a similar concentration of surface hydroxyl groups as that in the undried commercial 5A particles. The morphologies of $Mg(OH)_2$ formed on the uncalcined lab-made 5A particles, as shown in Fig. 5.2 are similar to that on the calcined lab-made 5A particles, and different from that on commercial undried 5A particles. The difference of hydroxyl group concentration cannot explain the different $Mg(OH)_2$ morphologies formed on commercial and lab-made 5A particles.

In order to check the effectiveness of the Sol-gel-Grignard treatment on other zeolites, high silica MFI particle was treated using the standard procedures. The results are shown in Fig. 5.3. Under all acidic conditions (pH from 7.0 to 0), $Mg(OH)_2$ always forms in flake morphology. The different $Mg(OH)_2$ morphologies on MFI, lab-made 5A (calcined and uncalcined), commercial 5A after the Sol-gel-Grignard treatment can be summarized into table 5.1. During the treatment on lab-made and commercial 5A, $Mg(OH)_2$ flakes turns to whisker morphologies at more acidic conditions. The conclusion may be drawn that more acidic conditions lead to more whisker morphology.

Table 5.1 Summary of different $Mg(OH)_2$ morphologies formed on different surfaces at 6S water addition

	pH=7	pH=1	pH=0
Commercial 5A	Short whisker + flake	Short whisker	Long whisker
Lab-made 5A	flake	flake	Independent whisker
Lab-made MFI	flake	flake	flake

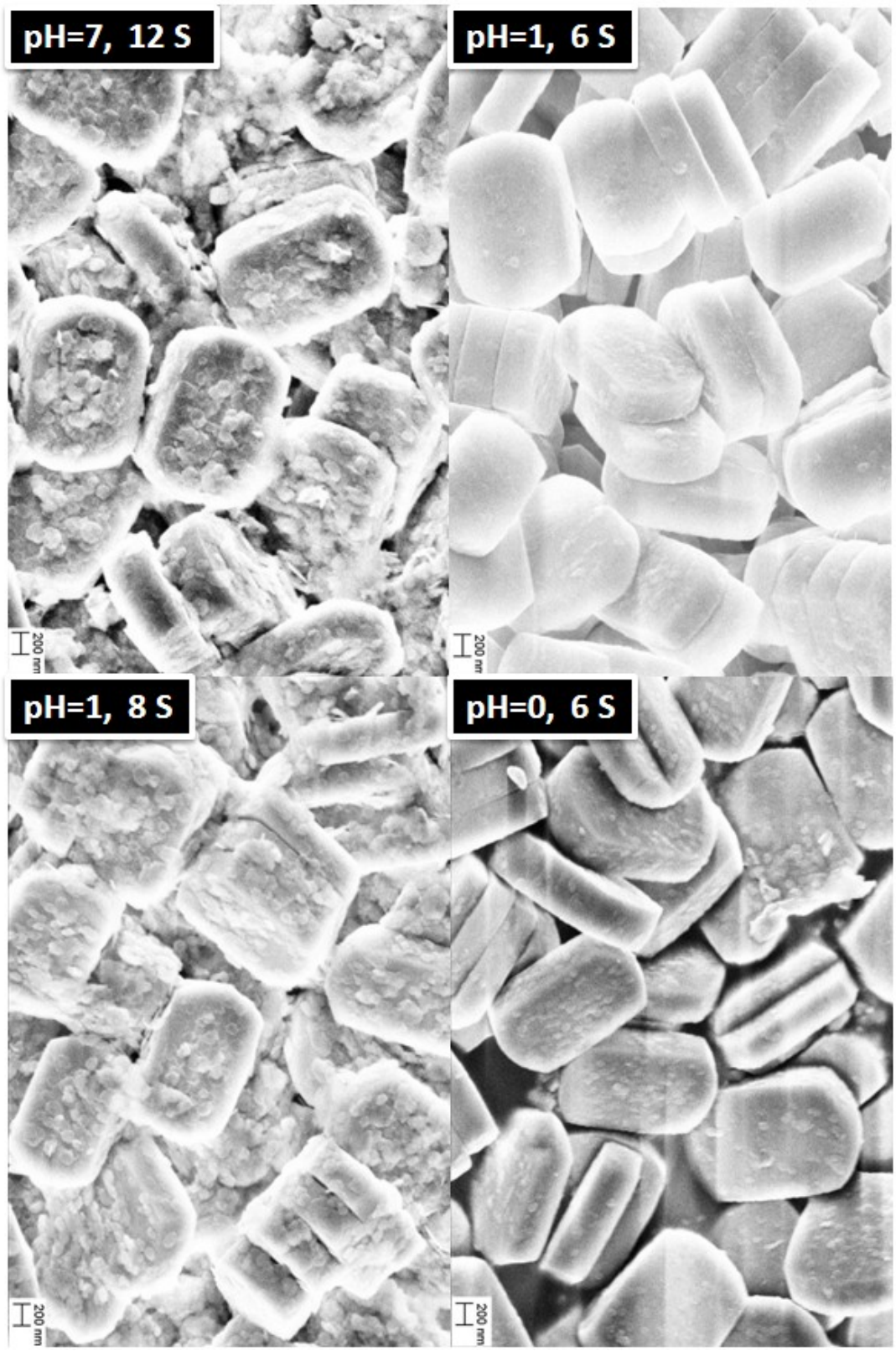

Figure 5.3 $Mg(OH)_2$ morphologies formed on the calcined lab-made MFI particles at various conditions

The acidic conditions promote the one dimensional whisker formation as shown in the treatment results on different zeolite particles. The acidity can come from two contributions: one is the HCl acid introduced, and the second one can be the acidity from zeolite, which is well known for their acidic properties in catalysis applications [3]. Since the same amount of HCl acid is introduced during the standard Sol-gel-Grignard treatment, it can be hypothesized that the different acidity of zeolite contributed to the difference of overall acidity, which leads to different $Mg(OH)_2$ morphologies. The order of acidity is commercial 5A > lab-made 5A > lab-made MFI, based on the degree of whiskered morphologies of $Mg(OH)_2$ formed. It is generally known that the structural Al in the LTA zeolite contributed to the acidity, therefore, the 5A is considered more acidic than MFI particles (no structural Al) [4]. It is unknown what factor contributed to the acidity difference between commercial and lab-made 5A particles. There can be a couple of hypotheses as shown earlier. The unwashed reagent for zeolite synthesis, or defects generated from template-free synthesis method on commercial 5A can contribute to the higher acidity than that of lab-made 5A particles. More investigation is needed on this aspect in the future.

5.3 SOL-GEL-GRIGNARD TREATMENT USING DEALUMINATED AlClx AS CATALYST

It is difficult to have the same kinds of acidity on lab-made 5A particles as that on commercial 5A particles, without knowing the source of the acidity; however, there are ways available to generate zeolite with more acidic properties. Acidic species of AlClx was found to be generated by the dealumination treatment on LTA zeolite [5]. These AlClx species can increase the acidity of zeolite, and act as the acidic catalyst for the sol-

gel reactions similar as the HCl acid. Dealumination treatment by $SOCl_2$ was performed before the sol-gel-Grignard treatment to raise the acidity of zeolite and promote the $Mg(OH)_2$ whisker formation. $SOCl_2$ (20 ml) was added into 5A particles (8 g) dispersed in toluene (80 ml). The dispersion is put in a sonication bath overnight to carry out the dealumination reactions. The detailed experimental conditions are shown in chapter 3. The treatment results on commercial and lab-made 5A are shown in Fig. 5.4. Different $Mg(OH)_2$ morphologies are formed on commercial 5A particles by the sol-gel-Grignard treatment, with and without dealumination treatment. Flakes and short whisker are formed on commercial 5A particles, without dealumination treatment, due to the insufficient acidity as discussed earlier. Longer $Mg(OH)_2$ whiskers are formed on commercial 5A by the dealumination & sol-gel-Grignard treatment. Apparently, the dealumination treatment on commercial 5A increased the acidity of commercial 5A particles by generating acidic AlClx species on the zeolite surface. The dealumination treatment by $SOCl_2$ is less effective on the lab-made 5A particles. The $Mg(OH)_2$ morphologies (flakes) are similar after sol-gel-Grignard treatment with and without dealumination pretreatment. $Mg(OH)_2$ flakes are formed on lab-made 5A even after dealumination treatment. This is probably because the acidity is insufficient through the AlClx species generated by dealumination treatment for the lab-made 5A particles.

The structural Al can be extracted to the zeolite surface and zeolite structures can be partially disrupted by the dealumination treatment using $SOCl_2$, as already known by previous researchers [5]. Gas transport properties of nC4 are investigated to understand the effect of dealumination treatment on the commercial and lab-made 5A particles. The results are shown in Fig. 5.6 and Fig. 5.7.

The commercial 5A shows reduced nC4 sorption capacity and kinetics after the dealumination and sol-gel-Grignard treatment (GT118). As shown in chapter 4, the sol-gel-Grignard treatment showed little effect on the gas transport properties of commercial 5A, therefore, the changes of gas transport properties are, therfore, due to the dealumination treatment. The shrinkage of pore size or the partially blockage of pores by dealumination are probably the reason for the change of gas transport properties in commercial 5A. Even though the roughened surface was formed by dealumination + sol-gel-Grignard treatment, the expected slow gas permeation rate, due to the huge reduction of diffusivity and solubilty, makes the treated 5A particles (GT118) undesirable to make mixed matrix membranes for C4s separation. In order to generate less disruption of zeolite strucutre by dealumination, half amount of $SOCl_2$ is used for the dealumination in a new treatment (GT4). The treated 5A has slightly reduced diffusion kinetics compared to as received 5A, which means less change of micropores in the zeolite. Mixed matrix membranes were made using the treated 5A particles (GT4), and the transport properties are shown in chapter 6. The flake morphology of $Mg(OH)_2$ formed by sol-gel-Grignard treatment, is probably due to a less acidity increase on lab-made 5A through dealumination. On the other hand, the gas transport properties are severely affected by the dealumination treatment. As shown in Fig. 5.6, the nC4 sorption capacity reduced to almost zero, and the sorption kinetcis is far slower after dealumination treatment. The gas transport properties of lab-made 5A particles is more adversely affected, while the acidity from AlClx species is not effectively increased by the $SOCl_2$ dealumination treatment. It seems the problem of insufficient acidity on lab-made 5A surfaces cannot be solved by the dealumination treatment.

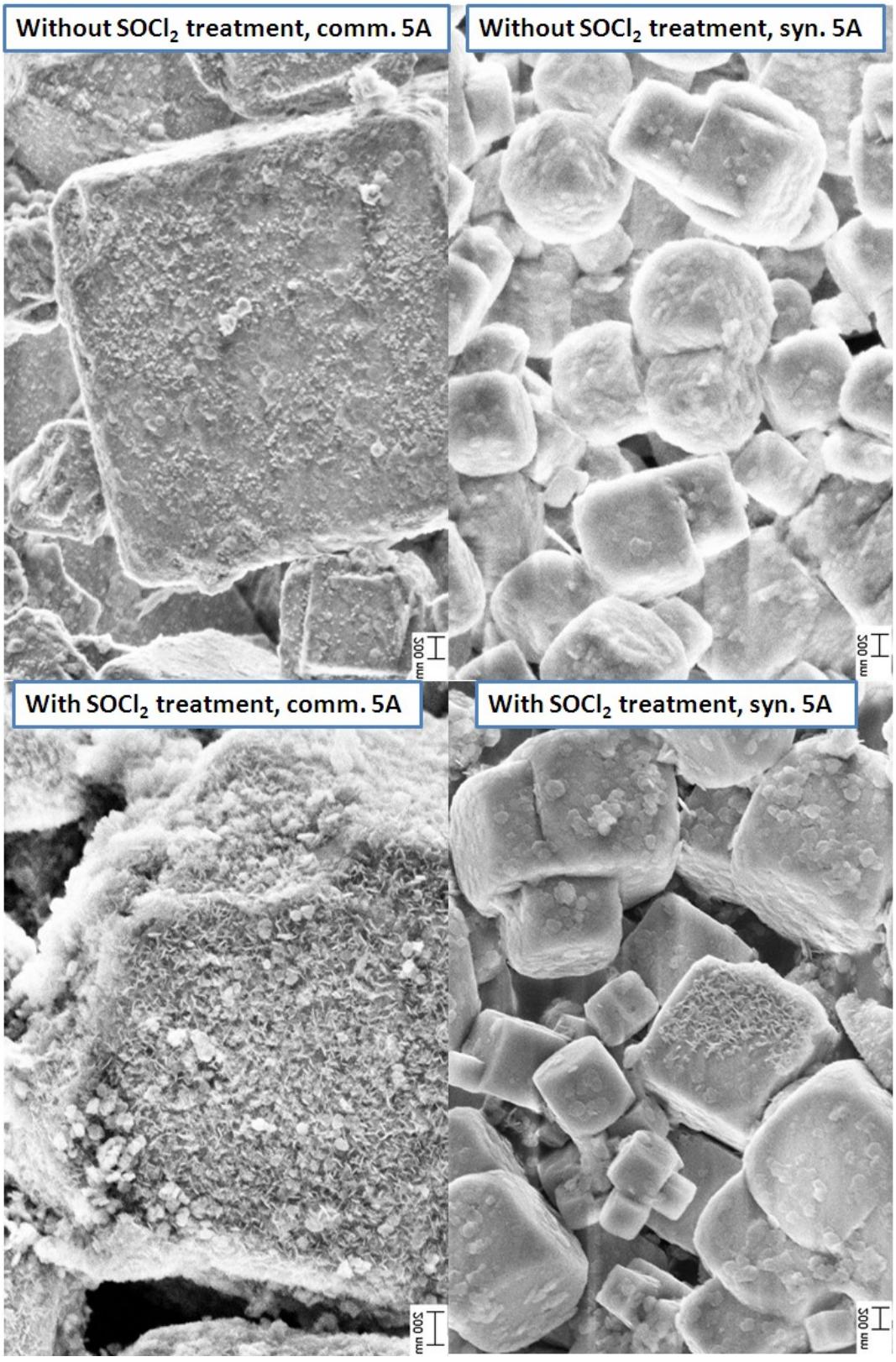

Figure 5.4 $Mg(OH)_2$ morphologies formed on the commercial(comm.) and lab-made (syn.) 5A particles with and without dealumination by $SOCl_2$.

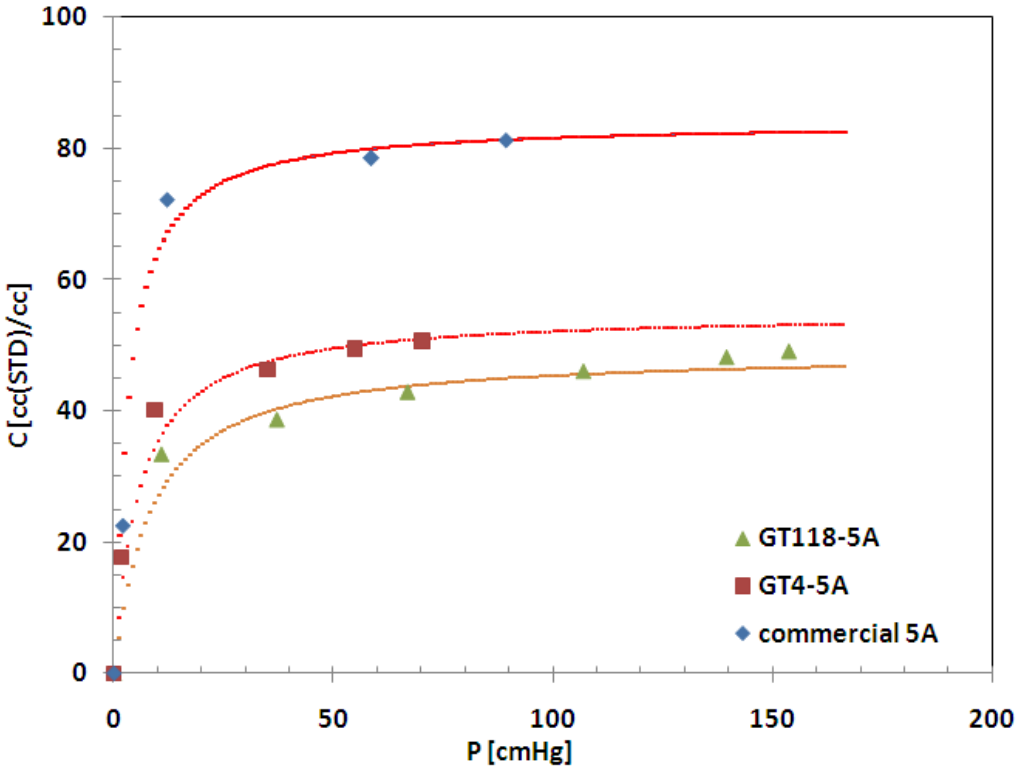

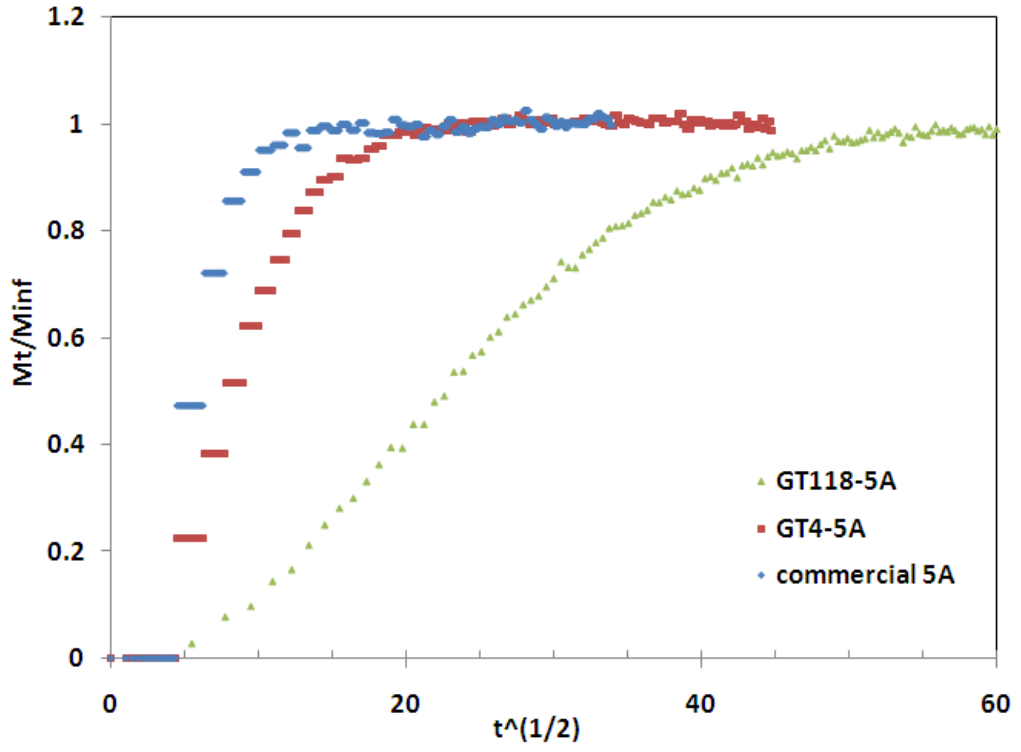

Figure 5.5 Sorption capacity and kinetics of commercial 5A and sol-gel-Grignard treated 5A partciles, pretreated by $SOCl_2$ dealumination(GT118), GT4 half amount of $SOCl_2$

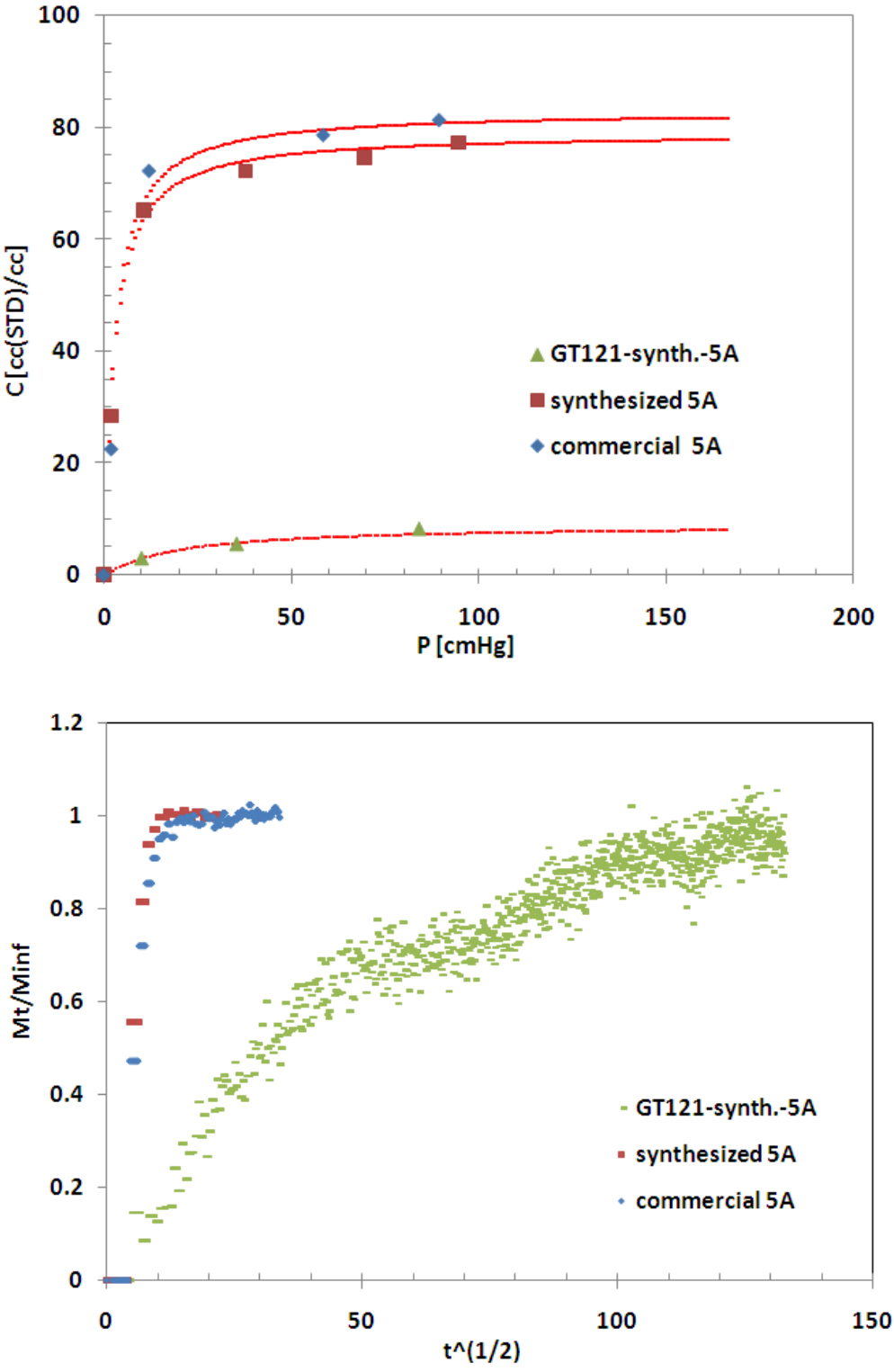

Figure 5.6 Sorption capacity and kinetics of commercial and lab-made 5A and sol-gel-Grignard treated 5A partciles, pretreated by $SOCl_2$ dealumination treatment(GT121)

5.4 SOL-GEL-GRIGNARD TREATMENT USING ANCHORED $AlCl_3$ AS CATALYST

The dealumination treatment is less effective to extract structural Al and form AlClx on the lab-made 5A surfaces. There are also zeolites which does not contain Al in the structure, such as pure silica MFI. Another way to generate $AlCl_3$ acidic sites on zeolite surfaces has already been discovered in the catalysis field. $AlCl_3$ can be anchored onto zeolite surfaces through the surface hydroxyl groups [6, 7]. Commercial 5A was first treated with the $AlCl_3$ anchoring treatment, followed by standard sol-gel-Grignard treatment. The $Mg(OH)_2$ morphologies are shown in Fig. 5.7. Different amount of $AlCl_3$ are used to anchor onto commercial 5A surfaces in order to find the minimum amount of $AlCl_3$ needed to supply enough acidity for the sol-gel reactions. More whiskers are formed on commercial 5A particles with more $AlCl_3$ anchoring as shown in table 5.2, because the highly acidic $AlCl_3$ can promote the whisker formation in the sol-gel treatment. When the amount of anchored $AlCl_3$ exceed 2 wt%, the $Mg(OH)_2$ whiskers are easily detached from zeolite surface, as shown in Fig. 5.7. The $AlCl_3$ probably hydrolyzes and forms a layer of $Al(OH)_3$ on the top of zeolite surface, with the presence of water during the sol-gel reactions. The thickness of $Al(OH)_3$ layer is anticipated to depend on the amount of $AlCl_3$ anchored onto the zeolite surface.

Table 5.2 Atomic composition of treated commercial 5A particles using different amount of anchored $AlCl_3$ as acidic catalyst

Atomic %	Na	Mg	Al	Si	Cl	Ca
4wt% $AlCl_3$ (GT120)	2.9	4.6	12.9	10.8	2.7	4.6
2wt% $AlCl_3$ (GT122)	3.3	3.9	13.1	11.9	0.8	4.8
1wt% $AlCl_3$ (GT123)	2.9	2.0	13.3	13.1	0.7	5.2

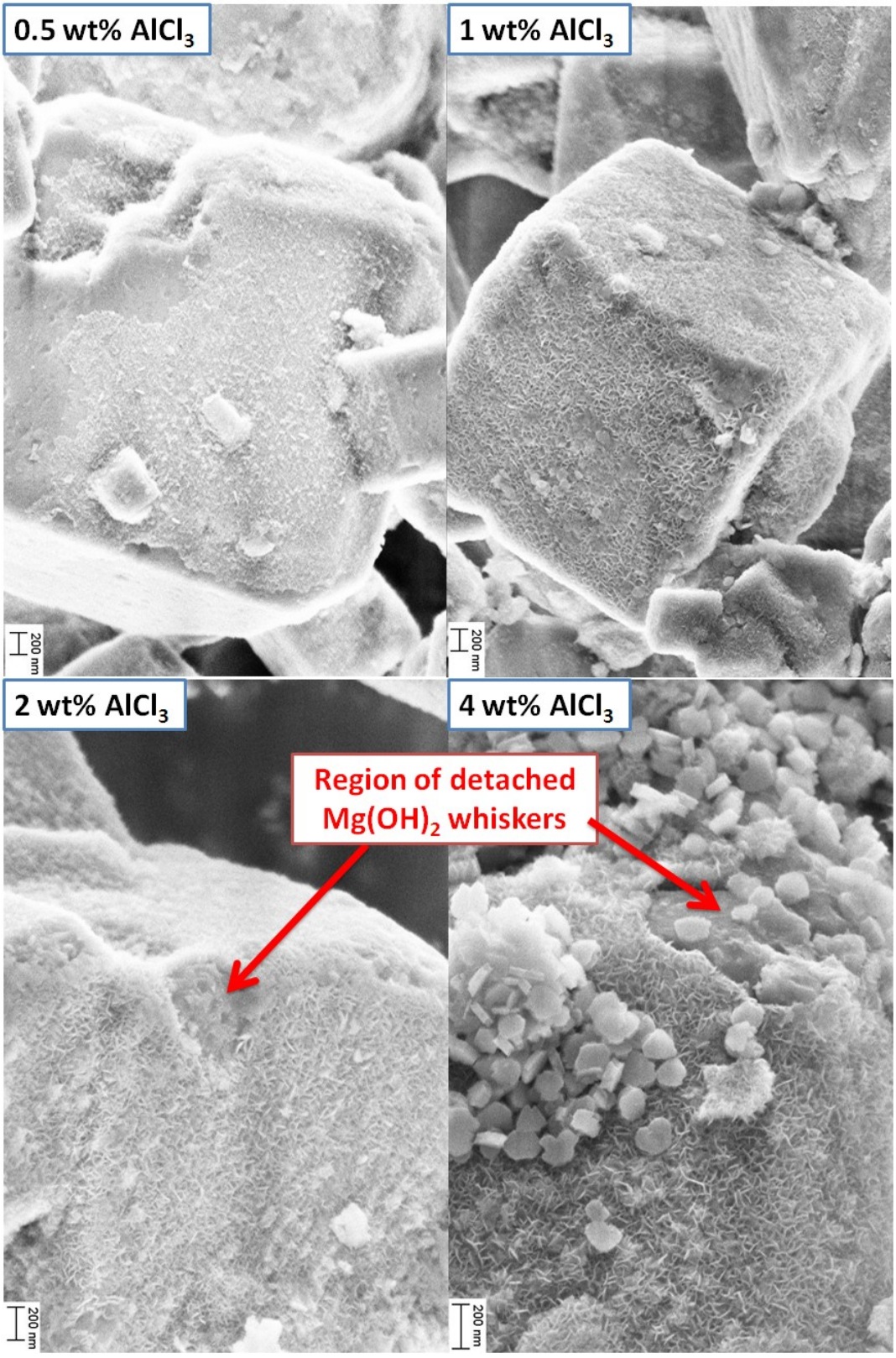

Figure 5.7 $Mg(OH)_2$ morphologies formed on the commercial 5A particles with different amount of anchored $AlCl_3$

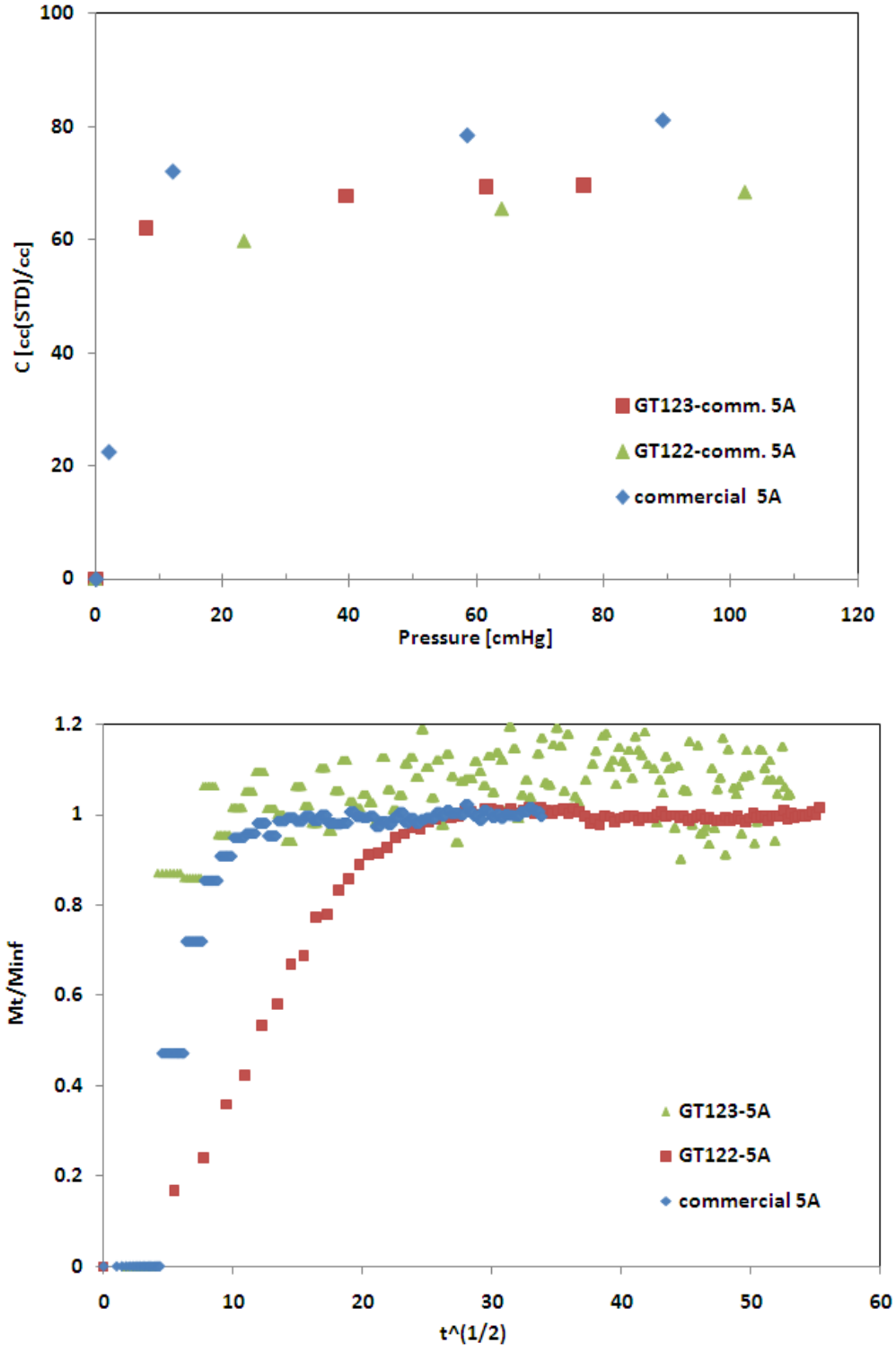

Figure 5.8 Sorption capacity and kinetics of commercial 5A after sol-gel-Grignard, anchored with different amount of $AlCl_3$ (GT122-2wt%, GT123-1wt%)

Transport properties of nC4 molecules in the treated 5A particles are measured by sorption method to investigate the effect of $AlCl_3$ anchoring on the micropore properties. As shown in Fig. 5.8, the nC4 sorption capacities in the treated 5A particles are lower than that in the commercial 5A particles. The sorption kinetics of 5A after anchoring 1wt% of $AlCl_3$ and sol-gel-Grignard treatment is similar to that of bare commercial 5A. The sorption kinetics slows down dramatically with 2wt% of $AlCl_3$ anchoring and treatment. The slower sorption kinetics can be explained by different ways: 1) an additional $Al(OH)_3$ barrier layer is formed on the top of 5A surfaces; 2) the micropore of 5A get affected (reduced pore size or plugged pore) with more acidic $AlCl_3$ anchored. In order to avoid the disruption of molecule diffusion in 5A particles, the amount of $AlCl_3$ is kept below 1wt% on commercial micron 5A particles. Further decrease of $AlCl_3$ amount (to 0.5wt%) leads to less $Mg(OH)_2$ whisker formation due to the insufficient acidity of zeolite, as shown in Fig. 5.7. The treated 5A particles anchored with 1wt% and 2wt% of $AlCl_3$ were used to make mixed matrix membranes. The C4s transport permeation tests were done on these films. As shown in table 5.3, mixed matrix films show huge increase of nC4 permeability with little change of nC4/iC4 selectivity, which is probably due to the voids between the zeolite and polymer matrix.

Table 5.3 C4s transport properties of mixed matrix membranes containing sol-gel-Grignard treated commercial 5A particles, with $AlCl_3$ anchoring pretreatment

membranes	PnC4 [Barrer]	nC4/iC4 [-]
6FDA-DAM (WQ0912)	3.2±0.2	21±2
25wt%-GT5A(1wt% $AlCl_3$)+6FDA-DAM	5.9±0.3	21±2
35wt%-GT5A(2wt% $AlCl_3$)+6FDA-DAM	6.8±0.3	18±2

As suggested by the SEM result shown in Fig. 5.10, the $Mg(OH)_2$ whiskers are probably formed on an $Al(OH)_3$ sheath layer, which can detach from zeolite surfaces. Voids can be generated when the sheath is detached from zeolite surface. The structure of the zeolite after $AlCl_3$ anchoring and sol-gel-Grignard treatment can be simplified to a tri-layer structure, as shown in Fig. 5.9. An additional layer of $Al(OH)_3$ is formed by the hydrolysis reaction of anchored $AlCl_3$, and the $Mg(OH)_2$ whiskers are formed on top of the $Al(OH)_3$ layer. Fig. 5.8 shows one example of detached layer of $Al(OH)_3$ and $Mg(OH)_2$ whisker from zeolite surface in the mixed matrix membrane. In the mixed matrix membranes, polymer chain can entangle onto the $Mg(OH)_2$ whiskers, but cannot diffuse through the $Al(OH)_3$ layer, therefore, the polymer matrix and zeolite particle is separated by a layer of $Al(OH)_3$. The gas molecules can bypass the zeolite through the $Al(OH)_3$ layer (if it is porous) or the voids when $Al(OH)_3$ layer detach from the zeolite surfaces. In either cases, the mixed matrix membranes show transport properties similar to that in membranes with ‘‘sieve-in-a-cage’’ morphologies.

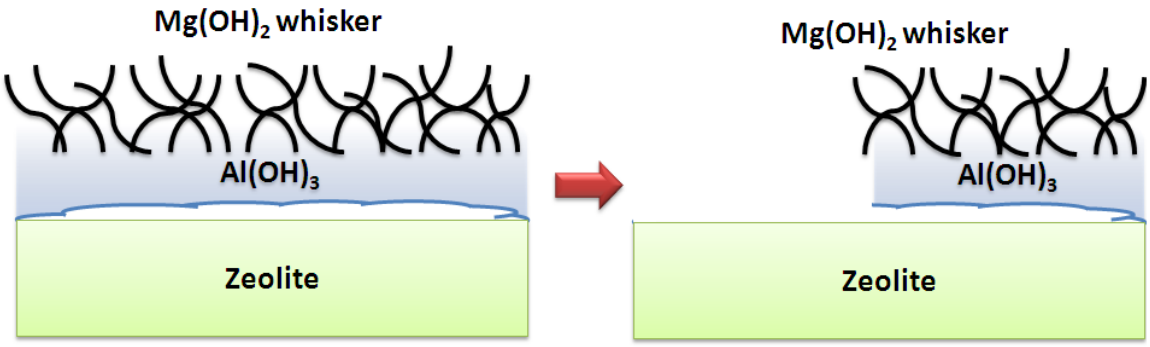

Figure 5.9 Tri-layer strucutre formed by $AlCl_3$ anchoring and sol-gel-Grignard treatment and its breakage

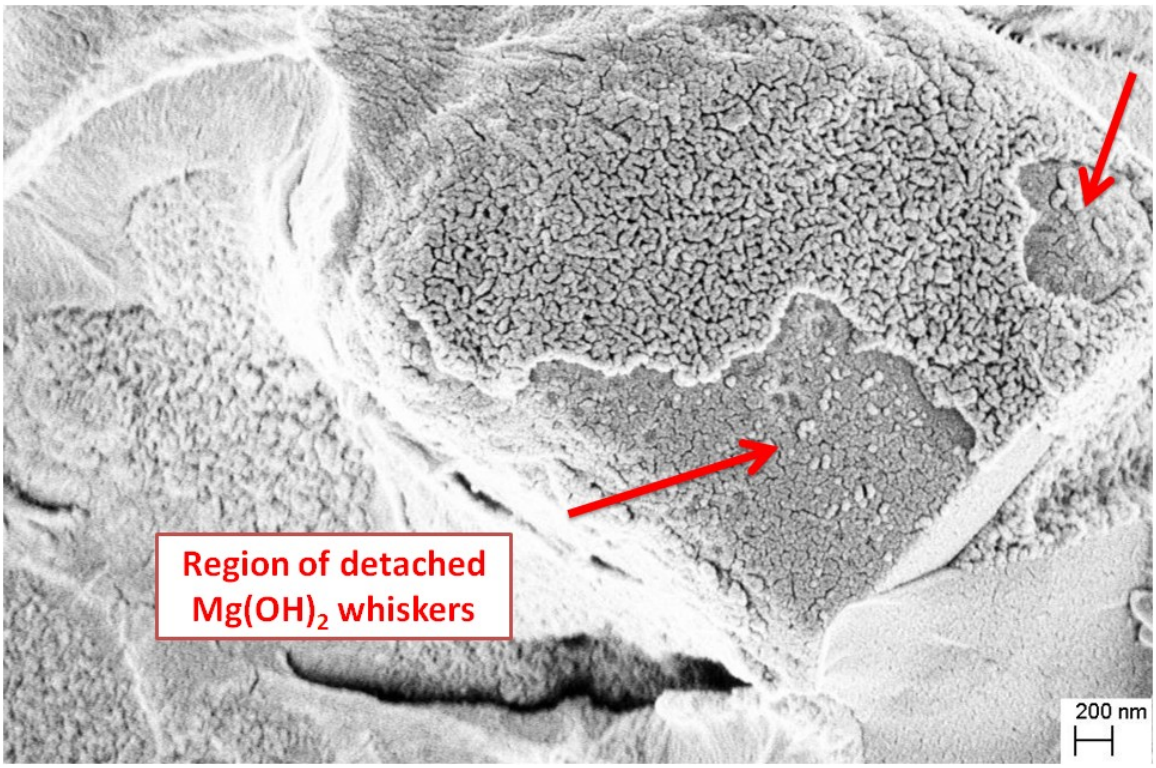

Figure 5.10 Cross section of mixed matrix memrbanes using 6FDA-DAM and 25wt% sol-gel-Grignard treated (with 2wt% $AlCl_3$ anchored, GT122) commercial 5A particles

Similar pretreatment of $AlCl_3$ anchoring was done on synthesized 5A particles of various crystal sizes before the standard sol-gel-Grignard treatment. In order to keep the amount of $AlCl_3$ per zeolite surface area the same on different size of crystals, 1wt%, 4wt% and 8wt% of $AlCl_3$ was anchored to the 1 μm, 300 nm and 150 nm zeolite 5A particles. Highly roughened surfaces are generated on all these synthesized 5A surfaces after the $AlCl_3$ anchoring and sol-gel-Grignard treatment, as show in Fig. 5.11. The nC4 sorption properties of these treated 5A particles are shown in Fig. 5.12. The nC4 sorption capacity drops as the amount of the amount of $AlCl_3$ increases, similar as the treated commercial 5A particles. The sorption kinetics is not dramatically slowed down, even after the treatment with 8wt% of $AlCl_3$ anchoring.

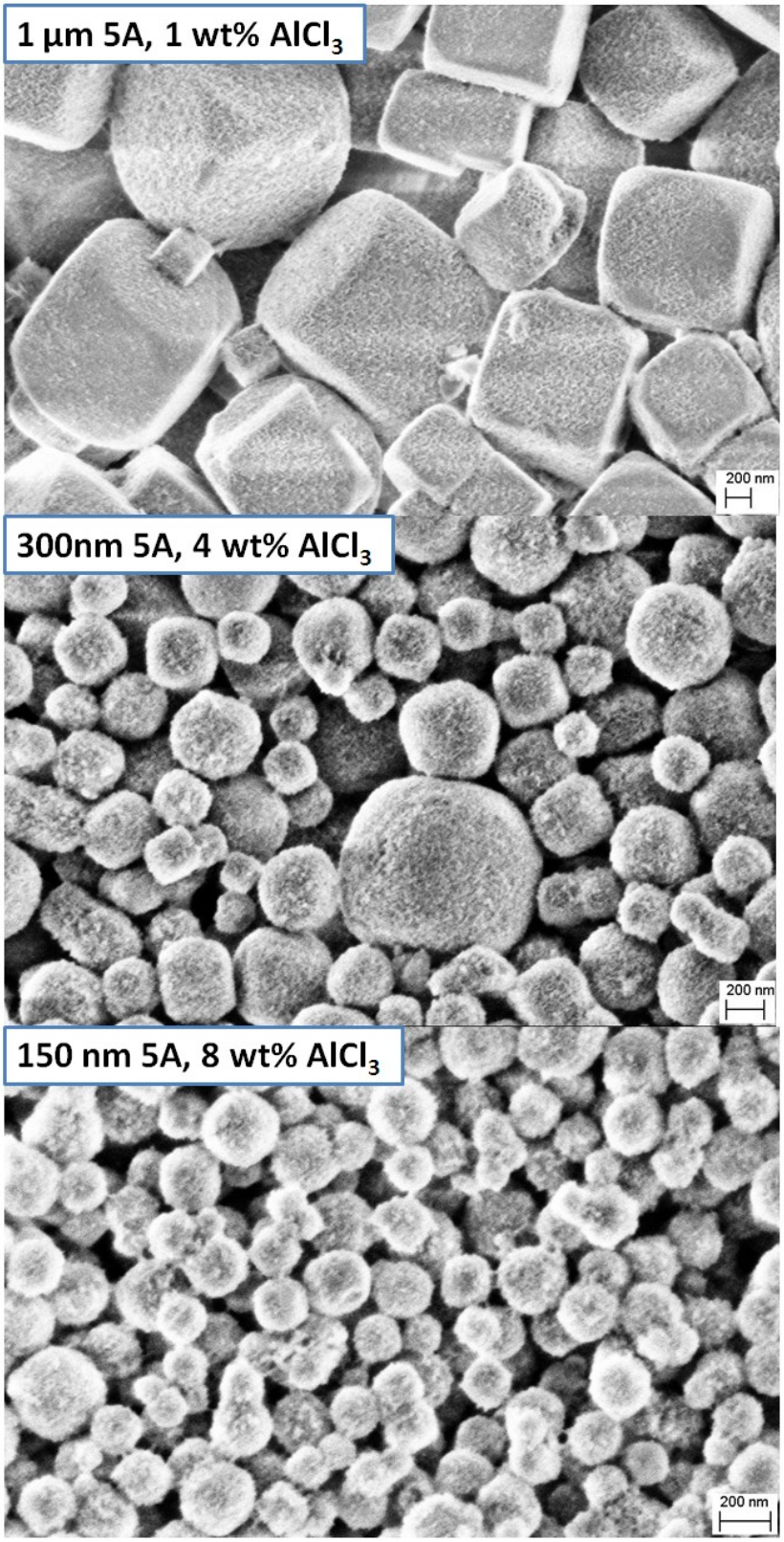

Figure 5.11 $Mg(OH)_2$ morphologies formed on the different sizes of lab-made 5A particles with different amount of anchored $AlCl_3$

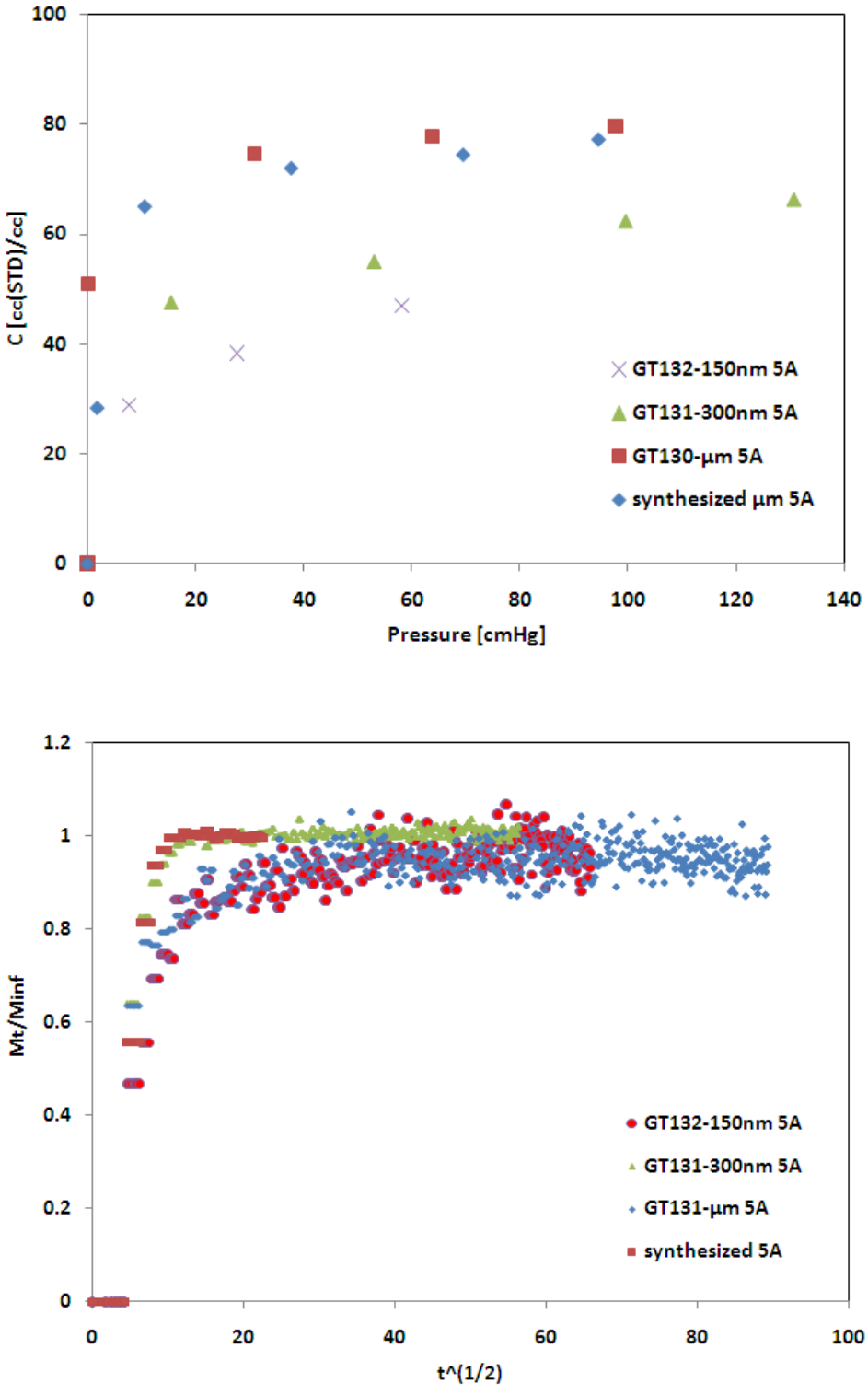

Figure 5.12 Sorption capacity and kinetics of different sizes of lab-made 5A after sol-gel-Grignard, anchored with different amount of $AlCl_3$

Mixed matrix membranes were made using the treated 5A particles. Good adhesion between the treated 5A particles and 6FDA-DAM matrix was observed as shown in Fig. 5.13. However, the gas transport properties of the mixed matrix membranes suggest a possible ‘‘sieve-in-a-cage’’ morphology, similar as the membranes containing treated commercial 5A particles. A calculation was done to approximate the thickness of $Al(OH)_3$ formed with few simplifications: 1) a uniform layer of $Al(OH)_3$ is formed on zeolite spheres; 2) zeolite and $Al(OH)_3$ has the same density. Assuming the radius of zeolite sphere is R and $Al(OH)_3$ thickness is δ. The volume of zeolite and $Al(OH)_3$ layer are $4/3\pi R^3$ and $4\pi R^2$ δ. If the volume of $Al(OH)_3$ (approximately amount of $AlCl_3$) is 1% of zeolite, then $4\pi R^2 \delta = 0.01 \times (4/3\pi R^3)$, therefore $\delta = R/300$. The thickness of $Al(OH)_3$ layer is 1.7 nm if the zeolite has diameter of 1 μm.

Considering the dimension of diffusing molecules of C4s (0.43-0.5 nm), a 1.7 nm thick $Al(OH)_3$ layer can cause the bypass problem through zeolite. It is needed to further investigate the morphologies of $Mg(OH)_2$ formed using anchored $AlCl_3$ as catalyst for the sol-gel-Grignard treatment. It is likely the $AlCl_3$ anchoring method cannot be used to pretreat zeolite to make acidic surfaces before the sol-gel-Grignard treatment due to the formation of byproduct of $Al(OH)_3$ layer, which affects the zeolite-polymer adhesion and gas transport properties of treated zeolite particles.

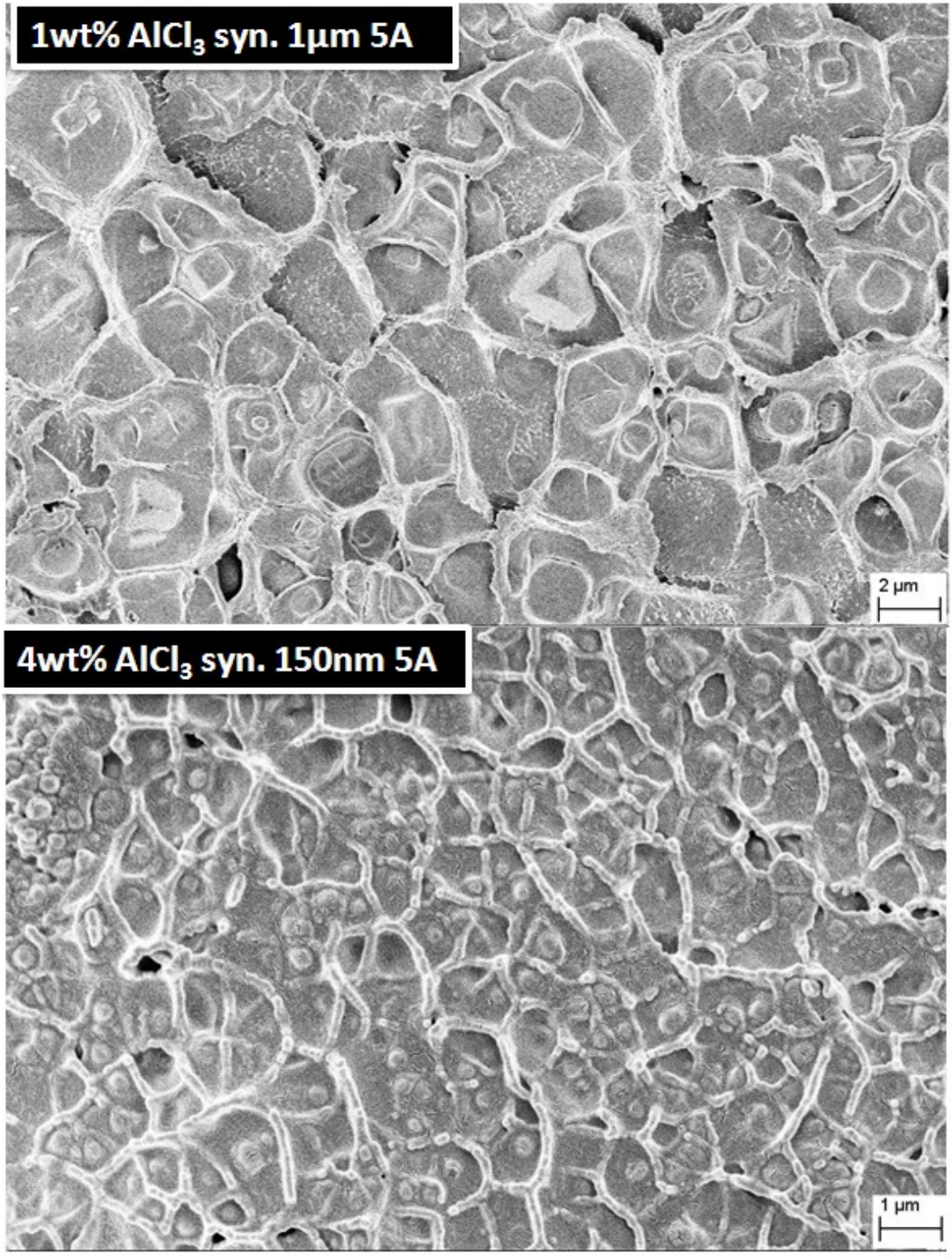

Figure 5.13 Cross section of mixed matrix memrbanes using 6FDA-DAM and 25wt% $AlCl_3$ anchoring & sol-gel-Grignard treated synthesized 5A particles of various sizes

Table 5.4 C4s transport properties of mixed matrix membranes containing sol-gel-Grignard treated synthesized 5A particles, with $AlCl_3$ anchoring pretreatment

membranes	PnC4 [Barrer]	nC4/iC4 [-]
6FDA-DAM (WQ0912)	3.2±0.2	21±2
25wt%-GT5A(1 μm)+6FDA-DAM	5.1±0.3	14±2
25wt%-GT5A(150 nm)+6FDA-DAM	5.5±0.3	21±2

5.5 SUMMARY

The acidic catalysts have profound influence on the sol-gel-Grignard treatment, and more thorough effort is needed on this aspect. The commercial 5A particles can be treated using HCl as acidic catalyst for the sol-gel-Grignard treatment. More whiskered $Mg(OH)_2$ morphologies are formed at higher acidic conditions. Different acidic catalysts were tried on the lab-made 5A. Homogeneous nucleation happened during the sol-gel-Grignard treatment using HCl as acidic catalyst. Controlled heterogeneous nucleation was achieved during the sol-gel-Grignard treatment using anchored $AlCl_3$ as acidic catalyst. The $Mg(OH)_2$ formed only on zeolite surfaces by anchoring acidic $AlCl_3$ sites on the zeolite surfaces. It seems the distribution as well as the strength of acidic sites affects the $Mg(OH)_2$ whisker formation.

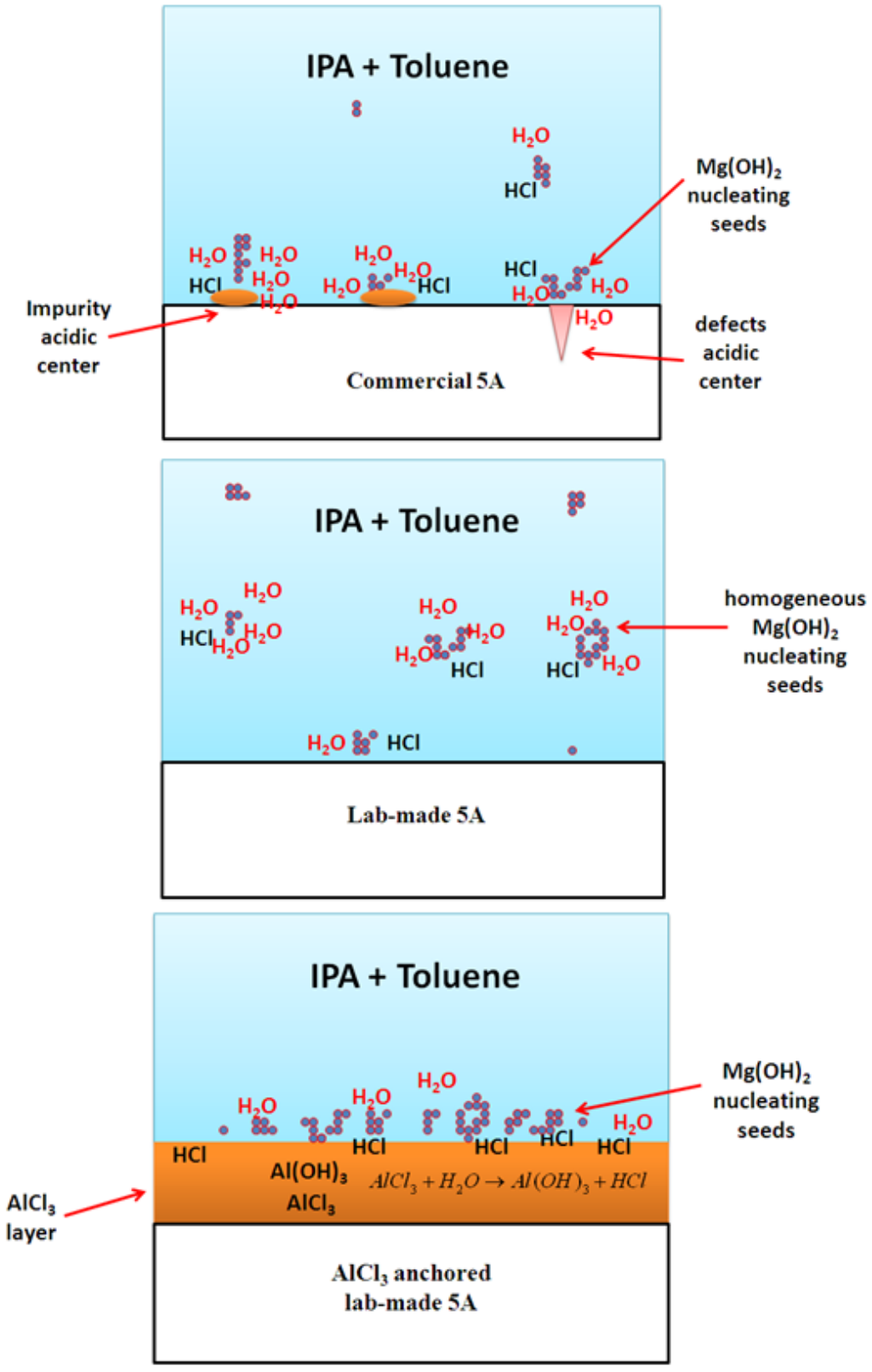

Figure 5.14 Homogeneous and heterogeneous $Mg(OH)_2$ nucleating seed generation around different acidic centers

The $Mg(OH)_2$ nucleation on different acidic surfaces can be explained as Fig. 5.14. $Mg(OH)_2$ nucleating seeds probably are generated around acidic (and water) centers, which can promote the sol-gel reactions. The impurities or defect sites on commercial 5A surfaces either are heterogeneous acidic sites or provide sites for HCl and water to adsorb on (and create heterogeneous acidic sites). The heterogeneous acidic sites on commercial 5A surfaces can assist the selective formation of heterogeneous $Mg(OH)_2$ seeds for the later whisker formation. Homogeneous nucleating seeds are formed during sol-gel reaction on lab-made 5A particles, because the acidic centers (HCl) are dispersed homogeneously in the sol-gel solution. $Mg(OH)_2$ whiskers will later form homogeneously on the seeds independent of zeolite surfaces. The HCl acid is released by the hydrolysis of $AlCl_3$ during the sol-gel treatment of $AlCl_3$ anchored 5A. $Mg(OH)_2$ seeds (and whiskers) form selectively on zeolite surfaces around the acidic center of $AlCl_3$.

Further investigation is needed for the treatment on synthesized 5A particles to generate heterogeneous acidic sites on the zeolite surfaces, while avoiding the problem of undesired additional layer formation. One choice is the application of organic acid, such as oxylic acid and citric acid, p-toluenesulfonic acid (PTSA), *etc*. These organic acids are reported to adsorb onto zeolite surfaces through the interaction with hydroxyl groups on zeolite surfaces [8, 9]. These adsorbed acids can act as heterogeneous acidic centers, in a similar way as the anchored $AlCl_3$. On the other hand, problems of additional layer will be avoided because the water soluble organic acid can be washed away.

5.6 REFERENCE

[1] C. J. Brinker, *Sol-Gel Science*, Academic Press, Inc. **1990**

[2] M.L. Hair, *Journal of Non-Crystalline Solids*, **1975,** 19, 299-309

[3] M. E. Davis, *Ind. Eng. Chem. Res*., **1991**, 30, 1675-1683

[4] D. Barthomeuf, *Mater. Chem. Phys.*, **1987**, 17, 49-71

[5] S. Shu, *Ind. Eng. Chem. Res.*, 46(2007), 767–772

[6] K. Wilson, *Pure Appl. Chem.*, **2000**, 72, 1313–1319

[7] X. Hu, *J. Catal*. **2000**, 195**,** 412–415

[8] Z. Xie, *J. Phys. Chem. B*, **2000**, 104, 2853–2859

[9] A. Corma, *J. Catal*. **1989**, 210, 78-87

CHAPTER 6

BUTANE ISOMER SEPARATION USING MIXED MATRIX MEMBRANES CONTAINING ZEOLITE 5A AND MFI PARTICLES

Proper matching of C4 isomer transport properties of polymer and zeolite components in formation of successful mixed matrix membranes is discussed in this work. The highly permeable zeolite MFI matches well with polydimethylsiloxane (PDMS) for C4s separation. This proper matching led to a nC4 Permeability increase of 2.4 fold and nC4/iC4 selectivity increase of 2.9 fold in PDMS-MFI mixed matrix membrane containing 50wt% of 5 μm MFI, compared to pure PDMS membrane. Despite the significant percentage enhancement, the beginning properties of PDMS are not very attractive. On the other hand, an nC4 permeability of 3.7 Barrer, and nC4/iC4 ideal selectivity of 21 was found in pure 6FDA-DAM polymer membrane. The attractive intrinsic nC4/iC4 selectivity makes 6FDA-DAM an attractive matrix polymer. Unfortunately, the difference of C4s permeability in MFI (>10000 Barrer) and 6FDA-DAM caused the 6FDA-DAM-MFI mixed matrix membrane to not show enhanced nC4/iC4 selectivity. It appears unlikely that any currently known, adequately selective glassy polymer can match the high permeability of nC4 in MFI to enable development of promising composite membrane for the C4s separation based on MFI. This issue is analyzed to emphasize the importance of ‘‘permeability matching’’ for the desired penetrant in the matrix polymer and dispersed sieve phase. This concept is extended to predict a better matched sieve/polymer pair. 6FDA-DAM-5A mixed matrix membranes are then shown to enhance nC4/iC4 selectivity, because the 5A sieve blocks iC4, and

allows nC4 to penetrate. An even better match is between 6FDA-DAM-DABA and 5A for C4s separation. The enhanced nC4/iC4 selectivity can potentially be achieved by both enhanced nC4 permeability and depressed iC4 permeability, therefore, a much larger selectivity enhancement than that in 6FDA-DAM-5A mixed matrix membranes by only iC4 permeability reduction.

6.1 6FDA-DAM-MFI (CALCINED) MIXED MATRIX MEMBRANES

Numerous studies have been done on intracrystalline diffusion of C4s in high silica MFI [1-3]. The accurate measurement of diffusion coefficients (therefore the permeability) for gases in zeolites historically has proven to be challenges for researchers in the molecular sieve area. Even though it is found that MFI is highly permeable and selective for C4s, values of diffusion constants measured for the same gas in the same zeolite measured by different investigators have been found to vary over several orders of magnitude [2]. At the same time, there were no studies on polymeric membranes for C4s separation, probably because of the slow diffusion in polymeric membrane caused by C4s' large kinetic diameter. In this research, C4s permeation property was studied using one of the most permeable polymer 6FDA-DAM, as the first step, due to the unknown permeation properties in both MFI and polymers.

The solubility of C4s in both MFI and 6FDA-DAM polymer were obtained from pressure decay sorption measurements. The solubility of C4s in MFI and 6FDA-DAM polymer at different pressure is shown in Figure. 6.1. The dual mode model (as shown in equation 2) sorption parameters are shown in table 6.1. C, C_D, and C_H stand for total sorption, dissolution domain sorption and hole-filling domain (Langmuir) sorption respectively. k_D is sorption coefficient for dissolution sorption ($k_D = 0$ for C4s'sorption in

MFI because there is no dissolution in MFI crystals). C_H' and b are capacity and affinity constants for Langmuir sorption. Pressure is shown as p in Eq. 6.2. The solubility of C4s was similar in 6FDA-DAM polymer, and the solubility of nC4 was higher than iC4 in MFI, because of different adsorption sites for C4s in MFI porous channels [4].

$$C = C_D + C_H = k_D p + C_H' bp/(1+bp) \quad (6.1)$$

The diffusivity of C4s in 6FDA-DAM polymer is shown in Figure 6.2. Both isomers show a strong diffusivity dependence on pressure (solubility), which agrees with the partially immobilization model [5]. The diffusivity of both C4s increased more than 4 fold from low pressure to high pressure. The diffusivity of nC4 was about 15 to 30 times higher than that of iC4 at same pressure, while the diffusivity selectivity of C4s in MFI was reported to be higher than 50, at 1.5 bar [1]. The diffusivity of nC4 at high pressure region in 6FDA-DAM polymer was around 6×10^{-9} cm^2/s, which is much slower than the typical reported diffusivity of nC4 in the MFI, 4×10^{-8} cm^2/s at 60 °C [2], and 5×10^{-6} cm^2/s at 100 °C [1].

Table 6.1 Sorption parameters of C4s in MFI and 6FDA-DAM at 100 °C

	C_H' [cc(STD)·cc^{-1}·cmHg^{-1}]	b [cmHg^{-1}]	k_D [cc(STD)·cc^{-1}·cmHg^{-1}]
nC4 in MFI	70.4	0.155	0
iC4 in MFI	38.9	0.150	0
nC4 in 6FDA-DAM	14.5	0.039	0.057
iC4 in 6FDA-DAM	12.8	0.047	0.063

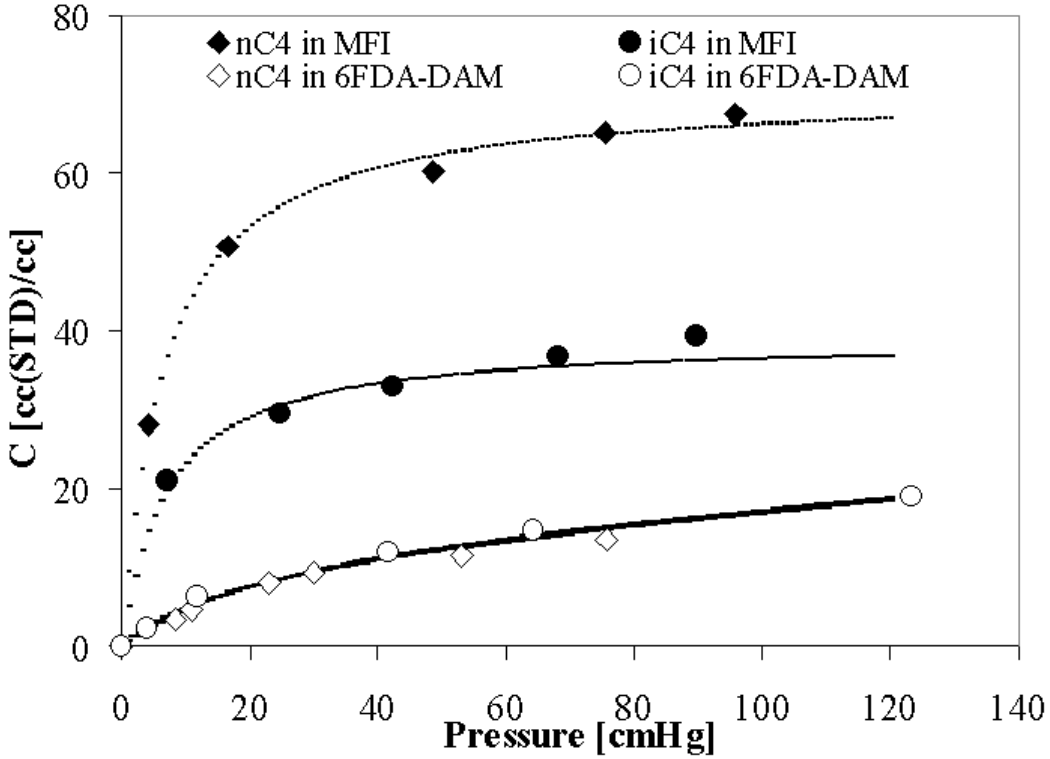

Figure 6.1 C4s' sorption capacity at different pressure in MFI and 6FDA-DAM (100 °C)

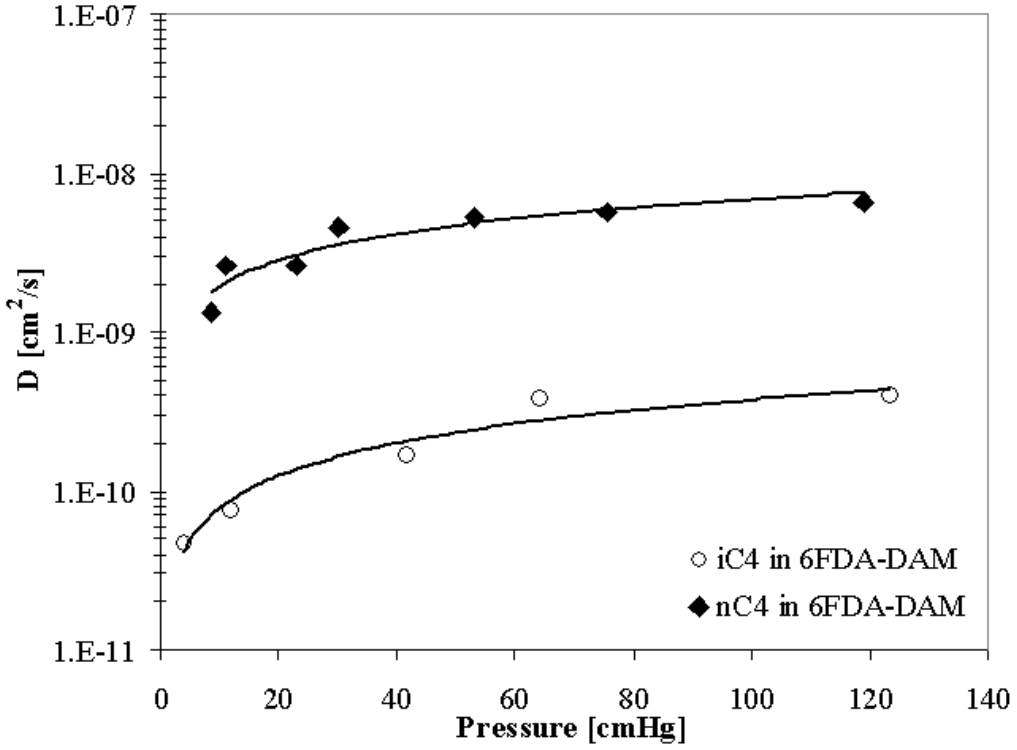

Figure 6.2 C4s' diffusivity at different pressure in 6FDA-DAM at 100 °C

As expected, much higher permeabilities of both C4s are observed in MFI than in 6FDA-DAM polymer, because of higher solubility and diffusivity in MFI. Moreover as noted earlier, a much higher selectivity for C4s in MFI has been reported as discussed previously [1, 2].

Figure 6.3 shows the MFI particles before and after Grignard treatment, demonstrating the roughened (fuzzy) surfaces produced after treatment. ICP measurement showed the Mg content in the total solid loading to be 4.2 wt%; this corresponds to 10.3 wt% of $Mg(OH)_2$ formed on the zeolite surface. Therefore, Grignard treatment is also effective on high silica zeolites if an aluminum-containing zeolite, like 4A is used as an aluminum source. In this case, it is suggested that the crystal seeds transfer from the external source, 4A, to the surface of the MFI.

It has been observed that the Grignard treatment is ineffective on silica or high silica zeolite particles because of the lack of appropriate crystal seeds, on which $Mg(OH)_2$ whiskers can grow [6, 7]. In this study, by treating zeolite 4A and MFI particles together, Al species from 4A particles created by dealumination process are speculated to transfer to the MFI particle surfaces and form nanocrystals that can act as crystal seeds. $Mg(OH)_2$ is formed on these transferred seeds later during the Grignard quenching and sonication process. It was hypothesized that the seed concentration can affect the crystal size and the morphology of the $Mg(OH)_2$ growth [8]. Factors such as crystal seed sources, and crystal seeds concentration should also affect the $Mg(OH)_2$ morphology; however they are beyond the scope of this paper. The focus of the current research is on the effectiveness of mixed matrix film formation using Grignard-treated, high silica MFI.

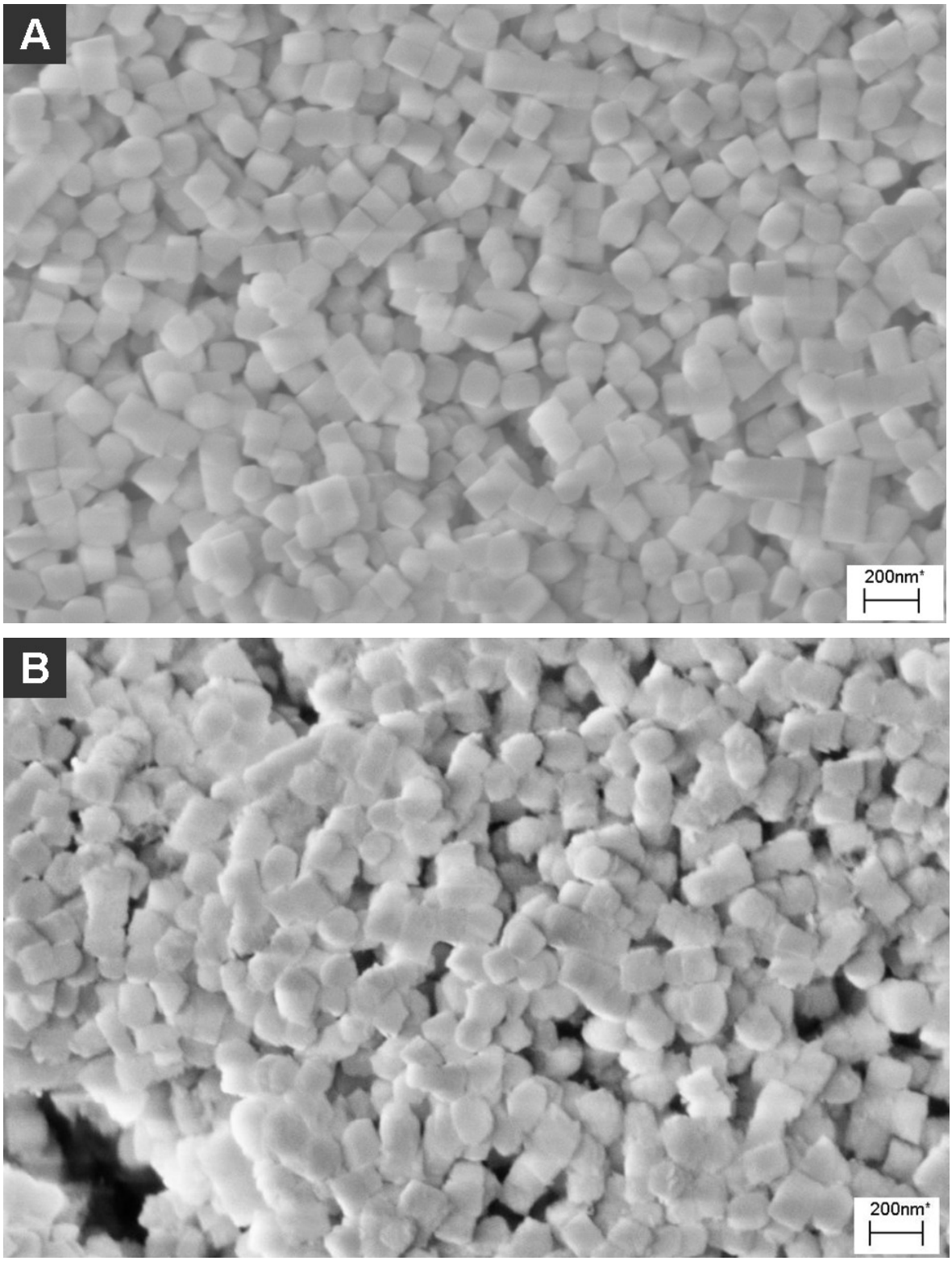

Figure 6.3 SEM images of Bare (A) and Grignard treated (B) calcined-MFI nanoparticles

To check the effect of $Mg(OH)_2$ formation on the porosity of MFI, an nC4 sorption capacity measurement was done at 50 °C. Figure 6.4 shows the nC4 sorption capacity in MFI before and after the Grignard treatment. There was an approximately 15% capacity decrease after Grignard treatment. Assuming the 10 wt% of $Mg(OH)_2$ crystal does not adsorb nC4 molecules, the capacity of Grignard treated MFI after accounting for the presence of essentially non-sorbing $Mg(OH)_2$ is similar to the intrinsic value of bare MFI. These data, therefore, suggest that $Mg(OH)_2$ did not plug or affect the inner pores of MFI.

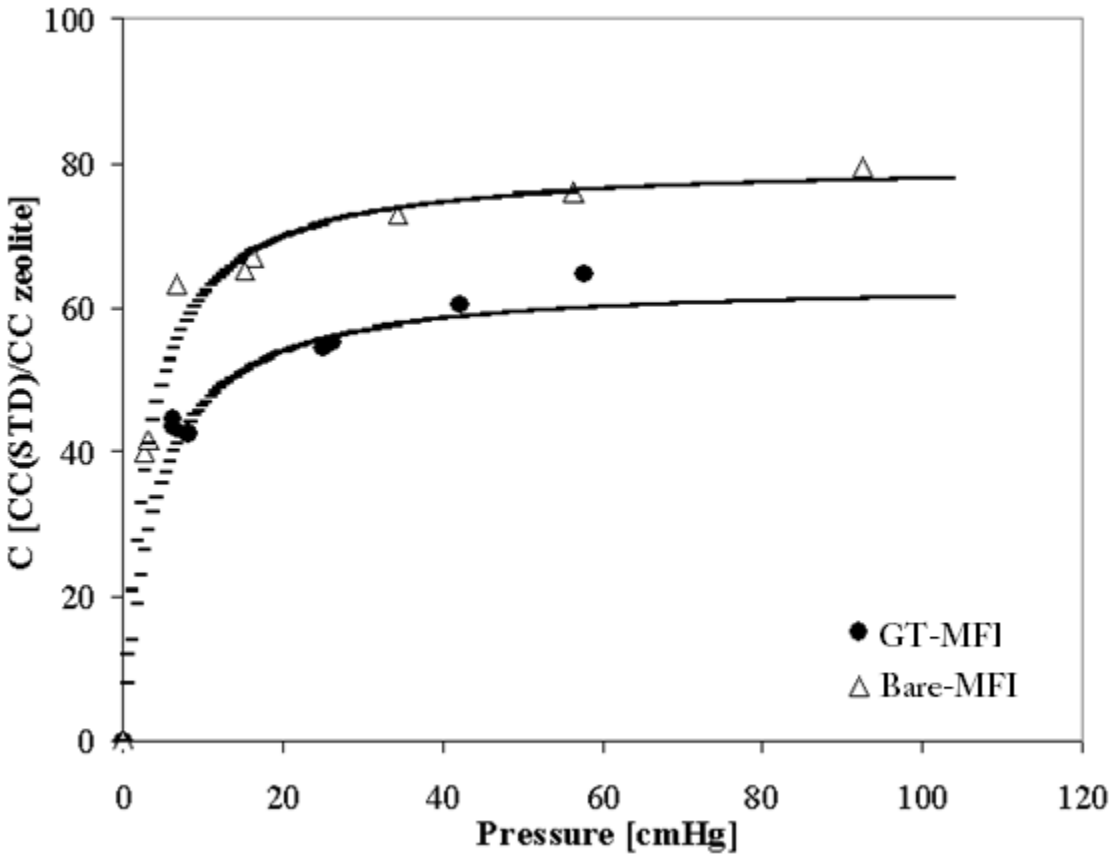

Figure 6.4 NC4 sorption capacity in MFI at 50 °C before and after Grignard treatment (the circles and triangular points are experimental results, the lines are the Langmuir fitting)

Mixed matrix membranes were made with bare and Grignard treated MFI particles at 25 wt% and 35 wt% loading in total solids. Figure 6.6 shows the cross section of mixed matrix membranes. The membrane made using bare MFI displayed significant zeolite agglomeration that occurred during mixed matrix membrane formation because of strong van der Waals attractions between the nanometer MFI particles. On the other hand, Grignard treated MFI particles were dispersed evenly in the polymer matrix. The relative transparencies of mixed matrix films with bare and Grignard treated MFI are shown in Figure 6.5 The micron size agglomerates in the bare MFI mixed matrix film diffract light and make the film opaque. The mixed matrix films with Grignard treated MFI particles are transparent because of good nanometer particle dispersion.

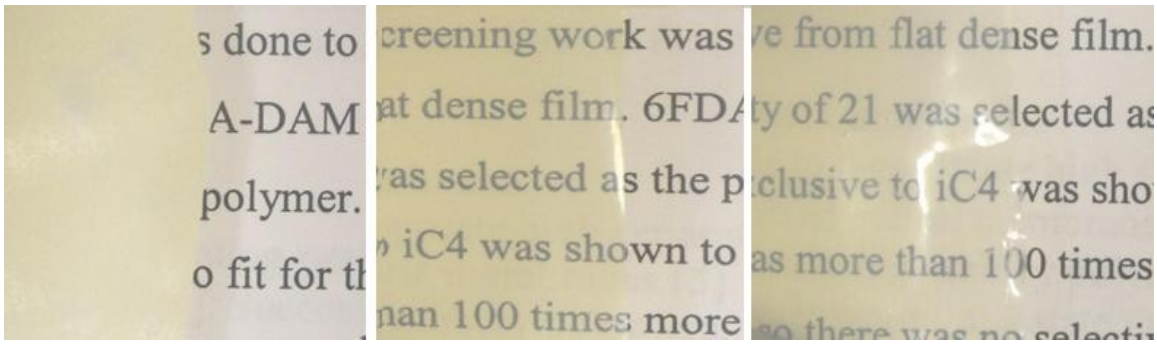

Figure 6.5 Transparency of 6FDA-DAM mixed matrix film with, from left to right, 25wt% bare MFI, 25 wt% Grignard treated calcined-MFI, and 35 wt% Grignard treated calcined- MFI

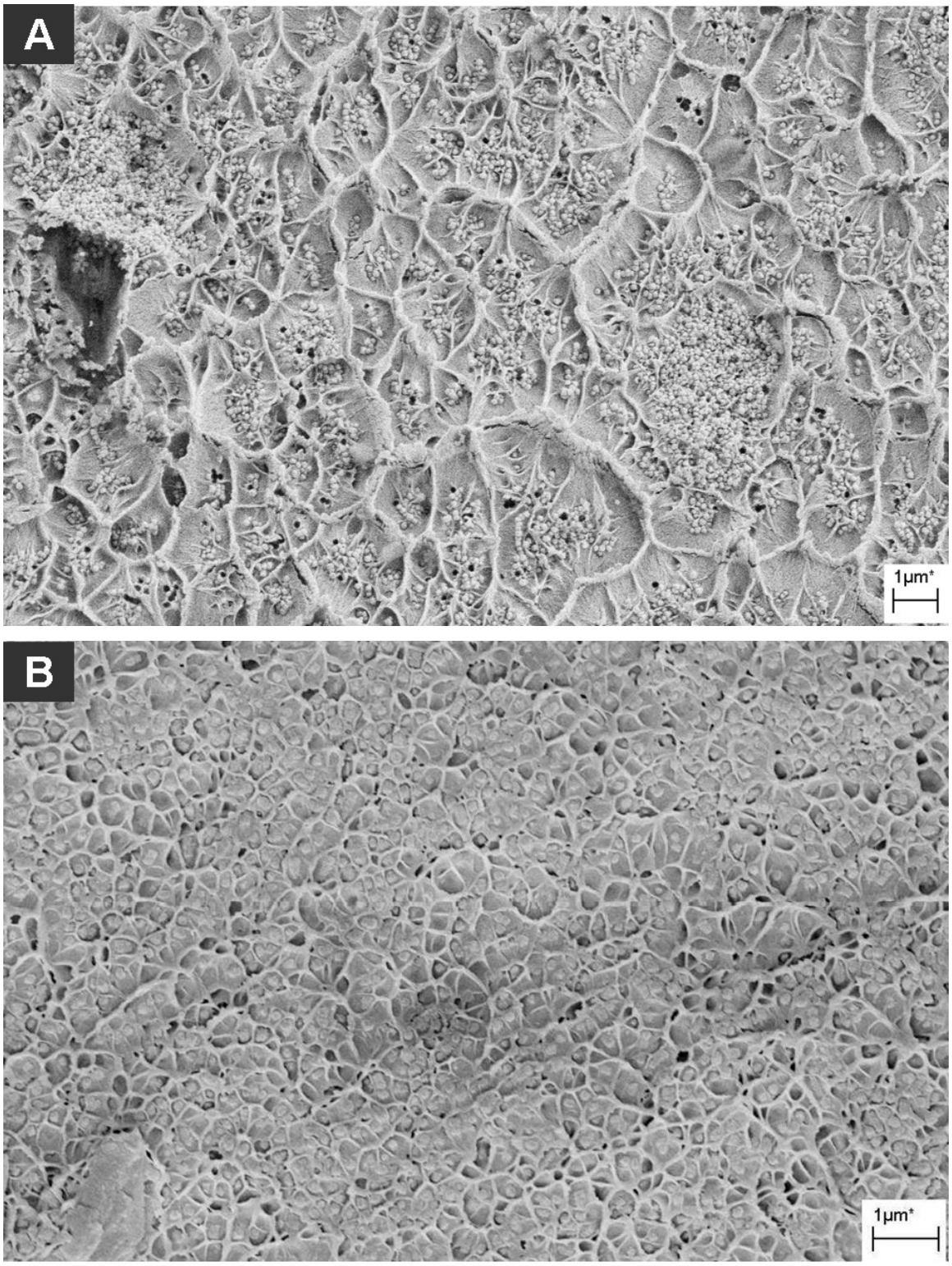

Figure 6.6 Dispersion of (A) bare calcined-MFI and (B) Grignard treated calcined-MFI in 6FDA-DAM matrix at 25 wt% loading

Agglomeration, driven by van der Waals attraction between nanoparticles, is detrimental to membrane separation performance. It is hypothesized that the $Mg(OH)_2$ formed during Grignard treatment enhanced the electrostatic repulsion between charged particles, effectively countering the van der Waals attraction, and therefore, stabilized the colloid dispersion of zeolite nanoparticles [9].

Table 6.2 Mixed matrix membrane performance using Grignard treated MFI particles

	35wt% GT-uncalcined	25wt% GT-uncalcined	Pure polymer	25wt% GT-calcined	35wt% GT-calcined
P_{nC4} [Barrer]	2.7± 0.2	3.0± 0.2	3.7± 0.2	6.4± 0.2	7.8± 0.2
Model P_{nC4}	*2.5*	*2.8*	-	*6.2*	*7.7*
nC4/iC4 [-]	23 ± 2	23 ± 2	21± 2	22 ± 2	23± 2
Model nC4/iC4	*21*	*21*	-	*21*	*21*

C4s permeation tests were done on pure 6FDA-DAM polymer and the mixed matrix membranes made with bare and Grignard treated MFI particles. The mixed matrix films with 25 wt% bare MFI were defective, with a significantly increased permeability and decreased selectivity for butane isomer compared to pure 6FDA-DAM polymers due to the presence of large potentially percolating defects. Table 6.2 shows the permeation results of the mixed matrix membranes and the pure polymer membrane. The membranes with 25 wt% and 35 wt% loading of GT-calcined-MFI have higher nC4 permeability than pure 6FDA-DAM polymer, while the selectivity of the nC4/iC4 was

the same within experimental uncertainty. The permeability of nC4 increased more than two-fold compared to pure polymer at 35wt% calcined- MFI loading. This permeability increase should not be the result of defective interfaces, because as shown in Figure 6.7, Grignard treated MFI particles appear to bond well with the polymer matrix.

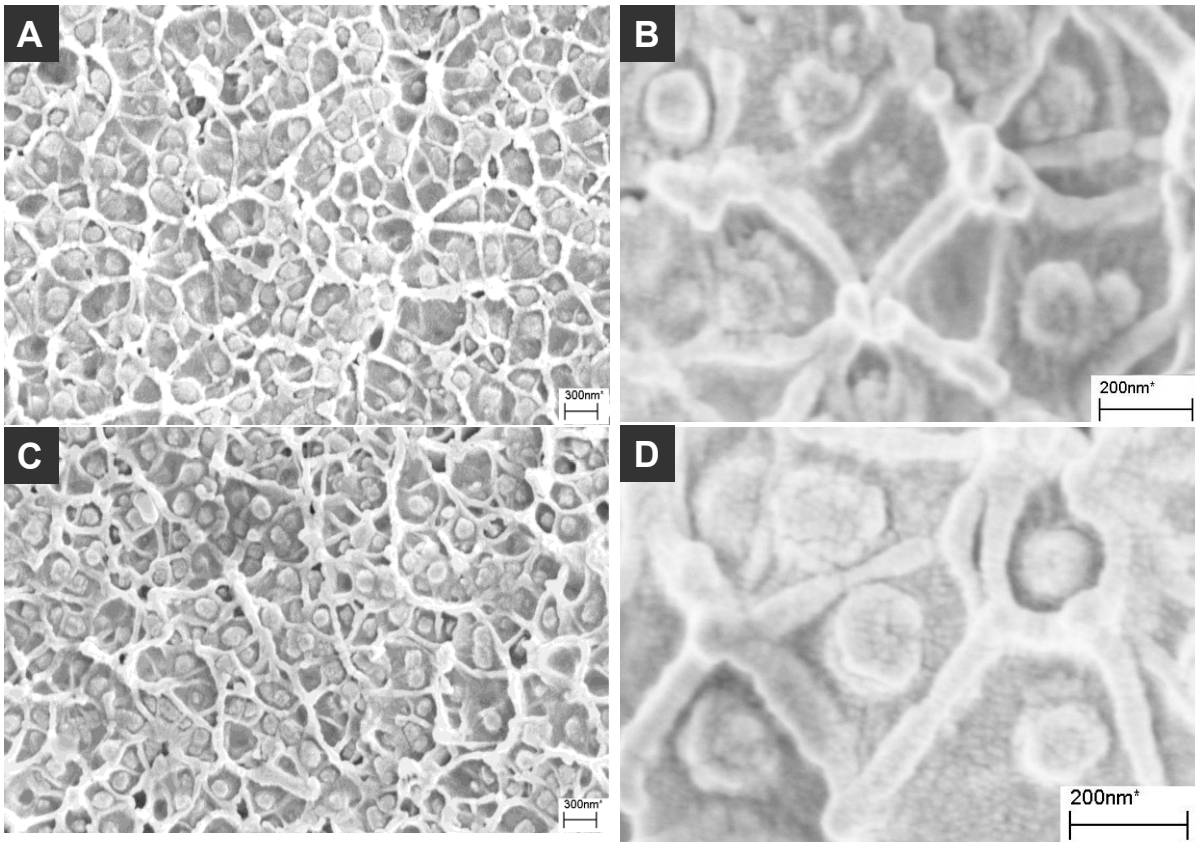

Figure 6.7 Cross-section of mixed matrix 6FDA-DAM films with Grignard treated particles: (A), (B) are films with calcined MFI and (C), (D) are films with uncalcined MFI in 6FDA-DAM, at 35wt% loading

Another possible reason for the mixed matrix membrane permeability increase can be that the MFI sieve is too permeable for C4s relative to the 6FDA-DAM polymer. The four different lines in Figure 6.8, indicate the 6FDA-DAM mixed matrix membrane permeation performance for C4s separation with different kinds of idealized highly

permeable sieves as estimated by the Maxwell model shown in Eq. 3.1. The high silica MFI and 6FDA-DAM polymer densities of 1.75 g/cm^3 [10] and 1.35 g/cm^3 [11], respectively, were used to convert weight concentration to volume concentration of sieves in polymer matrix. The four ideal sieves all have high nC4 permeability that is at least two orders of magnitude higher than that of the pure polymer. It was found that even with hypothetical sieves of different permeability and selectivity; all the mixed matrix membranes have the same permeability increase and constant selectivity at loadings up to 45 wt%, according to the Maxwell model. This modeling result showed that if the sieve permeability is far higher than that of the polymer matrix, the addition of sieve cannot enhance the mixed matrix performance at low loadings, and the sieves in the mixed matrix film act effectively as voids that cannot separate the C4s.

Most importantly, the mixed matrix film permeation results agree very well with the Maxwell model value with a sieve permeability of 1000 Barrer for nC4. Note in Figure 6.8. that a change of sieve selectivity from 1 to 50, and permeability from 500 Barrer to higher values does not change the model result significantly, if the sieve is too permeable than the polymer. G. Xomeritakis [12] showed that using a MFI membrane grown on Alumina porous support, the nC4 permeability was on the order of 1000 Barrer, far higher than the nC4 permeability of 3.7 Barrer in 6FDA-DAM polymer. The nC4 intracrystalline diffusivity of 5×10^{-6} cm^2/s [1] is also far higher than the nC4 diffusivity of 6×10^{-9} cm^2/s in 6FDA-DAM. Therefore, according to Maxwell model no selectivity enhancement should be expected even though the nC4/iC4 selectivity of more than 50 for MFI is higher than that in the polymer. It can be concluded (at low loading levels) that the MFI sieve is too permeable relative to the polymer, this being the main cause for the

increased permeability and constant selectivity in the mixed matrix membranes with Grignard treated MFI particles.

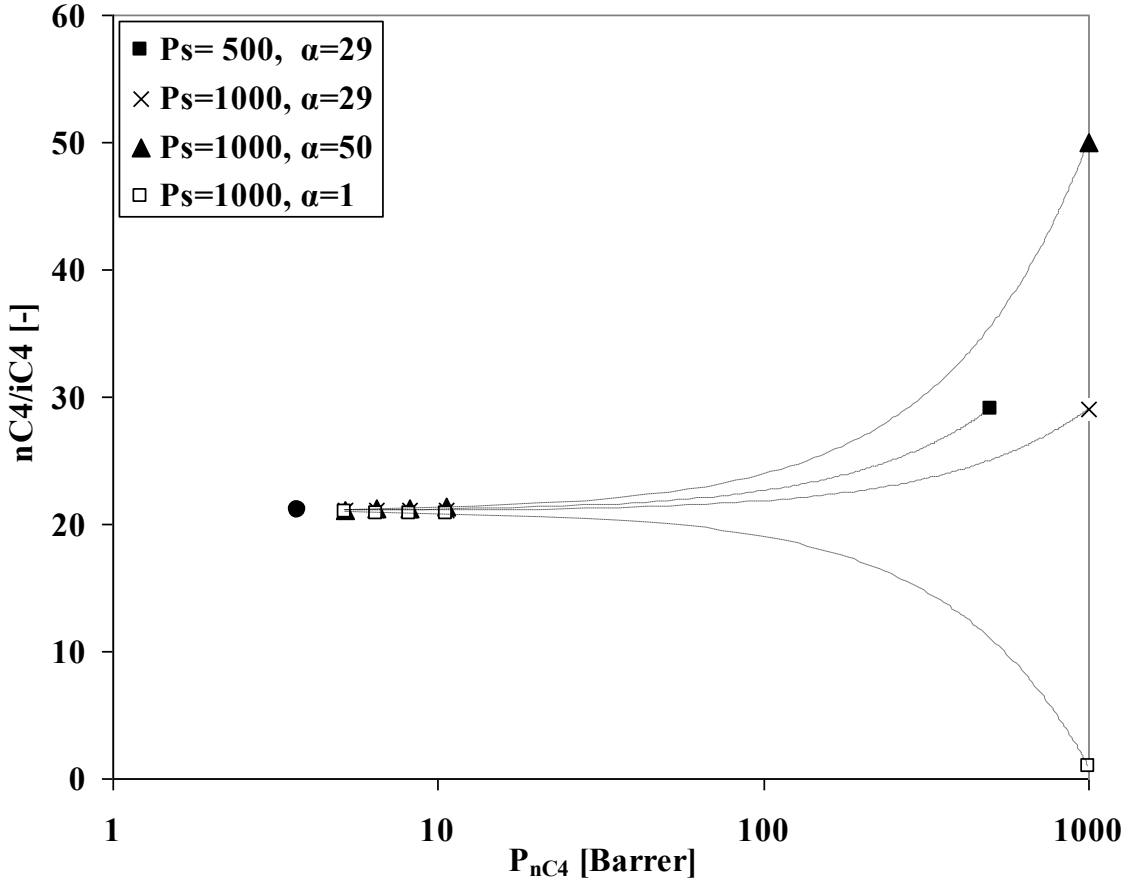

Figure 6.8 Prediction of mixed matrix membrane performance using 6FDA-DAM polymer and different highly permeable sieves, the solid point at left is pure polymer, and the other five points on every line from left to right are 15 wt%, 25 wt%, 35 wt% and 45 wt% loading using the Maxwell model and pure sieves

6.2 6FDA-DAM AND MFI(UNCALCINED) MIXED MATRIX MEMBRANES

To further verify the interfacial adhesion between the Grignard treated particles and 6FDA-DAM matrix is sufficient so that gaps do not contribute to the poor selectivity of the mixed matrix film, uncalcined-MFI particles, with template inside of the pores, were Grignard treated and made into mixed matrix membranes using the 6FDA-DAM

polymer at different sieve loadings. A similar surface roughening, as shown in Figure 6.3, was obtained on the uncalcined- MFI particles after Grignard treatment. Good interfacial adhesion with both Grignard treated calcined and uncalcined MFI particles can be verified with the SEM images shown in Figure 6.7. Permeation tests were done on the mixed matrix films with 25 wt% and 35 wt% Grignard treated uncalcined-MFI loading. The permeation results shown in table 6.2 indicate a permeability decrease, as anticipated since the uncalcined-MFI is impermeable with organic template occluding the zeolite pores. More importantly, the permeation results in mixed matrix films are very close to the Maxwell model results with a non-permeable sieve in the polymer matrix with perfect interfacial bonding. A higher sieve density of 2.0 g/cm^3 was used in the model based on the theoretical composition of $4TPAOH{\cdot}96SiO_2$ in uncalcined- MFI and the density of calcined- MFI. The agreement between experimental and model calculation suggest that a good interfacial adhesion was achieved between the Grignard treated MFI particles and 6FDA-DAM polymer. This observation further supports the hypothesis that the huge permeability increase observed in the Grignard treated, calined MFI mixed matrix films was not caused by defective interfacial bonding, but by the mismatch between the permeability of the sieve and the polymer.

In summary, an nC4 permeability of 3.7 Barrer, and nC4/iC4 ideal selectivity of 21 was found in pure 6FDA-DAM polymer membrane. High silica MFI nanoparticles were treated using a two-step Grignard method. Good interfacial adhesion between Grignard treated MFI and polymer was achieved. However, because of the mismatch between sieve and polymer, no selectivity enhancement for C4s separation is observed for mixed matrix membranes composed of MFI and 6FDA-DAM polymer. A zeolite with

smaller pore size than MFI (hence a lower C4 permeability) is needed to better match 6FDA-DAM and other glassy polymers to make promising mixed matrix membranes for butane isomer separation.

6.3 PDMS-MFI MIXED MATRIX MEMBRANES

Rubbery polymers such as PDMS have high permeability for hydrocarbons. C4s' sorption in PDMS obeys Henry's law, as shown in Figure 6.9. The Henry's constants for nC4 and iC4 in PDMS are 0.134 and 0.112 cc(STD)/(cc·cmHg) respectively, therefore, the solubility selectivity is only 1.20 for C4s in PDMS at 50 °C. The diffusivity of C4s in PDMS is strongly concentration dependent, as shown in the transient sorption results in Figure 6.9. This is because the presence of C4s molecules increases the mobility of PDMS chains. The diffusivity of nC4 and iC4 at 7.5 psi are 6.2×10^{-6} and 3.7×10^{-6} cm^2/s, therefore, the diffusivity selectivity is 1.7 for C4s in PDMS at 7.5 psi. The permeability of nC4 in PDMS increases from 4170 to 7100 Barrer when upstream pressure increases from 5 psi to 35 psi, because of enhanced diffusivity at higher pressure. The C4s selectivity changes little from 1.9 to 2.1 when pressure increases from 5 psi to 35 psi, because of similar mobility enhancement from the nC4 and iC4 molecules.

Sorption of C4s in MFI follows Langmuir law. As shown in Figure 6.9, the nC4 solubility reaches equilibrium at low pressure because of their high condensability. The nC4 molecules sorbs about two times more than iC4 molecules. In other word, C4s has a solubility selectivity about 2 in MFI, if we can simplify the transport process in MFI to a similar sorption-diffusion model as that in polymer. In the real case, the diffusion process through zeolites is more complicated than that in polymers. The diffusivity in zeolite is

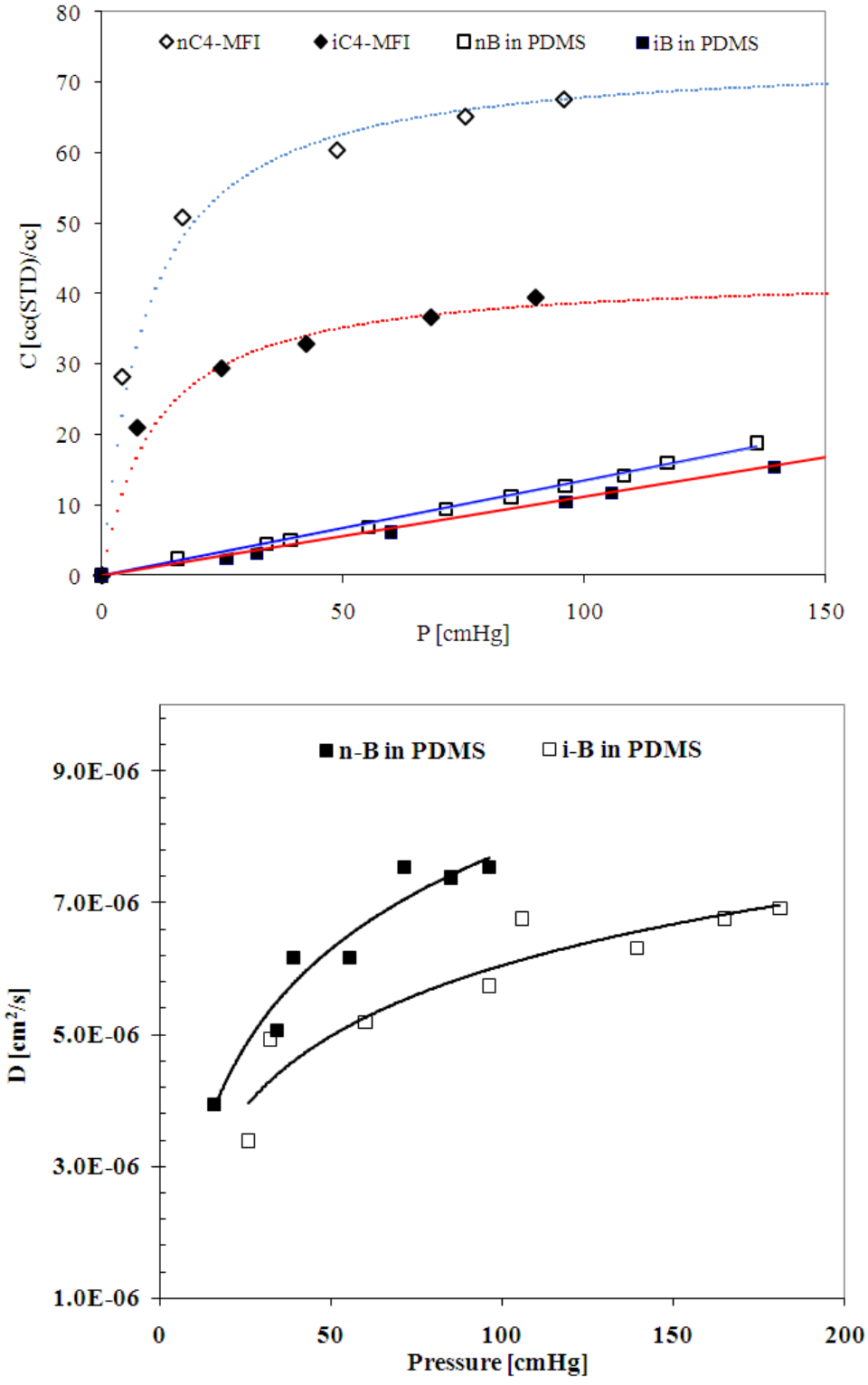

Figure 6.9 Solubility (top) and diffusivity (bottom) of butane isomer at various pressures in PDMS films (50 °C) and MFI particles (100 °C)

concentration dependent because of the non-linear relationship between pressure and solubility, and interaction between the diffusing molecules [25]. Different methods can be used to measure the diffusivity in zeolites. There is debate on the reliability of different techniques, but generally diffusivity results from different methods converge to a reasonable degree. The nC4 diffusivity in MFI is on the order of magnitude of 10^{-6} cm/s [1], which is close to the diffusivity in PDMS. The close nC4 permeability and much higher C4s selectivity in MFI compared to those in PDMS make PDMS-MFI a potential pair for mixed matrix membrane used for C4s separation.

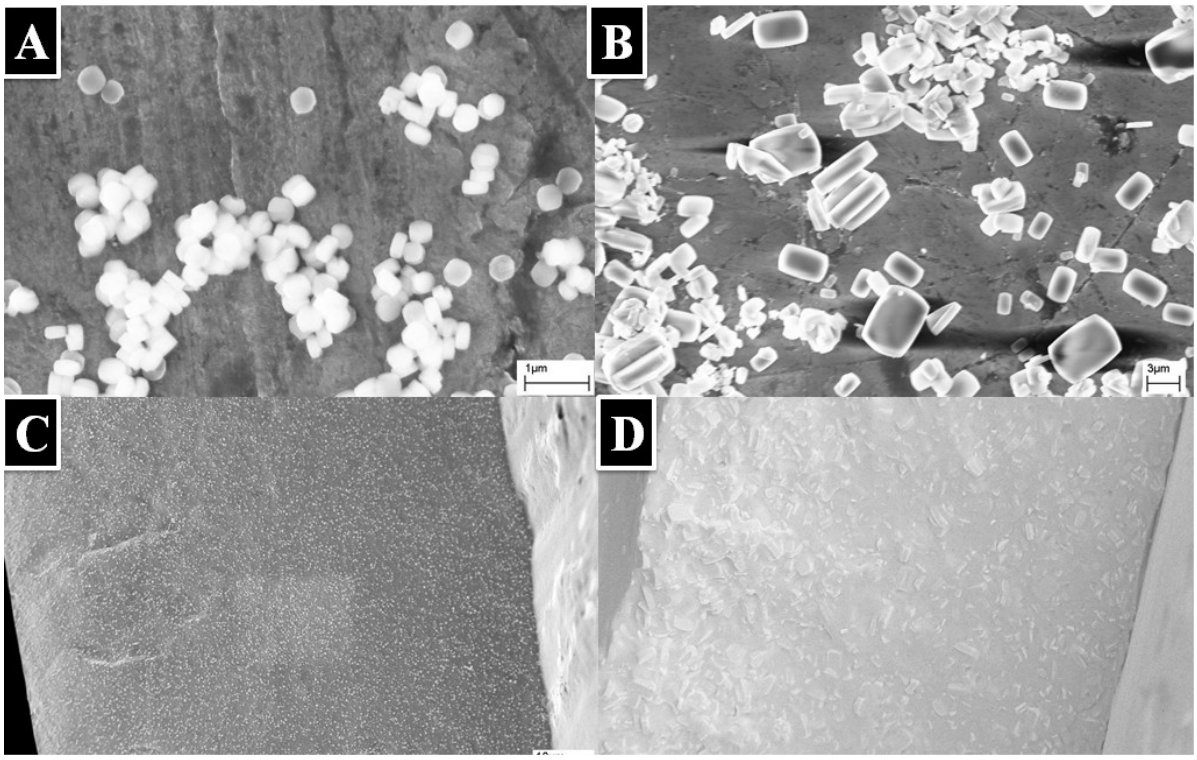

Figure 6.10 Zeolite MFI particles and cross section of PDMS-MFI mixed matrix membranes: 300 nm MFI (A, C); 5 μm MFI (C, D)

Mixed matrix membranes containing PDMS and MFI of different sizes were made. Figure 6.10 shows the good dispersion of MFI particles and interfacial adhesion

between PDMS and MFI particles. Because of the pressure dependence of C4s' permeability in PDMS, the permeation tests were done at fixed upstream pressure of 15 psi on mixed matrix membranes.

Table 6.3 Transport properties of PDMS-MFI mixed matrix membranes, test with upstream 15 psi, 50 °C

	P_{nC4}	$\alpha_{n/i}$
Pure PDMS	4980	1.9
50 wt% MFI(300nm)	8120	4.0
50 wt% MFI(5 μm)	12100	5.6
60 wt% MFI(300 nm)	11840	4.8
60 wt% MFI(5 μm)	11400	5.7

Table 6.3 shows the permeation results of different mixed matrix membranes. Both nC4 permeability and nC4/iC4 selectivity increase in all PDMS-MFI mixed matrix membranes. In membranes containing 300 nm MFI particles, both nC4 permeability and nC4/iC4 selectivity increase at higher particle loading. The effective nC4 permeability and nC4/iC4 selectivity in 300 nm MFI are 15500 Barrer and 11 respectively, back calculated using the Maxwell model (from 50wt% loading mixed matrix membranes). It is worth noting that the permeation test were done with upstream and downstream pressure at 15 psi and vacuum respectively, therefore, effective permeability is used because there is a diffusivity variation across the membrane. Mixed matrix membrane containing 50 wt% of 5 μm MFI particles shows higher permeability and selectivity for C4s separation compared to that with 50 wt% of 300 nm particles. Research shows that

MFI crystals grow preferentially along the direction of zig-zag channels [26], therefore, more nC4 selective straight channels are available in bigger MFI crystals. The mixed matrix membranes show higher C4s performance because of the addition of bigger crystals, which have higher C4s separation performances. Mixed matrix membranes containing 60 wt% of 5 μm MFI particles show little further selectivity enhancement but decreased nC4 permeability than the membrane with 50 wt% of 5 μm MFI particles, probably due to the more defective interfacial adhesion at higher loadings. The effective nC4 permeability and nC4/iC4 selectivity in 5μm MFI are 40000 Barrer and 28 respectively, back calculated using the Maxwell model.

In summary a good match between PDMS and MFI is found for C4s separation. The high C4s permeability in MFI further confirmed that no glassy polymer can be permeable enough to match the MFI to make useful mixed matrix membranes for C4s separations, as shown in previous research. PDMS-MFI mixed matrix membranes show enhanced selectivity for C4s separation, which is however, still much lower than that in glassy polymers. Because of the ability to make high surface area hollow fiber modules, glassy polymers are desired for membrane formation.

6.4 6FDA-DAM-5A MIXED MATRIX MEMBRANES

The molecule diffusion in glassy polymers is typically much lower than those in rubbery polymers. 6FDA-DAM and 6FDA-DAM-DABA (3:2) are two highly permeable polymers for gas separations. As shown in Figure 6.11, the nC4 diffusivity are about

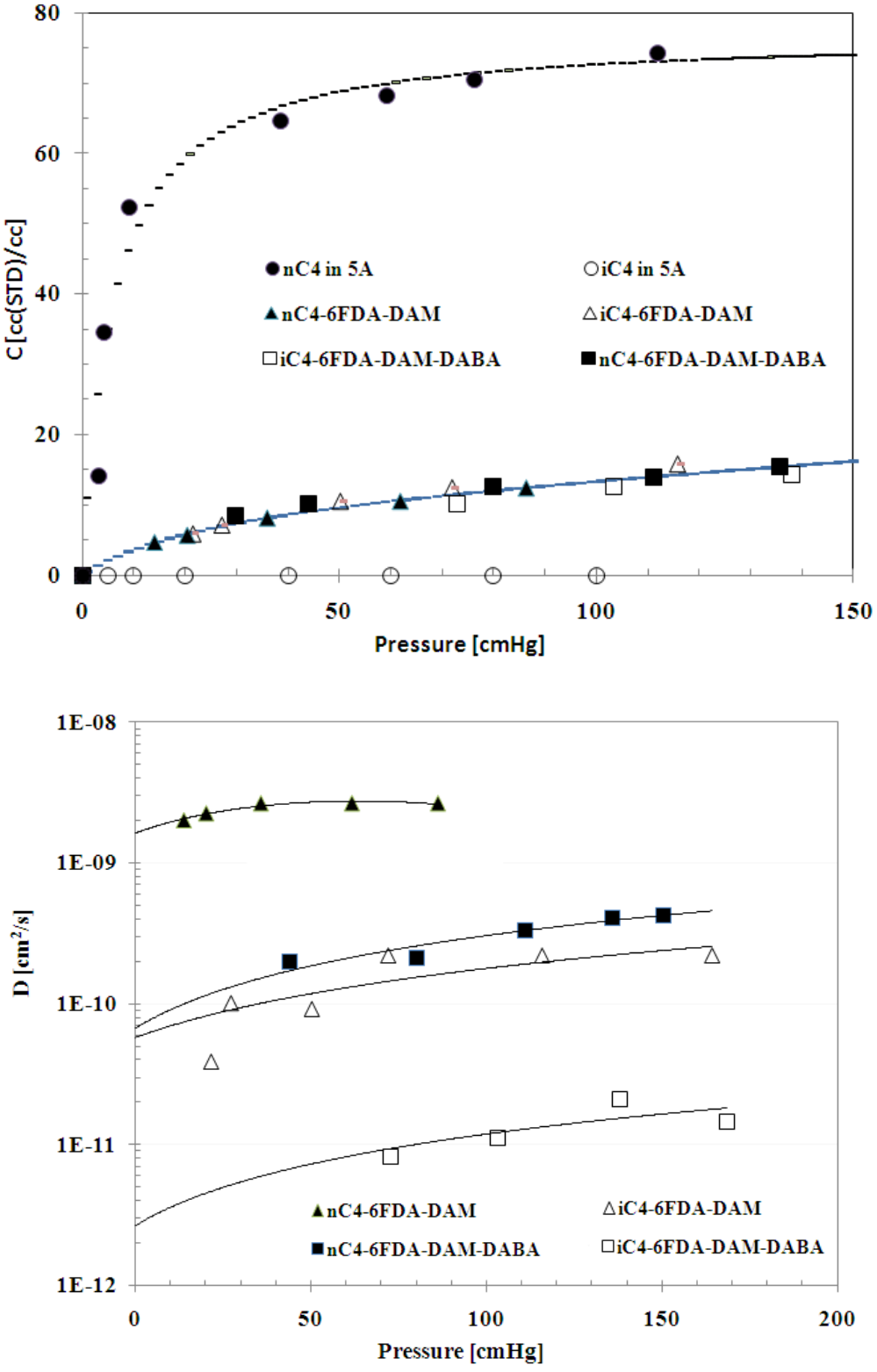

Figure 6.11 Solubility (top) and diffusivity (bottom) of butane isomer at various pressures in 6FDA-DAM and 6FDA-DAM-DABA (3:2) films and 5A particles at 100 ^{0}C

2×10^{-9} and 2×10^{-10} cm^2/s in 6FDA-DAM and 6FDA-DAM-DABA membranes respectively, which are three to four order of magnitudes lower than that in PDMS membrane. The C4s solubility is close in all three polymers, therefore the difference in C4s permeability is mainly due to the diffusivity difference.

The nC4 sorption is much higher than that in the two glassy polymers, while the iC4 shows negligible sorption in zeolite 5A. This confirms the practical infinite selectivity for C4s separation in zeolite 5A. The diffusivity (''corrected diffusivity'') of nC4 in zeolite 5A is reported to be 5×10^{-9} cm^2/s at 100 °C [16], which is very close to that in 6FDA-DAM polymer. The close nC4 permeability and infinite C4s selectivity in zeolite 5A compared to those in 6FDA-DAM make 6FDA-DAM-5A a potential pair for mixed matrix membrane used for C4s separation at loading higher than 20wt%.

Table 6.4 C4s transport properties in the mixed matrix membranes

	P_{nC4} [Barrer]	$\alpha_{n/i}$
6FDA-DAM (WQ0807)	3.7±0.2	21±2
20wt%-GT-5A-6FDA-DAM*	3.4±0.2	25±2
25wt%-GT-5A-6FDA-DAM*	3.4±0.2	26±2
25wt%-GT-5A-6FDA-DAM**	3.3±0.2	25±2
back calculated 5A	*2.5*	∞(ideally)
6FDA-DAM-DABA*	0.30±0.02	-
28.5 wt%-GT-5A-6FDA-DAM-DABA (WQ0903)	0.52±0.03	-
back calculated 5A	*3.5*	∞(ideally)

* Using Grignard treated commercial micron 5A particles (GT04)
** Using Sol-gel-Grignard treated commercial micron 5A particles (GT98-4)

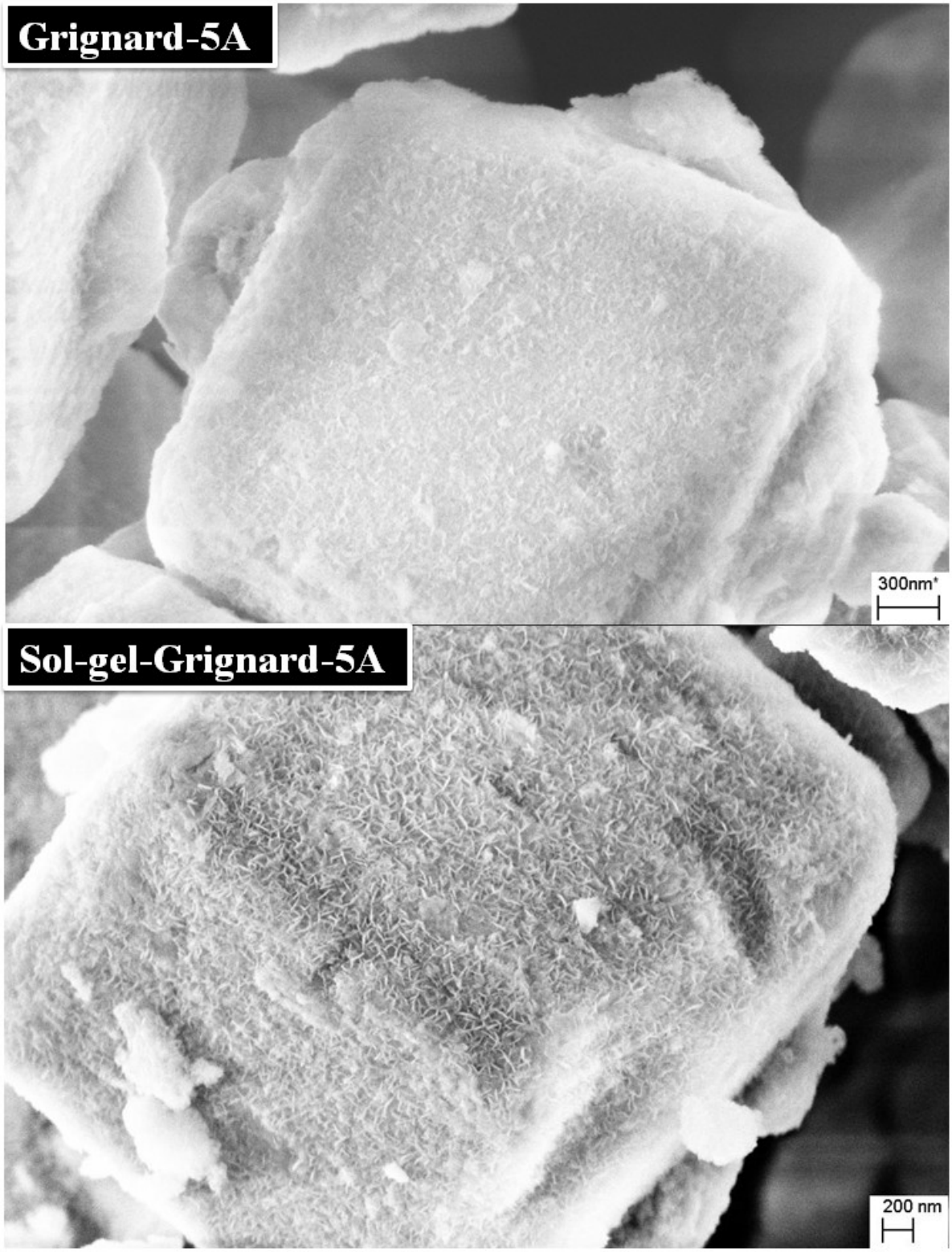

Figure 6.12 Surface treated 5A particles using traditional Grignard treatment (top) and Sol-gel Grignard treatment (bottom)

By adding zeolite 5A into polymeric membranes, the butane isomer performance should be enhanced if the zeolite and polymer is properly adhered. Defective interface (so called 'sieve-in-a-cage' morphology) is formed when bare 5A is added into 6FDA-DAM polymer, as shown in Figure 6.13. Gas molecules can bypass the zeolite through the defective interfaces. Pinholes can be generated if voids are interconnected in extreme cases.

It is reported that the $Mg(OH)_2$ nanowhiskers on zeolite surface can provide molecular scale interlocking with polymer chains and enhance the adhesion between zeolite and polymer [27]. $Mg(OH)_2$ whiskers, at a solid content of 9 wt%, were formed on zeolite 5A surfaces using sol-gel-Grignard treatment as described in chapter 4. For the mixed matrix membrane containing treated zeolite, the zeolite-polymer interfacial adhesion is improved significantly. The permeation results of these membranes are shown in table 6.4. The mixed matrix membrane containing bare 5A has increased n-butane permeability, but the selectivity for butane isomer is actually far lower than that in pure polymer. This is possibly due to the pinholes generated by the defective interfaces, which can reduce selectivity [28]. In the mixed matrix membrane containing treated 5A, the selectivity of butane isomer increased about 20% at 25wt% zeolite loading due to the addition of i-butane blocking 5A particles. The n-butane permeability decreases slightly in 6FDA-DAM-5A mixed matrix membranes compared to 6FDA-DAM polymer membrane. According to the Maxwell model, an effective 5A permeability of 2.5 Barrer can be back calculated using the pure polymer and mixed matrix membrane permeation properties. Because the nC4 has several times higher solubility in 5A than that in 6FDA-DAM polymer, the relatively lower nC4 permeability in 5A must be due to the lower nC4

diffusivity in 5A than in 6FDA-DAM polymer. The effective diffusivity of nC4 in 5A is therefore, lower than that in 6FDA-DAM polymer (2×10^{-9} cm^2/s) and the reported nC4 diffusivity in 5A (5×10^{-9} cm^2/s) [16].

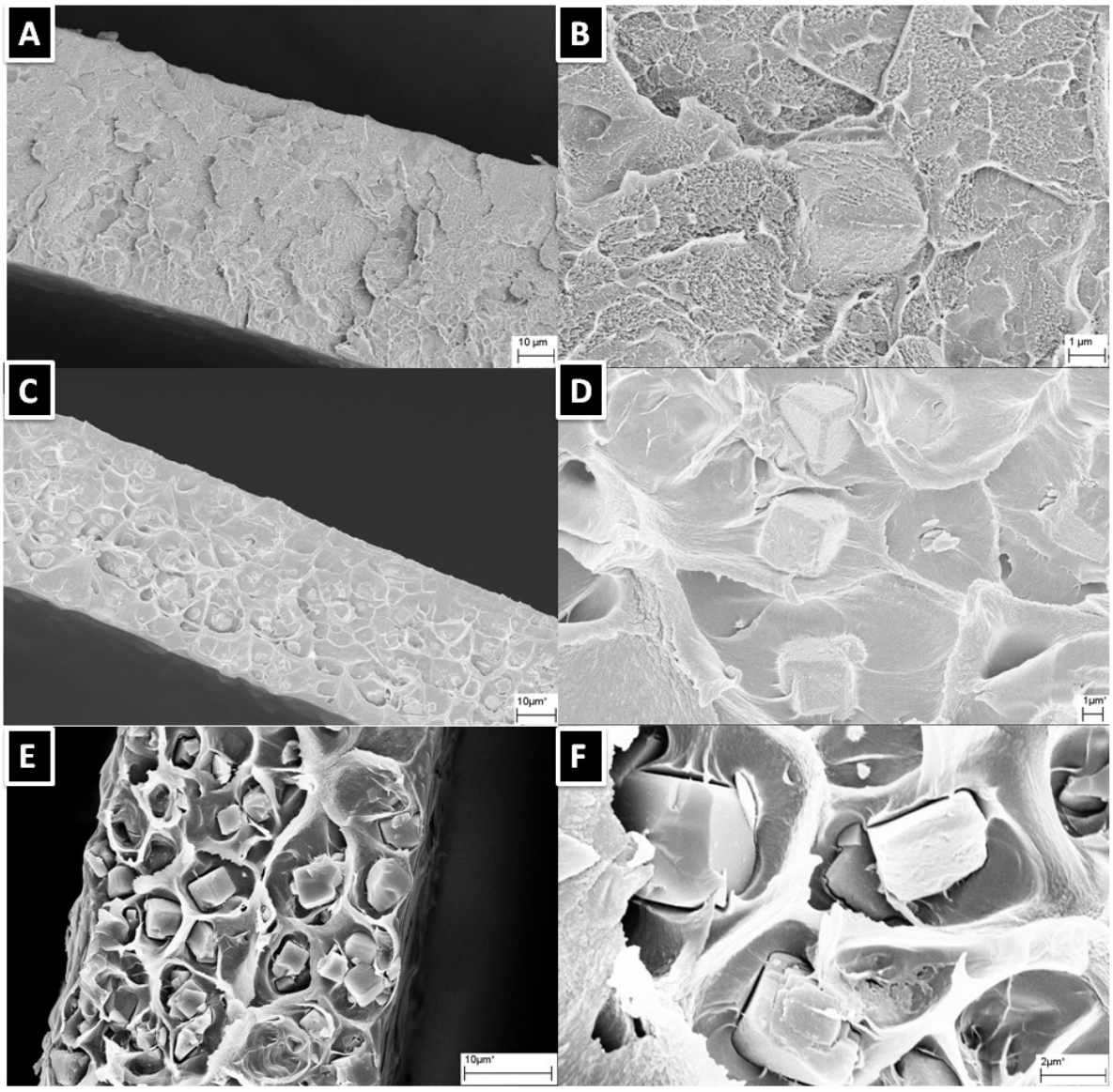

Figure 6.13 Cross section of mixed matrix films containing 6FDA-DAM polymer and 25wt% Sol-gel-Grignard treated 5A (A, B), Grignard-treated 5A (C, D) and bare 5A (E, F)

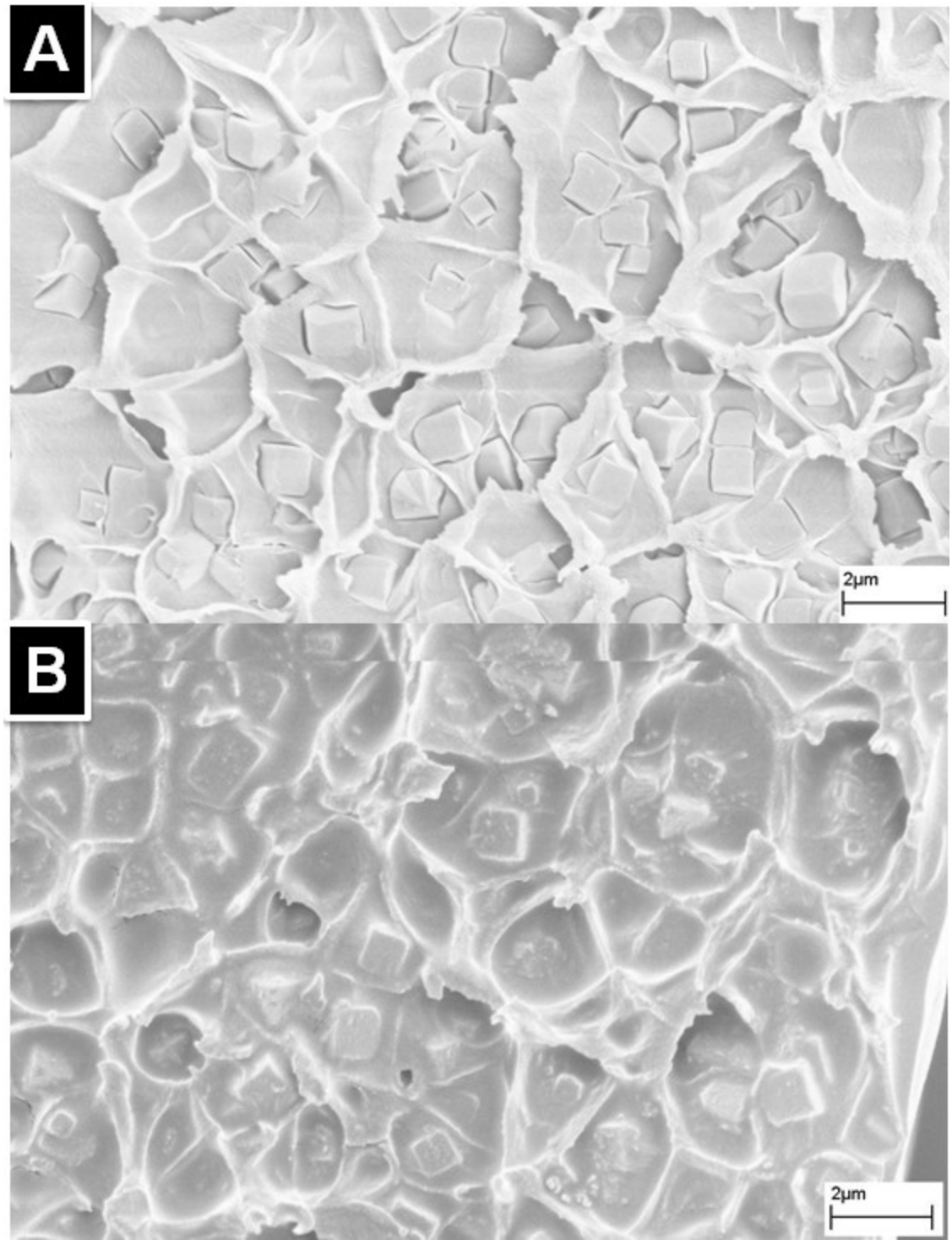

Figure 6.14 Cross section of mixed matrix films containing 6FDA-DAM-DABA (3:2) polymer and 25wt% bare 5A (top), and 28wt% Grignard treated 5A (bottom).

The diffusivity in zeolite 5A is reported to be dependent on factors such as the synthesizing procedures, Ca^{2+} ion exchange content, *etc.* At different Ca^{2+} exchange rate of 65% and 95%, the nC4 corrected diffusivity in 5A are 2×10^{-9} and 5×10^{-9} cm^2/s respectively at 100 °C. A much lower nC4 diffusivity is found in commercial Linde 5A than in lab made 5A, possibly because of partially blockage of zeolite pores in commercial 5A [16]. The commercial 5A used in this research has a Ca^{2+} ion exchange rate of 77%, higher than the requirement of 67% for fully open pores [25]. The zeolite 5A pores may also undergo a certain level of change during the surface treatment process, which possibly contributed to the slightly reduced diffusivity. Further study is needed on this aspect.

As shown in the introduction, a good match between polymer and zeolite can lead to mixed matrix membranes with both increased nC4 permeability and nC4/iC4 selectivity, *in other words, an increased nC4 permeability and decreased iC4 permeability*. Because of the relatively lower nC4 permeability in 5A versus 6FDA-DAM polymer, no nC4 permeability can be expected and the mixed matrix effect is somewhat compromised in 6FDA-DAM-5A mixed matrix membranes.

In order to better match the nC4 transport properties in 5A, 6FDA-DAM-DABA, which has an nC4 permeability 10 times slower than that in 6FDA-DAM, was used to make as the matrix polymer. Good adhesion can be found in 6FDA-DAM-DABA mixed matrix membranes containing surface treated 5A particles, compared to the defective interfaces in membrane with bare 5A particles, as shown in Figure 6.14. The carboxylic acid groups on 6FDA-DAM-DABA polymer chains may chemically or hydrogen bond

with the $Mg(OH)_2$ whiskers on treated zeolite 5A surfaces, through the strong acid-basic interaction. Further studies are needed on this aspect also.

The nC4 permeability increases by 73% in 6FDA-DAM-DABA-5A mixed matrix membrane at 28 wt% loading, compared to pure polymer membrane, because of the higher nC4 permeability in 5A than in 6FDA-DAM-DABA. According to the Maxwell model, an effective 5A permeability of 3.5 Barrer can be back calculated using the pure polymer and mixed matrix membrane permeation properties. This value generally agrees with the one back calculated from 6FDA-DAM-5A mixed matrix membranes. The iC4 permeability could not be measured because the system leak rate at high temperature approaches the permeation rate of iC4 through 6FDA-DAM-DABA membranes. A potential good match between 6FDA-DAM-DABA and zeolite 5A can lead to mixed matrix membranes with both increased nC4 permeability and nC4/iC4 selectivity. According to the Maxwell model, nC4 permeability of 0.49 Barrer and nC4/iC4 selectivity of 51 (assuming a selectivity of 25 in polymer) can be achieved using mixed matrix membrane containing 25wt% of 5A particles. The attractive high nC4/iC4 selectivity with an adequate nC4 permeability make 6FDA-DAM-DABA-5A mixed matrix membranes the most promising for C4s separation.

It needs to be noted that all the permeation experiment were done at fixed upstream pressure of 25 psi and a vacuum downstream using pure gas feed. The polyimides, however, showed no tendency to plasticize, so the ratio of pure gas permeabilities should provide good estimate of mixed gas feed performances. Mixed gas measurements are challenging in the system due to the very low iC4 permeabilities. In real cases, the diffusion in zeolite is pressure dependent, the C4s transport properties in 5A can be different from what derived in this research, under other operating conditions.

6.5. CONCLUSIONS

Polymer-zeolite matching of transport properties is a critical requirement for successful mixed matrix membrane formation. The highly permeable and selective zeolite MFI can match well with PDMS polymer for C4s separation. Permeability of nC4 and nC4/iC4 selectivity in PDMS-MFI mixed matrix membrane containing 50wt% of 5 μm MFI particles increased to 2.4 and 2.9 times of those in PDMS membrane. The nC4 permeability in MFI was back calculated to be on the order of magnitude of 10000 Barrer, according to Maxwell model. The large difference of C4s permeability in MFI and 6FDA-DAM (3.7 Barrer) caused the unsuccessful 6FDA-DAM-MFI mixed matrix membrane without enhanced nC4/iC4 selectivity. Zeolite 5A with smaller pore size and slower nC4 diffusion rate was used to match the 6FDA-DAM and 6FDA-DAM-DABA glassy polymers. 6FDA-DAM-5A mixed matrix membranes indicated significant enhanced nC4/iC4 selectivity, because the addition of iC4 blocking 5A particles caused the reduction of iC4 permeability. The nC4 permeability in 6FDA-DAM-5A mixed matrix membranes decreases slightly because the lower permeability in 5A than in 6FDA-DAM polymer. A potentially better match is between 6FDA-DAM-DABA and 5A for C4s separation. The enhanced nC4/iC4 selectivity can potentially be achieved by both enhanced nC4 permeability and depressed iC4 permeability, therefore, a much larger selectivity enhancement than that in 6FDA-DAM-5A mixed matrix membranes with only iC4 permeability reduction.

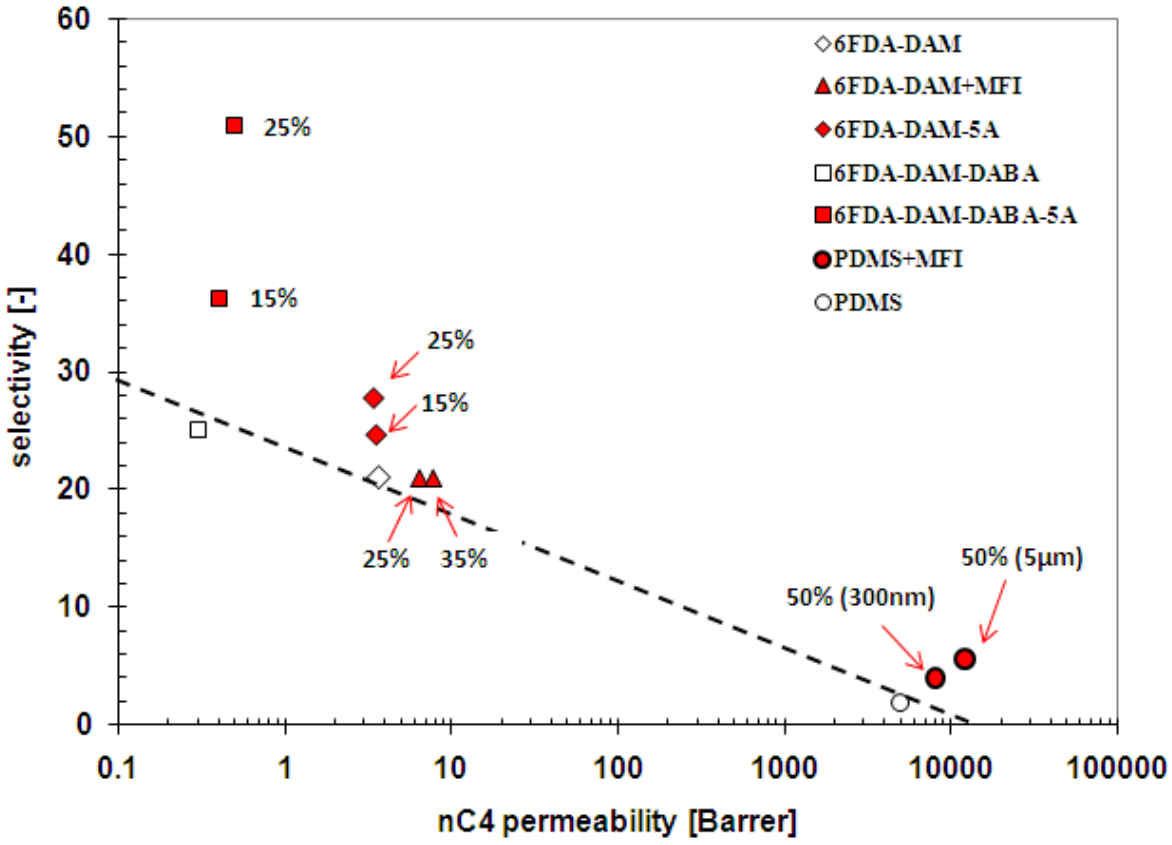

Figure 6.15 Butane isomer separation performances of various polymeric and mixed matrix membranes containing different amount of (weight percentage) 5A (according to the Maxwell model) and MFI particles (experimental results)

The matching between different polymers and zeolites can be summarized into Figure 6.15. The results of mixed matrix membranes containing MFI particles are from experimental measurements. The results of mixed matrix membranes containing 5A particles are calculated through the Maxwell model assuming nC4 permeability of 2.5 Barrer and infinite selectivity in 5A. Mixed matrix membranes containing zeolites showed higher C4s separation performances than the polymeric membranes. The most promising pair for C4s separation is 6FDA-DAM-DABA and zeolite 5A. Further study is needed to study this promising mixed matrix membrane for C4s separation.

6.6 REFERENCES

[1] B. Millot, Permeation of linear and branched alkanes in ZSM-5 supported membranes, *Micropor. Mesopor. Mat.*, **2000**, 38, 85-95

[2] D. T. Hayhurst, Diffusion of C1 to C5 normal paraffins in silicalite, *Zeolites*, **1988**, 8, 27-29

[3] H. Jobic, Diffusion of linear and branched alkanes in ZSM-5. A quasi-elastic neutron scattering study, *J. Mol. Catal. A-Chem.*, **2000**, 158, 135-142

[4] A. Ferreira, Adsorption and differential heat of adsorption of normal and iso-butane on Zeolite MFI, *Micropor. Mesopor. Mat.*, **2006**, 91, 47-52

[5] W.J. Koros, Carbon dioxide sorption and transport in polycarbonate, *J. Polym. Sci. Pol. Phys.*, **1976**, 14, 687-702

[6] S. Shu, Formation of nanostructured zeolite particle surfaces via a Halide/Grignard route, *Chem. Mater.***, 2007,** 19, 4000-4006

[7] S. Shu, Ph. D thesis, Georgia Institute of Technology, **2007**

[8] S. Shu, Sonication-assisted dealumination of Zeolite A with thionyl chloride, *Ind. Eng. Chem. Res.*, **2007**, 46, 767–772

[9] S. Husain, Ph. D thesis, Georgia Institute of Technology, **2006**

[10] E. Flanigen, ZSM-5, a new hydrophobic crystalline, silica molecular sieve, *Nature*, **1978**, 271, 512-516

[11] K. Tanaka, Permeation and separation properties of polyimide membranes to olefins and paraffins, *J. Membrane Sci.*, **1996**, 121, 197-207

[12] G. Xomeritakis, Transport properties of alumina-supported MFI membranes made by secondary growth, *Micropor. Mesopor. Mat.*, **2000**, 38, 61-73

[25] J. Karger, Diffusion in zeolites, **1999**, John Wiley & Sons

[26] M. C. Lovallo, AICHE, **1998**, 44, 1903-1913

[16] H. Yucel, *J.C.S. Faraday I*, **1980**, 76, 71-83

[27] S. Shu, *J. Phys. Chem. C*, **2007**, 111, 652-657

[28] T. T. Moore, *J. Mol. Struct*., **2005**, 739, 87-98

CHAPTER 7

DUAL LAYER HOLLOW FIBER SPINNING OF 6FDA POLYIMIDES

7.1 OVERVIEW

Macrovoid-free, delamination-free 6FDA-DAM/cellulose acetate dual layer hollow fiber membranes were fabricated. The $LiNO_3$ enhanced the phase separation rate of 6FDA-DAM sheath, which was slow otherwise. The effect of various spinning parameters on dual layer hollow fiber morphology is discussed. A longer time for polymer chain inter-diffusion at the interface before phase separation may assist interfacial adhesion, as probed by SEM investigations of morpholohy. The dual layer hollow fiber membrane showed defect-free gas transport properties for faster gas pairs, such as CO_2/CH_4, and O_2/N_2. The separation performance was below intrinsic value for slower gas pair n-C_4H_{10}/i-C_4H_{10}, because of possible presence of exceedingly minor defects that were undetectable for the higher flux gases. The fast phase separation rate of the $LiNO_3$ containing solution probably may have contributed to the minor defects. 6FDA-DAM-DABA/CA dual layer hollow fibers were fabricated using a similar way. The dual layer hollow fibers showed similar gas transport properties due to the addition of $LiNO_3$. The effectiveness of post treatment on these dual layer hollow fiber membranes was also discussed in this chapter.

7.2 CHALLENGES OF DUAL LAYER HOLLOW FIBER SPINNING

Because of the low cost associated with equipment installation, and large potential energy saving advantages, membrane based gas separations also provide an attractive

alternative to traditional thermally intensive cryogenic distillations and adsorption swing methods. A diverse array of gas processing applications using membranes exist, because polymeric membranes are relatively inexpensive, and can be processed into efficient and economical modules. A membrane material should have high selectivity and permeability in order to have wider economic membrane application for diverse gas separations, and 6FDA-polyimides with rigid fluorinated chains and high unrelaxed free volumes [1-5] satisfy these needs. Research has increased the stability of dense films using these polymers [6-8]. The material processing research to develop the practical asymmetric hollow fiber membranes using these advanced materials is a less developed area, and is the focus of this study.

Asymmetric hollow fiber membranes have high productivity, because of high surface area-to-volume ratios, low resistance to gas flow, and ability to withstand high transmembrane pressure drops. Hollow fiber membranes are effectively fabricated using a dry jet/wet quench process, as shown in Fig. 3.8. Within the air gap, the nascent selective skin layer is formed by evaporation of volatile component, while the porous structure is formed by phase separation of spinning dope in the quench bath. This support layer under the skin adds negligible permeating resistance, and supports the separating skin layer in the presence of high pressure. 6FDA polymers are however very expensive for spinning of single layer fibers; therefore, a dual layer fiber design can be used to reduce the cost. Such a composite structure is reported in this study. An inexpensive, commercial polymer is preferred to act as the support layer, and 6FDA polymers are only used in the sheath with a dense skin for separation purposes. This design can effectively cut as much as 90% of the material cost [9], however, the dual layer spinning process

adds additional technical challenges to the already complex spinning process. Delamination-free, macrovoid-free dual layer hollow fibers are needed for sufficient mechanical properties. There have been a number of studies on dual layer hollow fibers spinning using commercial polymers as both the support and sheath layer materials [10,11]. On the other hand, studies of dual layer hollow fibers using 6FDA polymers as a sheath layer has lagged behind, even though numerous studies have shown superior separation performance of these 6FDA polyimides in dense films. Li tried polyethersulfone (PES) as the support for 6FDA-durene-mPDA sheath layer [9]. A defect free, delamination free dual layer hollow fiber was reported by controlling the PES dope compositions and spinning parameters; however, the PES support layer contains many macrovoids, which are detrimental to mechanical strength of the hollow fibers. In this research, cellulose acetate (CA), a polymer used for commercial RO membranes, is used as the support layer for a 6FDA-DAM (shown as below) polymer sheath. The dual layer 6FDA-DAM/CA hollow fiber showed ideal morphologies, *i.e.*, macrovoid free, delamination free, and good gas transport properties.

7.3 DUAL LAYER HOLLOW FIBER SPINNING OF 6FDA-DAM POLYIMIDE

7.3.1 Formation of spinning dopes

Wallace [13] created a guideline for developing single layer hollow fiber membranes using novel polymers. An initial spinning dope is determined by the three phase diagram and viscosity measurement. The dope composition needs to be close to the spinodal line in order to have fast phase separation. A three phase diagram, as shown in Fig. 7.1, was created. Polymer dopes above a critical polymer concentration are necessary to provide sufficient polymer chain entanglement, and mechanical strength during the

spinning process to produce viable membranes [9]. As shown in Fig. 7.2, the critical concentration for the 6FDA-DAM polymer in NMP solution can be estimated to be between 20-25 wt% for practical purposes. An empirical dope viscosity, around 100 Pa·s, is preferred in order to have enough strength but still avoid excessive resistance to phase separation to prevent undesirable support layer resistance to mass transfers [13]. Initial sheath dopes, which compositions are shown in table 7.1, were used for spinning. The dope viscosities are around the empirical viscosity 100 Pa·s, as shown in Fig. 7.3.

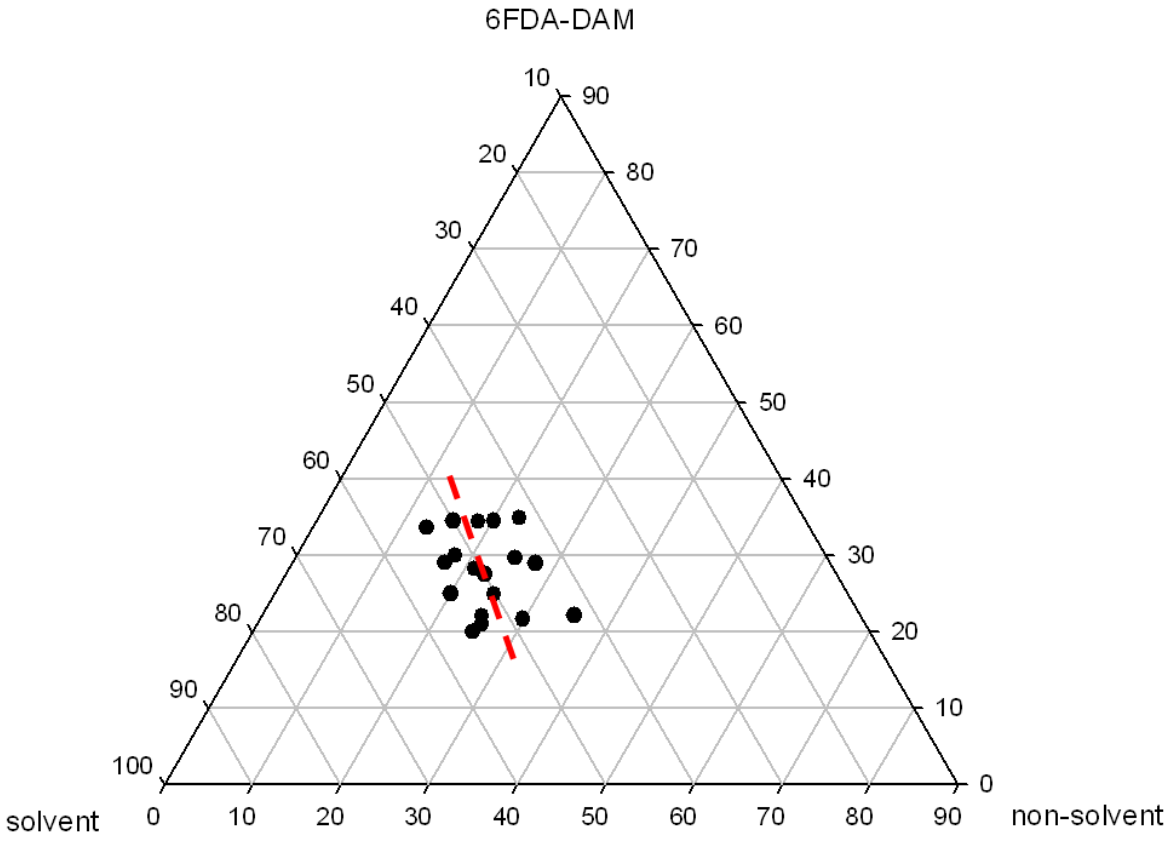

Figure 7.1 Three phase diagram for 6FDA-DAM polymer, solvent (NMP:THF=3:1) and non-solvent (EtOH:H_2O=3.5:1)

Phase separation tests using the asymmetric film method, was done on spinning dopes to approximate the phase separation kinetics. The phase separation times of both dopes were found to be around 10 seconds at room temperature. These slow phase separation rates are similar to that in dopes containing another 6FDA polymer reported before [13] and much slower than that in Matrimid® dopes. The slow phase separation rate can cause several problems during the fiber spinning process. Excessive thick skin or substructure due to slow phase separation rate can leads to compromised gas separation performance of hollow fibers. Defects can happen when fibers touch the guide or drum before the fibers become vitrified from sufficient phase separation. There can be several ways to facilitate the phase separation process, or diffusion process of solvents and non-solvents into and out of fiber membranes. Faster phase separation rate can be achieved using higher temperatures, either in the spinneret or water quench bath. A more powerful method is the use of solvent-additive complex, to reduce the solvent power [14-17]. The complex can aid in decreasing the phase separation time when water from the quench bath dissociate the complex. Kesting used organic acid-NMP base complex to enhance the formation of asymmetric polysulfone hollow fiber membranes [17]. Kurdi applied $LiNO_3$ –NMP complex for polyetherimide asymmetric membrane formation [14-16]. $LiNO_3$ and multiple NMP molecules form a complex, which acts as transient spacer for polymer chain packing. When water dissociates the complex by replacing the NMP molecules and associating with the $LiNO_3$, phase separation happens and micropores are formed. It is still unknown how the phase separation rates can be controlled while not affecting other properties, especially the core-sheath interfacial adhesion, in the dual

layer hollow fiber spinning. Nevertheless, with trial and error using various spin variables available, a workable compromise can often be achieved as it was here.

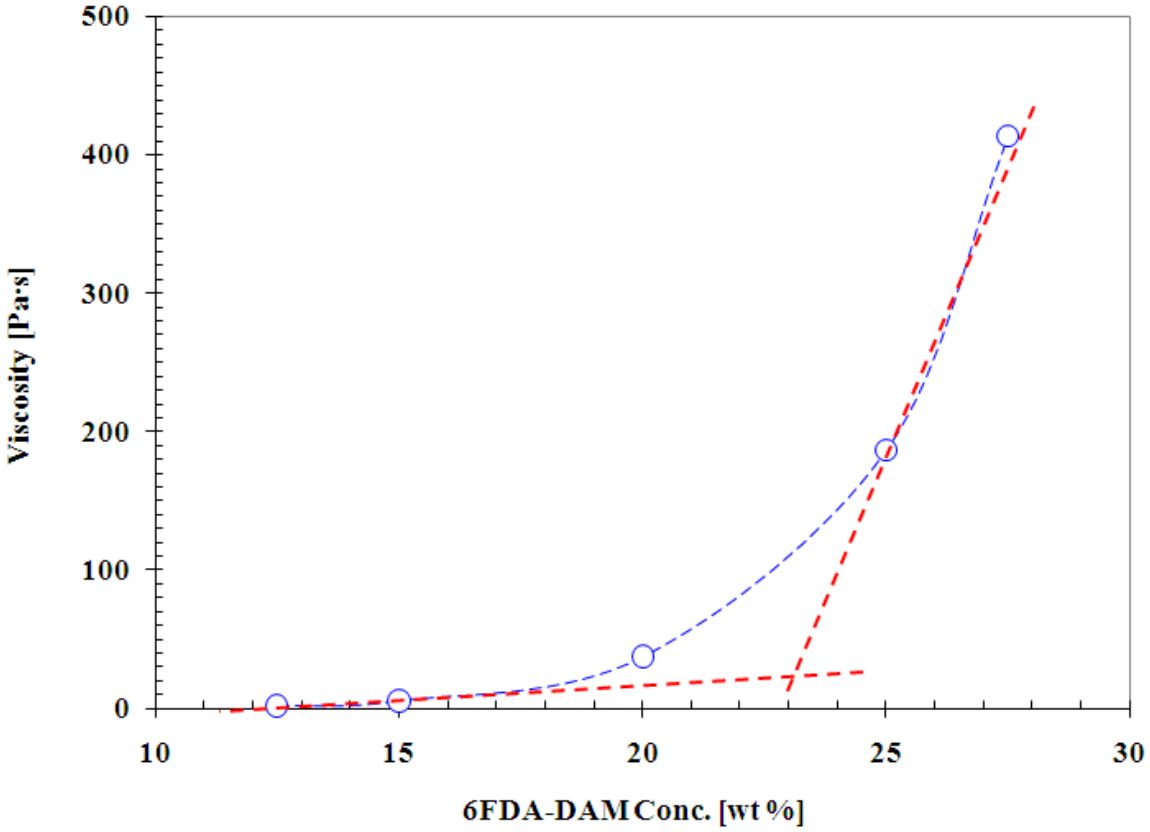

Figure 7.2 Viscosity of 6FDA-DAM solutions in NMP at different concentration and the critical concentration for sufficient polymer chain entanglement and mechanical strength

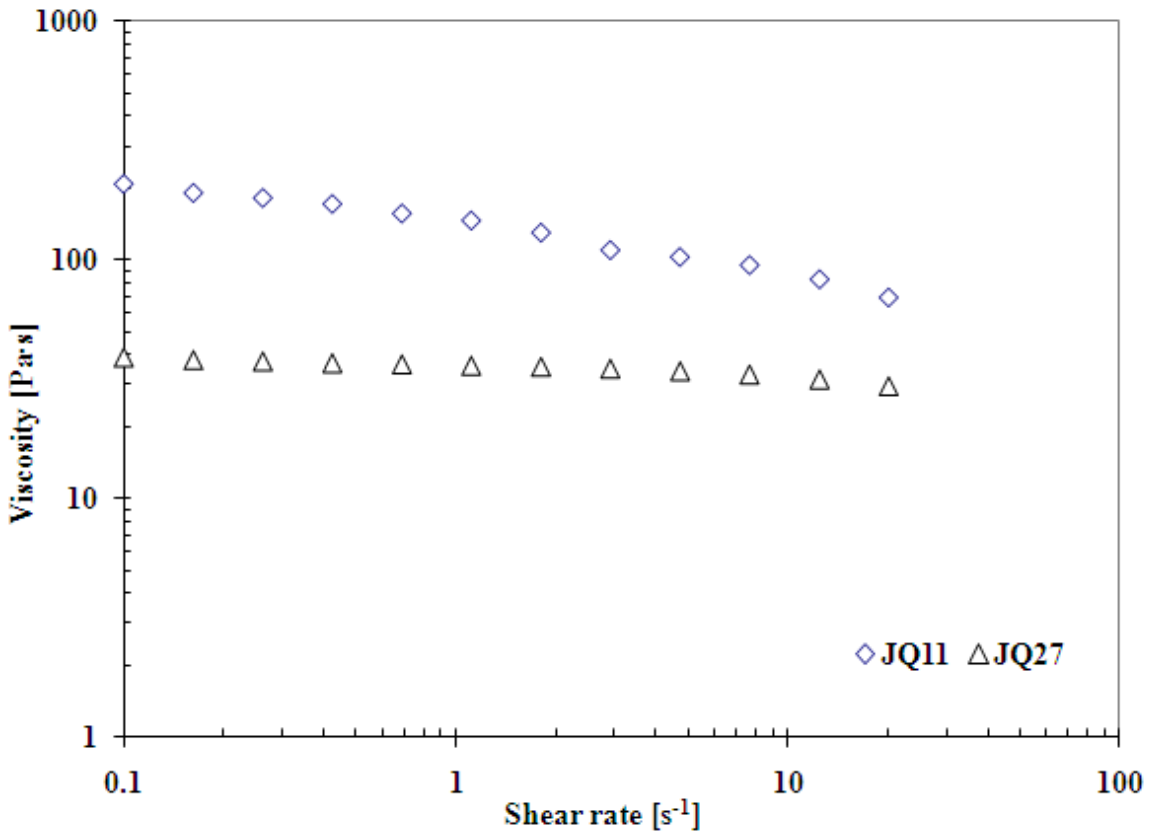

Figure 7.3 Viscosity of 6FDA-DAM spinning dopes different shear rates

7.3.2 6FDA-DAM dual layer fiber spinning without LiNO3

Dual layer hollow fibers (JQ27) were spun first using a 6FDA-DAM sheath dope (composition shown in table 7.1) without $LiNO_3$ addition, using a water quench bath at room temperature. The varying parameters are shown in table 7.2, and the constant parameters are shown in table 7.3. All dual layer hollow fibers seem concentric and show good core-sheath interfacial adhesion, as shown in Fig. 7.4. However, thick skins are formed on the 6FDA-DAM sheath layers probably due to the slow phase separation rate, as found in the asymmetric film test before. Spinning parameters were adjusted to raise the phase separation rate of the sheath layer. Reduced air gap, higher spinneret

temperature and thinner sheath layer thickness were used as shown in table 7.2, however, the dual layer hollow fibers spun at these conditions have either low permeance or defective skins, as shown in table 7.4. The dense skin thickness can be calculated from Eq. 7.1, ℓ is the skin thickness, P is gas permeability (Barrer) in dense film, p is gas permeance (GPU) in hollow fiber membrane.

$$\ell = \frac{P}{p} \qquad (7.1)$$

The N_2 permeance under 1 GPU is probably due to a cellulose acetate skin, because the calculated skin layer is thicker than the 6FDA-DAM sheath thickness (~10 μm). As shown in Fig.7.5, dense cellulose acetate layers exist at the interfaces of the dual layer hollow fibers. The defective skins, confirmed by CO_2/N_2 selectivity lower than intrinsic selectivity in dense films, were probably caused by the defects formed when the insufficiently phase separated fiber touching the guide.

Table 7.1 Compositions of 6FDA-DAM dopes

%	JQ27,JQ25 (without $LiNO_3$)	JQ11 (with $LiNO_3$)	XU35-1 (single layer)
6FDA-DAM	22	22	22
NMP	40	40	43
THF	9	13	10
EtOH	29	19.4	25
LiNO3		5.6	

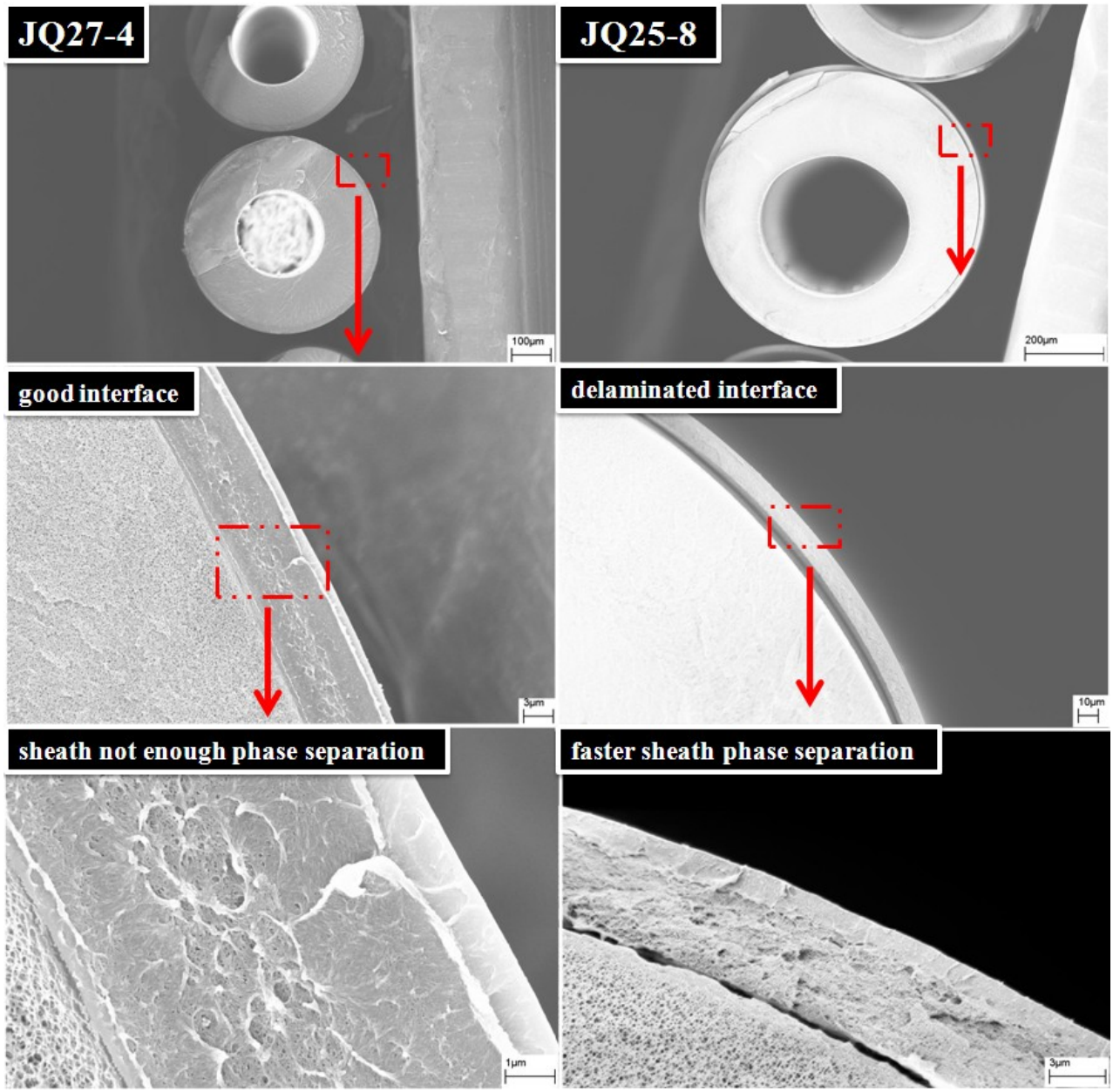

Figure 7.4 Dual layer hollow fibers spun in a cold quench bath (JQ27-4) and a hot quench bath (JQ25-8)

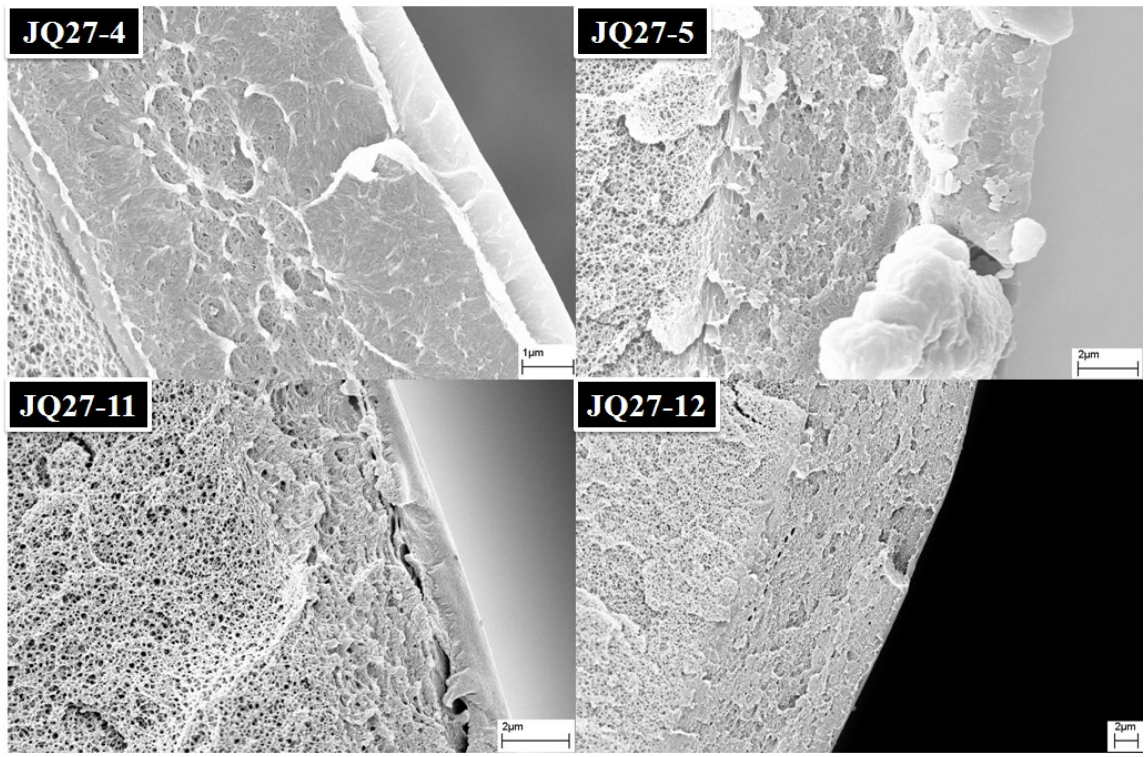

Figure 7.5 Interfaces and sheath layers of dual layer hollow fibers spun at various conditions using a cold quench bath, and sheath dope with no $LiNO_3$

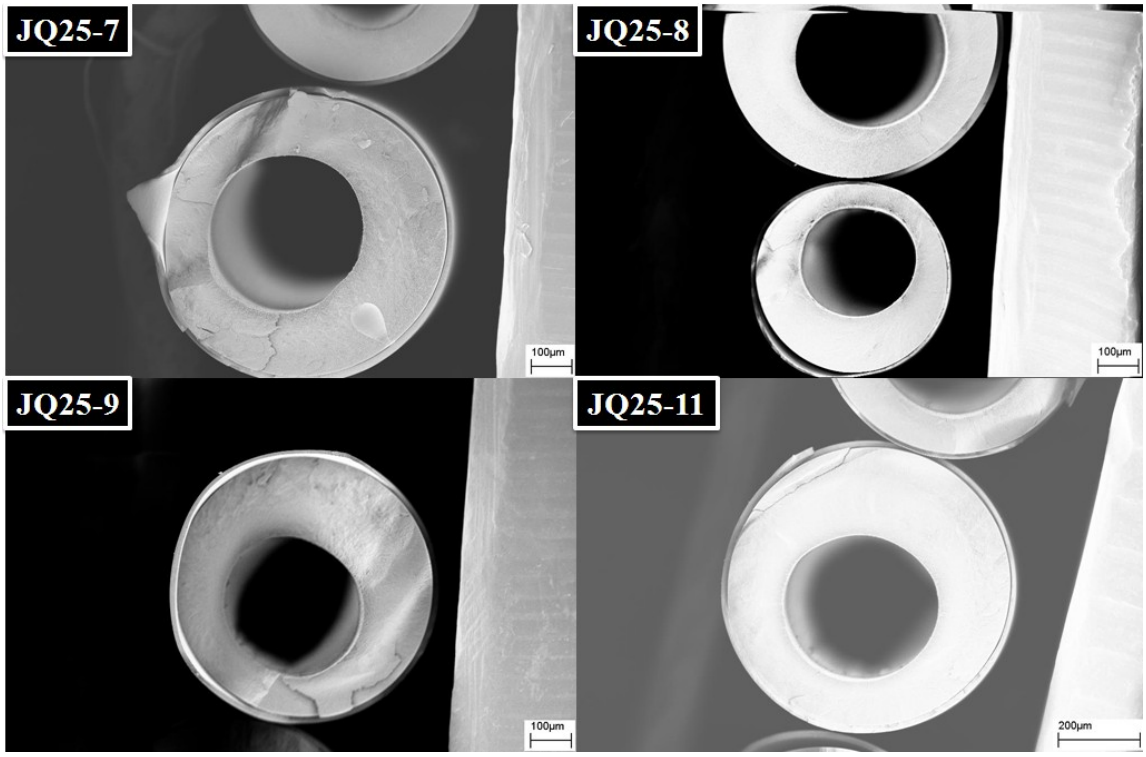

Figure 7.6 Delaminated interfaces of dual layer hollow fibers spun at various conditions using a hot quench bath, and sheath dope with no $LiNO_3$

Table 7.2 Varying parameters for dual layer hollow fibers spinning

	$LiNO_3$	bath temperature [°C]	sheath flow rate [ml/hr]	spinneret temperature [°C]	air gap [cm]	take up rate [m/min]
JQ11-1	with	22	30	50	6	15
JQ11-2	with	22	60	50	6	15
JQ11-3	with	22	30	60	6	15
JQ25-7	without	50	60	50	12	10
JQ25-8	without	50	60	50	3	10
JQ25-9	without	50	60	60	11	10
JQ25-11	without	50	60	40	12	10
JQ27-4	without	25	60	60	15	15
JQ27-5	without	25	60	60	3	15
JQ27-11	without	25	30	50	1.5	15
JQ27-12	without	25	60	50	1.5	15

Table 7.3 Constant parameters for dual layer hollow fibers spinning

Core dope	CA/NMP/H_2O (25:64:11)
Bore dope	NMP/H_2O (70:30)
Core flow rate	60 ml/hr
Bore flow rate	180 ml/hr

Table 7.4 Gas transport properties of dual layer hollow fiber membranes

		P_{N2} [GPU]	P_{CO2} [GPU]	$\alpha_{CO2/N2}$ [-]
Cold bath, with $LiNO_3$	JQ11-1	578	616	1.1
	JQ11-2	16	292	18
Cold bath, without $LiNO_3$	JQ27-4	0.6	22	35
	JQ27-5	103	154	1.5
	JQ27-11	12	55	4.4
	JQ27-12	0.7	-	-
Hot bath, without $LiNO_3$	JQ25-11	3.4	5.1	1.5

7.3.4 6FDA-DAM dual layer fiber spinning with LiNO3

In order to increase the phase separation rate of the sheath dope without $LiNO_3$, temperature of the quench batch was raised to 50 °C (JQ25). The delamination between core and sheath layers happened, as shown in Fig. 7.4. Spinning conditions were adjusted to increase the air gap, and to lower the spinneret temperature, which was found to assist the interfacial adhesion between the sheath and core layers, as shown in table 7.2. All fibers showed delaminated interfaces using a hot quench bath, as shown in Fig. 7.6. These fibers cannot be used for gas separations due to the anticipated poor mechanical strength of sheath layer. Gas transport properties on one of these delaminated fibers were done to check the fiber morphologies, together with SEM observation. Fibers (JQ25-11) showed low gas permeance and selectivity, which means a defective thick skin is formed due to the slow phase separation rate. The sheath also shows dense morphologies in Fig.7.4, which is in agreement with the permeation result. Therefore, the phase separation rate of 6FDA-DAM sheath was still inadequate using the quench bath of 50 °C. The phase separation rate of cellulose acetate core layer from bore coagulant probably increased, when the quench bath temperature was raised. The delamination is probably due to different shrinkage rates of a core with fast phase separation and a sheath layer with slow phase separation.

The initial dope composition was modified by adding $LiNO_3$ in order to further raise the phase separation rate of the 6FDA-DAM sheath dope. As shown in Fig. 7.3, the viscosity of 6FDA-DAM dopes with $LiNO_3$ is ~ 4 times more viscous than that without $LiNO_3$, at the same polymer concentration. The increase of dope viscosity normally leads to reduced water diffusion rate, and phase separation rate. The effect of enhanced water

diffusion through the $LiNO_3$-NMP complex is more pronounced than the viscosity factor, and leads to overall faster phase separation rate. Dual layer hollow fibers were spun using 6FDA-DAM sheath dope containing 5.6 wt% of $LiNO_3$ to raise the phase separation rate. A water quench bath at room temperature was used to avoid the delamination problem, thereby allowing more time for interface integrity building. The dual layer hollow fibers show good core-sheath interfacial adhesion and good phase separation in the sheath layers, as shown in Fig. 7.8. The core and sheath layers are both porous at the interface, while strongly adhered, possibly by some inter-diffusion of polymer chains between the two layers. Research shows the interfacial adhesion can be improved during the solvent exchange steps by relaxing the residual stresses in both inner and outer layers [9]. In order to investigate the effect of solvent exchange on the interfacial adhesion, fibers before and after solvent exchange were observed, the SEM images are shown in Fig. 7.7. The core and sheath layer both shrink if the fibers are taken out of water bath without solvent exchange. Delamination free interface was found both before and after solvent exchange. The sheath thickness was controlled by regulating the flow rate of sheath dope. As shown in Fig. 7.8, an 8 μm porous sheath is formed using a reduced sheath flow rate of 30 ml/hr (JQ11-1). The high gas permeance, shown in table 7.4, confirmed the porous sheath structure, which is due to the fast phase separation rate of the sheath dope. A thicker sheath with a dense skin is formed using a higher sheath flow rate of 60 ml/hr (JQ11-2). A dense skin was formed by slowing down the sheath phase separation rate, checked by both SEM (Fig. 7.8) and permeation results (table 7.4). Because the diffusion time is proportional to the second power of thickness, the diffusion rate of the solvent and non-solvent, *i.e.*, the phase separation rate, is effectively slowed down with a thicker

6FDA-DAM sheath. A porous sheath and delaminated interface were formed when the spinneret temperature was increased to 60 °C. As shown in Fig. 7.9, there is a correlation between sheath phase separation rate and the extent of interfacial adhesion. The interfacial adhesion is stronger when the phase separation rate of sheath is slower, using either a lower spinneret temperature, or a thicker sheath. The slow phase separation rate probably correlates with slower diffusion of water into the interfacial region, thereby providing longer time for the inter-diffusion of polymer chains between the two layers based on any potential miscibility between the two polymers.

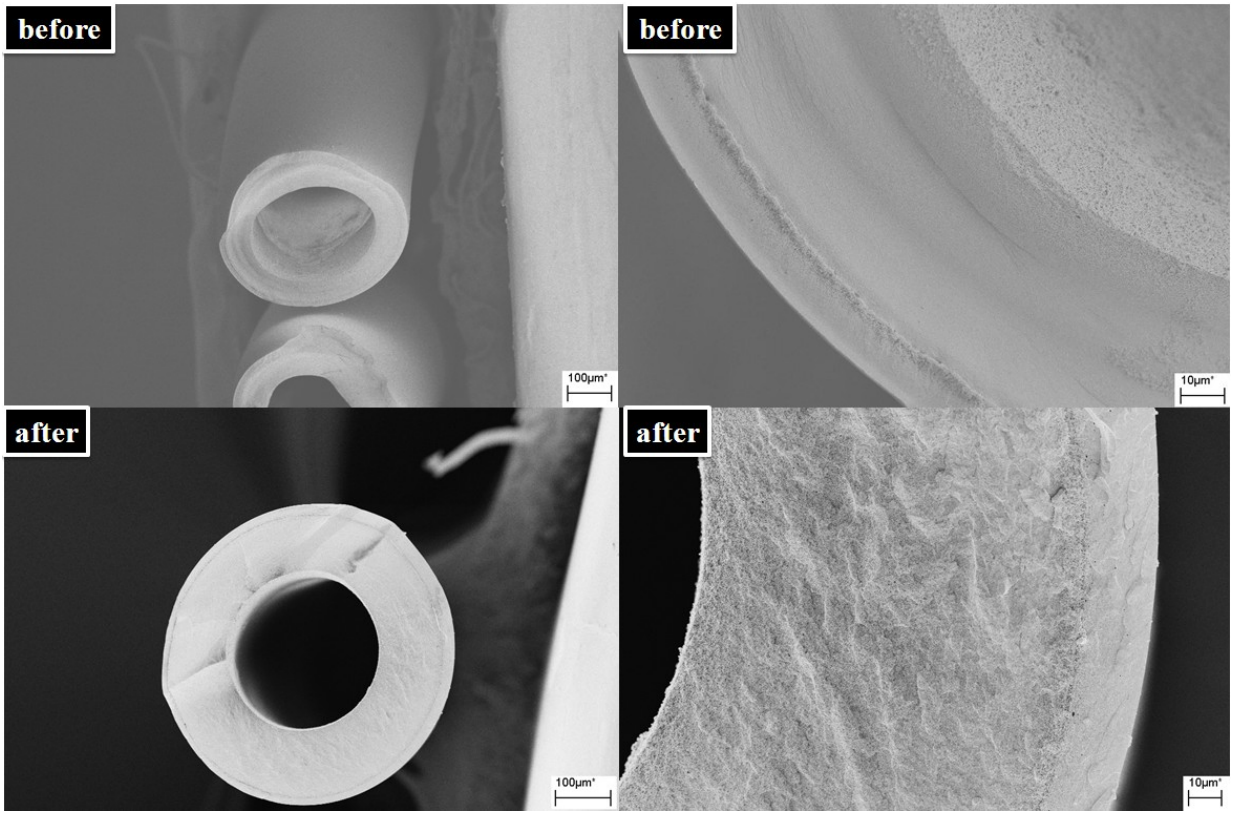

Figure 7.7 Dual layer hollow fibers before and after solvent exchange (JQ11-2)

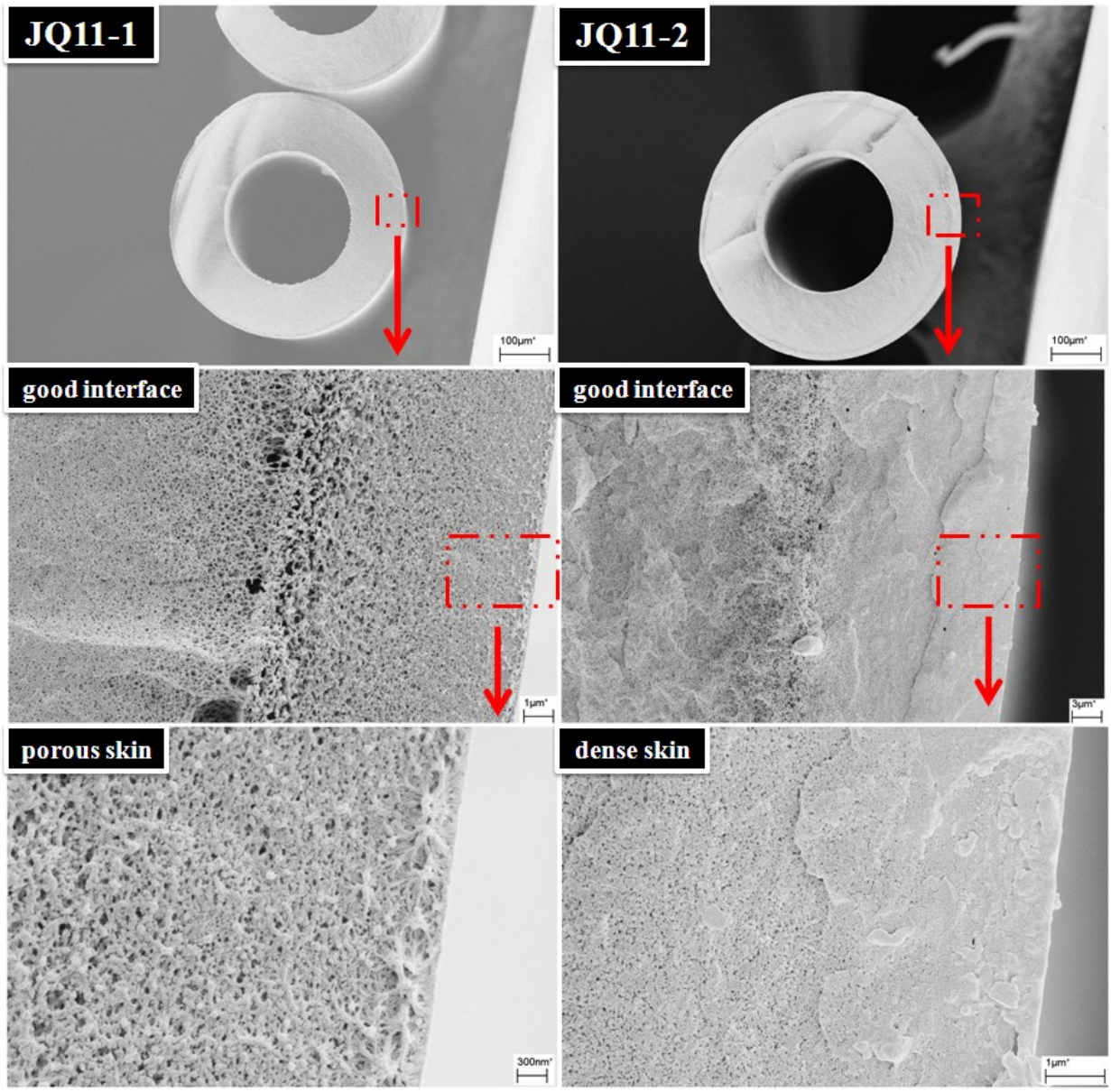

Figure 7.8 Dual layer hollow fibers using a $LiNO_3$ containing 6FDA-DAM sheath dope

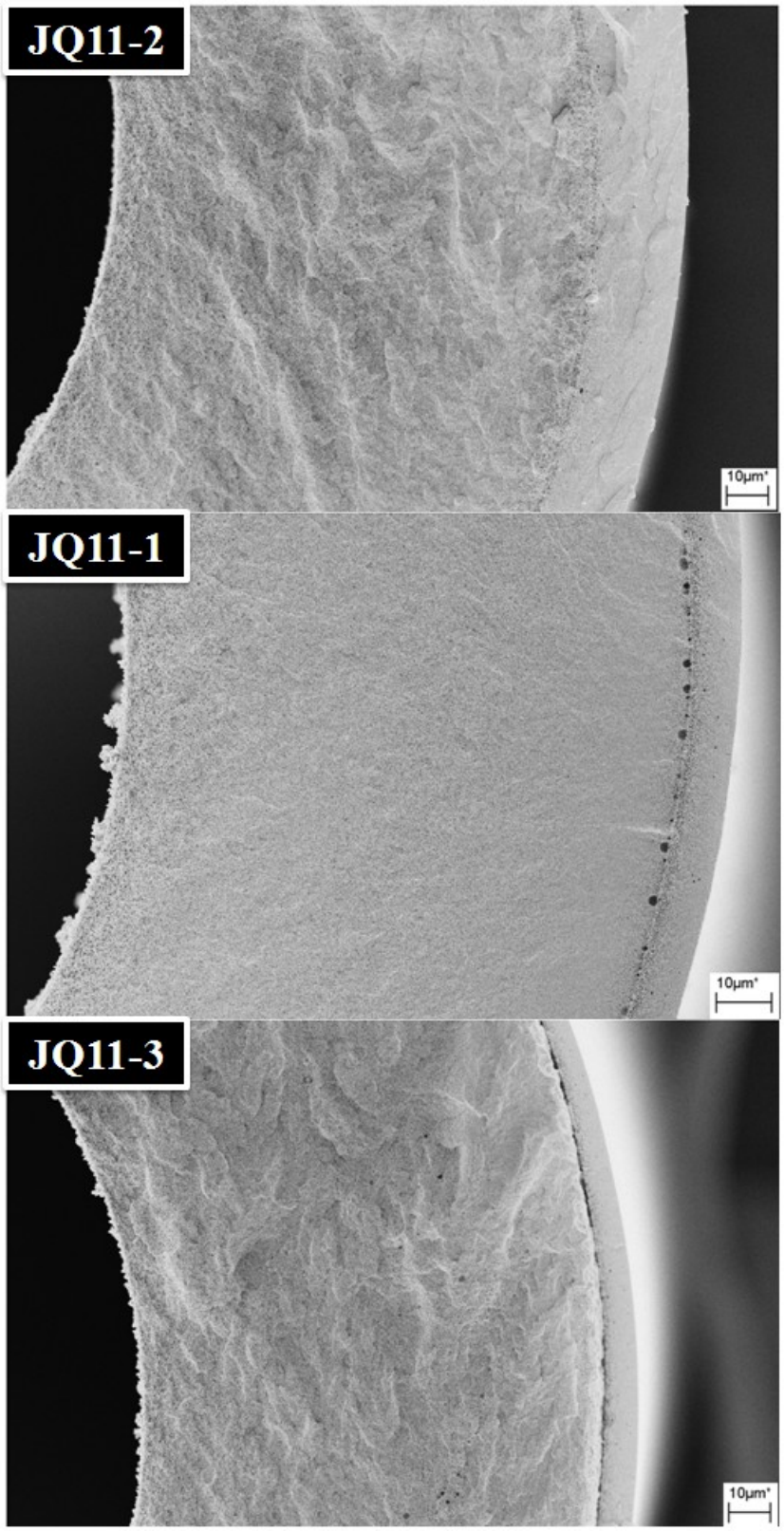

Figure 7.9 Core-sheath interfacial adhesions at different conditions

The bore coagulant also causes phase separation from the core side. The phase separation of the cellulose acetate core can also affect the interfacial adhesion properties in a similar way. As shown previously, the delaminated interface of fibers in a 50 °C quench bath may be due to an increased phase separation rate of the core layer, which may reduce the time for the interfacial diffusion of polymer chains. Future study is needed to systematically investigate this effect.

In summary, a slow phase separation rate of 6FDA-DAM sheath dope (without $LiNO_3$) was found. Slower phase separation at the interface is beneficial for the interfacial adhesion, by providing longer time for the polymer chain diffusion between the two layers. A quench bath at higher temperature can cause delamination problem but does not effectively raise the phase separation rate of the 6FDA-DAM sheath dope. The sheath phase separation rate cannot be effectively raised by other spinning parameters, such as spinneret temperature, air gap, sheath thickness, *etc*. Fortunately, the addition of $LiNO_3$ can enhance the phase separation of 6FDA-DAM sheath by forming a complex with the solvent.

Table 7.5 Parameters for monolayer 6FDA-DAM hollow fiber spinning

Spinneret temperature	70 °C
Quench bath temperature	50 °C
Core flow rate	75 ml/hr
Bore flow rate	75 ml/hr
Air gap	10 cm
Take up rate	5 m/min

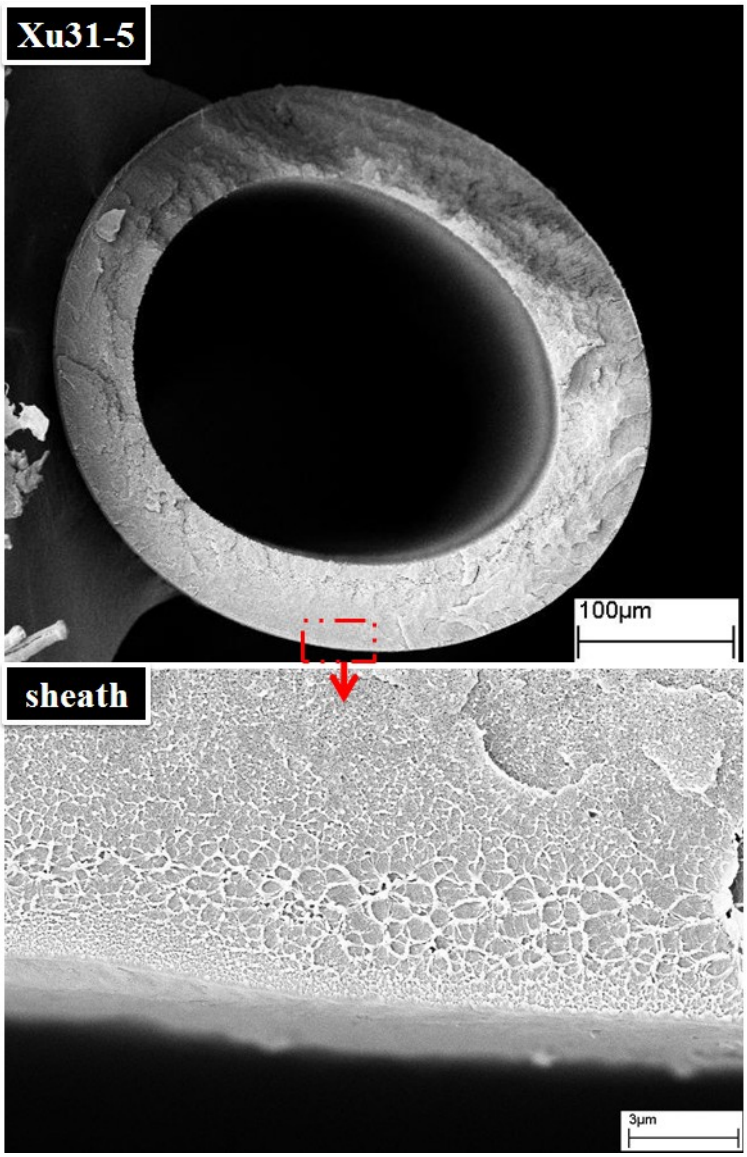

Figure 7.10 Monolayer 6FDA-DAM hollow fiber membrane

The gas transport properties of the delamination free and macrovoid free dual layer hollow fibers were shown in table 7.6. A single layer 6FDA-DAM hollow fiber, shown in Fig. 7.10 was used as a comparison. The dual layer 6FDA-DAM/CA hollow fiber shows selectivity higher than intrinsic values for O_2/N_2 and CO_2/CH_4 gas pairs. However, the selectivity for slower gas pair n-C_4H_{10}/i-C_4H_{10} was only 11% of the intrinsic values found in dense films. This is possibly because that the dual layer hollow

fiber is slightly defective. The total gas permeance can be considered as the combination of permeance through the membrane and the permeance through any minute defective sites. The diffusion through defective sites is presumably close to Knudsen diffusion, therefore, permeance of all gases through defective sites are about the same. For faster gases, such as CO_2, O_2, N_2 and CH_4, the permeance through the membrane are far larger than the permeance through defective sites, so the defective sites have negligible effect on the separation of these gases. On the other hand, such defective sites affect slower gases mostly because the permeance through the defective sites is closer to the very low permeance through the membrane. The permeance through the defective sites can be calculated out assuming C4s gases to have same permeance through the defective sites (x). The permeances of nC4 and iC4, after subtracting the permeance through defective sites from measured values, are (3.6-x) and (1.5-x). The selectivity of the gas pair through the asymmetric membrane is assumed the same as the intrinsic value in dense film (21) if all defective sites are plugged, *i.e.*, (3.6-x)/(1.5-x)=21, and the permeance through defective sites is x=1.4. The iC4 permeance increased about 10 fold by the defective sites (0.1 to 1.5 GPU), while n-C4 permeance only increased about 50% (2.2 to 3.6 GPU). Similarly for the ‘‘faster’’ gases (O_2, N_2, CO_2, CH_4), permeance through the defect free membrane regions is more than 10 times higher based on dense film estimate of intrinsic permeabilities. Therefore the selectivity of nC4/iC4 was dramatically affected by the defective sites. The single layer hollow fiber showed close to intrinsic selectivity for all gas pairs, therefore, it is defect free. As shown in table 7.1, the 6FDA-DAM spinning dope does not contain $LiNO_3$. In order to increase the phase separation rate, a quench bath at 50 °C, and a spinneret at 70 °C are used. As discussed previously, a

quench bath at 50 °C and spinneret above 60 °C will lead to delamination problems in a dual layer hollow fiber spinning process. A faster phase separation was achieved while maintaining a delamination free interface by introducing $LiNO_3$ salt to the 6FDA-DAM dope. The slightly defective nature of the membrane is probably due to the vigorous phase separation process with the presence of $LiNO_3$. It is reported that the addition $LiNO_3$ promotes the formation of 1 nm size micropores in polyetherimide asymmetric films [16]. The micropore volume increases as the content of $LiNO_3$ increases. These interconnected micropores possibly contribute to the formation of minute defects, which can lead to non-selective Knudsen type diffusion. Depending on the degree of defective sites formation, the gas separation performance of membranes is compromised differently. Previous works using $LiNO_3$ for membrane formations focused on faster gas separations, such as CO_2/CH_4, O_2/N_2 pairs [8, 16, 17]. These faster gases have higher permeance and therefore less affected by the defects. In this work, C4s gas pairs are used to characterize the degree of defects in the asymmetric hollow fiber membrane. The phase separation in the spinning process is dependent on several factors. A dope containing less amount of $LiNO_3$ can be used to reduce the $LiNO_3$-NMP complex effect, and the vigorous micropore formation leading to small pinholes. While a thinner skin or a higher temperature of spinneret can be used to enhance the phase separation rate of the 6FDA-DAM sheath. Future work is needed to further improve the quality of the 6FDA-DAM/CA dual layer hollow fiber membranes.

Table 7.6 Transport properties of different gas pairs in 6FDA-DAM dense film and dual layer hollow fiber membranes

	dense film[18, 19]	Dual layer fiber (JQ11-2)	Single layer fiber (XU31-4)
	[Barrer]	[GPU]	[GPU]
P_{CO2}	370	290	210
P_{O2}	109	65	66
P_{N2}	29	16	19
P_{CH4}	18	14	12
$\alpha_{CO2/CH4}$ [-]	***21***	***21***	***17***
$\alpha_{O2/N2}$ [-]	***3.7***	***4.0***	***3.5***
$P_{n\text{-}C4H10}$	3.7	3.6	3.0
$P_{i\text{-}C4H10}$	0.17	1.5	0.15
$\alpha_{nC4/iC4}$	***21***	***2.4***	***20***

7.4 DUAL LAYER HOLLOW FIBER SPINNING OF 6FDA-DAM-DABA

A 6FDA-DAM-DABA polymer, with a molecular weight about 100,000 was used for dual layer hollow fiber spinning. The sheath layer composition is shown in table 7.7. The CA core dope composition was the same as that used in 6FDA-DAM/CA dual layer hollow fiber spinning.

Table 7.7 6FDA-DAM-DABA sheath dope composition for dual layer hollow fiber spinning

%	JQ33 (with $LiNO_3$)
6FDA-DAM-DABA	23
NMP	28
THF	11.5
EtOH	32
LiNO3	5.5

The varying parameters for the 6FDA-DAM-DABA/CA dual layer hollow fiber were shown in table 7.8. Other unchanged parameters were the same as those in 6FDA-DAM/CA spinning.

Table 7.8 Spinning parameters for 6FDA-DAM-DAM dual layer hollow fibers

	bath temperature [°C]	sheath flow rate [ml/hr]	Spinning temperature [°C]	Air gap [cm]	take up rate [m/min]
JQ33-2	16	30	35	10	15
JQ33-3	16	60	35	10	15
JQ33-4	16	30	50	10	15
JQ33-8	16	20	60	2	15

Dual layer hollow fibers spun at two example states are shown in Fig. 7.11, and Fig. 7.12. Both showed good interfacial adhesion between the 6FDA-DAM-DABA sheath and the CA core. The 6FDA-DAM-DABA sheath layers have asymmetric structures, with a dense skin and porous support. Both fibers showed less porous sheath near the interface area, which may contributed to additional gas diffusion resistance. The additional skin at the interface for 6FDA-DAM-DABA/ CA dual layer hollow fiber is different from the completely porous interface in the 6FDA-DAM/ CA dual layer hollow fiber. The interfacial adhesion is good in 6FDA-DAM-DABA/CA fibers at spinneret temperature of 60 °C, compared to delaminated 6FDA-DAM/CA fibers at the same spinning conditions. These are probably caused by the slower phase separation rate of 6FDA-DAM-DABA sheath than that of 6FDA-DAM sheath. Future work is needed to optimize the phase separation rate of the 6FDA-DAM-DABA sheath, in order to achieve the ideal morphologies: good interfacial adhesion, defect free dense skin and porous support.

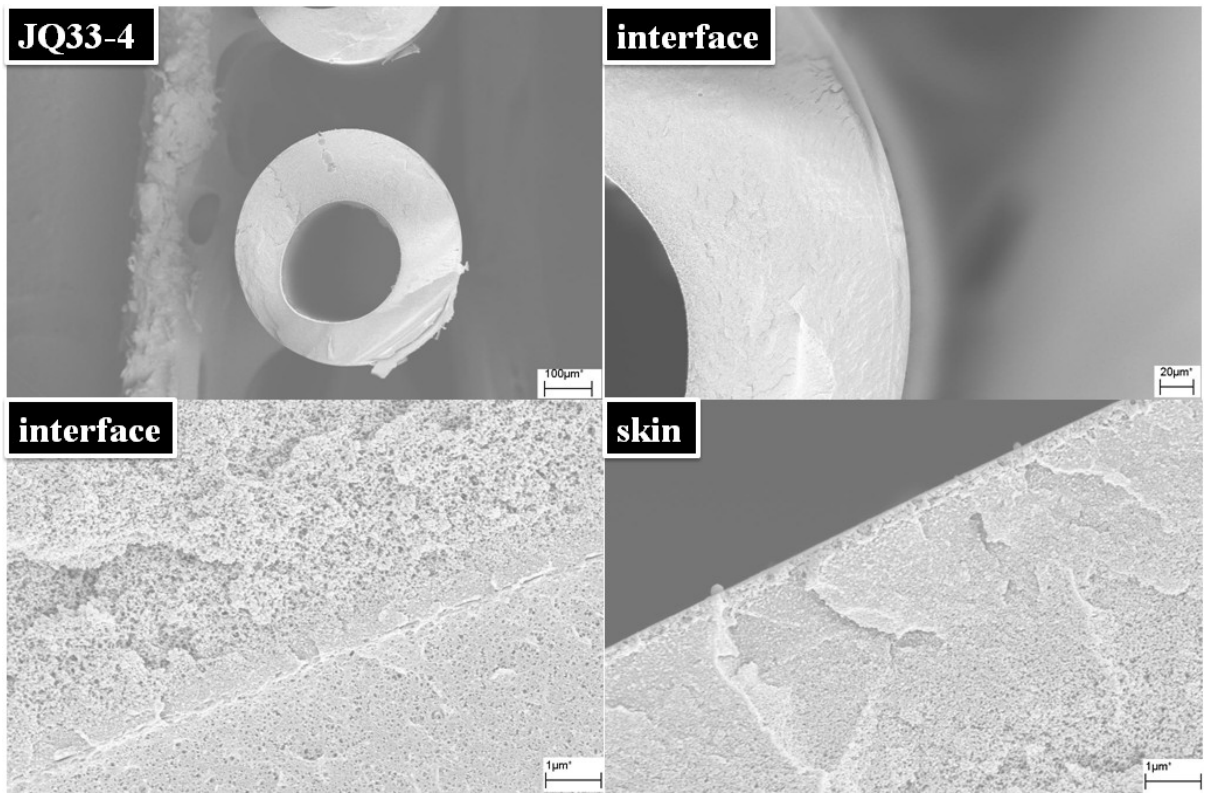

Figure 7.11 6FDA-DAM-DAM dual layer hollow fiber spun at 50 °C (JQ33-04)

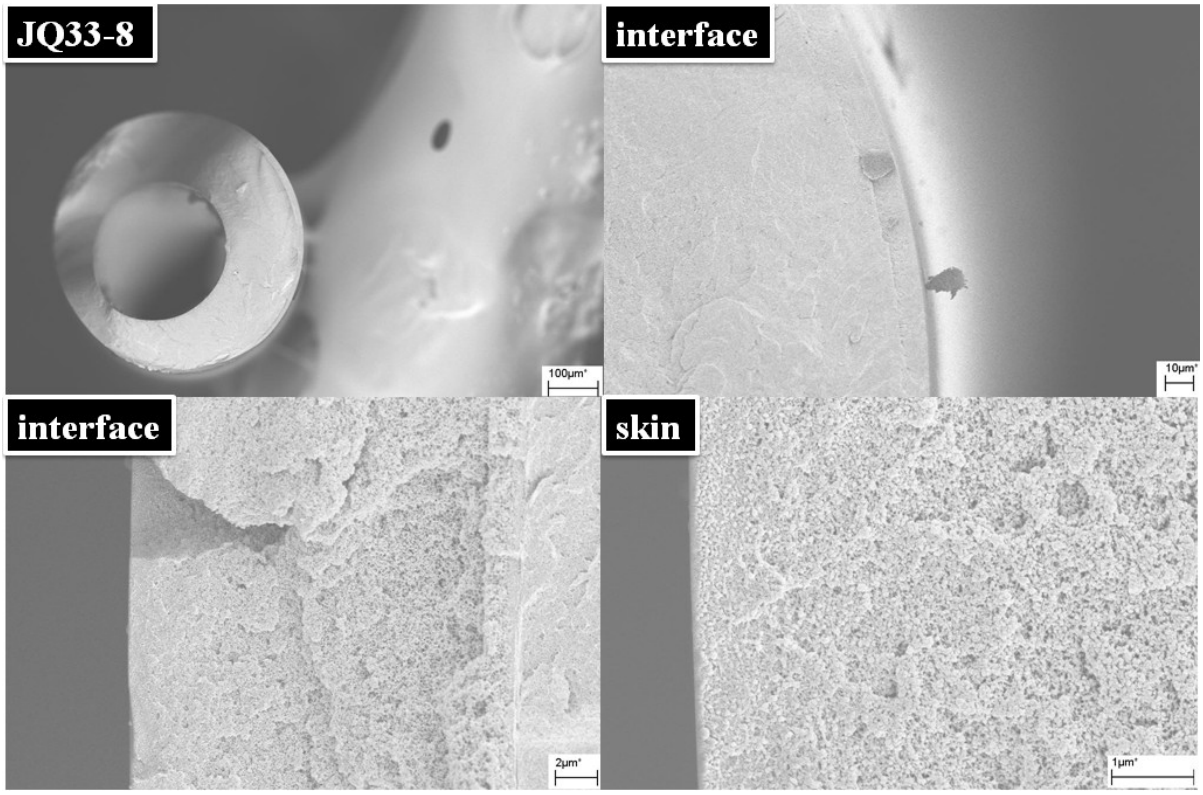

Figure 7.12 6FDA-DAM-DAM dual layer hollow fiber spun at 60 °C (JQ33-08)

Gas transport properties of fibers at several states are shown in table 7.9. Comparing the fibers at states JQ33-2 and JQ33-3, the gas permeance decreased when sheath thickness increases. This is probably due to the thicker dense skin formed, when phase separation of sheath layer is reduced with a thicker sheath. The selectivity of CO_2/N_2 in both fibers is lower than the intrinsic value, probably because of presence of defective sites in these fibers. When the spinneret temperature increase from 35 °C (JQ33-2) to 50 °C (JQ33-4), the gas permeance decreased and a selectivity increased, due to a thicker and more defect free skin is formed. A thicker skin at higher spinning temperature is probably due to the faster evaporation of volatile component.

Table 7.9 Transport properties of 6FDA-DAM-DAM dual layer hollow fibers

	P_{N2} [GPU]	P_{CO2} [GPU]	$\alpha_{CO2/N2}$ [-]
JQ33-2	8.1	118	15
JQ33-3	2.1	31	15
JQ33-4	3.8	88	23
JQ33-8	3.5	60	17

Various gas transport properties are done using fibers at one state. The results are shown in table 7.10. Similar to 6FDA-DAM/CA dual layer hollow fibers, the 6FDA-DAM-DABA/CA fibers shows defect free separation performances for faster gas pairs: CO_2/CH_4, O_2/N_2. However, the selectivity of slower gas pair nC4/iC4 is dramatically reduced. Similar defective sites are probably generated by fast phase separation in the dopes containing $LiNO_3$.

Table 7.10 Various gas separation performances of 6FDA-DAM-DABA dense film and dual layer hollow fiber

	dense film [Barrer]	JQ33-4 [GPU]
CO_2	152	88
O_2	35	17
N_2	7.4	3.8
CH_4	4.4	3.4
$\alpha_{CO2/CH4}$	***34.6***	***26.1***
$\alpha_{O2/N2}$	***4.7***	***4.5***
nC4	0.3	0.32
iC4	-	0.17
$\alpha_{n/i}$	***> 20***	***1.9***

7.5 POST TREATMENT ON DUAL LAYER HOLLOW FIBERS

Post treatments were done on the dual layer hollow fibers to plug the defective sites and enhance the separation performances using chemical post treatment method [20]. The fibers mounted in the module were put in contact with a first solution of 0.2% diethyltoluenediamine in iso-octane for 30 min. The solution was drained away, and a second solution containing 0.2% trimesolylchloride and 2% Sylgard 184® (Dow Corning) in iso-octane was put in contact for 30 min. The treatment solutions were diluted and treatment time was reduced if significant additional transport resistance is caused by post treatment. Then the fibers were dried overnight in an vacuum oven at 100 ^{o}C.

As shown in table 7.11, the dual layer hollow fibers are show dramatically reduced gas permeance, together with increased selectivity. Additional thick layers (PDMS) are formed during the treatment. As shown in Fig. 7.13, this layer can be formed

through two possible mechanisms: 1) layer on the top of dense skin, 2) layer formed inside the porous layer beneath the skin due to the chemical solutions draw in by capillary force. The second hypothesis is most probably true, considering the fact that no additional layers were formed during treatment on other fibers and the possible high porous nature of fiber due to the addition of $LiNO_3$. In order to reduce the thickness of additional post treatment layer while plugging the defective sites effectively, the concentration of chemicals in the solution and soaking time were adjusted. Two examples are shown in table 7.11, the selectivity of nC4/iC4 gas pair in both 6FDA-DAM/CA and 6FDA-DAM-DABA/CA both increased after post treatment with diluted treatment solutions. However, both fibers show nC4/iC4 selectivity below the intrinsic values. The post treatment method is less effective for plugging the defective sites in the membranes of this research than other membranes reported before [20]. The defects generated in these $LiNO_3$ containing dopes are probably different. Future work is needed to investigate the details on this aspect.

Table 7.11 Gas transport properties of dual layer hollow fiber membranes at different post treatment conditions

	6FDA-DAM/CA(JQ11-2)		6FDA-DAM-DABA/CA(JQ33-4)	
[GPU]	Diluted*	standard	Diluted**	standard
O_2	46	10.2	16.7	7.7
N_2	10	1.7	3.3	1.1
$\alpha_{O2/N2}$	***4.5***	***6.0***	**5.0**	**6.7**
nC4	0.93	0.085	0.22	0.07
iC4	0.09	0.007	***0.03***	*0.008*
$\alpha_{nC4/iC4}$	***10.4***	***11.0***	***7.5***	***8.4***

* using 5 times diluted solutions as that in the standard method, 2 min. soaking
** using 10 times diluted solutions as that in the standard method, 30 s soaking

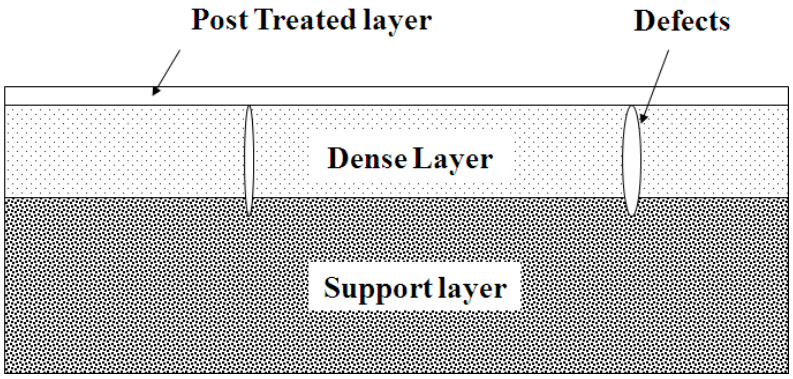

Figure 7.13 Post treatment to plug the pinholes in the membrane

7.6 CONCLUSIONS

The phase separation rate of the 6FDA-DAM, 6FDA-DAM-DABA sheath is raised by the addition of $LiNO_3$ salt. Cellulose acetate showed good properties as the support layer for a 6FDA polyimides sheath. Dalamination free, macrovoid free 6FDA polyimides /CA dual layer hollow fiber membranes were fabricated. The dual layer hollow fiber membranes showed good gas separation properties for faster gas pairs CO_2/CH_4, O_2/N_2. Slower C4s gas pair is used to probe the slight defects in the dual layer hollow fiber membrane. The slightly defective nature of the membrane is probably due to the vigorous phase separation process with the presence of $LiNO_3$. Parameters of a standard post treatment were adjusted to raise the effectiveness on these dual layer hollow fibers membranes spun from dopes containing $LiNO_3$. More systematic study is needed to further improve the gas separation performances of the dual layer hollow fiber membranes.

7.7 REFERENCES

[1] T. H. Kim, *J. Membr. Sci.*, **1988**, 37, 45-

[2] W. J. Koros, Prog. Polym. Sci., **1988**, 13, 339

[3] L. M. Robeson, *J. Membr. Sci.*, **1991**, 62, 165-185

[4] M. Mikawa, *J. Membr. Sci.* **2002**, 208, 405–414

[5] J. D. Wind, *Ind. Chem. Eng. Res.,* **2002**, 41, 6139–6148

[6] J. H. Kim, *Polymer,* **2006**, 47, 3094–3103

[7] W. J. Koros, *U.S. Patent* 6, 755, 900, **2005**

[8] I. C. Omole, *Macromolecules,* **2008**, 41, 6367-6375

[9] D. F. Li, *J. Membr. Sci.*, **2002**, 198, 211-223

[10] D. F. Li, *J. Membr. Sci.*, **2004**, 243, 155-175

[11] L. Jiang, *J. Membr. Sci.*, **2004**, 240, 91-103

[12] S.B. Carruthers, Ph.D. thesis, *University of Texas*, **2001**, 233

[13] D. W. Wallace, *J. Membr. Sci.*, **2006**, 278, 92-104

[14] J. Kurdi, *J. Appl. Polym. Sci*., **1999**, 73, 1471-1482

[15] R.Y.M. Huang, *J. Appl. Polym. Sci*., **1995**, 57, 613-621

[16] R.E. Kesting, US Patent 4,871,494, **1989**

[17] J. Kurdi, *J. Membr. Sci.*, **2001**, 184, 175-186

[18] R. L. Burns, *Macromolecules,* **2003**, 36, 2374-2381

[19] J. Liu, *J. Membr. Sci*., **2009**, 343, 157-163

[20] O.M. Ekiner, US patent, 6,663,805, **2003**

CHAPTER 8

DUAL LAYER MIXED MATRIX HOLLOW FIBER SPINNING

8.1 OVERVIEW

Mixed matrix hollow fiber membranes with high zeolite loading (> 40wt%) were first fabricated using Ultem® as the polymer matrix, because of its known easy fiber forming properties. The mixed matrix spinning dopes containing Grignard (traditional) treated zeolite nanoparticles showed greater dispersion stability than those containing untreated zeolite nanoparticles. The stabilization of Grignard treated nanoparticles are probably through two mechanisms: 1) electrostatic stabilization by the $Mg(OH)_2$ dissolved slightly in polar solvent NMP; 2) steric stabilization by the polymer chains entangled onto the zeolite surface. Dual layer mixed matrix hollow fiber membranes were spun using a pure polymer, Ultem®, as the core layer, and Ultem®/zeolite mixed matrix layer as the sheath. The mixed matrix hollow fibers have strong mechanical strength from the pure Ultem® core layer, but the mixed matrix membrane showed gas transport properties close to pure polymeric membranes. No significant selectivity enhancement were found on mixed matrix membranes containing GT-4A (traditional Grignard treatment) nanoparticles, probably due to the lack of adhesion between the polymer and 4A nanoparticles. Mixed matrix fibers with sheath layers containing two different zeolites: pure silica MFI and aluminosilicate 4A, were fabricated to find the effect of zeolite properties on the membrane formation. The thickness of dense skin in the mixed matrix hollow fiber membranes containing MFI nanoparticles are thicker than those of membranes containing the same amount of 4A nanopartciles. The addition of hydrophilic

4A nanoparticles probably raises the phase separation rate by promoting the non-solvent water diffusion into the mixed matrix sheath. The dense skin in mixed matrix hollow fiber membrane containing 40wt% of GT-MFI nanoparticles (~1 μm) is about 10 times thicker than that in membranes containing 40wt% of GT-4A nanoparticles (~ 100 nm) fabricated under similar spinning conditions. The profound effect of zeolite type on the mixed matrix membrane morphology needs to be investigated in the future, however, the preliminary goal is met to confirm the possibility to spin high loading (40wt%) mixed matrix hollow fiber.

Mixed matrix hollow fiber membranes for C4s separation with high zeolite loading were then fabricated using 6FDA-DAM-DABA as the sheath polymer matrix and cellulose acetate as the core layer. During the optimization process of zeolite-polymer matching and surface treatment on zeolite nanoparticles (as shown in chapter 4-6), two preliminary trials were made to spin mixed matrix hollow fibers for C4s separation. Mixed matrix sheath dopes were made in the absence of $LiNO_3$ to avoid the micropore formation as discussed in chapter 7. Lower polymer concentrations were used to raise the phase separation rate of 6FDA-DAM-DABA mixed matrix sheath. The phase separation was not enough in the sheath containing 18.7wt% of 6FDA-DAM-DABA polymer and 3.3% of GT-5A nanoparticles, and undesirable double skin sheath morphology was formed. A second trial was made using a mixed matrix sheath with lower polymer concentration (14.7wt%) to raise the phase separation rate. The desired morphology: ~2 μm dense skin, delamination-free interface, macrovoid-free support layer, was achieved on the dual layer mixed matrix hollow fibers. The treatment of zeolite 5A nanoparticles

(150nm-300nm) is critical for the further development of mixed matrix hollow fibers membranes used for C4s separation.

8.2 STABILITY OF MIXED MATRIX SPINNING DOPES

The MFI nanoparticles were first used because of the short supply of 5A nanoparticles and the resultant delayed surface modification work. A GT-MFI/Ultem® spinning dope with high sieve loading was prepared using the procedures shown in chapter 3. The spinning dope composition was determined to have the right polymer/sieve ratio to achieve the right ratio in solid fibers, the appropriate amount of evaporating THF was added to form a dense skin layer, and a suitable distance from spinodal line for dope composition was established to achieve the desired phase separation. After considerable optimization, a weight percent composition of Ultem® 21%, NMP 49%, THF (non-solvent) 16%, GT-MFI 14% was selected. Surface modified MFI nanoparticles and NMP was mixed in a 150ml jar. The mixture was sonicated in a sonication bath for a few hours to help the dispersion. I speculate the sonication helps to dissolve $Mg(OH)_2$ in NMP to increase the ionic strength in the colloid mixture. Once trace amounts of $Mg(OH)_2$ dissolved, the electrostatic repulsion can keep the GT-MFI/NMP colloid stable. Even though the GT-MFI was 40wt% in the solid base, the beginning GT-MFI in NMP colloid was only 22wt% particle loading, which is a stable gel mixture. THF was added into the gel and a significant viscosity decrease was observed with unchanged stability. Roughly 10% of the ultimately required Ultem® polymer was first added into the mixture to help the stabilization, according to past experience. The remaining polymer was added later to form the final spinning dope. Fig.

8.1 shows the stability comparison with dopes of 15wt% non-treated sieves and 15wt% treated SSZ-13. The spinning dope showed similar stability as that in lower sieve loading, and the dope had high strength to form fibers from visual observation.

Figure 8.1 Stability of mixed matrix dope with 15wt% non-treated SSZ-13[1], 15wt% GT-SSZ-13[1] and 40wt% GT-MFI

8.3 ULTEM®+GT-ZEOLITE MIXED MATRIX HOLLOW FIBERS SPINNING

The mixed matrix dual layer hollow fibers were spun using Ultem® pure polymer dope to form the core layer and mixed matrix Ultem®/GT-zeolite dope to form the sheath layer. A core dope with composition of Ultem® (32%)/NMP(56%)/THF(9)/$LiNO_3$(3%) was used, which was the same for all the mixed matrix hollow fibers. A neutral bore fluid of NMP(90%)/H_2O(10%) was used as that used for pure Ultem® fiber spinning. The bore and sheath dope flow rates were held constant at 60 and 180 ml/hr respectively. The sheath dope compositions for different mixed matrix hollow fiber spinning are shown in table 8.1. The dope viscosity, an empirical parameter for spinning, increases due to the addition of polymer or zeolite nanoparticles. The total solid (polymer+zeolite) concentration in the sheath dope are held constant at 35wt% as that in pure Ultem® hollow fiber spinning, in order to make dopes with viscosities around the empirical value

~100 Pa·S (from eye observation). The ratio of polymer to zeolite varies to achieve the desired zeolite loading in the final mixed matrix membranes. For example, sheath dope with polymer and zeolite concentrations of 21% and 14% was used to form a 40wt% mixed matrix membranes.

Table 8.1 Mixed matrix sheath compositions

	JQ08 20wt%-MFI	JQ09 40wt%-MFI	JQ14 20wt%-4A	JQ12 40wt%-4A
Ultem®	28	21	28	21
NMP	49	49	49	49
THF	16	16	16	16
Zeolite	7	14	7	14

Table 8.2 Detailed spinning parameters for the Ultem® based mixed matrix hollow fiber spinning

	bath temperature [°C]	sheath flow rate [ml/hr]	Spinning temperature [°C]	Air gap [cm]	take up rate [m/min]
20wt%-GT-MFI (JQ08-03)	16	20	50	15	25
40wt%-GT-MFI (JQ09-03)	17	20	70	15	25
20wt%-GT-4A (JQ14-07)	22	20	70	15	25
40wt%-GT-4A (JQ12-04)	25	20	75	15	25

Table 8.2 shows detailed spinning parameters for the mixed matrix hollow fibers containing 20% and 40% GT-zeolite nanoparticles. Higher spinning temperature (>50

°C) and larger air gap (15cm) are used to ensure the formation of dense skin in all the mixed matrix hollow fibers membranes. Fig. 8.2 and Fig. 8.3 show the mixed matrix hollow fibers containing GT-MFI and GT-4A nanoparticles respectively. In all the mixed matrix hollow fibers, no clear interface between the zeolite containing sheath and pure Ultem® core can be observed, because of the good adhesion between the two layers containing the same Ultem® polymer. Uniform mixed matrix sheath layers (~5 μm) were formed on the pure Ultem® core sheath, with a sheath flow rate (20ml/hr), which is about 1/10 of the core flow rate (180 ml/hr).

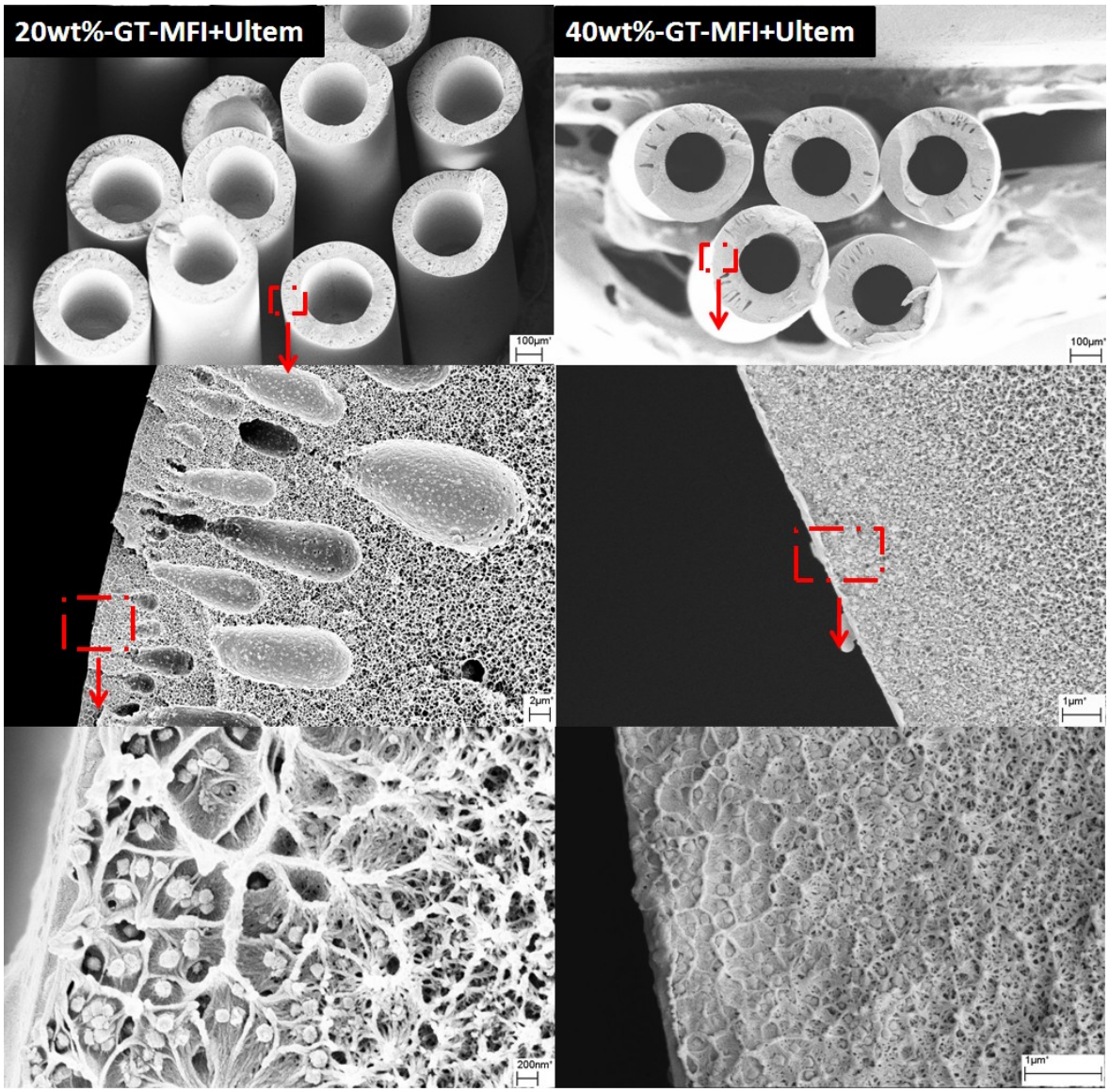

Figure 8.2 Mixed matrix Ultem® hollow fiber with 20wt% and 40wt% GT-MFI loading

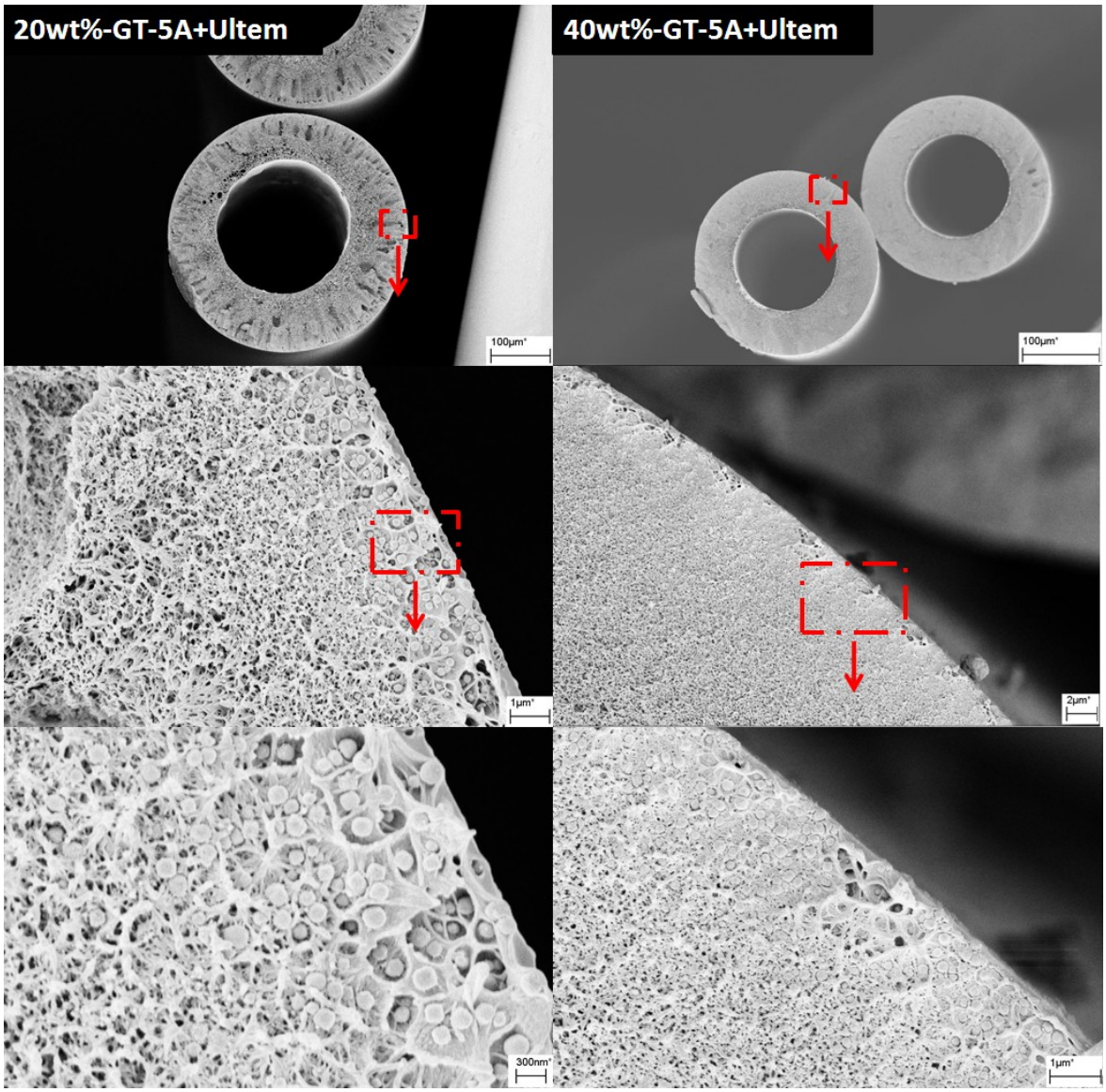

Figure 8.3 Mixed matrix Ultem® hollow fibers with 20wt% and 40wt% GT-4A loading

All the mixed matrix hollow fibers showed good spinnability, and the spinning parameters, such as spinning temperature, take up rate, *etc.,* can vary in large operating windows. For example, the take up rate of 40wt% mixed matrix hollow fiber can increase to 65 m/min, as in pure polymeric hollow fiber spinning, because the mechanical strength of the mixed matrix hollow fibers are mainly due to the pure Ultem® core layer. The dispersion of GT-zeolite nanoparticles is good in the sheath of all the mixed matrix

hollow fibers. The gas transport properties of CO_2/CH_4 and O_2/N_2 pairs are shown in table 8.3. The thickness of dense skin in the asymmetric hollow fibers can be derived from the gas permeance in mixed matrix hollow fiber and the intrinsic gas permeability in the mixed matrix films. The dense skin thickness varies significantly in mixed matrix membranes with addition of different kind of zeolite and at different amount of zeolite loading. With the same amount of zeolite added, thicker skins are always formed on mixed matrix sheath containing MFI nanoparticles, presumably because the addition of hydrophobic high silica MFI suppressed the water diffusion rate (and the phase separation rate) in the mixed matrix sheath layer. The skin thickness of mixed matrix fibers containing 40wt% of GT-MFI nanoparticles (1180nm) is about 10 times thicker than that in fibers containing 40wt% of GT-4A nanoparticles(110nm). More fundamental research is needed on the dramatic difference of dense skin thickness formed in the mixed matrix hollow fibers containing different kinds of zeolite.

Table 8.3 Gas transport properties Ultem® based mixed matrix hollow fiber membranes after post treatment [2], permeation tests were done using a downstream vacuum method at 2 atm, 35 °C

	Pure Ultem®	JQ08-3 20wt%-MFI	JQ14-7 20wt%-4A	JQ09-3 40wt%-MFI	JQ12-4 40wt%-4A
P_{O2} [GPU]	0.4	0.70	1.37	0.34	3.73
O_2/N_2	***7.6***	***7.0***	***7.7***	***7.9***	***6.7***
P_{CO2} [GPU]	1.4	2.7	5.4	1.3	13.7
CO_2/CH_4	***37.5***	***35***	***41***	***48***	***32***
Calculated skin thickness [nm]	***1000***	***570***	***290***	***1180***	***110***

The selectivity of O_2/N_2, CO_2/CH_4 was not expected to change due to the addition of MFI particles, because the lack of molecular sieving effect in the large pores of MFI. The 4A is reported to enhance the O_2/N_2, CO_2/CH_4 selectivities in the mixed matrix dense films [3]. The O_2/N_2 selectivities of the mixed matrix membranes containing GT-4A nanoparticles are around the intrinsic selectivity in the Ultem® polymer membranes (7.6). The lack of good polymer/zeolite interfacial adhesion probably causes the lack of selectivity shown in the Ultem®/4A mixed matrix hollow fiber membranes. The CO_2/CH_4 selectivities in the mixed matrix hollow fiber membranes, except the 40wt%-GT-MFI mixed matrix hollow fibers membranes, are close to that in Ultem® dense films (37.5) after post treatment. Two possible explanations for the high CO_2/CH_4 selectivity in the 40wt%-GT-MFI mixed matrix hollow fibers are: 1) the polymer chains align to a certain degree during fiber spinning process, the addition of nanoparticles slows down the chain relaxation process to random coils state before vitrifying to form the dense skin. The membrane with partially aligned polymer chains has higher gas selectivity than that in the normal state. 2) the diethyltoluenediamine used in the chemical post treatment method [2] can selectively enhance the CO_2 solubility, thereby the CO_2 permeance in the membrane is selectively enhanced over other gases after post treatment. More research is needed to find the reason for the selectivity enhancement. The dense skin of 40wt%-GT-4A mixed matrix hollow fibers is 110nm, according to the calculation. The zeolite nanoparticles are about 150nm in diameter, therefore, a dense skin of 500nm-1000nm is desirable to encapsulate the 150nm nanoparticles in the dense skin, with defect free polymer-zeolite interfaces. One way to increase the skin thickness is to raise the polymer

concentration in the dope, and suppress the phase separation rate of the mixed matrix sheath layers containing GT-4A nanopaticles.

8.4 ANNEALING OF MIXED MATRIX HOLLOW FIBER MEMBRANES

Annealing post treatment (around Tg) is widely used to remove the voids between zeolite and polymer phase and enhance the adhesion. Here, one example shows the effect of annealing treatment on the morphology of mixed matrix hollow fiber membranes.

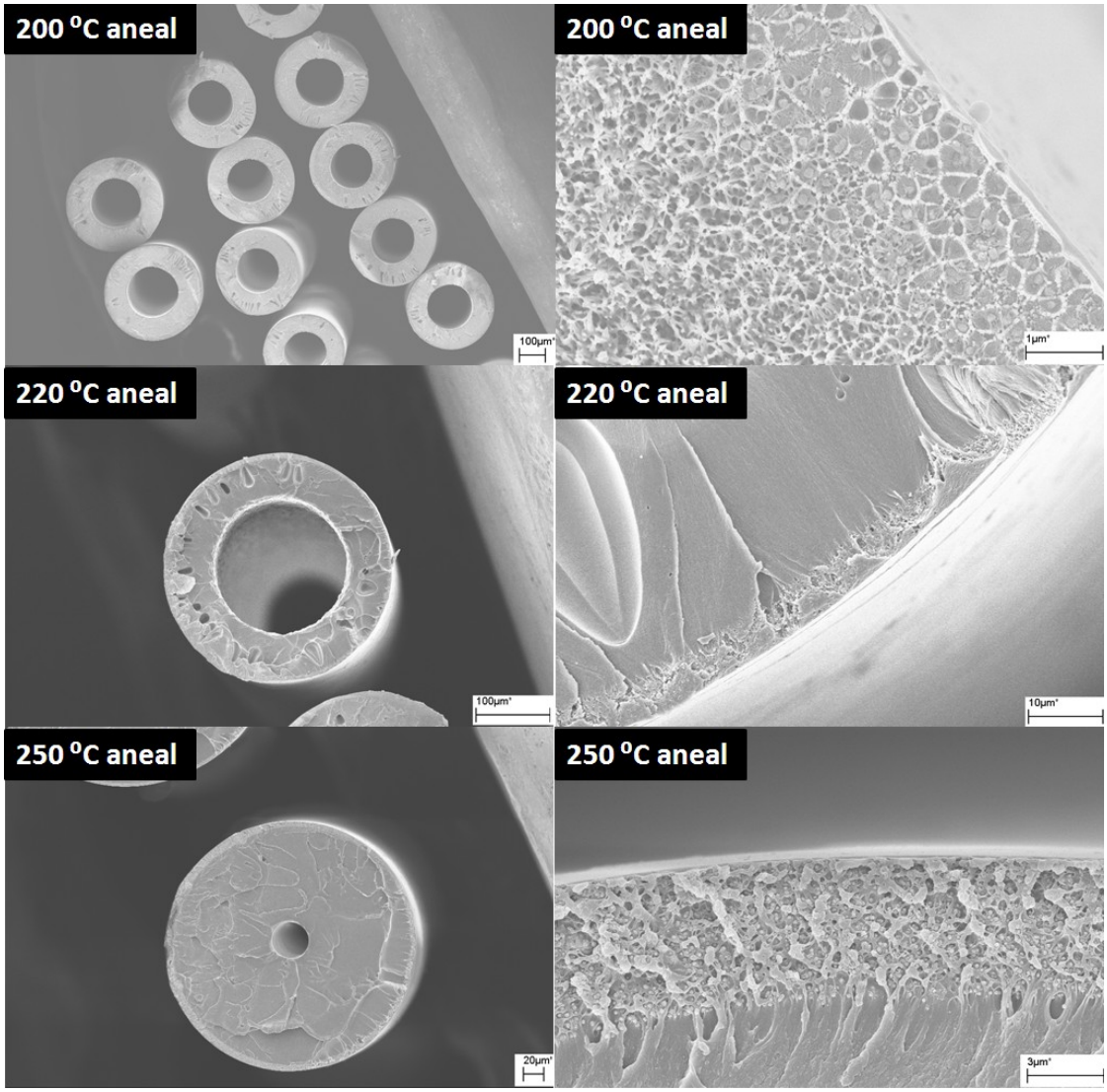

Figure 8.4 Mixed matrix hollow fiber (20wt% GT-MFI) annealed at different temperatures

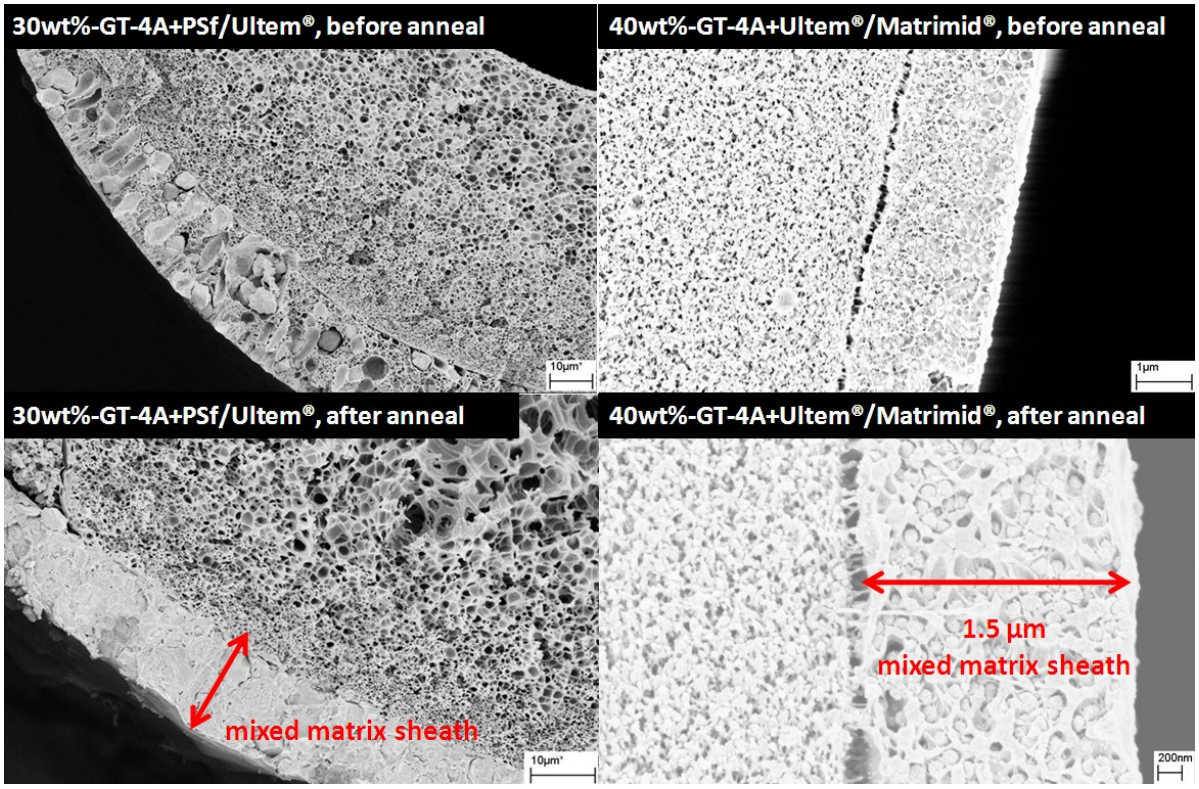

Figure 8.5 Dual layer mixed matrix hollow fibers before and after annealing treatment

Fig. 8.4 shows the 20wt%-GT-MFI mixed matrix hollow fibers annealed at different temperatures. The Tg of Ultem® polymer is about 215 °C [4], and three annealing temperature are used, slightly below Tg (200 °C), slightly above Tg (220 °C) and above Tg (250 °C). The structure of the hollow fiber, *i.e.,* porous support, dense skin is maintained after annealing at 200 °C for overnight. The porosity of both support and sheath layers diminish after overnight annealing at 220 °C. The hollow fibers shrink overall at even higher annealing temperature of 250 °C. Due to the same Ultem® polymer used in the core and sheath layers, it is difficult to selectively anneal the sheath layer above Tg to fix the defective interfaces between zeolite and polymer, while maintaining a porous support layer.

Another mixed matrix hollow fiber design for the convenience of annealing treatment is as follows: a polymer with lower Tg (T_l) is used for the sheath layer, a polymer with higher Tg (T_h) is used for the core layer. The annealing treatment can be carried out in the range of T_l to T_h. Two examples are shown in Fig. 8.5, a polysulfone (Tg=190 °C) [5] sheath containing zeolite particles on an Ultem® core, and an Ultem® sheath containing zeolite particles on a Matrimid (Tg=305 °C) core [6]. The sheath changed from porous to dense layer after annealing at temperatures above the Tg of sheath polymers (200 °C for polysulfone and 250 °C for Ultem®). The porosity of core layers is maintained because the annealing temperatures are still below the Tg of core layer polymers. As shown in Fig. 8.5, a thin sheath layer (1.5 μm) is achieved by using low sheath dope flow rate (20 ml/hr) and higher take up rate (50 m/min). The mixed matrix hollow fiber design with a thin mixed matrix sheath layer densified by annealing post treatment, may provide an alternative to the design of forming the mixed matrix dense skins during the spinning process in the future.

8.5 MIXED MATRIX HOLLOW FIBERS MEMBRANES FOR C4S SEPARATION

The project started with the goal of spinning mixed matrix hollow fibers membranes for C4s separation, with the assumption that high silica MFI is the right zeolite for C4s separation, and proper surface modification on the synthesized zeolite nanoparticles (as on commercial μm LTA particles) can be done to achieve sufficient zeolite/polymer interfacial adhesion. It was found by later work that 6FDA polyimides are the most promising polymer choice for the bulky C4s gas separations. As discussed in

chapter 7, significant optimization work was done to spin dual layer hollow fibers with 6FDA polyimides as the sheath layer polymer. More work is shown here to add zeolite nanoparticles to the 6FDA polyimide sheath to form dual layer mixed matrix hollow fiber membranes. As discussed in the chapter 5, the development of a surface treatment method on synthesized zeolite nanoparticles (based on the sol-gel-Grignard treatment) is part of the process. Dense film work (shown in chapter 6) using the Grignard (and sol-gel-Grignard) treated commercial 5A particles shows the 6FDA-DAM-DABA and 5A are the polymer and zeolite choices to form C4s separating mixed matrix membranes.

Preliminary mixed matrix hollow fibers were spun using the Grignard treated zeolite nanoparticles (not necessarily having ideal interfacial adhesion with the polymer matrix). The morphologies of mixed matrix hollow fibers can be optimized initially, so that the future well treated nanoparticles will replace the current particles in the initially optimized mixed matrix hollow fiber membranes.

As discussed in chapter 7, the addition of $LiNO_3$ enhances the phase separation rate of 6FDA polymer sheath, but possibly induces micropore formation in the skin, which is especially detrimental to the slow gas separations, such as C4s. As shown in table 8.4, if total solid concentrations (polymer+zeolite) in the mixed matrix sheath dopes are held constant at 22wt%, the ratio of polymer to zeolite can be adjusted to have the desired zeolite loading in the final membrane. The compositions of cellulose acetate core dope and bore fluid are the same as those in dual layer hollow fiber spinning as shown in table 7.3. Other spinning parameters are shown in table 8.5. Compared to dual layer mixed matrix hollow fibers using Ultem® as the core and sheath polymers, it is more difficult to spin dual layer mixed matrix hollow fibers using cellulose acetate as the core

and 6FDA-DAM-DABA as the sheath. The mixed matrix hollow fibers showed insufficient mechanical strength due to the slow phase separation rate of both core and sheath layer, therefore, bigger fibers were spun using higher dope flow rates and lower take up rates to avoid the breakage of fibers during the spinning process.

Table 8.4 Compositions of the mixed matrix sheath dopes

%	15wt%-GT-5A+DABA (JQ30)	35wt%-GT-MFI+DABA (SH56)
6FDA-DAM-DABA	18.7	14.7
THF	78	77.5
GT-Zeolite	3.3	7.8
zeolite % in total solid	15wt%	35wt%

Table 8.5 Detailed parameters for dual layer mixed matrix hollow fiber spinning

	Bore/core/sheath flow rate [ml/hr]	Spinning temperature [°C]	Air gap [cm]	Take up rate [m/min]
15wt%-GT-5A (JQ30-4)	80/240/30	40	4	10
15wt%-GT-5A (JQ30-5)	100/300/50	40	4	10
15wt%-GT-5A (JQ30-7)	100/300/50	50	4	10
35wt%-GT-MFI (SH56-1)	100/400/50	22	10	10

Fig. 8.6 shows the morphology of the 15wt%-GT-5A mixed matrix hollow fiber. A GT-5A+6FDA-DAM-DABA mixed matrix sheath (~8 μm) is formed uniformly on the cellulose acetate core layer. Good interfacial adhesion between the CA core and mixed matrix sheath is achieved. However, the sheath layer shows closed cell pores and double skin layers due to the slow phase separation rate of the sheath layer. The calculated skin

thickness (from gas transport properties) is 6 µm, which means the majority of sheath (~8 µm) is not phase separated yet. Other spinning conditions were tried to increase the phase separation rate of the sheath layer, as shown in table 8.5. Thinner sheath layer and higher spinning temperature were tried, and the mixed matrix sheath morphologies are shown in Fig. 8.7. Similar double skin morphologies on sheath layers are found on both hollow fiber membranes. The phase separation rate of sheath layer can be enhanced by further reducing the polymer concentration in the sheath, or adding pore forming agent such as $LiNO_3$. There may be concerns regarding the ion exchange into the cation containing zeolites by the $LiNO_3$. Other pore forming polyvinylpyrrolidone (PVP) or polyethyleneglycol (PEG) [7] can be tried in the future to raise the phase separation rate of 6FDA polymer sheath, while avoiding the possible ion exchange issue.

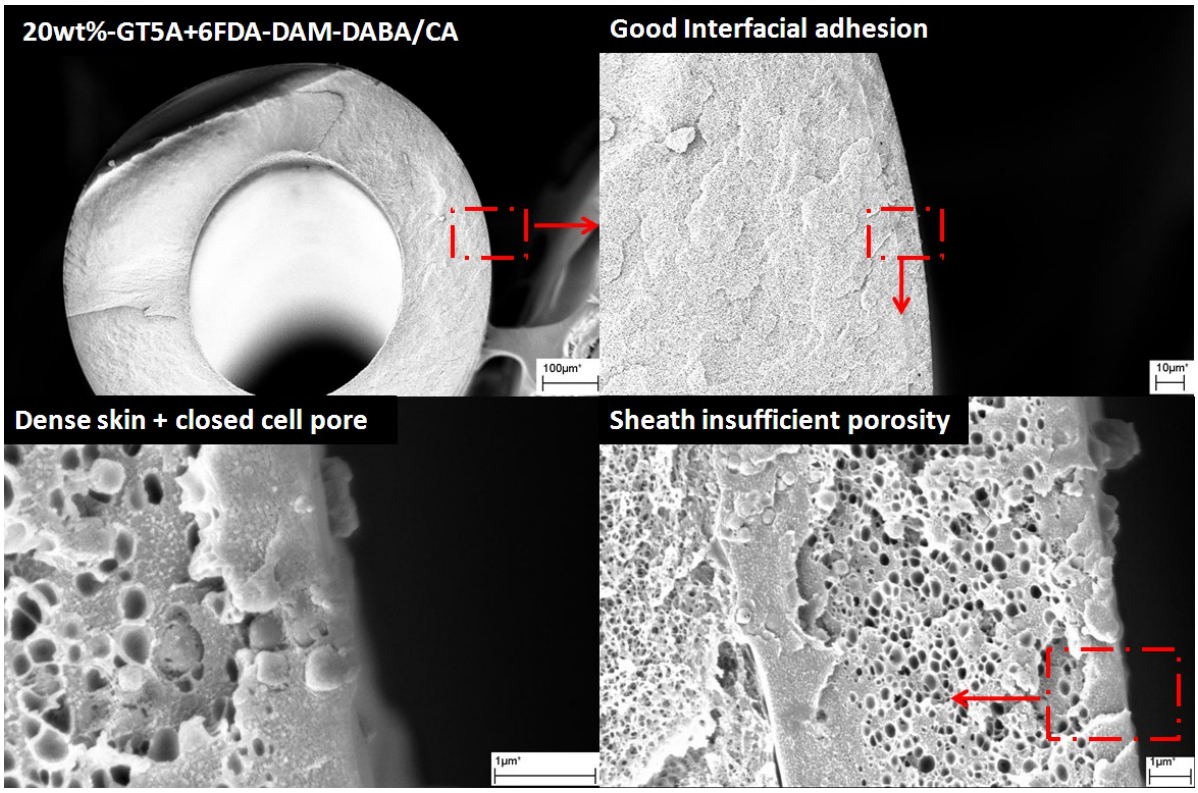

Figure 8.6 15wt%-GT-5A+6FDA-DAM-DABA/CA mixed matrix hollow fiber (JQ30-5)

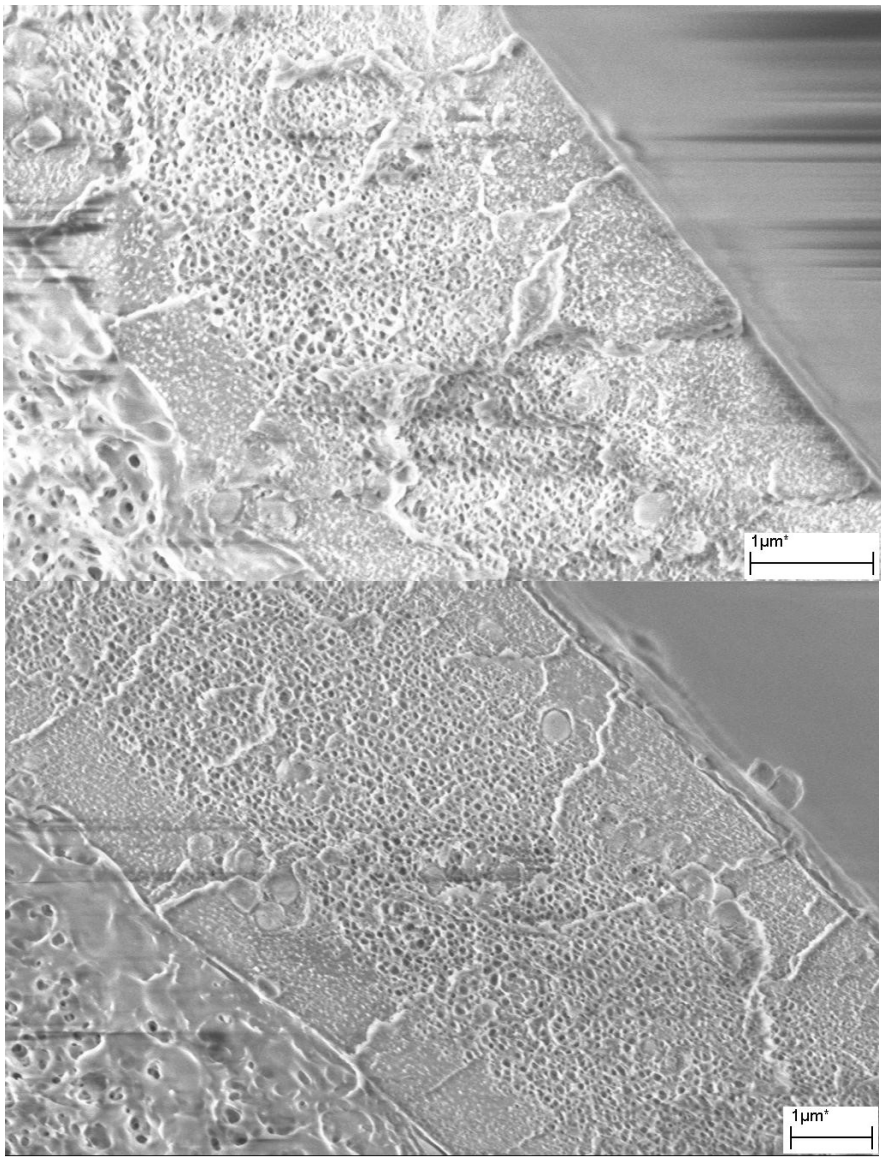

Figure 8.7 15wt% GT-5A+6FDA-DAM-DABA/CA mixed matrix hollow fiber spun with a thinner sheath layer (top) and high spinning temperature (bottom)

Fig. 8.8 shows the morphology of 35wt%-GT-MFI dual layer mixed matrix hollow fiber membranes. Good interfacial adhesion is observed between the CA core and the mixed matrix sheath layer. The porosity of sheath layer is significantly higher than that of 15wt%-GT-5A mixed matrix hollow fibers. The higher gas permeance, shown in table 8.6, verified the porous sheath. The calculated skin thickness is about 2 µm, which is slightly thicker than the desired mixed matrix skin thickness (0.5-1 µm), as discussed

in the previous section. The 6FDA-DAM-DABA concentration in the sheath dope is only 15wt%, far below the critical concentration to have high mechanical strength. The low O_2/N_2 selectivity in the as-made 35wt%-GT-MFI mixed matrix membrane suggests a defective skin layer is formed. The defective skin is probably caused by the low polymer concentration in the sheath dope, or low spinning temperature. The defective fiber membranes are post treated using the same method shown in chapter 7. The permeance of slower gases decreases more after the post treatment, while the permeance of faster gas such as O_2 hardly changes. This suggests only diffusion through the defective sites are plugged by the post treatment. The chemical post treatment method applies to 6FDA-DAM-DABA mixed matrix membranes without additional layer formation. The C4s selectivity after post treatment is 17, very close to the intrinsic selectivity in pure 6FDA-DAM-DABA polymer (~25). As discussed in chapter 6, no selectivity enhancement is anticipated by adding zeolite MFI to 6FDA-DAM-DABA polymer, due to the mismatching of transport properties. The skin layer thickness (~2 μm) and high nC4/iC4 selectivity (after post treatment) are both approaching the desired properties in a mixed matrix hollow fiber membrane. Further optimization can be done by increasing the polymer concentration to have more defect free skin, and adding pore forming agents such as PVP, PEG to raise the phase separation rate. Preliminary work shows mixed matrix hollow fiber spinning using 6FDA-DAM-DABA as sheath polymer is feasible, but more optimization work is needed. Mixed matrix hollow fiber can be spun using the future well treated zeolite 5A nanoparticles for C4s separations, using the partially optimized dual layer mixed matrix platform.

Table 8.6 Gas transport properties of the dual layer mixed matrix hollow fibers

P [GPU]	As spun 15wt%-GT5A-DABA	As spun 35wt%-GT-MFI-DABA	Post treated 35wt%-GT-MFI-DABA
O_2	5.7	18.5	17.8
N_2	1.8	7.1	2.8
selectivity O_2/N_2	***3.2***	***2.6***	***6.2***
nC4		1.8	0.20
iC4		1.6	0.012
selectivity nC4/iC4		***1.1***	***17***
skin thickness	***6***	***1.9***	***2***

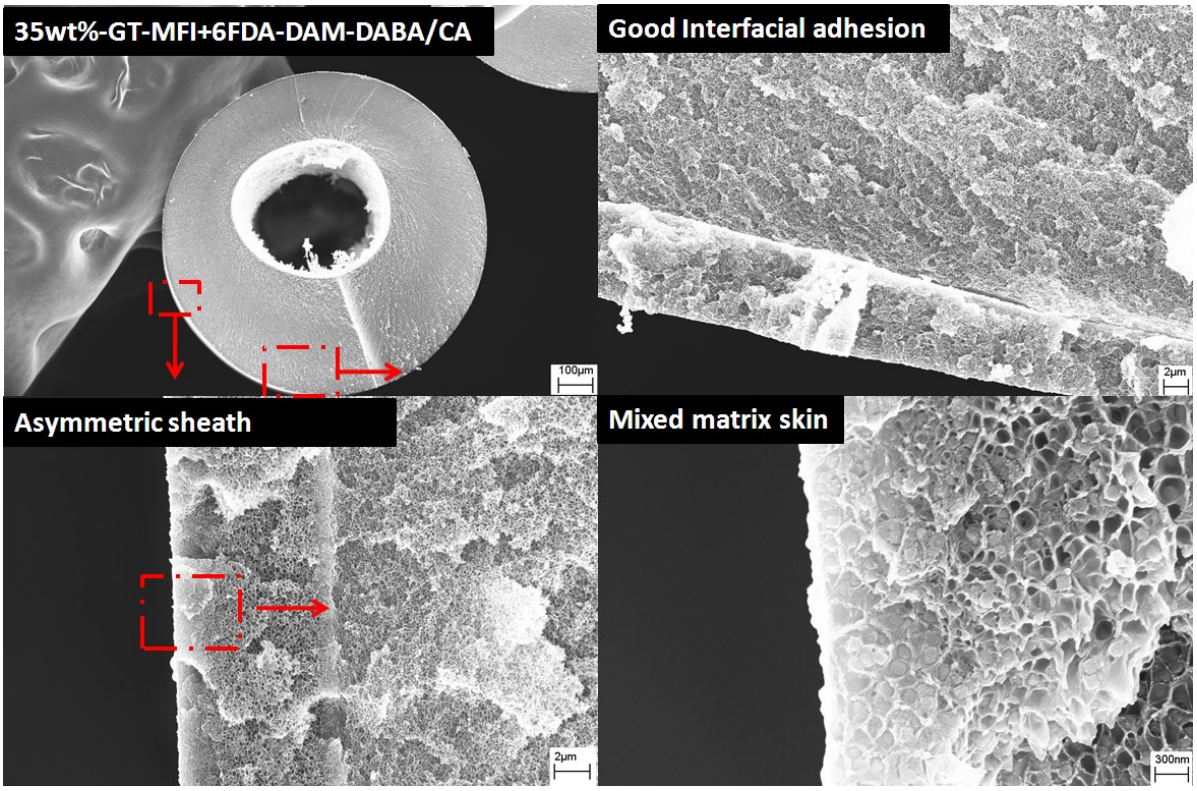

Figure 8.8 35wt%-GT-MFI-6FDA-DAM-DABA/CA mixed matrix hollow fiber

8.6 SUMMARY

The high loading (>40wt%) mixed matrix hollow fiber spinning using Ultem® as the polymer matrix is less technically challenging due to the good fiber formation properties of the Ultem® polymer. Preliminary work is done to spin mixed matrix hollow fibers aimed for C4s separation, using 6FDA-DAM-DABA as the polymer matrix. Future work is needed to optimize the mixed matrix hollow fiber spinning process, before the well treated 5A nanoparticles are ready.

8.7 REFERENCE

[1] S. Husain, Ph. D thesis, *Georgia Institute of Technology*, **2006**

[2] O.M. Ekiner, US patent, 6,663,805, **2003**

[3] S. Shu*, J. Phys. Chem. C*, **2007**, 111, 652-657

[4] *Ultem® Product Data Sheet*, **1997**, GE Plastics: Pittsfield, MA

[5] *Polysulfone Product Data Sheet,* **2002**, Solvay: Alpharetta, GA

[6] *Matrimid® Product Data Sheet*, **2000**, Vantico, Inc.: Brewster, NY.

[7] J.R. Hwang, *J. Appl. Polym. Sci*., **1996**, 60, 1343-1348

CHAPTER 9

SUMMARY AND RECOMMENDATIONS

9.1 SUMMARY AND CONCLUSIONS

The goal of this four year project was to develop high loading mixed matrix hollow fiber membranes for C4s separation. The research set out to address following objectives.

9.1.1 Identify proper sieve and polymer for butane isomer separation

There was limited research on C4s membrane separations using glassy polymer membranes previously. A group of fluorinated polyimides were selected for C4s separation. There are two advantages to using these polymers. First, high nC4 permeability (0.3 - 3.7 Barrer) is possible in this family of high FFV polymers. By a comparison, nC4 permeability in one of the most permeable commercial polymers, Matrimid®, is only ~0.1 Barrer. Second, the family of fluorinated polyimide covers a large nC4's permeability window, which is beneficial for the polymer-zeolite matching.

High silica MFI was first explored to make mixed matrix membranes for C4s separation. The nC4 permeability in MFI (~10,000 Barrer) matches well with that in the rubbery polymer PDMS (4980 Barrer). There is no glassy polymer permeable enough to match zeolite MFI for successful mixed matrix membrane formation used in C4s separation. Zeolite 5A, with lower nC4 permeability and practically infinite nC4/iC4 selectivity, was then used to match the less permeable glassy polymers. Different separation performances can be achieved using mixed matrix membranes composed of

zeolite 5A and different polymer pairs. The most promising pair for C4s separation is 6FDA-DAM-DABA and zeolite 5A.

9.1.2 Surface modify zeolite particles

The $Mg(OH)_2$ whiskers formed on the sieve surfaces proved to be effective to improve the adhesion between polymer and sieve, in both mixed matrix dense films and hollow fibers. Unfortunately, insufficient knowledge exists regarding the $Mg(OH)_2$ formation. New facile solvothermal treatment method was developed by Tae-Hyun Bae in Dr. Nair and Dr. Jones group, and I played the assistance role. It was later found that the solvothermal and ion exchange induced $Mg(OH)_2$ whisker formation methods were less effective on the LTA particles, which were to be used for C4s separation. There was the need for revival of Grignard treatment and elucidating the whisker formation mechanism. I proposed a sol-gel-precipitation mechanism to explain the $Mg(OH)_2$ whisker formation. The effect of two major parameters: water amount (hydrolysis ratio), and pH were studied to control the sol-gel $Mg(OH)_2$ morphology. $Mg(OH)_2$ whiskers were successfully formed on commercial 5A particles at 6 stiochoimetric amount of water (pH=0, HCl solution) addition.

It was found that not only the $Mg(OH)_2$ whisker morphology develops under acidic conditions, but also the $Mg(OH)_2$ nucleation highly probably happens on acidic sites on the zeolite. Therefore, the acidity control (sites and strength) is important for the sol-gel-Grignard treatment. Three kinds of acidic species: HCl acid solution, AlClx species by dealumination, and $AlCl_3$ supported on zeolite surface, were introduced into the sol-gel system. All three acidic species promoted the one dimensional $Mg(OH)_2$ whiskers formation by providing acidic catalyst for the sol-gel reactions. The different

distribution of acidic species probably caused the different nucleation place of $Mg(OH)_2$. Undesired homogeneous nucleation of $Mg(OH)_2$ happens when HCl acid is added homogeneously to catalyze the sol-gel reactions. $Mg(OH)_2$ whiskers selectively nucleate on zeolite surfaces when $AlCl_3$ (anchored onto zeolite surfaces) was used as the acid catalyst for sol-gel reactions. The heterogeneous $Mg(OH)_2$ whisker formation is possible on all kinds of zeolite surface, supported with a $AlCl_3$ acid layer. However, the $AlCl_3$ later can hydrolyze and form a byproduct layer of $Al(OH)_3$ between zeolite surface and $Mg(OH)_2$ whiskers. New ways have to be designed to introduce surface acidic sites on zeolite surfaces to promote the surface nucleation of $Mg(OH)_2$ whiskers, while not affecting the bonding between zeolite and $Mg(OH)_2$ whiskers.

9.1.3 Spin dual layer hollow fibers using 6FDA polymers.

The drawbacks of using 6FDA polymers are their high cost and less studied spinning properties. A dual layer design is needed to cut the cost of sieves and polymers in mixed matrix hollow fibers. Dual layer hollow fiber membranes using 6FDA polymers as the sheath layer (without zeolite addition) were first developed. Several commercial polymers were tried as the core layer material and cellulose acetate showed the best adhesion with 6FDA polymer sheath. The phase separation of 6FDA polymer sheath can be enhanced by the addition of pore forming agent $LiNO_3$, without losing the good core/sheath interfacial adhesion. The dual layer hollow fiber membrane showed defect-free gas transport properties for faster gas pairs, such as CO_2/CH_4, and O_2/N_2. The separation performance was below intrinsic value for slower gas pair n-C_4H_{10}/i-C_4H_{10}, because of possible presence of exceedingly minor defects that were undetectable for the

higher flux gases. The fast phase separation rate of the $LiNO_3$ containing solution probably may have contributed to the minor defects.

9.1.4 Spin dual layer mixed matrix hollow fibers.

Mixed matrix hollow fiber membranes with high zeolite loading (> 40wt%) were first fabricated using Ultem® as the polymer matrix, because of its known easy fiber forming properties. The mixed matrix hollow fibers have good mechanical strength due to the pure Ultem® core layer, but the mixed matrix membrane showed gas transport properties close to pure polymeric membranes. No significant selectivity enhancement were found on mixed matrix membranes containing GT-4A (traditional Grignard treatment) nanoparticles, due to the lack of adhesion between the polymer and 4A nanoparticles.

Mixed matrix hollow fiber membranes for C4s separation with high zeolite loading were fabricated using 6FDA-DAM-DABA as the sheath polymer matrix and cellulose acetate as the core layer. The desired morphology: ~2 μm dense skin, delamination-free interface, macrovoid-free support layer, was achieved on the GT-MFI+6FDA-DAM-DABA dual layer mixed matrix hollow fibers. The treatment of zeolite 5A nanoparticles (150nm-300nm) is critical for the further development of mixed matrix hollow fibers membranes used for C4s separation.

The following conclusions can be made through this research:

1. The family of fluorinated polyimides matches for the C4s separation. Zeolite MFI, with too high nC4 permeability and limited nC4/iC4 selectivity, does not match 6FDA polymers for C4s separation. Zeolite 5A, with lower nC4 permeability and practically infinite nC4/iC4 selectivity matches 6FDA polymers for C4s separation.
2. Cellulose acetate matches well for 6FDA polymers to spin delamination-free, macrovoid-free dual layer hollow fibers. High loading (> 40wt%) mixed matrix hollow fibers is feasible, based on the platform of 6FDA polyimides/Cellulose acetate dual layer hollow fibers.
3. A sol-gel-precipitation mechanism explains the $Mg(OH)_2$ whisker formation in the Grignard treatment. Zeolite surface acidic sites promotes the heterogeneous $Mg(OH)_2$ whisker formation.

9.2 RECOMMENDATIONS

The good interfacial adhesion between zeolite and glassy polymers is the core engineering challenge for future mixed matrix membrane development. The interfacial adhesion enhancement through whisker-roughened surface is a promising universal solution. The question remains is there universal ways to grow $Mg(OH)_2$ whiskers on different kinds of zeolite surfaces. More work needs to be done, in order to answer this question.

9.2.1 Introducing surface acidity by adsorbed organic acid

The heterogeneous acidic site by supported $AlCl_3$ on zeolite surface promoted the heterogeneous nucleation of $Mg(OH)_2$ whiskers. The $AlCl_3$ is supposed to be able to

attach all kinds of solids surfaces through the chemical bonding with hydroxyl groups. The acidic strength can be adjusted by the amount of $AlCl_3$ supported onto the zeolite surfaces. Sol-gel-Grignard treatment can be applied to the $AlCl_3$ attached to the zeolite to form $Mg(OH)_2$ whiskers; however, the byproduct $Al(OH)_3$ prevented the application of this promising method.

Organic acids, such as p-toluenesulfonic acid (PTSA), can be used to replace the $AlCl_3$ to introduce the surface acidity on zeolite. The acid molecules can absorb on zeolite surfaces through the strong interaction with surface hydroxyl groups. The strong polarity of zeolite also attract the polar acid molecules physically adsorb on the zeolite surfaces in a tolune/IPA dispersion during the sol-gel-Grignard treatment. Sol-gel species of $Mg(OH)_2$ precursor can form around the adsorbed acid molecules (catalyst) close to zeolite surface, and then attach to zeolite surfaces through the condensation reaction with the hydroxyl groups. The water soluble organic acid will be washed away during the water washing steps, therefore, no layer exist between the zeolite surfaces and $Mg(OH)_2$ whiskers. It is potentially a universal solution to grow $Mg(OH)_2$ whiskers on all zeolite surfaces by introducing a layer of physically adsorbed organic acid layer, which acts as the semi-heterogeneous catalyst for the sol-gel reactions.

9.2.2 Study the difference between commercial and synthesized LTA

There are also huge differences between commercial and synthesized LTA particles, during the sol-gel-Grignard treatment, as shown in table 9.1. The current hypothesis is the existence of macropore (defective sites) or layer of amorphous species (unreacted reagent after synthesis) on commercial 5A surfaces, as discussed in chapter 5. The elucidation of the different surface property can help design new treatment method.

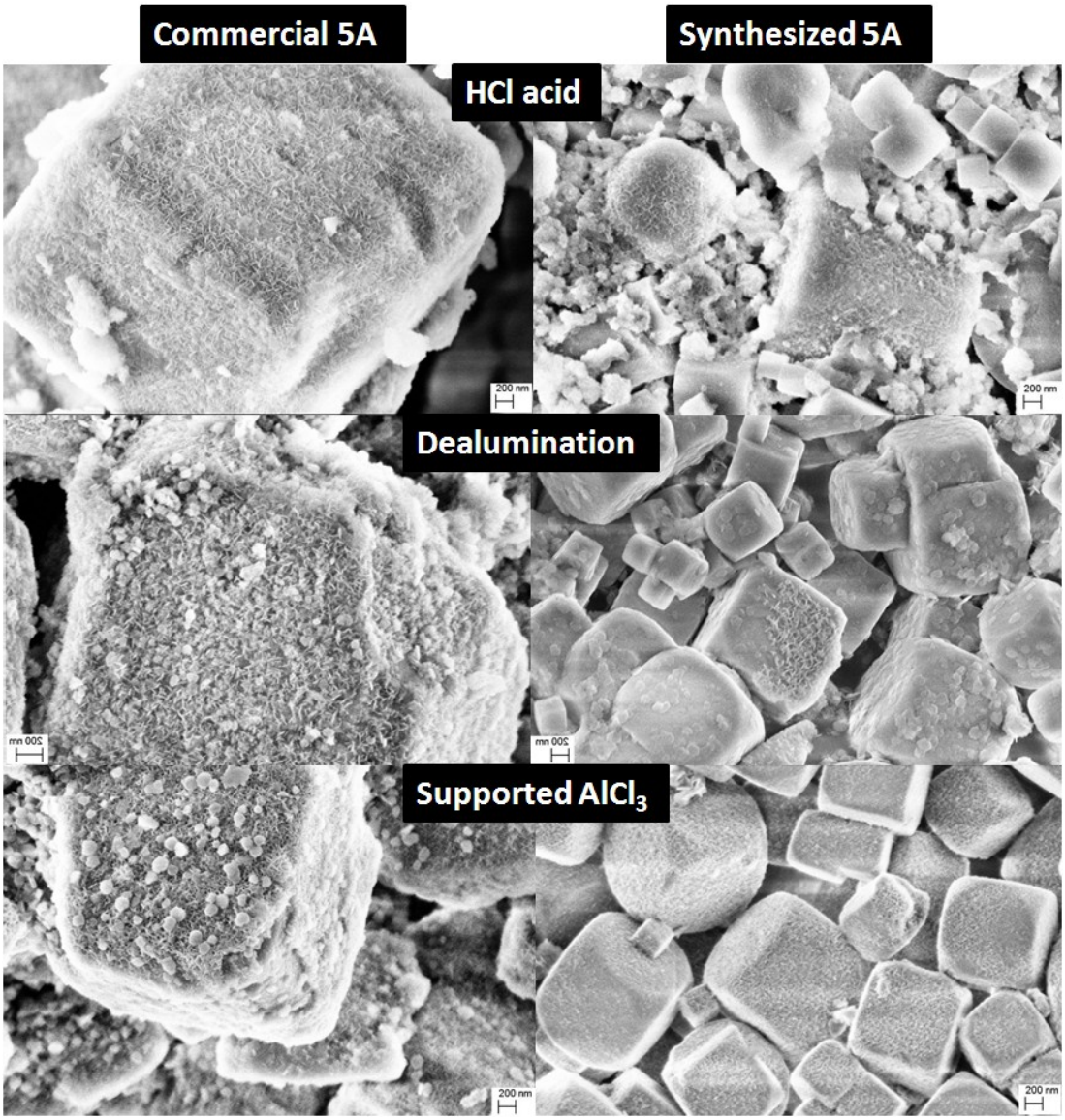

Figure 9.1 Effectiveness of sol-gel-Grignard treatment on commercial and synthesized zeolite 5A surfaces using different acidic catalyst

9.2.3 Sol-gel treatment using magnesium alkoxide as the Magnesium source

Currently, the magnesium isopropoxide used for sol-gel-Grignard treatment, comes from quenching of methylmagnesium bromide by isopropoxide. Magnesium alkoxide can be directly used for the sol-gel treatment. Fig. 9.2 shows two preliminary

$Mg(OH)_2$ morphologies formed using magnesium alkoxide. Further study is needed to optimize the $Mg(OH)_2$ morphology.

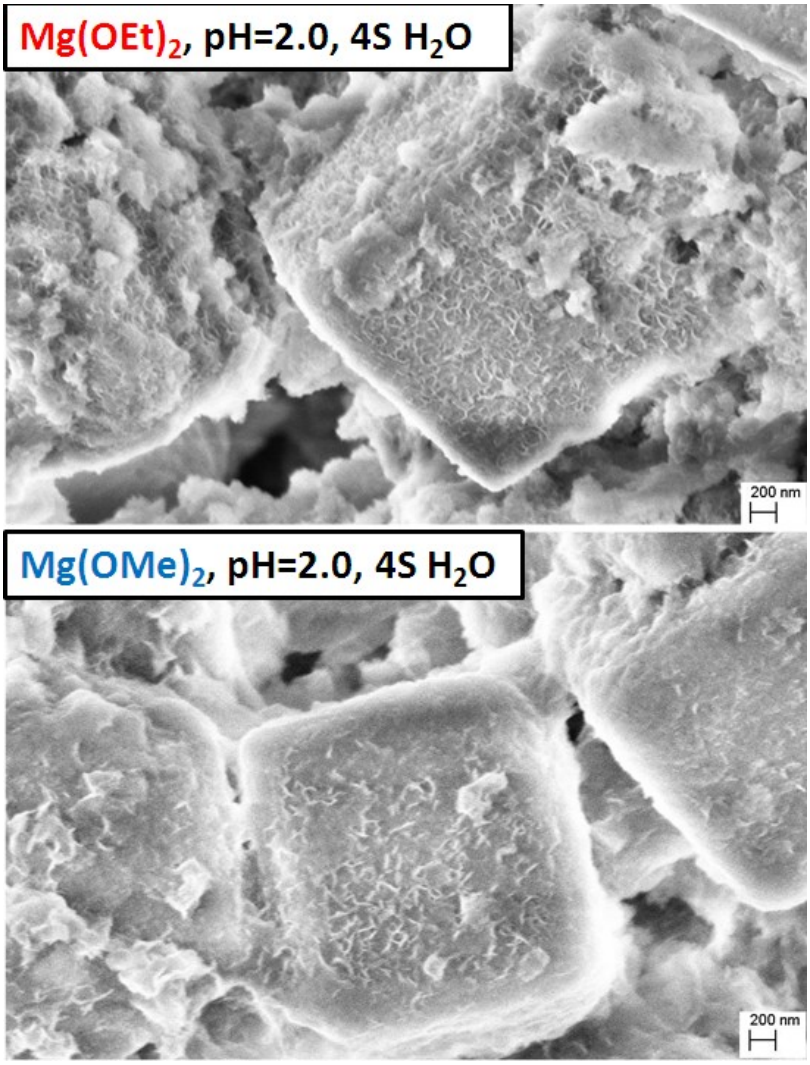

Figure 9.2 $Mg(OH)_2$ morphologies formed on zeolite 4A surfaces by sol-gel treatment using magnesium methoxide and magnesium ethoxide

APPENDIX A

MORPHOLOGIES DURING SOL-GEL TREATMENT

The sol-gel method is widely used to synthesize microporous metal oxide (or hydroxide) materials, through hydrolysis of the precursor metal alkoxide, such as $Si(OR)_4$, $Ti(OR)_4$, $Al(OR)_3$, $Mg(OR)_2$, *etc*.[1, 2] The advantage of sol-gel method is the relative easiness to control the morphologies of product. As shown in Fig. A.1, depending on the processing parameters, product of different morphologies (from high surface area porous networks to dense particles and fibers) can be formed.

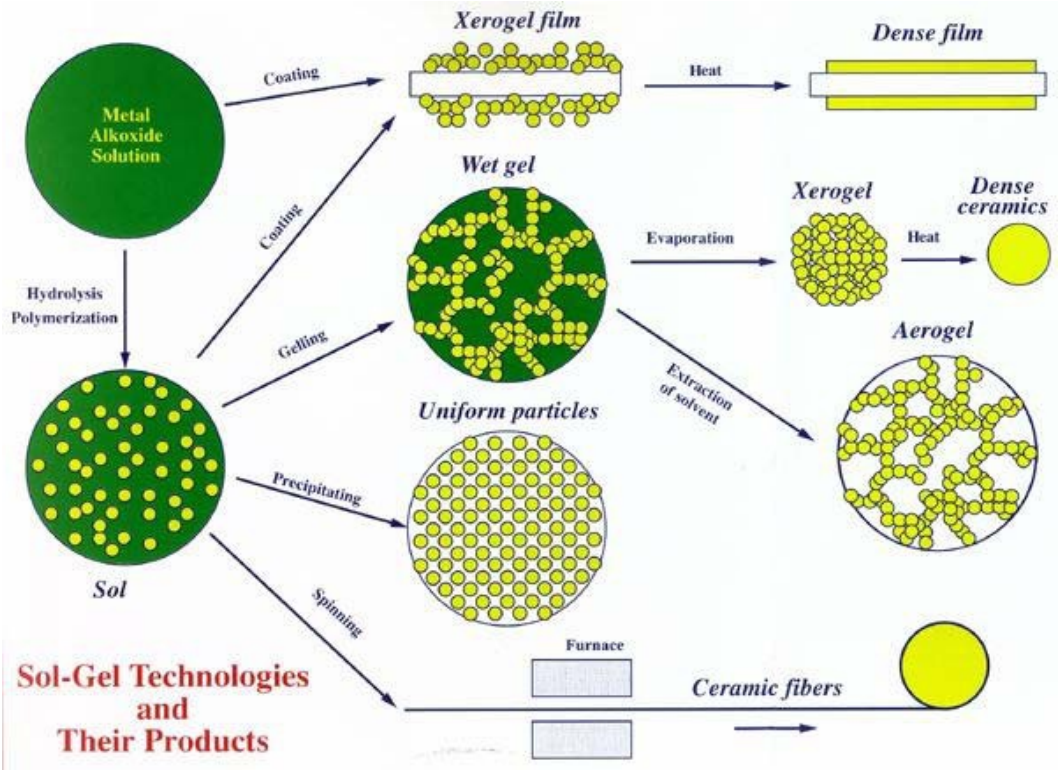

Figure A.1 Richness of morphologies of sol gel products

Former works on the MgO or $Mg(OH)_2$ synthesized from sol gel method are mainly xerogel or aerogel (under low acidic or basic conditions), which are suitable for catalysis applications due to the high porosity and larger surface area [3-8]. This work shows for the first time, the possibility of $Mg(OH)_2$ one dimensional structure formed by sol gel method (under high acidic condtions). Fig. A.2 is a reminder of the dramatic morphology variation depending on the acid catalyst for sol gel reactions, as discussed in chapter 4, 5.

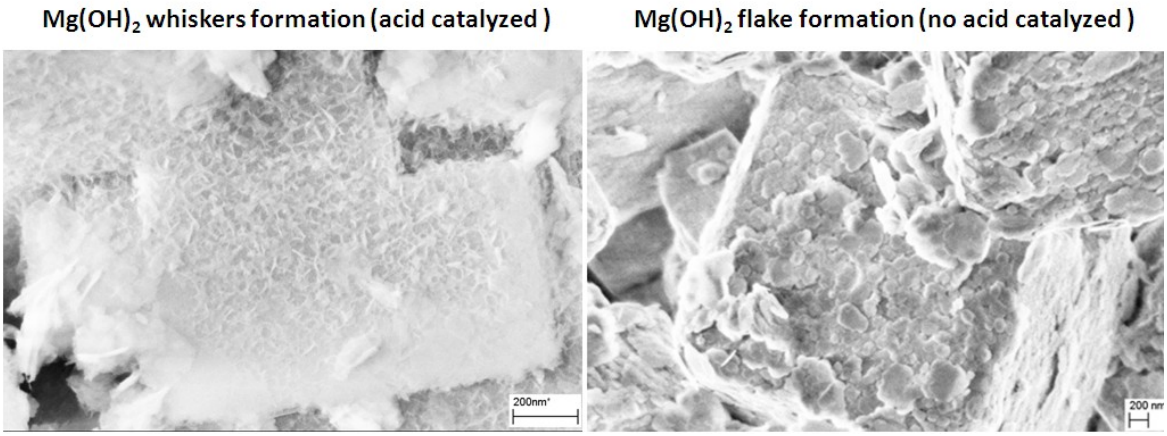

Figure A.2 Different $Mg(OH)_2$ morphologies formed under different acidic conditions

The possible structures of solution precursors (gel) range from weakly branched polymeric species to uniform (non-fractal) particles that may or may not be aggregated. During the deposition and drying stages (evaporation of solvent, slightly different from precipitation through toluene/IPA to water phase change in this work), these various species are rapidly concentrated on the substrate surface. How efficiently they pack (i.e. the volume fraction solids) depends on the extent of branching or aggregation and on the condensation rate. For branched clusters or aggregates, the precursor or aggregates size is also important.

The precursor species freely penetrate one another but do not stick as they are forced into close proximity by the increasing concentration [6]. De Gennes visualized such networks as ‘‘entangled worms’’ [7]. Alternatively, when the sticking intersection increases, the structures, even though porous, are much like an assemblage of tumbleweeds, as shown in Fig. A.3. The *sticking probability* depends on the condensation rate of reaction, which causes the crosslinking of the precursor species. In silica systems, the sticking probability is highest at intermediate pH, where the condensation rate is the greatest. The sticking probability is lower near pH=2 and above pH=10 (for high-molecular-weight species) where silanols tend to be deprotonated causing mutual repulsion of silicate particles [8].

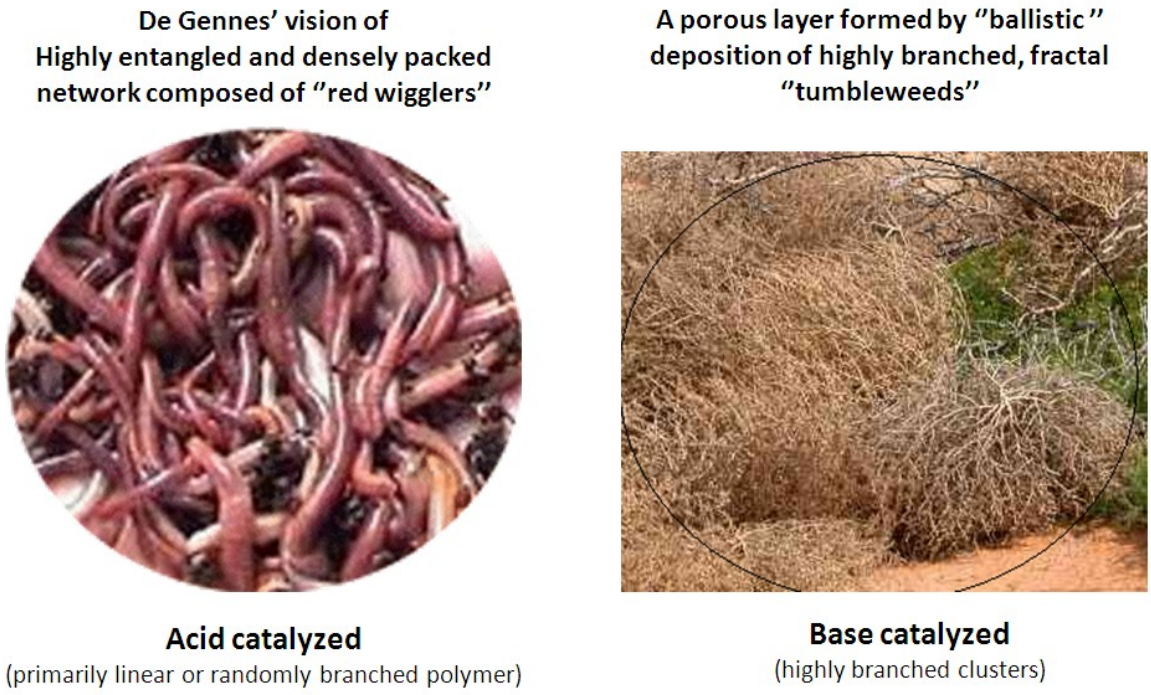

Figure A.3 Visualization of morphologies formed by sol gel species with low and high sticking probability

The pH may has similar effects on the sol gel morphologies in both silica and magnesium systems. At higher acidic environment, the protonated -$MgOH_2^+$ sol gel species mutually repulse with one another and have less sticking probability. Apparently, the pH window to form one dimensional (linear) sol gel product is different between the well studied silicon system and our magnesium system, which needs to be studied in the future.

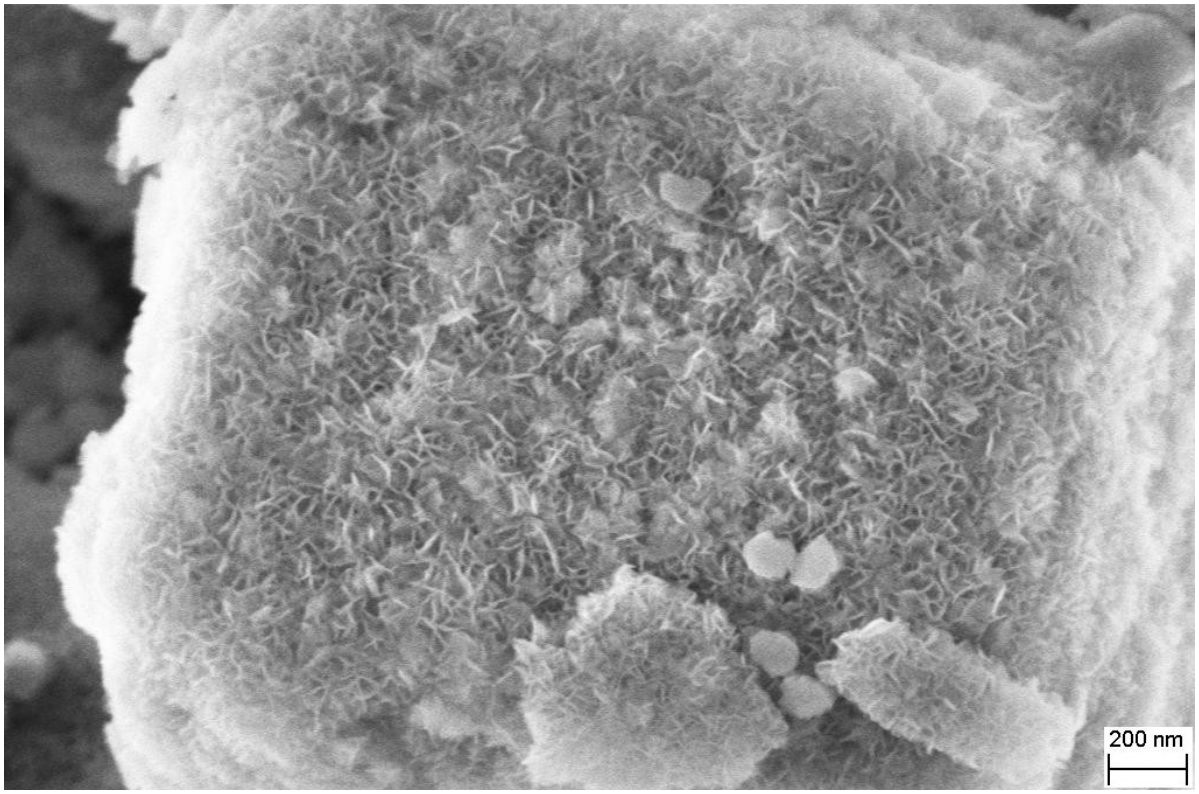

Figure A.4 Imagine the $Mg(OH)_2$ as entangled wigglers (nanosize) on the zeolite surface

During the sol-gel-Grignard treatment, some interesting morphologies evolved unexpectedly. More work is needed to elucidate the detailed mechanism of those morphologies formation, here two examples are shown to exemplify the variety of sol gel product morphology. Fig. A.5 shows the unexpected long fibers formed during the sol-

gel step. The treatment was done on 300 nm 5A particles with no external acid added. After 12S (stoichiometric amount of) water was added to the sol-gel precursor dispersion, the solution was shake overnight, after which a significant viscosity increase was observed on the sol gel precursor dispersion (the dispersion kept still overnight did not show any viscosity increase). The sol-gel product was centrifuged out and the solid was observed under SEM. As shown in Fig. A.5, long fibers are formed by the sol-gel reactions, which explains the viscosity increase of the sol-gel dispersion. The sol-gel species may have higher probability to collide and align to form the long fibers, during the overnight shaking process. The sol-gel species can only collide and align with neighbor species under still condition, due to the limited diffusivity of the large sol-gel species. Similar fiber morphology sol-gel products were found if the dispersion is constantly stirred. The long fibers were broken down to small pieces after the isopropanol phase is changed into water phase. It can be hypothesized that the fiber contains water soluble part, such as $MgBr_2$ and $Mg(OR)_2$, so that when those parts dissolve into water solutions, the fibers break down to smaller pieces.

Fig. A. 6 shows a sticky polymer like morphology of sol-gel product. After 8S of water addition (with no acid addition), the sol-gel product undergoes one time of IPA wash and three times of water washing. Despite the fact that XRD pattern shows the majority of sol-gel product is $Mg(OH)_2$ crystals after 3 times of water washing (Fig. 4.5), there seems to be some amorphous sticky product exist, which probably corresponds to the polymer like sol-gel aggregates (Fig. 4.6). Due to the limited time frame for this research , no thorough investigation into these sol-gel products are done, however, the preliminary results indicates the potential complexity of sol-gel morphology.

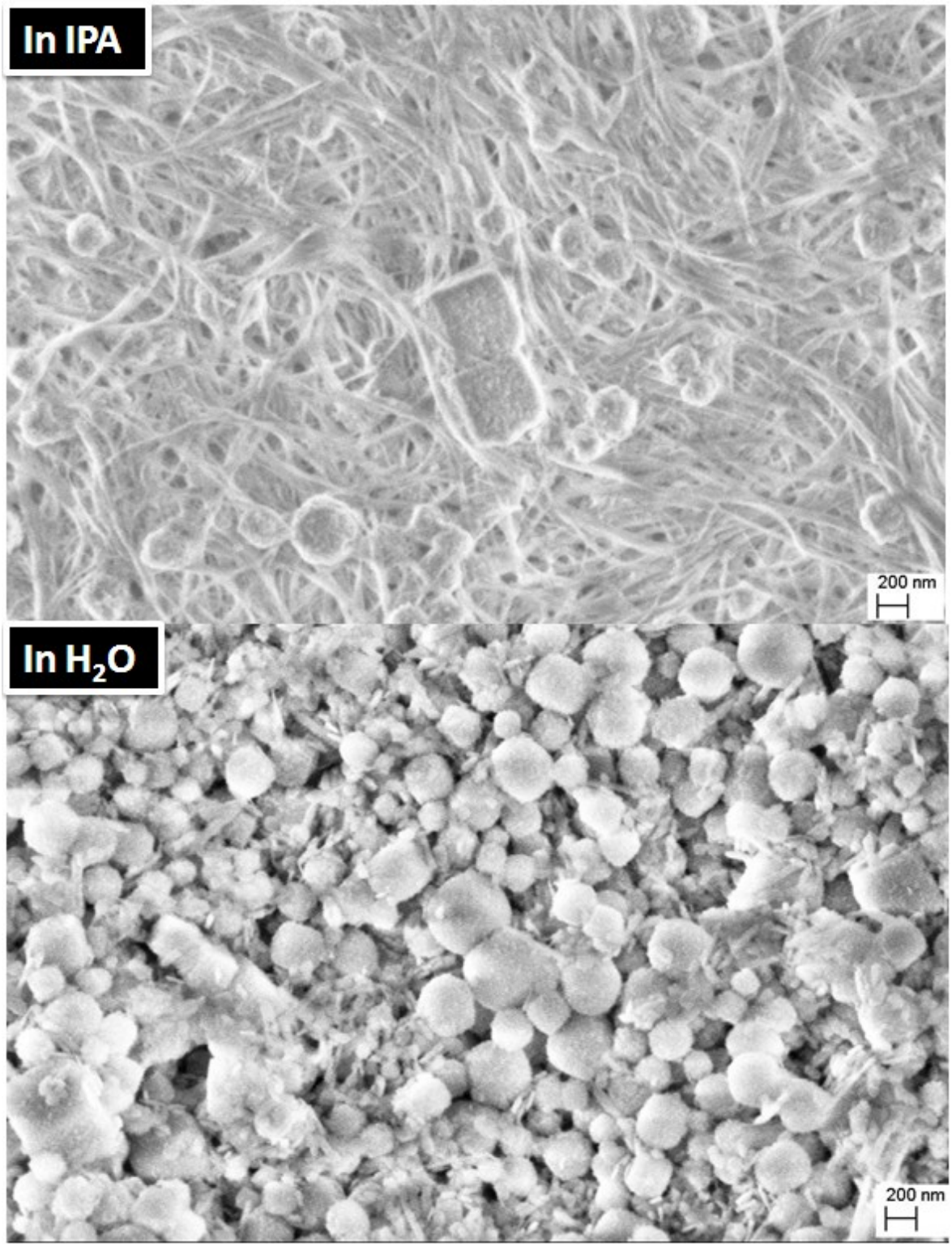

Figure A.5 Long fibers formed in the sol gel step and broken fibers during water washing steps (GT88-2)

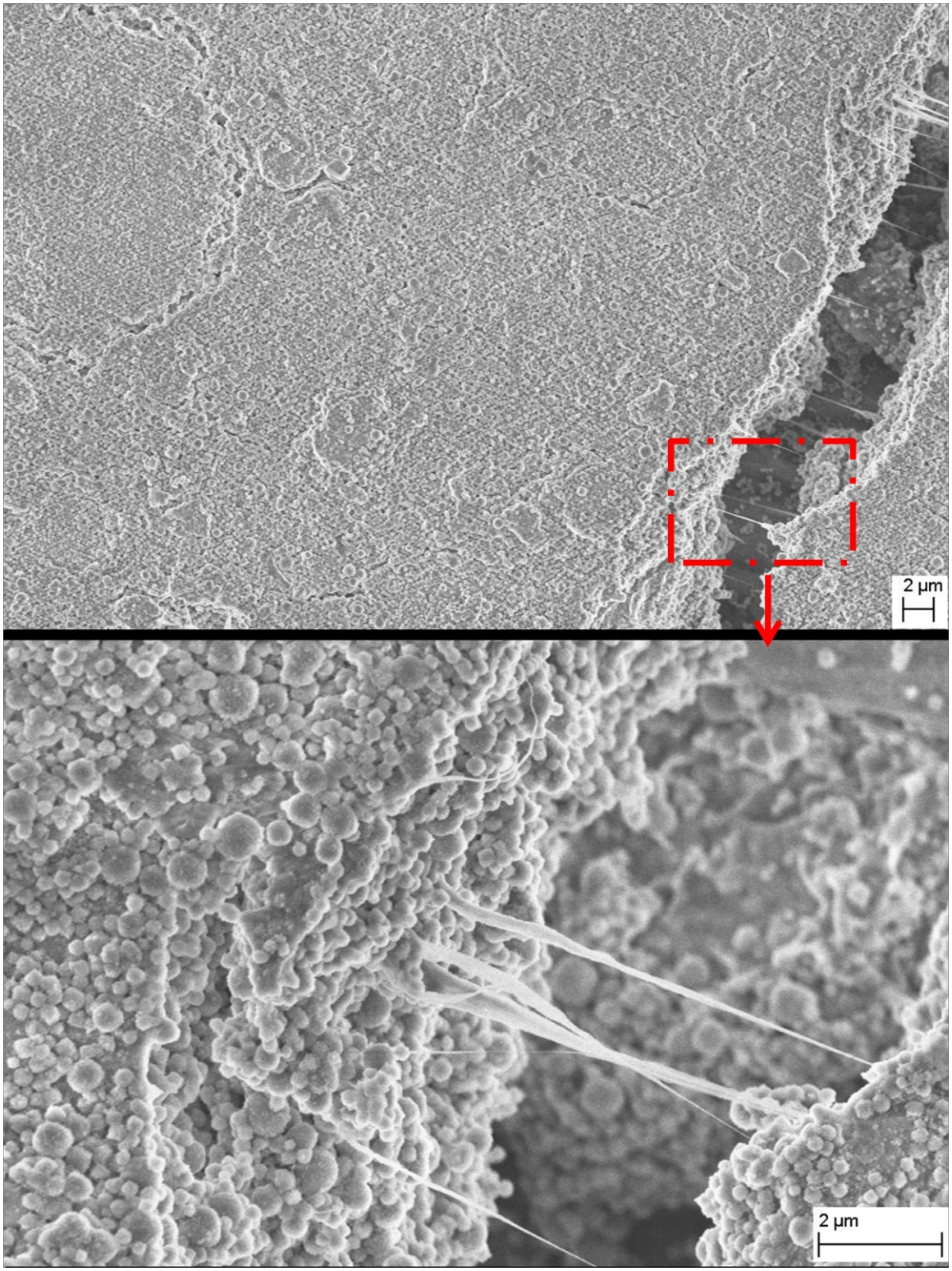

Figure A.6 Polymer like sticky species formed in the sol-gel-Grignard treatment (GT77-3)

In the current sol-gel-Grignard treatment, the precursor magnesium isopropoxide, together with magnesium bromide are formed by the reaction between Grignard reagent and isopropanol. It is well known that salt ions can distribute homogeneously in the sol-gel product [2]. During the water washing steps on the sol-gel product, it was found the conductivity of supernatant water drops gradually, probably because the magnesium bromide embedded in the sol-gel product slowly diffuses out. The effect of this diffusion process on the sol-gel $Mg(OH)_2$ morphology is unknown. An interesting SEM observation, Fig. A.7 shows the potential importance of the separation process between the water soluble $MgBr_2$ and the sol-gel product. One sol-gel Grignard treatment was done without zeolite addition. After 8S of water addition (no acid catalyst), one drop of the sol-gel dispersion (toluene/IPA phase) was dispersed on a SEM sample mount and observed by SEM. (It is worth noting that during the evaporation process of toluene and IPA, moisture from air can get in). Two phases were found: islands of skeleton appearance crystals dispersed in fine amorphous structure. Considering the limited variety of solid contents in the sol-gel product, the skeleton appearance crystal probably is $MgBr_2$, and the fine structures are the sol-gel product $Mg(OH)_2$. The regular patterns formed by the phase separation of sol-gel product (and $MgBr_2$) shows the potential importance of $MgBr_2$ on the sol-gel $Mg(OH)_2$ morphology. Further work is needed on this aspect.

In summary, more factors except for hydrolysis ratio (water amount), pH can affect the sol-gel Mg(OH)2 morphology. Fundamental research is needed to elucidate the roles of each factor.

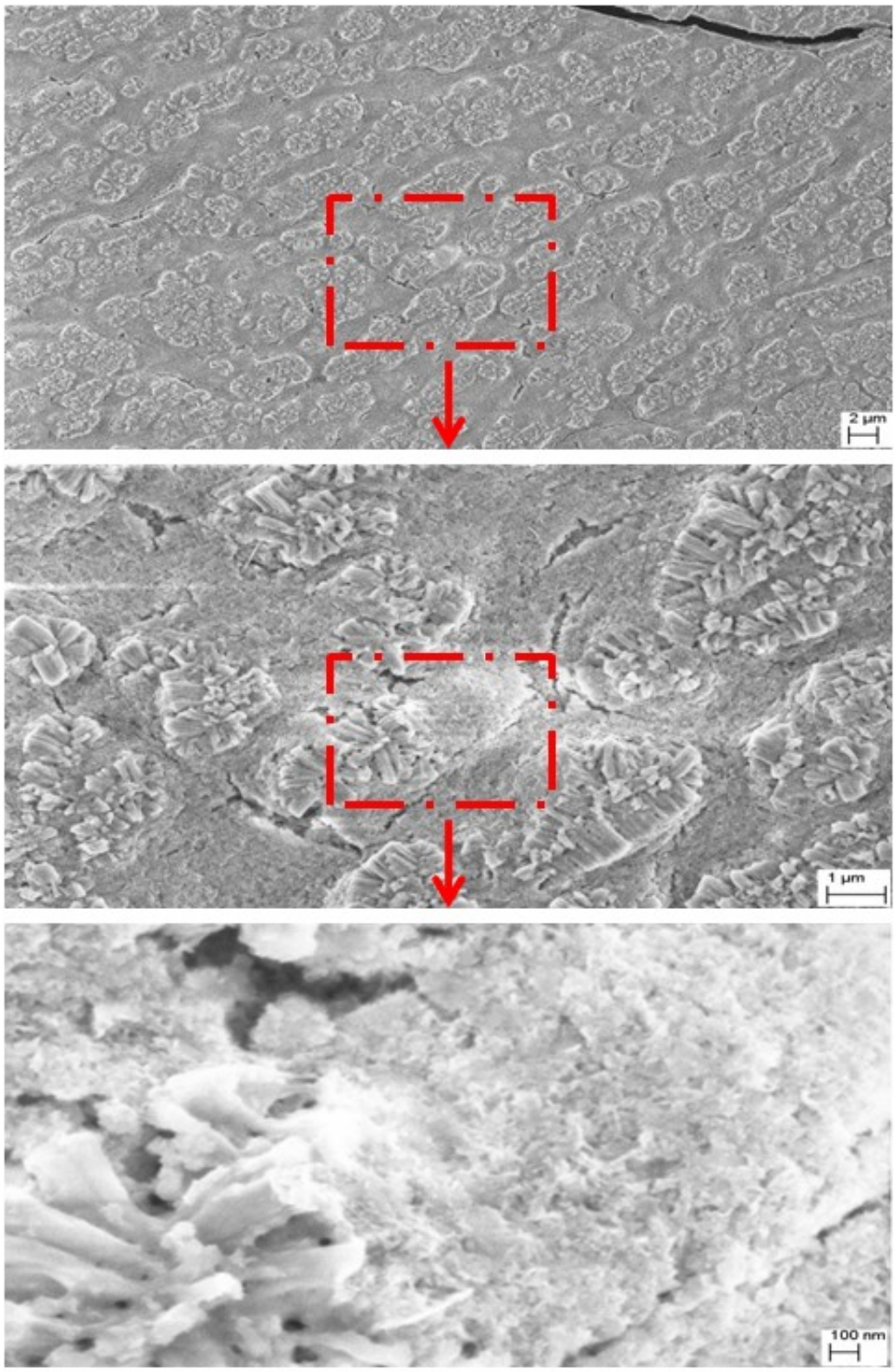

Figure A.7 Phase separation induced regular patterns of sol-gel $Mg(OH)_2$ containing equimolar of $MgBr_2$ (GT72-3)

REFERENCES

[1] C. J. Brinker, Sol-gel science, **1990**, *Academic Press Inc.*

[2] L. F. Francis, Sol-gel methods for oxide coatings, *Mater. Manuf. Process*, **1997**, *12(6),* 963-1015

[3] Y. Diao, Hydrolysis of magnesium methoxide. effects of toluene on gel structure and gel chemistry, *Chem. Mater.,* **2002**, *14*, 362-368

[4] J.G. Yoon, Growth of (111) oriented MgO film on Si substrate by the sol-gel method, *Appl. Phys. Lett.* **1995**, *66(20),* 2661-2663

[5] T. Lopez, Synthesis of magnesium oxide by the sol-gel method: effect of the pH on the surface hydroxylation, *J. Catal.,* **1991,** *127*, 75-85

[6] T.A. Witten, *science,* **1986**, 232, 1607

[7] P.G. de Gennes, *Physics Today*, **1983**, 36, 33-39

[8] R.K. Iler, *The chemistry of silica*, Wiley, New York, **1979**

APPENDIX B

MEMBRANE PLANT SIMULATION

Based on the membrane performance on C4s separation, a hypothetical hollow fiber membrane, with nC4 permeance of 4 GPU and nC4/iC4 selectivity of 40 is used to simulate a membrane separator. It is challenging to achieve these performances based on the discussion shown in chapter 6, a best case scenario can be used to simulate a membrane separator, and compare with the existing distillation method, in order to show the maximum potential of membrane based separation.

Simulation was carried out using the program developed by Koros group members [1]. A countercurrent flow is used and other detailed parameters are shown in table B.1.

Table B.1 Membrane separator (250,000 tons/yr) using hollow fiber membrane modules, which has nC4 permeance of 4 GPU, and nC4/iC4 selectivity of 40

temperature	100 °C
feed pressure	8 atm
permeate pressure	1 atm
feed gas composition	40% nC4 /60% iC4
permeate composition	79.4% nC4/20.6 % iC4
retentate composition	2% nC4/ 98% iC4
feed flow rate	26000 kg/hr
permeate flow rate	12740 kg/hr
retentate flow rate	13260 kg/hr
Membrane area	340,000 m^2
packing density	10,000 m^2/m^3 [2]
membrane unit volume	34 m^3

The simulated membrane separator can be integrated into the isomerization-separation-alkylation process as shown in Fig. B.1. The high temperature, high pressure C4s mixture gas from the isomerization reactor can be feed into the membrane separator. The membrane based separation utilizes the pressure difference (between feed side and permeate side) as the driving force, therefore, no outsource of energy is needed to drive the separation. The 98% purity iC4 from retentate can be feed into the alkylation process. The nC4 rich permeate gas will be pressurized, and recycled back to the isomerization reactor. The only source of energy supplied to the membrane separator is the compressor used to pressurize the permeate gas. The power needed for the compressor can be approximated using the pressure difference and the gas flow rate [3].

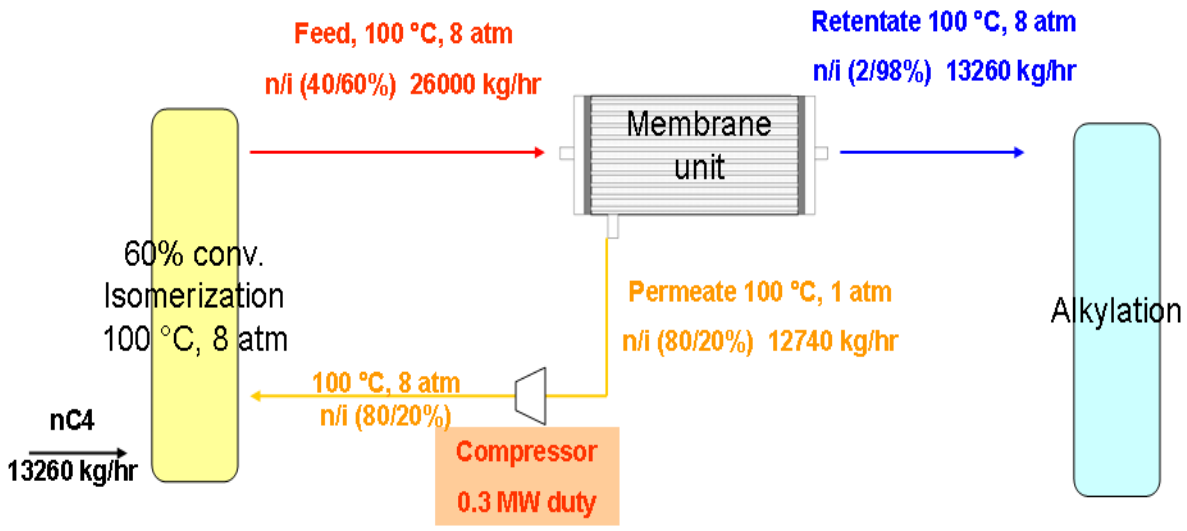

Figure B.1 Flow diagram of isomerization-separation-alkylation process

Based on the simulation results, a membrane separator with capability of 250,000 tons/yr separation capability can be compared with the existing distillation method [4]. As shown in table B.2, a membrane separator is significantly smaller in size and more efficient in energy consumption than a distillation tower with similar separation capabilities.

Table B.2 Comparison between distillation and membrane method for C4s separation

	Size	Energy usage
Membrane	34 m^3	0.3 MW (compressor)
Distillation [4]	500 m^3 (2.9 m by 60 m)	10 MW (boiler)

REFERENCES

[1] D.T. Coker, *AICHE*, **1998,** 4, 1289-1302

[2] R. W. Baker, *Ind. & Eng. Chem. Res.,* **2002**, 41, 1393-1411.

[3] Compressor duty table, BPH Pump & Equipment, Inc.

[4] K. T. Klemola, *Ind. Eng. Chem. Res.*, **1996**, 35, 4579-4586

APPENDIX C

MIXED MATRIX MEMBRANES CONTAINING ALUMINA WITH SURFACE NANOWHISKERS

To understand the entropic contribution to the enhanced adhesion from $Mg(OH)_2$ whiskers, polymer adhesion with other whiskered surfaces can be used to find if similar good adhesion exist. Alumina nanopowder with highly whiskered surface, as shown in Fig. C.1, was used in this preliminary work. Aggregates of alumina nanopowder can be found in mixed matrix membranes, as shown in Fig. C.2, but the polymer adhesion with the independent particles appears good, from SEM observation. The gas permeabilities in the mixed matrix membrane are far higher than the Maxwell model results, assuming non-permeable Alumina particle. If the alumina powder is highly porous, the gas permeabilities in the mixed matrix membrane may be due to the large gas permeabilities in the alumina, instead of defective interfaces. More research is needed on this aspect.

Table C.1 Gas transport properties of mixed matrix membranes (theoretical and experimental results)

	P_{O2}[Barrer]	$\alpha_{O2/N2}$	P_{nC4}[Barrer]	$\alpha_{nC4/iC4}$
6FDA-DAM	176	3.7	3.7	21
25wt%-$Mg(OH)_2$+6FDA-DAM	282	3.6	7.6	20
Maxwell model (P=0 in $Mg(OH)_2$)				
25wt%-$Mg(OH)_2$+6FDA-DAM	***103***	***3.7***	***2.2***	***21***
Maxwell model (P=∞ in Al_2O_3)				
25wt%-$Mg(OH)_2$+6FDA-DAM	***327***	***3.7***	***6.9***	***21***

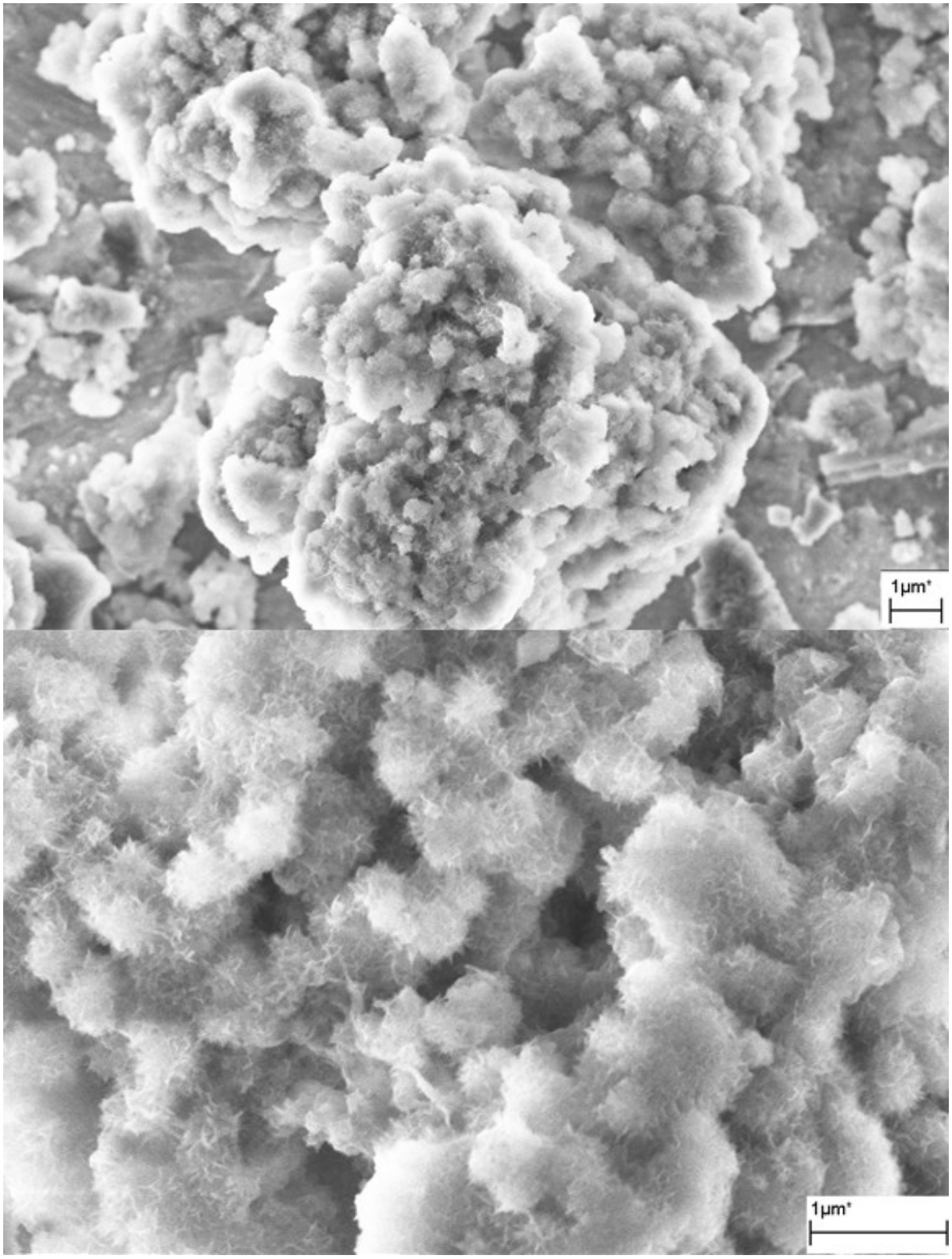

Figure C.1 Alumina nanopowder (whisker) for mixed matrix membrane formation

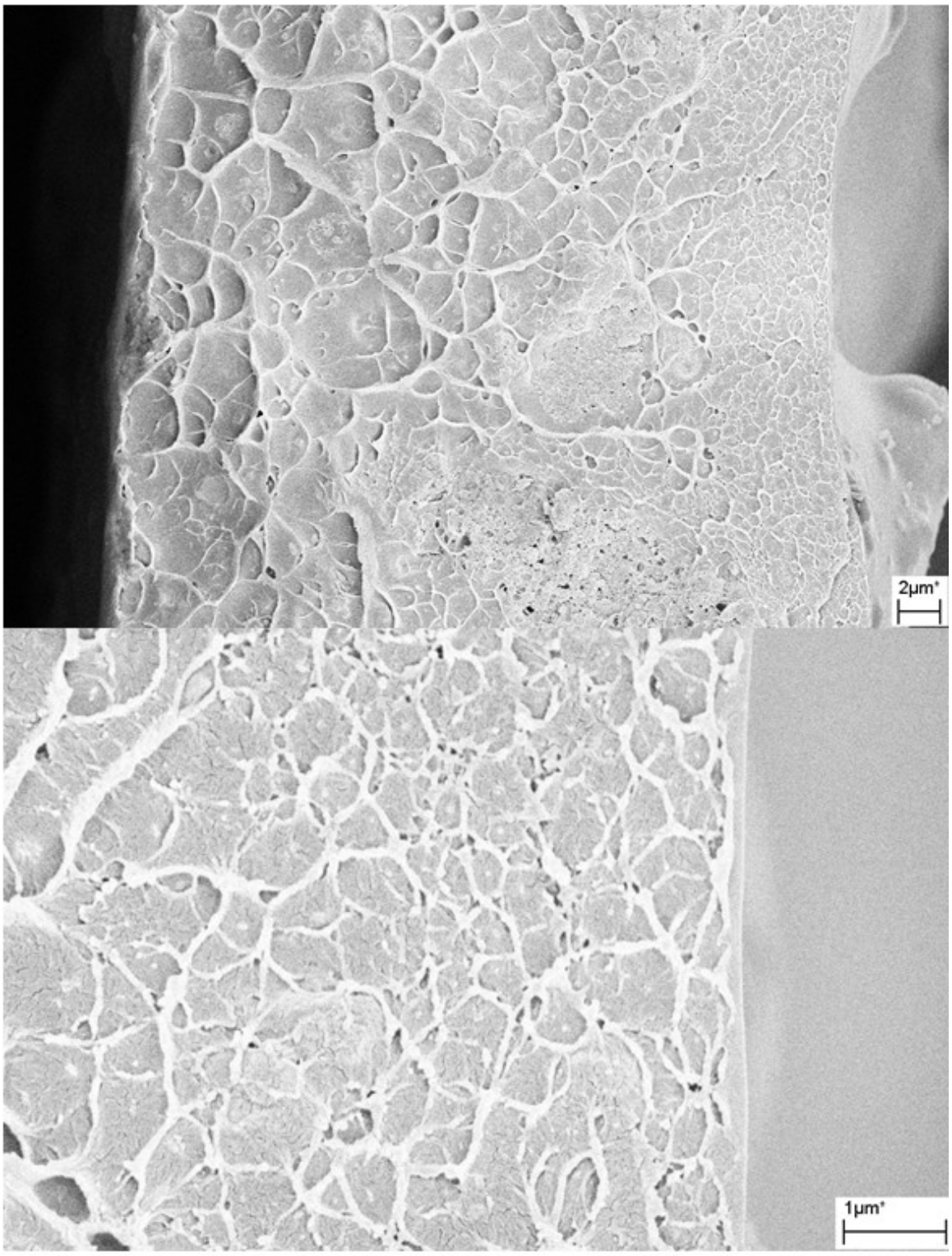

Figure C.2 Cross-section of Alumina +6FDA-DAM mixed matrix membranes

APPENDIX D

MIXED MATRIX MEMBRANES CONTAINING MAGNESIUM HYDROXIDE NANOPARTICLES

Previous researchers suggested to study the enthalpic and entropic contribution of zeolite/polymer adhesion enhancement through $Mg(OH)_2$ whiskers formed on zeolite surfaces. A powerful microscopic tool to study the adhesion between $Mg(OH)_2$ and polymer is AFM. Jung-Hyun Lee in Dr. Meredith group carried out the AFM work to study the adhesion force between polymer and zeolite surfaces. The adhesion force between the high silica MFI and different polymers are measured and it was found the acid (zeolite surface hydroxyl)-basic(polymer carbonyl group) interaction is the primary factor for the difference of adhesion force. Similar AFM study, using a $Mg(OH)_2$ micron particle attached to AFM tip, lagged behind due to the lack of micron $Mg(OH)_2$ crystal. Mixed matrix membrane method is used here to study the adhesion between polymer and $Mg(OH)_2$ particles. $Mg(OH)_2$ nanoflakes and 6FDA-DAM polymer are used to make mixed matrix membranes. As shown in Fig. D.1, $Mg(OH)_2$ flakes have dimension of 500 nm length and 100 nm thickness, and smooth surfaces. Aggregates of $Mg(OH)_2$ flakes can be observed in the cross section of mixed matrix membranes, as shown in Fig. D.2 . The adhesion between polymer and $Mg(OH)_2$ particles, from SEM observation, is better than that of polymer and zeolite particles, however, the gas permeation results of mixed matrix films, as shown in table D.1, suggest a non-ideal interfacial adhesion. The gas permeabilities are higher than the Maxwell model values, assuming the $Mg(OH)_2$ flakes as non-permeable.

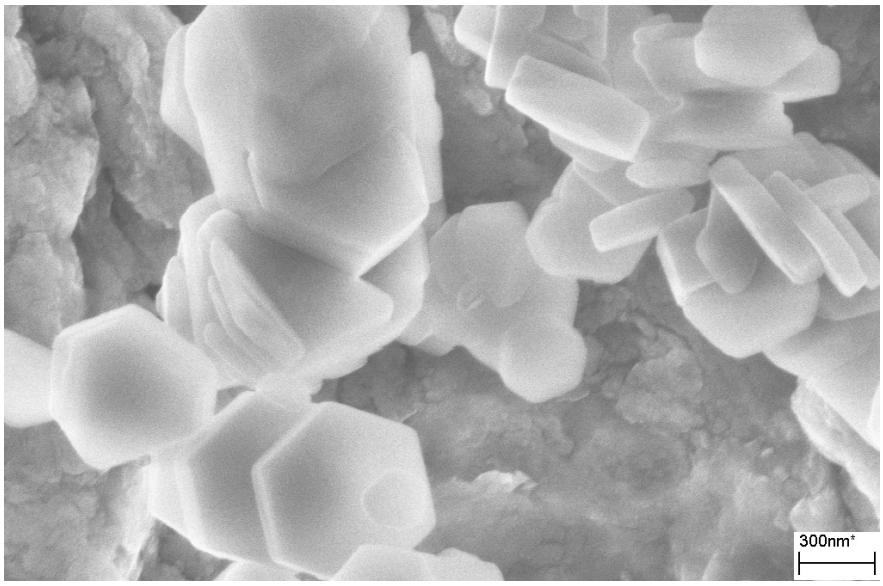

Figure D.1 $Mg(OH)_2$ nano-flakes for mixed matrix membrane formation

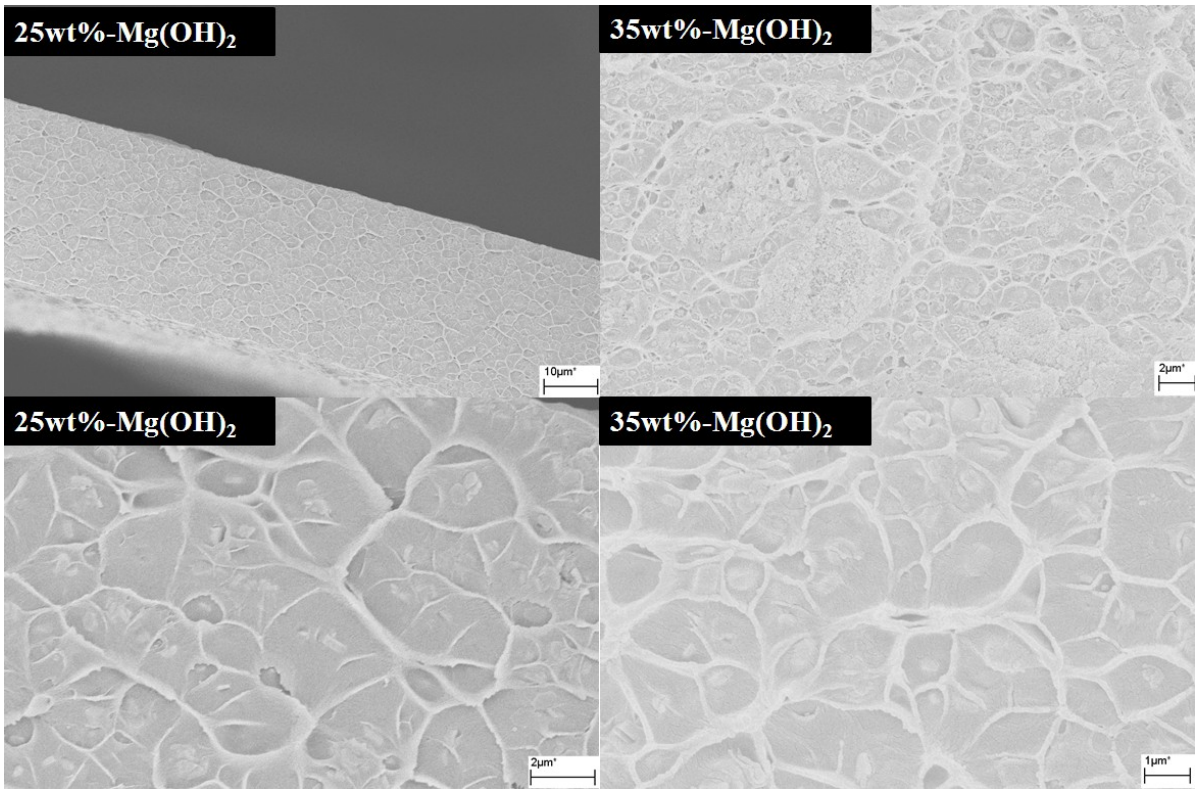

Figure D.2 Cross-section of $Mg(OH)_2$ +6FDA-DAM mixed matrix membranes

Preliminary results suggest the interfacial adhesion between the smooth $Mg(OH)_2$ surfaces and 6FDA-DAM polymer is probably not enough to achieve good mixed matrix membranes. Similar works can be done using bigger $Mg(OH)_2$ particles (to avoid agglomeration) and other polymers to study the interactions.

Table D.1 Gas transport properties of mixed matrix membranes (theoretical and experimental results)

	P_{O2}[Barrer]	$\alpha_{O2/N2}$	P_{nC4}[Barrer]	$\alpha_{nC4/iC4}$
6FDA-DAM	176	3.7	3.7	21
25wt%-$Mg(OH)_2$+6FDA-DAM	178	3.4	4.5	21
Maxwell model				
25wt%-Mg(OH)$_2$+6FDA-DAM	***123***	***3.7***	***2.6***	***21***
35wt%-$Mg(OH)_2$+6FDA-DAM	161	3.5	4.8	22
Maxwell model				
35wt%-Mg(OH)$_2$+6FDA-DAM	***103***	***3.7***	***2.2***	***21***

VITA

Junqiang Liu was born in Weifang, China in 1982. He is the third and youngest son of Ruiping Liu and Ailan Sun. After completing his high school studies at No.7 middle school, Weifang in 1999, he entered East China University of Science and Technology, from which he received a Bachelor degree on Chemical Engineering. He went to Tokyo University of Agriculture and Technology in 2002 as an exchange senior student for one year. He continued to study at Tokyo University of Agriculture and Technology and obtained a Master degree on Applied Chemistry in 2006. He crossed the Pacific and enrolled in Georgia Institute of Technology in the fall of 2006. In December 2010, he fulfilled the requirements for Doctor of Philosophy degree in Chemical & Biomolecular Engineering. Thereafter, he began working in the Chemistry& Catalysis group at Dow Chemical Company, Midland, Michigan.